Proceedings of the National Conference on

Preparation and Characterization of Crystalline Materials

(NCPCCM 2016)

4th & 5th August 2016

Chief Editor & Convener

Dr.S.M. RAVI KUMAR

Organised by

PG and Research Department of physics

Government Arts College,

Chengam Road, National Highway 66, Tiruvannamalai, Tamil Nadu 606603
Telephone No : 04175 – 236553, Website : http://gactvm.in

Sponsored by

TANSCHE, Chennai.

Government Arts College, Tiruvannamalai.

In Association with

ISPA,Chennai

Proceedings of the National Conference on

Preparation and Characterization of Crystalline Materials

(NCPCCM-2016)

Edited by

Dr.S.M. RAVI KUMAR
AssistantProfessor,
PG and Research Department of Physics,
Government Arts College, Tiruvannamalai-606 603
Email Id: smravi78@rediffmail.com, Ph: 8608953139

JACS DIRECTORY
Research Journals and Books Publishing Group
Tamil Nadu, India.

Proceedings of the National Conference on Preparation and Characterization of Crystalline Materials (NCPCCM-2016)

Edited by

Dr.S.M.RAVI KUMAR
AssistantProfessor,
PG and Research Department of Physics,
Government Arts College,
Tiruvannamalai-606 603, Tamilnadu, India.
Email Id: smravi78@rediffmail.com., Ph: +91 8608953139

Published by

JACS Directory, Research Journals and Books Publishing Group,
2/127, Puthiyamputhur, Tuticorin, Tamilnadu, India – 628 402.
Email: editor@jacsdirectory.com; Ph: +91 9943365389

First Print: August 2016
No. of Pages: 248

ISBN: 978-81-931566-1-2

Printed at INDIA

Dr. S.M.Ravi Kumar
Convener-NCPCCM '16
Government Arts College
Tiruvannamalai

PREFACE

It is a great pleasure for us to organize the National Conference on Preparation and Characterization of crystalline Materials (NCPCCM '16) at PG & Research Department of Physics, Government Arts College, Tiruvannamalai during 4 & 5 August 2016. We extend a cordial welcome to all the honourable delegates of this two days national event. The PG and Research Department of Physics of Government Arts College is committed for the Research and Development of modern technologically and industrially important crystalline materials.

The purpose of this conference is to bring together scientists, experts, academicians and other researchers from different parts of the country actively engaged in the forefront of Preparation and characterization of crystalline materials for exchange of knowledge and ideas and an in depth analysis of the subject. It will cover the entire field of preparation and characterization of macro, micro and nano crystalline materials, from basic physical phenomena to the recent significant advancements in preparation techniques, materials characteristics, characterization techniques, etc. Special attention will be paid to the prospects for future development of crystal preparation and characterization techniques.

I am very much pleased to note that there are 9 Invited talks and more than 125 contributed papers from various institutions covering different aspects of preparation and characterization of crystalline materials. It is our sincere hope that the young researchers will gain a lot from these high profile dedicated invited speakers and authors of contributed papers and will pave a way for many productive and collaborative pursuits in this technologically important area of research.

I am grateful to our **Principal** who has given us great strength and encouragement in organizing this national conference. We express our sincere thanks to the Founder of ISPA **Dr. S. Gunasekaran**, Dean-Research, St. Peters University, Avadi, Chennai for extending collaboration and support in organizing this conference successfully. We express our gratitude to **Dr. P. Sagayaraj**, Head, Department of Physics, Loyola College, Chennai and **Dr. R. Jayavel**, Dean-Research, Anna University, Chennai for their kind and valuable guidance in this effort. We also thankful to the advisory board members from various institutions for their kind support and help.

I express my sincere thanks to my colleagues in our Department for their valuable help and support in making this National level event successful. I thank all the invited speakers for their technical and enlightening lectures, sharing their innovative ideas and knowledge. Special thanks are due to the participants who have come from various parts of India to share their scientific inventions and ideas in this conference.

The financial support extended by Tamil Nadu State Council for Higher Education (TANSCHE) and Indian Spectrophysics Association (ISPA), Chennai are gratefully acknowledged.

Dr. S.M.Ravi Kumar

Dr. P. Sagayaraj
Head &Associate Professor
Loyola College (Autonomous)
Nungambakkam
Chennai-600 034

I am very happy to know that a “National Conference on Preparation and Characterization of Crystalline Materials” is organized by the Department of Physics, Government Arts College, Tiruvannamalai, Tamil Nadu, India.

Crystalline materials provide the foundation of our modern technologically driven world. The supremacy of materials is achieved through detailed scientific research. Advances in the techniques of growing and characterizing ever more perfect crystals of a wide range of materials lie at the roots of today's advanced technology. The growth of crystal involves research by dedicated scientists and scholars in academic world as well as industry involving a broad field of disciplines including physics, chemistry, biology, material sciences and engineering. Significant applications in information technology, photonics, energy storage and harvesting, environmental protection and medicine require a deep understanding and control of crystal growth.

The reason for growing single crystals is, many physical properties of solids are obscured or complicated by the effect of grain boundaries. Hence, in order to achieve high performance from the device, high quality single crystals are required. The strong influence of single crystals in the present technology is evident from the recent advancements in the above mentioned fields. The mostdynamic campaigns of this conference shall be its intensive interaction with research community to inculcate excitement regarding crystal growth, assessment and scientific method of knowledge transfer. I am sure that this conference would rejuvenate younger minds to get new ideas in the field of crystal growth and characterization.

I wish and thank the organizers for arranging such a conference and my best of luck to all the organizing staffs and students, and all the participants.

Dr. P. Sagayaraj

Dr. S. Gunasekaran, M.Sc.,Ph.D.,D.Sc.
TANSA Awardee
Dean, Research & Development
Peter's Institute of Higher Education and Research, St. Peter's University
Avadi, Chennai – 600 054. Tamil Nadu, India.
E-mail: deanresearchspu@gmail.com
Mobile: 0091-9962574210
Founder President: Indian Spectrophysics Association (ISPA)
Former Registrar: Periyar University
Former Head: PG & Research Department of Physics, Pachaiyappa's College, Chennai – 600 030.

25.07.2016

Message

Hearty Greetings from ISPA!!!

In the modern era of science, contributions and significance of Physics thither technology is remarkable. Dodging Physics and its adaptability to advancements is unpardonable but to form a forum among the students, researchers, professors and scientists, **The Department of Physics**, Government Arts College, Tiruvannamalai, Tamilnadu, India has organizing a **National Conference on Preparation and Characterization of Crystalline Materials** (NCPCCM 2016), during 4th &5th, August 2016.

It is appropriate to extend my greetings and felicitation to **The Patron** of this Conference Prof**. K. Kalidasan**, Principal, Government Arts College, Tiruvannamalai, for his enthusiastic encouragement and support for this scientific event.

I deem it a pleasure to wish **The Conference Chairman Prof. R. Arunchunai Annadurai**, Head, PG & Research Department of Physics, Government Arts College, Tiruvannamalai. His rapport towards the successful sculpturing of this National Scientific event is a bench mark.

My congratulations and best wishes to the Convener **Dr. S. M. Ravi Kumar,** Assistant Professor, Department of Physics and the Organizing Secretary **Dr. M. Balakrishnan**, Associate Professor, Department of Physics, for being successful captains in uniting their team to bring out this scientific mega event as a victorious one. I extend my wishes to their dedicated and sincere team members of the department of Physics.

I once again congratulate each and everyone, who worked behind the screen to make NCPCCM'16 an event of razzmatazz and nostalgic.

(S. GUNASEKARAN)

ANNA UNIVERSITY

CENTRE FOR RESEARCH

Sardar Patel Road, Chennai - 600 025, India

Prof. R. JAYAVEL, Ph.D.
DIRECTOR

MESSAGE

I am very much delighted to know that the Post Graduate and Research Department of Physics, Government Arts College, Tiruvannamalai is organizing the National Conference on Preparation and Characterization of Crystalline Materials during 4-5, August 2016. Crystalline materials play a vital role in diverse field of importance like Energy, Environment, Electronics, Photonics, Spintronics, Biotechnology, Defense technology, Space Technology, etc., Nanocrystalline materials are believed to be the promising class of advanced materials with an opportunity to ride the leading edge of a groundbreaking wave of new science heading our way. In order to nurture the advancement of these class of materials and realize their industrial applications, it becomes essential to have constant interaction among researchers, professional, academicians and students and this kind of conference would provide the stage for such interactions.

I take this opportunity to express my heartfelt congratulations to the Principal, Convener, Head of the Department, and the dedicated team of faculty members of the Post Graduate and Research Department of Physics, Government Arts College, Tiruvannamalai for organizing this kind of conference focusing on the Preparation and Characterization of Crystalline Materials. My very best wishes for the success of the conference and hope this experience would be carried by all to enrich their Scientific career.

29/7/16

R. JAYAVEL

Tel. : +91 44 22357354, +91 44 22357366 • Fax : +91 44 22201213 • E-mail : dirresearch@annauniv.edu, dirresearch@gmail.com

அரசு கலைக் கல்லூரி
திருவண்ணாமலை – 606603.
GOVERNMENT ARTS COLLEGE
Tiruvannamalai, 606603
(NAAC Accredited 'B' Grade College)
Affiliated to Thiruvalluvar University, Serkkadu, Vellore

Prof. K.Kalidasan
Principal (i/c)

FOREWORD

I am happy to note that the PG & Research Department of Physics, Government Arts College, Tiruvannamalai organized the "**National Conference on Preparation and Characterization of crystalline Materials (NCPCCM '16)**" during 4 & 5 August 2016 in association with Indian Spectrophysics Association (ISPA) and sponsoring by Tamil Nadu State Council for Higher Education (TANSCHE). This conference aimed at brings out the relevance of the preparation and characterization of crystalline materials for advanced applications in the various fields. It is an evident that these types of conferences will encourage exchange of ideas, spreading knowledge and innovations and report the progress in crystalline materials. I am very glad to promulgate that conference days are fruitful for research delegates so that those objectives of the conference will be accomplished to a very great extent. I wish to express my appreciation to the convener Dr. S. M. Ravi Kumar for his dynamic work in encouraging participants and securing substantial inputs of the papers from different parts of India. I extend my sincere thanks to all the learned speakers and participants for their commitments to come over Government Arts College, Tiruvannamalai and share their experiences with us. I extent my heartfelt gratitude to all the organizers, faculty members of various committees and student volunteers on their worth full efforts to make this conference a great success.

I take this opportunity to welcome all the participants to Government Arts College to make NCPCCM '16 a memorable event and wish you all tot stay at TIruvannamalai.

I wish NCPCCM '16 a grand success

K.Kalidasan

EDITORIAL BOARD

CHIEF EDITOR Dr. S.M. RAVIKUMAR

PG & Research Department of Physics,
Government Arts College, Tiruvannamalai – 600 603

National Conference on
PREPARATION AND CHARACTERIZATION OF CRYSTALLINE MATERIALS
(NCPCCM '16) Program Schedule

Thursday, 4 August 2016	
Time	**Program**
8.30 A.M – 9.30 A.M	**Registration**
9.30 A.M – 10.30 A.M	**Inauguration Function**
10.30 -11.00	**Inaugural Tea**
11.00 – 12.00 P.M	Development of Morphology engineered DAST derivatives of DSCHS, DASC and DAAS crystals for Terahertz applications **Dr. P. Sagayaraj** Head & Associate Professor, Department of Physics, Loyola College, Chennai – 600 034
12.00 – 1.00 P.M	ATR Technique – A Fortune To FTIR Spectroscopy For Materials Characterization **Dr. S. Gunasekaran** **Dean, Research & Development** St. Peter's Institute of Higher Education and Research, St. Peter's University, Avadi, Chennai – 600 054.
1.00 P.M – 2.00 P.M	**Lunch Break**
2.00 P.M – 2.45 P.M	Improvement in crystallinity of unidirectional method grown nonlinear optical (NLO) and ferroelectric single crystals for Second Harmonic Generation and Infrared (IR) Detector Applications **Dr. Muthu Senthil Pandian** Research Scientists, SSN Research Centre, SSN College of Engineering, Chennai-603 110, Tamilnadu
2.45 P.M -3.30 P.M	Anisotropic growth of silver nanostructures from silver spheres and Cu@Ag nanoparticles for enhanced nonlinear optical applications **Dr. M. Jose,** Assistant Professor Department of Physics, Sacred Heart College (Autonomous), Tirupattur, Tamilnadu, India
3.30 P.M -3.45 P.M	**Tea Break**
3.45 P.M -5.15 P.M	**POSTER/ORAL Presentation -1**

PG & Research Department of Physics,
Government Arts College, Tiruvannamalai

National Conference on
PREPARATION AND CHARACTERIZATION OF CRYSTALLINE MATERIALS (NCPCCM '16)

Program Schedule

Friday, 5 August 2016	
Time	**Program**
9.30 A.M – 10.15 A.M	Role Of GaAs Nano-Electronic Materials And Devices Fabrication Technologies In Select Space And Defence Applications-A Bird's Eye View **Dr. V.N.Mani** Scientist, Centre for Materials for Electronics Technology, Hyderabad 500 051
10.15 A.M – 11.00 A.M	Growth And Characterisation Of Pure And Copper Dopped Lithium Sulphate Nlo Single Crystals **Dr. M. Selvapandiyan** Associate Professor, Department of Physics, Periyar University PG Extension Centre, Dharmapuri, India-636 705.
11.00 A.M -11.15 A.M	**Tea Break**
11.15 A.M - 12.00 Noon	Pump-probe thermal lens near-infrared spectroscopy and Z-Scan study of (Tris) Thiourea Cadmium Sulphate **Dr. R. Rajasekaran** Former Professor & Principal,Government Arts and Science College, Tiruvannamalai, Tamil Nadu, India.606 603
12.00 Noon – 1.00 P.M	Bimetallic Thiocyanate Complex Crystals for Optoelectronic Devices **Dr. Ginson P. Joseph** Assistant Professor, Department of Physics, St. Thomas College, Pala, Kerala
1.00 P.M – 2.00 P.M	**Lunch Break**
2.00 P.M – 3.00 P.M	Development of nano hybrid structures for DSSC and QDSSC applications **Dr. R. Jayavel** Director-Research, Anna Univeristy, Chennai-25 Centre for Nanoscience and Technology, Anna University, Chennai-25
3.00 P.M -3.15 P.M	**Tea Break**
3.15 P.M - 4.15 P.M	**ORAL / POSTER Presentation -2**
4.15 P.M -5.00 P.M	**Valedictory Function**

PG & Research Department of Physics
Government Arts College (Grade 1)

(NAAC Accredited ' B ' Grade College)

Tiruvannamalai-606 603.

In association with

Sponsored by

Cordially invites you for the National Conference on

PREPARATION AND CHARACTERIZATION OF CRYSTALLINE MATERIALS (NCPCCM '16)

04th, 05th August 2016

Registration:
8.30 am - 9.30 am

Inaugural Function

04.08.2016
Thursday
9.30 am - 10.30 am

Invocation

Lighting of Kuthuvilakku

Welcome Address	:	Prof. **R. Arunchunai Annadurai** Head, Department of Physics
Focal Theme of the Conference	:	Dr. **S.M. Ravi Kumar** Convener
Presidential Address	:	Prof. **K. Kalidasan** Principal (i/c)
Inaugural Address	:	Dr. **P. Sagayaraj** Head, Department of Physics, Loyola College Chennai.
Key-note Address	:	Dr.**S.Gunasekaran**, TANSA Awardee Dean, Research & Development, St.Peter's University, Chennai.
Vote of Thanks	:	Dr.**M.Balakrishnan** Associate Professor

VALEDICTORY FUNCTION

05.08.2016
Friday
4.15 pm - 5.15 pm

Welcome Address	:	Dr. **S.Vetrivel**, Assistant.Professor
Presidential Address	:	Prof. **K. Kalidasan**, Principal (i/c)
Overview of the Conference	:	Prof. **R. Arunchunai Annadurai** Head, Department of Physics
Valedictory Address	:	Dr. **R. Jayavel** Director - Research, Anna University, Chennai.

Feed back & Distribution of Certificates

Vote of Thanks	:	Dr. **S.M. Ravi Kumar** Convener

Invited Talks

Development of Morphology engineered DAST derivatives of DSCHS, DASC and DAAS crystals for Terahertz applications

Dr. P. Sagayaraj

Head & Associate Professor, Department of Physics, Loyola College, Chennai - 34
psagayaraj@hotmail.com

Terahertz (THz) waves are located between microwaves and infrared light, which contain molecular information such as phonon modes of crystals and combined modes of low frequency vibrations with rotation and tunneling in fluids. THz technology offers diverse applications such as wireless communications, inspection of drugs, detection of explosives and metals, analysis of DNA, gas sensing, imaging and spectroscopy. Organic non-centrosymmetric, nonlinear optical (NLO) crystals are regarded as highly efficient THz emitters due to their very large NLO properties when compared to semiconductors and inorganic materials. In this regard, an organic crystal DAST has attracted much attention due to its very high NLO coefficients and its low dielectric constant making it highly suitable for THz generation. It offers vast design possibilities to tailor the linear and nonlinear properties, and owing to the almost completely electronic origin of the nonlinearity, they are well suited for future high speed devices. Though DAST is considered as one of the best THz emitters, its development is limited by its crystal growth characteristics. DAST has a high tendency to form multi-nucleation leading to poly-crystallization and twinning which at the same time reduces the quality and size of the single crystals. In this context, a number of stilbazolium derivatives with different types of counter anions have been synthesized and investigated to understand the influence of counter anions on the growth, NLO and THz properties. In this presentation, along with DAST, stilbazolium derivatives such as4-N,N-dimethylamino-4-N'- methylstilbazolium 3-carboxy-4-hydroxy benzenesulfonate(DSCHS),4-N,N-dimethylamino-4-N'-methylstilbazolium 4-aminotoluene-3-sulfonate (DAAS),4-N,N-dimethylamino-4-N'- methylstilbazolium p-styrenesulfonate(DSSS), 4-N,N-dimethylamino-4-N'-methylstilbazolium p-methoxybenzenesulfonate (DSMOS), 4-N,N-dimethylamino-4-N'-methylstilbazolium p-chlorobenzenesulfonate (DASC) , 4-N,N-dimethylamino-4-N'-methylstilbazolium m-nitrobenzenesulfonate (DSMNS) are discussed from the view point to improve the growth conditions of these potentially useful materials. The advantages of counter ion approach and slope nucleation technique will be highlighted based on the hands on experience of the THz crystals developed by our research group.The present investigation provides the growth aspects of the DAST- like crystals and their morphology control by varying the supersaturation. The improvement in the size and the ability to control the shape of the crystal assumes much significance as the materialsare environmentally more stable than DAST and at the same time equally efficient.

IR TECHNIQUE – A FORTUNE TO FTIR SPECTROSCOPY FOR MATERIALS CHARACTERIZATION

Dr. S. Gunasekaran, Ph.D., D.Sc.
TANSA Awardee
Dean, Research & Development
St. Peter's Institute of Higher Education and Research,
St. Peter's University, Avadi, Chennai – 600 054.
Founder President, Indian Spectrophysics Association
Former Head, Department of Physics, Pachaiyappa's College, Chennai – 600 030,
Former Registrar, Periyar University, Salem.
E-mail : deanresearchspu@gmail.com
Website: www.ispa.wiki

Materials are the main source for revolutions, one such revolution is made in the infrared spectroscopy is FTIR – ATR technique. The vital role in characterizing materials is played by matrix materials which are transparent to infrared radiation.

Mid-infrared spectroscopy is an extremely reliable and well recognized finger printing method. Many materials can be characterized, identified and also quantified. It is an analytical technique to obtain spectra from a very wide range of solids, liquids and gases. However to good quality of spectrum in the transmission, sample preparation is rectified for traditional infrared spectrometers. Where the sample is in a liquid or solid form, the intensity depends more on the thickness or concentration of the sample. The technique of Attenuated Total Reflectance has made revolutions in the analysis of solid and liquid samples because it combats the most challenging aspects of infrared analysis.

The two most common forms of sample preparation for solids both involve grinding the material to a fine powder and dispersing it in a matrix. The ground material can be dispersed in a liquid to form a mull. The most commonly used liquid is mineral oil (nujol). Potassium bromide (KBr) is probably the most widely used matrix material. Between 1 and 3 mg of ground material needs to be mixed thoroughly with about 350 mg of ground KBr. The mixture is now transferred to a die that has a barrel diameter of 13 mm. This is then placed in a suitable press and pressed at around 12,000 psi for one to two minutes. Re-crystallization of the KBr results in a clear glassy disk about 1 mm thick. This disk is now ready to be analyzed by transmission.

Liquids are traditionally analyzed as thin films in cells, a cell consists of two IR transparent windows. A Teflon spacer is generally used to produce a film of the desired thickness or path length. A constant path length is highly desirable when performing quantitative analyses. Overall, sample preparation is easier for liquid transmission studies when compared to solid transmission sampling but both suffer from inevitable reproducibility issues given the complexity of the sample preparation methods. In addition, preparation can be very messy and time consuming and is further complicated by difficulties in getting sample to matrix ratios correct and homogenous throughout the sample. The materials involved are fragile and hydroscopic and the quality of measurements can be adversely affected if handled or stored incorrectly. The technique of Attenuated Total Reflectance addresses these issues.

An attenuated total reflection accessory operates by measuring the changes that occur in a totally internally reflected infrared beam when the beam comes into contact with a sample. An infrared beam is directed onto an optically dense crystal with a high refractive index at certain angle. This internal reflectance creates an evanescent wave that extends beyond the surface of the crystal into the sample held in contact with the crystal. It can be easier to think of this evanescent wave as a bubble of infrared that sits on the surface of the crystal. This evanescent wave protrudes only a few microns (0.5 µ - 5 µ) beyond the crystal surface and into the sample. Consequently, there must be good contact between the sample and the crystal surface. In regions of the infrared spectrum where the sample absorbs energy, the evanescent wave will be attenuated or altered. The attenuated energy from each evanescent wave is passed back to the IR beam, which then exits the opposite end of the crystal and is passed to the detector in the IR spectrometer. The system then generates an infrared spectrum.

For the technique to be successful, the following two requirements must be met:

The sample must be in direct contact with the ATR crystal, because the evanescent wave or bubble only extends beyond the crystal 0.5 μ - 5 μ. The refractive index of the crystal must be significantly greater than that of the sample or else internal reflectance will not occur – the light will be transmitted rather than internally reflected in the crystal. Typically, ATR crystals have refractive index values between 2.38 and 4.01 at 2000 cm-1. It is safe to assume that the majority of solids and liquids have much lower refractive indices.

When measuring solids by ATR, it is essential to ensure good optical contact between the sample and the crystal. The accessories have devices that clamp the sample to the crystal surface and apply pressure. This works well with elastomers, other deformable materials and also with fine powders, but many solids give very weak spectra because the contact is confined to small areas. The effects of poor contact are greatest at shorter wavelengths where the depth of penetration is lowest. The issue of solid sample/crystal contact has been overcome to a great extent by the introduction of ATR accessories with very small crystals, typically about 2 mm across. The most frequently used small crystal ATR material is diamond because it has the best durability and chemical inertness. These small area ATR crystal top-plates generally provide only a single reflection but this is sufficient, given the very low noise levels of modern FT-IR spectrometers. Much higher pressure with limited force can now be generated onto these small areas. A much smaller area of contact is now required in comparison to the HATR units. As a result, spectra can be obtained from a wide variety of solid materials including minerals.

Diamond is by far the best ATR crystal material because of its robustness and durability. The original purchase cost is obviously higher than that of other crystal materials available, but over the instrument's lifetime replacement costs should be minimal. The same cannot be said of Zinc Selenide or Germanium, both of which can scratch and break with improper use. As with all FT-IR measurements, an infrared background is collected, in this case, from the clean ATR crystal.

The crystals are usually cleaned by using a solvent soaked piece of tissue. Typically water, methanol or isopropanol are used to clean ATR crystals. The ATR crystal must be checked for contamination and carry over before sample presentation, this is true for all liquids and solids.

After the crystal has been cleaned and an infrared background has been collected, the liquid is simply poured onto the crystal. The whole crystal must be covered if performing a quantitative or qualitative analysis. The crystal is recessed into the metal plate to retain the sample. Pastes and other semi-solid samples are readily measured by spreading them on the crystal. Horizontal ATR units are often used for quantitative work in preference to transmission cells because they are easier to clean and maintain.

Solids are generally best analyzed on the single reflection ATR accessories; diamond being the preferred choice for most applications because of its robustness and durability. After the crystal area has been cleaned and the background collected, the solid material is placed onto the small crystal area. Experience has shown that ideal results from powder samples have been achieved by placing just enough samples to cover the crystal area. The sample height should not be more than a few millimeters. Once the solid has been placed on the crystal area, the pressure arm should be positioned over the crystal/sample area. When using the Spectrum 100 Series' Universal ATR accessory, the pressure arm locks into a precise position above the diamond crystal. Force is applied to the sample, pushing it onto the diamond surface.

ATR is an IR sampling technique that provides excellent quality data in conjunction with the best possible reproducibility of any IR sampling technique. It has revolutionized IR solid and liquid sampling through:

- Faster sampling
- Improving sample-to-sample reproducibility
- Minimizing user to user spectral variation

Most importantly, the improved spectral acquisition and reproducibility associated with this technique leads to better quality database building for more precise material verification and identification. ATR is clearly an extremely robust and reliable technique for quantitative studies involving liquids.

Improvement in crystallinity of unidirectional method grown Nonlinear optical (nlo) and ferroelectric single crystals for Second harmonic generation and infrared (ir) detector applications

Muthu Senthil Pandian*, P. Ramasamy

SSN Research Centre, SSN College of Engineering, Chennai-603 110, Tamilnadu
Email: senthilpandianm@ssn.edu.in

Gravity driven concentration gradient is used in the uniaxially solution-crystallization method of Sankaranarayanan-Ramasamy (SR). TGS, GPI, KAP, SSDH, DGZCD, DGBCM, benzophenone and many more crystals have been successfully grown by SR method. Longest benzophenone crystal having dimension of 1350 mm length and 55 mm diameter was grown for the first time in solution growth by SR method. Starting with a thin plate as seed a large size crystal can be grown. Facets can be generated after cylindrical growth which may have its own added advantage in device making effort. Crystals with different crystallographic faces can be grown from conventional method and for practical applications where the specimen should have more size along a particular direction, therefore after the studies, the conventional method grown crystals with unique properties are collected and the chosen seeds are mounted in the SR method set up to get very high quality large size single crystals with minimum duration. Using slotted ampoule it was possible to avoid the accumulation of the segregated impurities while using not so very pure crystal ingredients. The experimental parameters involved in the present study were investigated in detail and a constant growth rate was achieved by compensating the loss of growth units in the solution. Using conventional and SR methods crystals have been grown and they were subjected to various studies like HRXRD, laser damage threshold, chemical etching, Vickers microhardness, birefringence, UV-Vis NIR, dielectrics and piezoelectrics. The SR method grown crystals show excellent optical, mechanical, dielectric and piezoelectric behavior and higher laser damage threshold capability compared to the conventional method grown crystals. HRXRD and etching studies showed that the quality of the SR method grown crystal is better than conventional method grown crystal. Similar enhanced performance was discovered in all the crystals studied. 100% solute-crystal conversion efficiency of SR method is an added advantage. We have performed real time and in-situ optical imaging of concentration and convection fields during unidirectional growth of benzophenone crystal. The shadowgraph technique is used to visualize convection, to quantify the thickness of the solutal boundary layer and the crystal growth rate. The Mach-Zehnder interferometry is used to quantify the gravity driven concentration profiles during growth. Special growth apparatus was designed and fabricated for performing the imaging experiments.

Anisotropic growth of silver nanostructures from silver spheres and Cu@Ag nanoparticles for enhanced nonlinear optical applications

A. SakthiSabariMoorthi and M. Jose*

Department of Physics, Sacred Heart College (Autonomous), Tirupattur, Tamilnadu, India

*Corresponding author E-mail id: mjosh1231@gmail.com, jose@shctpt.edu

A well-designed two-step solution-based method has been proposed to switch isotropic silver nanospheres to anisotropic nanoprisms using sodium carboxy methyl cellulose as surfactant. This method has several clear advantages including simplicity and high stability. Silver prisms with a nanometer scale diameter could be judiciously prepared when the precursor concentration was slightly changed. The obtained samples have been characterized by X-ray diffraction, UV–Vis absorption spectroscopy, scanning electron microscopy, and transmission electron microscopy. The experiments show that the concentration of $AgNO_3$, is an important factor for controlling the morphology of the products.

We also prepared core-shell structured Cu@Ag nanoparticles by a facile redox-transmetalation process at room temperature. The SPR band at 405 nm is indicative of the formation of Cu@Ag nanoparticles. The powder X-ray diffraction and energy dispersive X-ray analyses were carried out to elucidate the structure and chemical composition respectively. The morphological investigations made by electron microscopes revealed that the particles are spherical in shape with core-shell structures having size of about 50 nm. The X-ray photoelectron spectroscopy was performed to elucidate surface state composition of the core-shell structured nanoparticles based on the binding energies and confirmed the formation of Cu@Ag core-shell nanoparticles. The enhanced non-linear optical response of the Cu@Ag core-shell nanoparticles was demonstrated by z-scan experiment using He-Ne laser.

ROLE OF GaAs NANO-ELECTRONIC MATERIALS AND DEVICES FABRICATION TECHNOLOGIES IN SELECT SPACE AND DEFENCE APPLICATIONS-A BIRD's EYE VIEW

V. N. Mani
Centre for Materials for Electronics Technology,
Department of Electronics & Information Technology, Govt. of India,
Cherlapalli, Hyderabad 500 051, India
E-mail: vnmanicrystal272001@gmail.com

Solid State Electronics has become the key technology of our time. Whatever the major field of social activity or world industry is selected, it will be realized that electronics is playing an increasingly dominant role in it. The invention of the transistor and the laser has provided the starting blocks for incredible developments in technology and application or solid-state electronics. So impressive it was that the last two decades of technological development in the field are often quoted as unique in the whole history of human technological achievements. The long lasting period of development in micro-optoelectronics has produced a wide range of distinct high purity electronic materials, single crystals, epitaxial structures and devices where Silicon and III-V binary, ternary and quaternary compounds are of pivotal importance. Among the process technologies, epitaxial growth represents a building block upon which many device structures have been developed. Epitaxial layers have been used for the fabrication of integrated circuits and discrete devices. Much progress in micro-optoelectronics technology during the last decade has been based on epitaxial technologies in the growth of multilayered structures for device applications. The success of advanced multi-layered structures and devices in the laboratory and in production depends heavily on the advanced epitaxial techniques used to grow them. The various forms of epitaxial methods appear to be leading candidates for the fabrication of these devices.

In this overview talk, our decade long efforts in developing ultra hig pure (7N) gallium, indium and recent results on germanium, GaN, which are required for epitaxial opto and nano- electronics and optoelectronics will be highlighted. The talk will also cover technological issues namely multi-pass zone-refining, directional solidification and associated chemical engineering, instrument development aspects, preparation of bulk crystals and substrates including VLSI principles and practices. The class clean and green processing scheme(s) for sample homogenization, preparation, processing analysis and packaging, the usage of the class clean room (1000), clean benches (100) environment and characterization issues will be dealt with.

References

1. K. Ghosh, V. N. Mani and S.Dhar Jl. Appl. Phys Vol.13, 133(2009)
2. V. N. Mani et al Materials Science Research India Vol. 6, No.1 (2008)
3. K. Ghosh, V. N. Mani, S.T. Ali and MRP Reddy Metals Materials and Processes 20(2008), 153
4. K. Ghosh, V. N. Mani and S.Dhar Transaction of the Indian Institute of Metals (TIIM) 61 (2008) 1
5. V. N. Mani et al, Metals Materials and Processes Vol.18 (2), 2006, pp 107-118
6. V. N. Mani et al Physics of Semiconductor Devices Vol.1, pp.203-205 (2004) Eds. K.N. Bhat etal, Narosa Publishers, New Delhi
7. V.N.Mani et al , Physics of Semiconductor Devices Vol.2, pp.1142-1146 (2001) Eds. Vikram Kumar etal, Allied Publishers, New Delhi
8. V.N.Mani et al.; Jl. Cryst.Growth (Netherlands) 99(1990) 333-340
9 . V.N.Mani et al.; Jl. Appl. Phys.(USA) 69,1399 (1991).
10. V.N.Mani, Bull. Mater. Sci. (India), Vol. 17, pp. 469-478, 1994.

GROWTH AND CHARACTERISATION OF PURE AND COPPER DOPPED LITHIUM SULPHATE NLO SINGLE CRYSTALS

M. Selvapandiyan

Department of Physics, Periyar University PG Extension Centre, Dharmapuri, India-636 705

***Email:** mselvapandiyan@rediffmail.com

Crystals are the pillars of modern technology. Without crystals, there would be no electronic industry, no photonic industry, and no fibre – optic communications. Nonlinear optical materials are reputed candidates for device fabrication due to good mechanical strength, better nonlinearity, high thermal stability and large laser damage threshold. The large second order non linear optical materials find in various fields of applications such as laser technology, laser telecommunications, optical computing, Optical data storage devices, frequency conversion, modulation, optical memory storage and optical switching. In this paper describes that the growth and characterisations of pure and copper doped single crystals. The energy band gap of the pure and copper doped Lithium sulphate crystals are found to be 3.24 eV and 3.25 eV. The observed results confirmed that the grown materials belong to the categories of typical insulating materials. The presence of functional group on the modes of vibration of the grown pure and copper doped Li_2SO_4 single crystal were analysed by using Perkin Elmer spectrum two FTIR / ATR spectrometer with the frequency range between 4000 cm^{-1} and 450 cm^{-1}. The results of the Vickers hardness studies suggests that the grown materials are belongs to soft in nature and working in the load range between 1 gm and 100 gm. The dielectric constant of material decreases with increasing of frequency. The dielectric loss of material also decreases with increasing of frequency. The grown materials are well suited to apply the optoelectroinic device application because the dielectric loss of material very low at high frequencies. The sharp endothermic peaks of Differential Thermal Analysis curves are 145˚C and 167˚C which represents the melting point of the grown pure and copper doped Li_2SO_4 crystals.

Bimetallic Thiocyanate Complex Crystals for Optoelectronic Devices

Ginson P. Joseph
Assistant Professor, Department of Physics, St. Thomas College, Pala, Kerala
Email: ginsonpj@gmail.com

Nonlinear optics (NLO) has emerged as one of the most attractive fields of current research in view of its vital applications in areas like optical modulation, optical switching, optical logic, frequency shifting and optical data storage for developing technologies in telecommunications and signal processing. Materials with large SONLO properties, short transparency cut off wavelengths and stable physicochemical performance are needed to realize many of the above applications. Bimetallic thiocyanates of type $AB(SCN)_4$ with A=Zn, Co, Ni, Mn, Cd and B=Cd, Hg are one among those which satisfy the above mentioned features. Their crystal structure consists of two kinds of slightly flattened tetrahedral: AN_4 and BS_4. The most striking features are the –N=C=S– bridges, which connect the center atoms of the infinite three dimensional–A–N=C=S–B– networks. The metal ligand bonding in organometallics gives rise to the large macroscopic nonlinearities and excellent physicochemical stabilities due to the transfer of electron density between the metal atoms and the conjugated ligand systems. The double ligand model theory facilitates the researchers to develop this new class of materials. These materials have the potential for combining the high optical nonlinearity and chemical flexibility of organics with physical ruggedness and excellent transmittance of inorganic. Like organic materials, organo-metallic compounds also offer the advantage of architectural flexibility and ease of fabrication and tailoring. The main focus of this talk is on the synthesis, growth, electrical, thermal and non-linear optical properties of thiocyanate complex and its lewis base adduct crystals.

Pump-probe thermal lens near-infrared spectroscopy and Z-Scan study of (Tris) Thiourea Cadmium Sulphate

Rajasekaran.R* & M.Porchelvi
*E-Mail:rrsekar57@yahoo.com

Former Professor & Principal,Government Arts and Science College, Tiruvannamalai, Tamil Nadu, India.606 603
Research Scholer Dept. of Physics,Goverentment Arts College,Tiruvannamalai

Abstract

A novel use of the pump-probe thermal lens spectroscopy and Z-Scan techniques for the measurement of the small absorption coefficient in a semi organic-nonlinear optical crystal (Tris) Thiourea Cadmium Sulphate.The absorption spectrum and the absolute values of the absorption of the crystal in the near infrared region(700 nm-980 nm).A maximum absorption coefficient of ~ 0.04 cm-1 is reported.

Development of nano hybrid structures for DSSC and QDSSC applications

R. Jayavel*

Centre for Nanoscience and Technology, Anna University, Chennai 600-025, India.

* rjvel@annauniv.edu

Hybrid (organic/inorganic) nanostructures continue to attract research interest owing to their potential applications in electronic and optoelectronic devices. Recently, nanostructures of inorganic semiconducting materials are looked upon for energy conversion aspects along with their organic counterparts. Fabrication of a new class of hybrid organic/inorganic material systems has envisaged a new dimension in the field of Dye sensitized solar cells (DSSC). The study of such systems could be of great help in improving the device performance and lowering their fabrication cost considerably. In this regard, a systematic approach has been made on the development of PPy/TiO_2 and PPy/ZnCoO hybrid layers. Undoped and Co doped ZnO nanocrystallite were prepared through a simple two-step chemical approach. The hybrid layers have been fabricated at room temperature through electro-polymerization reactions (assisted by UV radiation). FT-IR and Raman spectroscopy have been used to ensure the formation of polypyrrole deposits. The flat band potential for the hybrid systems assimilated from the Mott Schottky plots was observed to shift towards the negative direction, presumably due to the higher concentration of the polymer composites, which gives rise to a more negative potential. Preliminary photovoltaic studies were carried out under AM1.5, 1 sun condition for these photoelctrodes, which showed a photovoltage of 0.45 V. One of the critical issues in dye sensitized solar cell structure is the poor stability of dye molecules. Recently, Quantum Dots have been considered as a potential substitute for dye molecules with improved stability. Fabrication of QDSSC structures and their device performance will be discussed in detail.

Spectroscopic analysis on thiourea complex of nonlinear optical crystals

S. Selvakumar
Assistant Professor
Government Arts College for Men (Autonomous)
Nandanam, chennai – 600 035

Spectroscopic investigations in different regions of the electromagnetic spectrum provide information regarding translational, rotational, vibrational and electronic energy levels of molecules. Vibrational spectroscopy deals with the interaction of electromagnetic radiation with molecular vibrations and this is one of the most useful spectroscopic tools for basic research. Information regarding molecular structure, stereochemistry of complex molecules, hydrogen bonding and inter and intra molecular processes can be obtained from the vibrational spectra. Fourier Transform Infrared (FTIR) is one of the most exciting scientific investigations which can be attempted to understand the basic units of matter and how they are held together.

Thiourea is potentially capable of forming co-ordinate bonds through both sulphur and nitrogen. Both these possibilities will be reflected in the FT-IR spectra of the complexes. Bonding through sulphur, the C-S stretching frequency should decrease and C-N should increase. If, on the contrary, a nitrogen – metal bond is formed just the opposite effect is to be expected. Furthermore, the N-H frequency should decrease if the metal is coordinated through nitrogen, while remaining substantially unaffected if the bonding is through sulphur. Among the semi-organic materials, complexes of thiourea are interesting because of their large nonlinear property, lower UV cut off, wide transparency and good thermal stability. Thiourea as a ligand possesses a large dipole moment and has the ability to form extensive network of hydrogen bonds. The well known thiourea complex which are proved to have good SHG efficiency are bis (thiourea) cadmium chloride (BTCC), bis(thiourea) zinc chloride (BTZC), bis(thiourea) cadmium acetate (BTCA), bis(thiourea) cadmium formate (BTCF). The FTIR results of some of the thiourea complex will be discussed in detail.

CONTENTS

Core@Shell for Quantum Dots for Q- LED Applications

G. Ramalingam[*1], P. Kathirgamanathan[2], K.Gurunathan[1], V. Veeraputhiran[3]

[1] *Department of Nanoscience and Technology, Science Campus, Alagappa University, Karaikudi-Tamil Nadu. India-630 003.*

[2]*Department of Electronic Materials Engineering, Brunel University, Uxbridge, UB8 3PH, London.*

[3]*Department of Chemistry, M.D.T Hindu College, Tirunelveli*

ABSTRACT

In the present work, CdSe/ZnS core-shell quantum dots (QDs) were synthesized via chemical route using bio-conjugated organic amino acid (L-Cysteine). The high intensity XRD result (002) plane the right panel of CdSe/ZnS QDs is identical with the *c*-axis of the wurtzite structure. The diameter of the resulting QDs was about 3 nm with uniform size distribution. The synthesized QDs exhibited an absorption and emission peak at 515 and 525 nm respectively, at room temperature. QDs with emission in the spectral range of 516-535 nm are special for their application in green LEDs and white-light generation.

Keywords: CdSe/ZnS, Core-shell quantum dots, Luminescence, Optical properties, green and white-light LEDs.

1. INTRODUCTION

Core-shell quantum dots (QDs) have attracted considerable attention as potential candidates in various applications including LED displays, photoluminescent, chemiluminescent and biological labels [1-3]. The CdSe/ZnS core- shells QDs with emission in the spectral range of 516-535 nm are used for application in LEDs [4]. The various semiconductor QDs of II -VI group metal chalcogenides such as ZnS, CdSe and CdTe have been studied by researchers because of their quantum confinement effects which include size dependent photoemission properties. The photoluminescence (PL) spectra of these QDs can be turned over a wide range of the electromagnetic spectrum with control in size and composition. Studies are being carried out on the effect of size on their physico-chemical properties. As their size decreases to their Bohr radius (usually around a few nanometers), all the electronic properties changes. QDs have many advantages compared to organic dyes, such as high PL intensity with narrow bandwidth and high photo-stability against photo bleaching [5]. Due to these properties QDs have potential application in biomedical tags and light harvesting devices.

Many synthesis routes have been developed during the past decades including organometallic precursor route , non-organometallic precursor route, microwave irradiation route , solvothermal route and sonochemical route All these methods include the hot co-ordination solvent method using tri-n-octylphosphine oxide (TOPO) and trioctylphosphine (TOP) which is identified as a prominent method to synthesize semiconductor QDs. However, these methods require higher temperature and toxic materials. Therefore, we have succeeded in developing an environmental friendlier method to synthesis CdSe/ZnS QDs for the first time unlike previous researchers. The as-prepared QDs were characterized by structural (XRD), morphological (SEM/EDAX, TEM) and optical properties (UV & PL) studies.

2. EXPERIMENTAL PROCEDURE

2.1 Synthesis

The synthesis procedure of CdSe is already described by our group [6]. The as prepared ZnS

and CdSe are mixed thoroughly with 25 ml L-Cysteine. After stirring for 2 hrs, the mixture was transferred into a Teflon lined stainless autoclave of 200 ml capacity (with 75 % filling). The autoclave was sealed tightly and heat treated at 200 °C in an electrical oven for about 6 hrs and then allowed to cool down to room temperature naturally. Finally, a deep dark red powder was collected, after centrifugation and it was repeatedly washed with water and ethanol to remove unwanted species present in the product. Finally the sample was dried at 120°C for 3 hrs.

3. RESULTS AND DISCUSSION

3.1 Powder X-ray Diffraction and EDAX Analysis

Powder XRD patterns of monodispersive CdSe/ZnS QDs are shown in Figure 1. The evolution of the powder X-ray diffraction patterns during the growth of the shells around spherical ZnS nanoparticles shows that the hexagonal (wurtzite) phase of CdSe. The higher intensity and the smaller width (002) of the reflection (Fig.1) show that the right panel of CdSe/ZnS QDs is identical with the *c*-axis of the wurtzite structure. All the observed peaks can be indexed to the wurtzite structure, with a lattice constant slightly compressed from that of bulk CdSe due to the CdSe/ZnS coating, which were well consistent with the characterized peaks of wurtzite hexagonal CdSe/ZnS core-shell (JCPDS card No:77-2307, 89-7385).

3.2. SEM & TEM Analysis

The size and shape of the particles of CdSe/ZnS core-shell QDs was investigated by TEM. The Figures shows the XRD, molecular structure and TEM image of hydrothermally grown CdSe/ZnS core-shell QDs. It is interesting to note that the presence of highly monodispersed and absolute spherical QDs. Further, a close examination of last figure below suggests that the less agglomeration of QDs. As seen in the TEM image, honeycomb of QDs size is ranging from 2-4 nm. We surveyed approximately 150 QDs and their histograms confirm the average diameter is about 3 nm and the particles have a narrow size distribution.

3.4 Optical Properties Studies

From the Figure below shows, a sharp absorption features (λ_{abs} ~ 515 nm) suggest monodispersity of CdSe/ZnS nanoparticles and the narrow PL emission λ_{emi} ~ 525 nm) indicates near band edge emission. The fact that the PL emission maximum lies close to its absorption-onset indicates that the PL emission arises as a result of the direct recombination between LUMO and HOMO charge carriers [7-8].

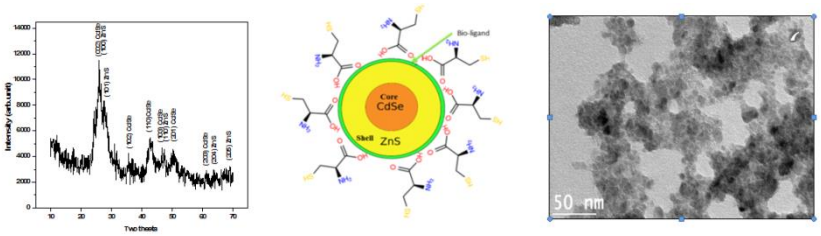

3.4 Optical Properties Studies

From the Figure below shows, a sharp absorption features (λ_{abs} ~ 515 nm) suggest monodispersity of CdSe/ZnS nanoparticles and the narrow PL emission (λ_{emi} ~ 525 nm) indicates near band edge

emission. The fact that the PL emission maximum lies close to its absorption-onset indicates that the PL emission arises as a result of the direct recombination between LUMO and HOMO charge carriers [7-8]. QDs with emission in the spectral range from 516 to 538 nm are of special interest for the preparation of QDs based green and white LEDs. So, we suggest that CdSe/ZnS core shell QDs prepared in the present study is promising candidates [9-10] for light harvesting applicationsaround R=3 nm in the present work. Thus, the decreased ($R << a_B$) regime indicate that the strong-quantum confinement effect.

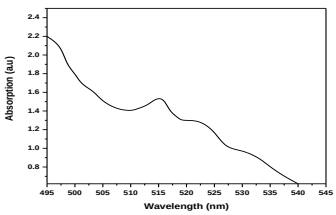

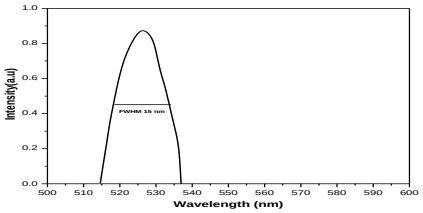

4. CONCLUSIONS

Summarizing, we have developed a novel type synthesis of luminescent semiconductor nanocrystals consisting of CdSe core and ZnS as outer shell. The size of CdSe/ZnS QDs was successfully controlled by environmental friendly solvent. The powder XRD pattern and EDX analysis confirmed the structure, purity and composition of the obtained product. X-ray diffraction analysis confirmed the crystallization of hexagonal CdSe/ZnS QDs. The absorption and emission edge is a clear indication of visible light response of the particles and thus showing the promise for various light harvesting and fluorescence applications. QDs with emission in the spectral range of 516-535 nm are special for their application in green LEDs and white-light generation.

References

1. Jr .Bruchez Marcel, Moronne Mario, Gin Peter, Weiss Shimon, and Alivisatos A. Paul. *Science*, 25 (1998) 2013
2. S. Coe, W-K. Woo, M. Bawendi, Bulovic., Nature. 420 (2002) 800.
3. J. Lee, A. O. Govorov, and N. A. Kotov, *Nano Lett*, 5 (2005) 2063-2069
4. M. Protiere and Dr.P.Reiss, small, 3(2007)399.
5. Chan Warren and Nie Shuming, *Science*, 28 (1998) 12016.
6. G. Ramalingam, N. Melikechi., P. Dennis Christy., S. Selvakumar and P. Sagayaraj, J. Cryst. Growth, 311 (2009) 3138
7. Weiling Luan, Hongwei Yang, Ningning Fan and Shan-Tung Tu, Nanoscale Res. Lett, 3(2008)134.
8. S. Sapra, J. Nanda, D. D. Sarma, Abed El-Al F and G. Hodes., Chem. Comm. 21 (2001) 2188.
9. . Peng, Z. A. Peng and Xiaogang Peng, *J. Am. Chem. Soc*, 123 (2001) 183.
10. Y. Kayanuma and H. Nakayama, Phys. Rev. B, 57 (1998) 13099-13112.

Synthesis and Characterization of Lead Sulfide Nanoparticles

L.Kungumadevi*, P.Jeya Kiruba

Department of Physics, Mother Teresa Women's University, Kodaikanal, Tamilnadu-624001.

**E-Mail id:sivarivudevi@gmail.com*

ABSTRACT

PbS nanoparticles were synthesized using wet chemical method. The synthesized product has been characterized by X-ray diffraction (XRD), FE-SEM, energy dispersive X-ray spectroscopy (EDX), Optical,FTIR studies and their results have been discussed in detail.

1. Introduction

Lead sulfide is a good IV-VI group semiconductor, which has attracted considerable attention due to its special small direct band gap (0.41 eV) and large excitonic Bohr radius of 18nm[1,2]. PbS has been widely used in many fields such as Pb2+ ion selective sensor, IR detectors, solar absorber and photography[3-5]. The band gap of PbS can be easily adjusted up to a few electron volts when the size of the particles is reduced. Such a significant widening of the band gap is associated with small effective masses of electrons and holes ($m_e = m_h = 0.09\ m_0$) as well as with a large exciton Bohr radius (20 nm) of PbS [1]. Nanomaterials of PbS have been discovered to have exceptional third-order nonlinear optical property with potential applications in optical devices such as optical switches [2]. A lot of effort has been focused on the synthesis of PbS nanostructures and recently complex PbS structures such as dendritic or flower-like structures have attracted much attention because of their interesting morphologies and potential applications [3-6]. Aqueous phase routes have been employed to obtain PbS microcrystals with a flower-shaped or clover-like structure [4, 5]. Different dentritic PbS nanostructures can be synthesized through a surfactant-assisted hydrothermal process [3].Nano-particles of lead sulfide have been synthesized recently by different chemical method with controlled particle size distribution [6-9]. During wet chemical synthesis of nanoparticles organic stabilizers are normally used to prevent them from aggregation by capping their surface. Moreover, the introduction of stabilizers influences on the chemical properties as well as the physical properties of semiconductor materials. Therefore, the choice of a suitable capping agent, the dynamic of binding, and its concentration becomes the pre-requisite for the particle size regime, stabilization against aggregation and high quantum yield during synthesis of nanoparticles. In this paper, we have prepared PbS nanoparticles by simple method and characterized by different techniques and their results were discussed.

2. Experimental details

Lead acetate trihydrate was dissolved in deionized water and stirred at room temperature. Then PEG was added drop wise to lead acetate solution and the sodium sulfide was dissolved in deionised water. The prepared sodium sulfide solution was added drop wise to lead acetate solution under constant magnetic stirring. The colour of the solution changed to black. The above mixed solution was stirred at 50ºC for 2 hours and the products were separated by centrifugation at 2000rpm. The solution was washed with deionised water, acetone and ethanol to remove the impurities of the sample. After completing washing the sample was dried in hot air oven at 100ºC for 4 hours and collected as the yield. The crystal structure of as synthesized PbS NCs was investigated using X-ray

diffraction model Bruker D8 advance with monochromated Cu, kα radiation (λ=1.541A°). The morphology of the synthesized samples was investigated by using field emission scanning electron microscopy (FESEM, ZEISS). The ultraviolet-visible spectra were recorded at room temperature (UV-ESECDB-205). The FTIR analysis of the sample was recorded in a range from 400cm^{-1} to 4500 cm^{-1}. The formation of PbS crystals were confirmed using EDAX(Bruker).

3. Results and discussion

The XRD pattern of synthesized PbS nanoparticles are shown in figure1. It shows several diffraction peaks at 2θ values of 26.48, 30.575, 43.544,51.444,53.895,63.001,69.322, 71.374 and 79.336 which correspond to the miller index of the reflecting planes for (111), (200),(220),(311),(222),(400),(331),(420) and (422). All the diffraction peaks in the spectra are analogous to the literature pattern of cubic phase powder (JCPDS file no 01-005-0592) of the PbS. This confirms the formation of PbS nanoparticles. The strong and sharp diffraction peaks suggest that the particles are well crystallized. No other impurity peas have been observed from the XRD pattern which confirms the formation of pure PbS nanocrystals. It is observed that all the peaks are very much prominent which implies the high crystallinity of the PbS nanocrystals. The crystallite size was calculated using Debye-Scherrer formula. $D=K\lambda/(\beta \cos \theta)$ Where, λ is the wavelength of X-rays (1.5404Å), β is the full width at half maximum, and θ is the Bragg's diffraction angle obtained from 2θ value corresponds to the maximum intensity peak in XRD pattern.

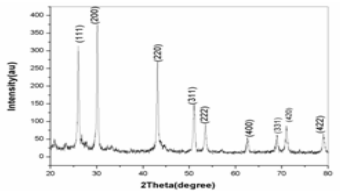

Fig.1.XRD pattern of synthesized PbS

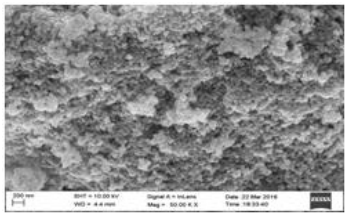

Fig.2 FESEM image of PbS

The average calculated particle size is 24.9nm and they are agglomerated. It clearly indicates the formation of spherical shaped PbS nonaparticles. The formation of PbS nanoparticles was confirmed from EDAX spectrum which is given in Fig.3. The morphology of as synthesized PbS nanoparticles was investigated using field emission scanning electron microscopy (FESEM). The FESEM image of PbS nanoparticles is shown in Fig 2. It shows that the synthesized PbS nanoparticles contain mainly the grains of spherical particles

FTIR was used to study the purity and functional group composition of the PbS nanoparticles. The dried PbS nanoparticles were mixed with KBr to form pollets and then characterized with FTIR. The transmittance peak in the range from 4500-500cm^{-1}corresponds to the OH group of water observed by the sample. Since PbS had no characteristic absorption peaks in the range 4000 – 500 cm^{-1}, the observed peaks at 1113 and 623 cm^{-1} were attributed to the PEG.

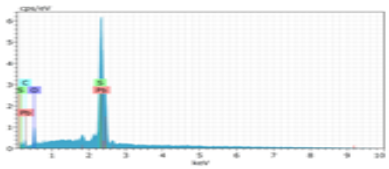

Fig.3.EDAX Spectrum of PbS

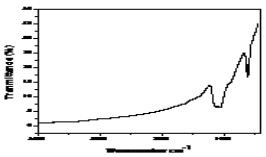

Fig.4. FTIR spectrum of PbS nanoparticles

A fundamental property of semiconductor is the band gap-the energy separation between the filled valence band and the empty conduction band. The room temperature UV-visible spectrum in the absorption mode was measured for PbS nanoparticles and given in Fig.5. The optical band gap of the nanoparticles is calculated from the UV absorption study using the following formula. $E = hc/\lambda$

The samples exhibit a strong absorption at 823 and 880nm. The band gap energies of the samples corresponding to the absorption edge are found to be 1.507 and 1.409 eV which are higher than the bulk value (0.41 eV). It shows that the absorption edge is shifted to blue region which may be due to the quantum size effect.

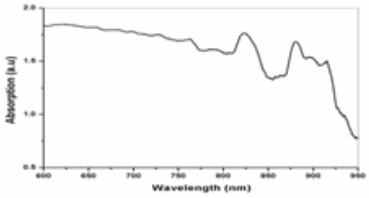

Fig.5. Optical absorption spectrum of PbS

CONCLUSION

PbS nanoparticles are successfully synthesized by wet chemical method. X-ray diffraction pattern indicates the formation of good crystalline cubic structure of PbS nanoparticles. The FESEM image reveals that the PbS nanoparticles have regular spherical shapes. The optical analysis reveals that the spectrum of PbS nanoparticles shows a blue shift in the band gap energy due to small crystallite size.

References

[1] J.L. Machol, F.W. Wise, R.C. Patel, D.B. Tanner, Phys. Rev. B48 (1993) 2819.
[2] S. Zhou, Y. Feng, L. Zhang, J. Mater. Res. 18 (2003) 1188.
[3] H. Hirata, K. Higashiyama, Bull. Chem. Soc. Jpn. 44 (1971) 2420.
[4] P.K. Nair, O. Gomezdava, M.T.S. Nair, Adv. Mater. Opt. Electron. 1 (1992) 139.
[5] T. Ding, J.K. Zhang, S. Long, J.J. Zhu, Microelectron. Eng. 66 (2003) 46.
[6] R. Houbertz, W. Krauss, R. Birringer, V. Hartmann, Nanostruct. Mater. 9 (1997) 339.
[7] S.H. Yu, Y.S. Wu, J. Yang, Z.H. Han, Y. Xie, Y.T. Qian, X.M. Lin, Chem. Mater. 10 (1998) 2309.
[8] J.K. Salem, T. M. Hammad, M. Abu Draaz, R. Hempelmann, J. Mater. Sci.: Mater. Electron. 25 (2014) 2177.
[9] A.L. Alvarez, J. Tito, M.B. Vaello, P. Velasquez,Thin Solid Films 433 (2003) 277.

Syzygium Cumini Leaf Extract As A Green Source To Synthesize of Sno_2 Nanoparticles And Their Characterization

[1]Senthilkumar.S, [1]Siva.E, [1]Rajendran*. A,

[1]PG and Research Department of Physics, Nehru Memorial College(Autonomous), Puthanampatti, Trichirappalli, Tamilnadu, India -621007.

**Corresponding author: neelrajnmc@gmail.com*

ABSTRACT

The present study reveals green synthesis of SnO_2 nanoparticles (NP's) that is non-toxic, novel and eco-friendly using syzygium cumini. This synthesis approach is cost effective, eco-friendly and promising for applications in medical field. The characterization such as XRD, FTIR, FESEM, and Dielectric studies and were analyzed for synthesized SnO_2 NP's.

Keywords: SnO_2 nanoparticles, Green synthesis, *syzygium cumini* leaf extract

INTRODUCTION

Currently there has been a signification increase in the area of nanotechnology in terms of research due to the applications of nanoparticles. The development of green processes for the synthesis of Tin oxide nano particles (SnO_2NPs) is evolving an important branch of Nanotechnology [1]. Biologically synthesized SnO_2NPs have drawn the attend of scientist[2], because of the extensive applications in the development of new technology in the areas of electronics , material science and medicine at the nanoscale [3].The process involved in biosynthesized of Tin oxide nanoparticles have already reported from the leaf extract of Eucalyptus chapmania Lantharana camera, etc. SnO_2 nanoparticles it is usually synthesis from medical applications from cancer, bacteria fungal tolerance towards metal high bonding capacity and intracellular uptakes metals [4]. SnO_2NPs have been widely employed due to their physicochemical properties. In the present study, Tin oxide nanoparticles are synthesized by using the leaf extract of the plant *Syzygium cumini* (also known as Jamun) belongs to Mirthaze family; The plants are used for the regulation of menstrual cycles [5]. In addition the plant is known to possess many pharmaceutical activities. Synthesis of Tin oxide nano particles with the extract of the plant leaf may increase their properties in lesser quantities and can act as a potential application in the field of medicine.

2. MATERIALS AND METHODS

2.1 Biosynthesis of Tin oxide nanoparticles

The collected *Syzygium cumini* plant leaves were surface cleaned with tap water followed by distilled water. A plant leaves, dried at room temperature and powdered Then weighted for 10g, dried powder mixed with 100 ml ethanol and mixture was heated at 90°C , for 4hours .It was filtered by using whatmann filter paper and the filtrate was collected. This leaf extract mixed with 90 ml tin oxide aqueous solution in 250 ml solution. The colour of solution is changed greenish yellow to pale yellow colour. It is the primilary identification at a formation of Tin oxide nanoparticles.

3. RESULTS AND DISCUSSION

3.1 X-ray diffraction pattern (XRD)

Figure 1 shows X-ray diffraction patterns obtained for the SnO_2 nanoparticles synthesized using leaf extract confirmed the formation of Tetragonal structure SnO_2 nanoparticles. The crystal

structure of biosynthesized SnO_2 Nps different temperature 400^{o} C, and 600^{o} C at 2 hours, which shown well defined diffraction peaks at 26.75^{o}, 37,343^{o}, 37.88^{o},51.95^{o},54.50^{o},57.93^{o}, 62.09^{o},64.95^{o},66.8^{o},71.70^{o},and 79.13^{o} can be indexed to (1 1 0),(1 0 1),(2 0 0) ,(2 1 1),(2 2 0), (0 0 2), (3 1 0),(1 1 2), (3 0 1),(3 2 0) and (3 2 1) crystal planes of tetragonal SnO_2 compared JCPDS card no(41-1445).

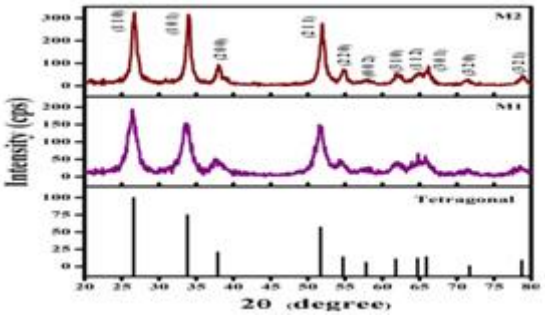

Fig 1. XRD patterns of (400^{0}C, (M1). (600^{0}C) (M2) of biosynthesized SnO_2 Nps

The formation of the biosyntheses of high purity SnO_2 Nps . The diffracted pattern using Debye's Scherer's formula D= (0.9λ)/βcosθ. Sample M1 Crystalline size D=6nm,and lattice parameters a=4.764, c=3.203nm, and lattice strain=0.492 **ε x10$^{-3.}$** The M2 crystalline average size 11 nm, calculated lattice parameters a=4.720, c=3.179 and lattice strain 4.1 nm obtained.

3.3 FESEM analysis:

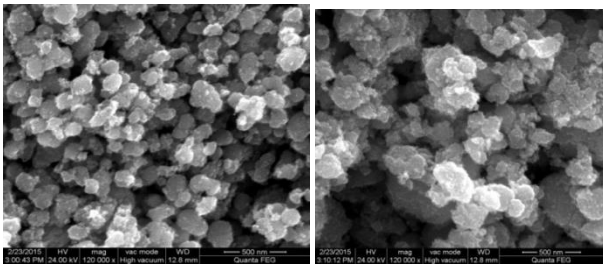

Fig.2.FESEM analysis of biosynthesized SnO_2 Nps

The morphology of biosynthesized SnO_2 Nps was obtained by FESEM as shown figure.2.FESEM images of SnO_2 Nps at different temperature 400^{o} C, 600^{o} C at 2hours. It's formed SnO_2 Nps shows spherical shape structure. The biosynthesized of SnO_2 Nanoparticles particle size analyzed average size 54nm.

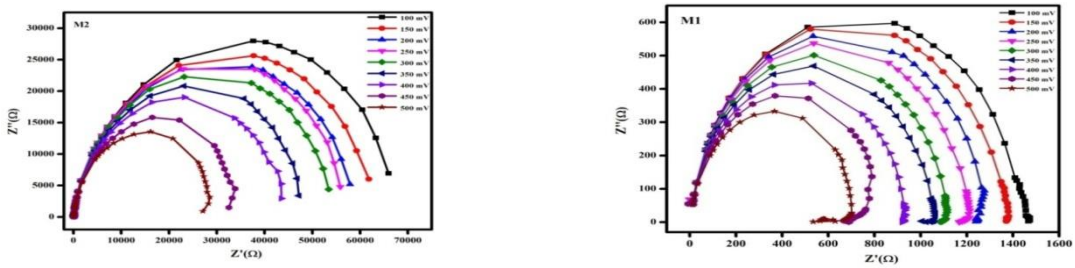

Fig.3. Dielectric – complex impedance analysis of biosynthesized SnO_2 Nps

3.4 Dielectric –– Complex Impedance analysis

The dielectric properties of the SnO_2 nanoparticles studied dielectric -complex impedance analysis as shown figure 3. The impedance is measured at different frequency. The electrical current of SnO_2

NP's found to be frequency dependence which increased linearly with applied frequency and also measure dielectric constant (∑r) for SnO2 nanoparticles at various frequency.

Conclusion

The SnO_2 nanoparticles synthesized successfully with leaf extract by green synthesis method. The physic – chemical properties of synthesized SnO_2 nanoparticles were investigated by XRD , UV-Visible , FT-IR , FESEM, and Dielectric study analysis indicating the properties of synthesized SnO_2 nanoparticles.

References

1. Ghassan Mohammad sulaiman, Wasnaa Hatif Mohammed, Thorria Marzoog, Ahmed Abdul Amir Al-Amir, Abdul Amir H. Abu baker Mohamed. Green synthesis, Antimicrobial and cytotoxity effects of Silver nanoparticles using Eucalypytus chapmania leaves extract Asian Pac J Trop Bio med 2013.
2. Sivakumar. J, Premkumar. C.santhanam. P. and saraswathi. Biosynthesis of silver Nanoparticles using calotropis giantean leaf, African journal of basic applied sciences.
3. Akal M Awwad, Nida M Salem and Amany O Abdeen. Green synthesis of silver nanoparticles using carob leaf extract and its trial antibacterial activity. International journal of Industrial chemistry 2013, Pp 4:29
4. R.Das, M.Saha, S. A. Huaaain and S.S Nath, Silver nanoparticles and their antimicrobial activity on a few bacteria", BioNanoscience, vol. 3, no.1, pp 67-72, 2013.
5. M.K.Rai, S.D.Deshmukh, A.P. Ingle, and "Silver nanoparticles best by callus and leaf extract from salt marsh plant, Sesuvium portulastrum L; colloids and surface B: Biointerfaces, Vol 79, no: 2, pp.448-493, 2010.

Crystal Growth and Charaterization of 8- Hydroxyquinoline

T.Jothi,* K.Venkatesan1 L.Anandraj

[*]PG and Research Department of Physics NKR Arts and Science College, Namakal
[1]PG and Research Department of Physics, SVM College of Arts and Science, Uthangarai.
[2]PG and Research Department of Physics, Sacred Heart College Tirupattur.
E-mail:kvphy6@gmail.com

Abstruct

The single crystals of 8-hydroxyquinoline, a organic material, were grown by the solvent evaporation technique from an ethyl alcohol solution of at ambient temperature. The novel non-linear optical single crystal 8-hydroxyquinoline has been successfully synthesized by Good optical quality single crystals of size were grown in a period of 5 days. A since the morphology found to depend on dielectric crystal, electric susceptibility studies. Powder X-ray diffraction (XRD),UV and Fourier transform infrared transmission (FTIR) have confirmed the formation of the new crystal. The grown crystals were characterized by single-crystal XRD analysis to study the crystal structure. From this analysis we found that the quality of the crystal was quite good. UV–Vis spectrum was recorded to study the optical transparency of the grown crystals and functional group of above crystal was finding by FTIR.

Introduction

Crystalline organic compounds represent a new class of multifunctional group of material with introducing simultaneously optoelectronic and photo refractive properties of a wide range of application. Molecular materials are considered now as a very important alternative for electrodes of a crystalline stricter compounds and electrical active device manufacturing energetic structure, electrical compounds and optical properties are determined by their molecular configuration and particularity applications of the construction. For future application in electronics it will necessary to utilize the compounds with big molecule, less volatile and in very small geometrical configuration to complete with the modern tendency of the miniaturization.

Solid can defined by the way their constituent atoms or ions (or) molecule packed. If the packing of specific material is regular, forming an infinite three domination array exhibiting long-range Oder, it is said to crystallization plays a part in almost every area of science and technology.

To attempt this aim very important the crystal purity and quality. The purity requirements for the organic materials are difficult and problem that as to be solved. Ordinarily, we can characterize a material after its capacity to crystalline good. Transparent crystalline structures and its spectra in the optical wavelength range. But these measurements are not very sensitive to the pressure of the impurities traces that an affect the crystal growth process.

A good knowledge of the fundamental aspects of crystallization is particularly important in the optical and communication industry for number of reasons. Firstly, crystallization is generally carried out on a large scale. So the system must be well understood to ensure a good yield to material. Secondly, to avoid the classic formulation problems associated with pure filtering. It is vitally important that the crystalline product exhibits manufacturing and uniformly from batch-to-batch (i.e.) the particles exhibit similar sizes and morphologies. This crystal has the same structure and a similar degree of perfection.

Molecular structure

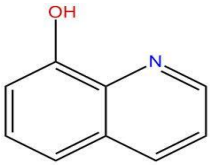

Fig Structure of 8-Hydroxyquinoline

An off white needles crystal derived from quinoline-8-sulfonic acid and commonly used as a chelating agent and also used as liquid bandages.

3.4 Preparation of 8-hydroxyquinoline

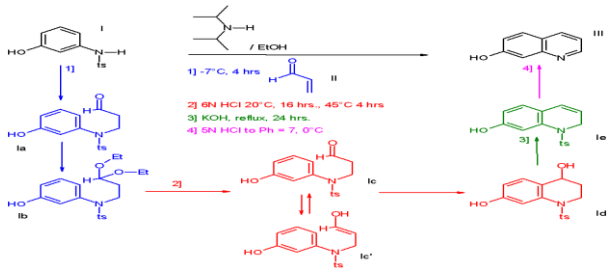

Physical nature

The appearance of the 8-hydroyxyquinoline colorless crystalline needles, it is and in the same times a bi-functional hydrogen bonding molecule. The conjugated organic materials that are functionalized by electron-donor moiety coupled, through a π conjugated bridge to an electron-acceptor moiety, can exhibit large optical non-linear (NLO) properties. The new materials exhibiting NLO effects are of great technological importance for use in application with in electronic and photonics.

8-hydroxyquinoline is easily soluble in acetone, insoluble in cold water, hot water, freely soluble in alcohols, chloroform and aqueous mineral acids soluble in acetic, hydrochloric and formic acids, alkalis

Experimental Details

The starting materials are commercially available . The solvent evaporation technique was used to grow single crystals of 8-HQ. The corresponding 8-HQ salt was dissolved in acetone to prepare a saturated solu-tion and the solution was filtered using Whatmann filter paper. The filtered solution was then taken in a beaker which was hermetically sealed to avoid the evaporation of the solvent. Optically defect free good quality single crystals of 8-HQ with reasonable dimensions were harvested in a month. In the present work, good optical quality crystals of pure 8-HQ are harvested.

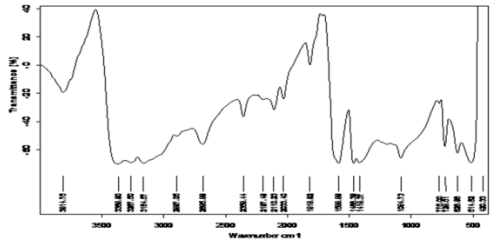

Result and Discussion

FTIR spectroscopy

The 8- HYDROXYQUINOLINE crystal is characterized by FTIR, UV and XRD analyzing techanique.These are discussed below. Fourier transform spectroscopy is to study the infrared spectra now been developed into a very powerful technique for the detection of very weak signals from their environmental technique to resolve a complex wave into its frequency components. The FTIR spectrum of the sample was recorded in mid and far IR regian and is used for the present investigation. Interpretation of FTIR spectrum of 8- HYDROXYQUINOLINE:

1) Amines in 8- HYDROXYQUINOLINE (N-H)
   Its observed at 3300 cm^{-1}.It represents in an primary Amines group present in 3388.8 ,its due to N-H stretching mode of vibration.
2) Amino in 8- HYDROXYQUINOLINE (N-H)
   It's observed at 3287 cm^{-1}.It represents in amino group present in 8- HYDROXYQUINOLINE due to N-H stretching mode of vibration.
3) Heteroaromatics in 8- HYDROXYQUINOLINE(ring structure)
   It's observed at 2110.69 cm^{-1}.It represents in Heteroaromatics group present in 8- HYDROXYQUINOLINE due to Ring stretching mode of vibration.
4) C-N Amines in 8- HYDROXYQUINOLINE(C-N)
   It's observed at 1488.80 cm^{-1}.It represents in amines group present in 8- HYDROXYQUINOLINE shows strong band due to C-N stretching mode of vibration.
5) Thicarbonys in 8- HYDROXYQUINOLINE(C=S)
   It's observed at 1351.51 cm^{-1}.It represents in Thicarbonys group present in 8- HYDROXYQUINOLINE due to C-N stretching mode of vibration.
6) Silicon components in 8- HYDROXYQUINOLINE(Si-X)
   It's observed at 1084.73 cm^{-1}.It represents in Silicon components group present in 8- HYDROXYQUINOLINE shows a Weak band due to S-X stretching mode of vibration.
7) Phosphorus Compounds in 8- HYDROXYQUINOLINE(S-S)
   Its observed at 928.01 cm^{-1}.It represents in Silicon components group present in 8- HYDROXYQUINOLINE shows a Weak band due to S-X stretching mode of vibration.
8) Pyrrole in 8- HYDROXYQUINOLINE(C-H)
   It's observed at 828.01 cm^{-1}.It represents in Pyrrole components group present in 8- HYDROXYQUINOLINE shows a Weak band due to C-H stretching mode of vibration.
9) Iodides in 8- HYDROXYQUINOLINE(C-X)
   It's observed at 770.00 cm^{-1}.It represents in Iodides components group present in 8- HYDROXYQUINOLINE shows a Weak band due to C-H stretching mode of vibration.
10) Disulfides in 8- HYDROXYQUINOLINE(S-S)
   It's observed at 514.82 cm^{-1}.It represents in Disulfides components group present in 8- HYDROXYQUINOLINE shows a Weak band due to S-S stretching mode of vibration.

UV Absorption spectrum:

UV visible spectral studies the cut off wave length and transmission band are occur at 204 nm.The UV Absorption study it identifies the π- π^* transition.

XRD Interpretation

The powder XRD Interpretation for the grown crystal 8- HYDROXYQUINOLINEis taken in XRD curve source that the material 8- HYDROXYQUINOLINE in in crystalline nature. The planes of reflection are shown in the graph that is the graph is indexed. The X-axis of the graph is 2θand the Y-axis gives the intensity the units are arbitrary. The 8- HYDROXYQUINOLINE single crystal is belongs to the structure of MOMOCLINIC.and also its having a = 11.765Å ; b = 6.9092Å ; c = 14.571Å and also, $\alpha = \beta = 90^{o}$ ‡Ɣ.

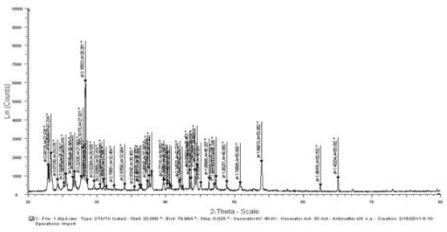

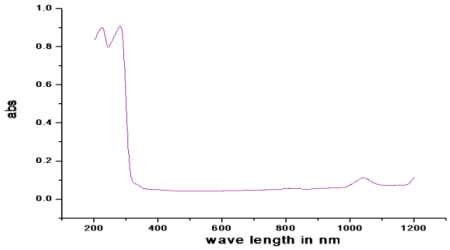

CONCLUSION

Good quality of 8- HYDROXYQUINOLINE single crystal was grown successfully by slow evaporation technique using the solvent Ethyl Alcohol at ambient temperature. The crystal was light yellow transparent. Powder X – Ray diffraction studies were carried out. It shows sharp peaks confirming its crystalline and the lattice parameter were calculated. The XRD data of the crystals confined that the 8- HYDROXYQUINOLINE grown crystal in monoclinic system. FTIR analysis confirms the presence of functional group in the grown crystals. The FTIR spectrum 8-HYDROXYQUINOLINE contains amines at wave number 3388.80cm^{-1} and other datas are tabulated. UV visible spectral studies the cut off wave length and transmission band are occur at 204 nm.The UV Absorption study it identifies the π- π^* transition.

REFERENCES

1. Harry.J.Simpson, Richard E.Marshi, *Acta Cryst.*, **20**, 550 (1966).
2. S.Palaniswamy and O.N.Balasundaram, *R. J.Chem.*,**2(1)**, 49-52 (2009).
3. R.Khanna and P.J.Miller, *Spectro Chem. Acta* ,**26A**, 1667, (1970).
4. S.Palaniswamy and O.N.Balasundaram , *R. J.Chem.*,**2(1)** 28-33(2009) .

Quantum Chemical Determination of Molecular Geometries and Interpretation of FT-IR and FT-Raman Spectra of 4 Butyrylbiphenyl

K. Rajalakshmi*[a] and S. Narayanan [a]

[a]*Department of Physics, Sri Chandrasekharendra Saraswathi Viswa MahaVidhyalaya, Kanchipuram,*
Corresponding author: k_rajalakshmi123@yahoo.com

Abstract

The Fourier-transform Infrared spectrum (FT-IR) and Fourier-transform Raman spectrum (FT-Raman) of 4-Phenylbenzophenone were recorded in the region 4000-400 cm^{-1} and 4000-100 cm^{-1} respectively. The spectra were interpreted with the aid of full structure optimization based on HF (Hartree Fock) using 6-31 G(d,p) and DFT (Density Functional Theory) B3LYP using 6-31 G(d,p) basis sets. A complete vibrational assignment aided by the theoretical harmonic frequency analysis has been compared with experimental FT-IR and FT-Raman spectra. Stability of the molecule arising from hyperconjugative interactions, charge delocalization have been analyzed using natural bond orbital analysis (NBO). The results show that charge in electron density (ED) energies confirm the occurance of ICT (Intramoleculr Charge Transfer) within the molecule. The calculated HOMO and LUMO energy gap also confirms that charge transfer occurs within the molecule. A Sufficient general agreement between the experimental and theoretical spectra have been achieved.

Keywords: 4 Butyrylbiphenyl; HF; DFT; FT-IR; FT-Raman; HOMO-LUMO; NBO.

1. Introduction

Biphenyl is an organic compound and used to prevent the growth of molds and fungus, and also used as a preservative particularly in the preservation of citrus fruits during transportation. It is mildly toxic, but can be degraded biologically by conversion into nontoxic compounds. Some bacteria are able to hydroxylate biphenyl and its polychlorinated biphenyls (PCBs) [1, 2].

2. Experimental: Structure and Spectra

The sample was obtained from M/s. Sigma Aldrich Co., with a stated purity of 99% and was used as such without further purification. The Fourier transform infrared spectra are recorded using Perkin Elmer spectrometer in KBr dispersion in the range of 4000 to 400 cm^{-1}. The FT-Raman spectrum was recorded using the 1054 line of a Nd:YAG laser as excitation wavelength in the region 4000-100 cm^{-1} on a Bruker model IFS 66 V spectrophotometer equipped with an FRA 106 FT-Raman module accessory.

3. Computational details

In the present work, the density functional method (DFT) [3] has been employed using Becke's three parameter hybrid exchange functional with the Lee-Yang –Parr correlation functional [4] to optimize the structure of the molecule and also to calculate the electronic structure of the title molecule. The entire calculations were performed at ab-initio Hartree Fock(HF) and DFT method using B3LYP levels at 6-31 G(d,p) basis sets on a Pentium V/ 1.6 GHz personal computer using Gaussian 09W program package [5-7] and applying geometry optimization Initial geometry generated was minimized at the Hartree Fock level using 6-31 G (d,p) basis set.

4. Results and Discussion

The optimized structure of 4 Butyrylbiphenyl is shown in Figure 1. The FTIR and FTRaman spectra is given in Figure 2 and Figure 3.The global minimum energy obtained by DFT structure optimization is

found to be -694.5942 Hartree. The optimized values of bond length and bond angle are shown in Table 1. The carbonyl group draws electrons and thereby weakens the resonance. Hence the inductive effect predominates resulting in an increase in the C=O force constant and slight increase in the corresponding bond length than the standard C=O bond length (1.220 Å) [8].

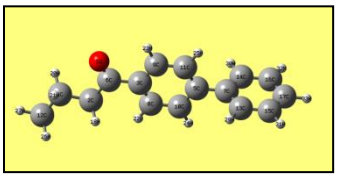

Figure 1.The Optimized Structure of 4 Butyrylbiphenyl at DFT/B3LYP/6-31 G(d,p)

Table 1: Optimized geometrical parameters of 4 Butyrylbiphenyl obtained by B3LYP/6-31G density functional calculations

Bond Length / Å		Bond Angle / o	
O1 – C2	1.223	O1-C6-C3	120.364
C8– C10	1.391	O1-C6-C2	120.763
C3 – C6	1.499	C5-C7-C14	120.949
C4 – H21	1.095	C14-C16-H32	119.659
C16 –H32	1.086	C2-C4-C12	112.611

4.1 Vibrational Assignments

The molecule 4 Butyrylbiphenyl contains 33 atoms, and it has 93 normal modes of vibration. According to group theory, the point group for this molecule is C_1 symmetry and all the fundamental vibrations are IR active.

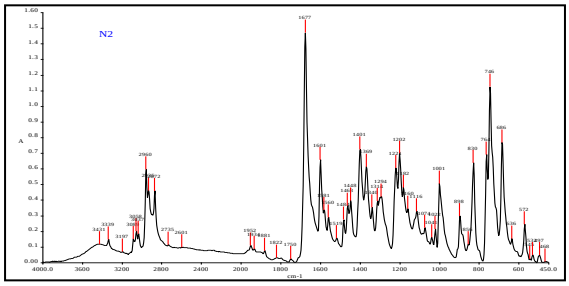

Figure 2. FTIR spectrum of 4 Butyrylbiphenyl

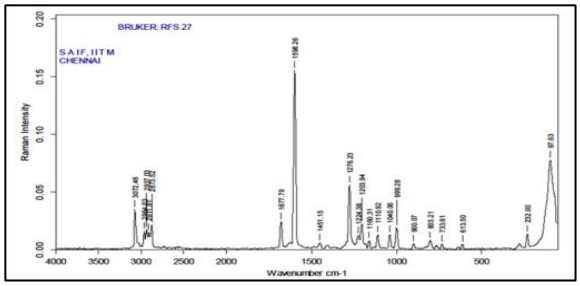

Figure 3. FTRaman spectrum of 4 Butyrylbiphenyl

C-H Vibrations

Normally, aromatic compounds commonly exhibit multiple weak band in the region 3100-3000 cm^{-1} due to aromatic C-H stretching vibrations. In the present study, the C-H vibrations of the title compound are observed at 3187 cm^{-1} in the DFT/B3LYP method and it is observed at 3197 cm^{-1} in the FT-IR spectrum and 3072 cm^{-1} in the FT-Raman spectrum [9]. All the compounded bands for the C-H vibrations by DFT/B3LYP method show excellent agreement with recorded spectrum as well as with the literature values.

C-C Stretching Vibrations

The ring stretching vibrations are very important in the spectrum of pyridine and its derivatives and are highly characteristic of the aromatic rings. The aromatic ring carbon-carbon stretching vibrations occur in the region 1625-1430 cm^{-1}. In the present work, the C-C aromatic stretch is

observed in the region 1644-1588 cm^{-1} in the DFT/B3LYP calculations. In FT-IR spectrum, it is observed in the region 1601and 1581 cm^{-1} and in Raman spectrum, it is observed in the region 1677 and 1588 $cm^{-1.}$ These vibrations are in good agreement with the calculated values. The C-C in-plane and out-of-plane vibrations are in good agreement with the literature values [10].

CH_2 Vibrations

The symmetric CH_2 stretching vibration is observed at 3031 and 2987 cm^{-1} in DFT/B3LYP method and the asymmetric CH_2 stretching vibration is observed at 3081 and 3056 cm^{-1} in DFT/B3LYP method. The observed bands at 3058 and 3089 cm^{-1} in IR spectrum is assigned to symmetric and asymmetric CH_2 stretching vibration. In FTRaman, CH_2 stretching vibration is observed at 3072 cm^{-1}. The CH_2 wagging is observed at 1330 cm^{-1} in DFT method and in FTIR spectrum it is observed at 1340 cm^{-1} and in FT Raman spectrum, a band observed at band at 1330 cm^{-1} is assigned to CH_2 wagging. The CH_2 scissoring is observed at 1456 cm^{-1} in DFT method and in FTIR spectrum it is observed at 1448 cm^{-1} and in FT Raman spectrum, a band observed at band at 1459 cm^{-1} is assigned to CH_2 wagging. The CH_2 rocking is observed at 1239 cm^{-1} in DFT method and in FTIR spectrum it is observed at 1222 cm^{-1} and in FT Raman spectrum, a band observed at band at 1234 cm^{-1} is assigned to CH_2 rocking. The CH_2 twisting is observed at 1313 cm^{-1} in DFT method and in FTIR spectrum it is observed at 1314 cm^{-1} and in FT Raman spectrum, a band observed at band at 1320 cm^{-1} is assigned to CH_2 twisting. The most important ring stretching vibration is the ring breathing vibration at mode 43. In this mode, all bonds of the rings appear to stretch and contract in-phase with each other [11,12]. In the experimental infrared spectrum of ciprofloxacin, this mode appears at 1001 cm^{-1} in FT-IR and in FTRaman it is observed at 999 cm^{-1} and the computed value by DFT/B3LYP method was found to be 1013 cm^{-1}.

Thermodynamic parameters	HF/ 6-31 G (d,p)	DFT/B3LYP/ 6-31 G (d,p)
SCF energy (a.u.)	-690.111	-694.594
Total energy (thermal) E_{total}(Kcal mol^{-1})	194.006	182.806
Vibrational energy, E_{vib}(Kcal mol^{-1})	192.228	181.029
Zero point vibrational energy(Kcal mol^{-1})	185.041	173.263
Specific heat, C_v (cal $mol^{-1}K^{-1}$)	54.091	58.496
Entropy, S(cal $mol^{-1}K^{-1}$)	122.956	126.588
Rotational constants (GHz)		
X	1.789	1.761
Y	0.164	0.163
Z	0.153	0.151
Dipole moment μ (Debye)		
μ_x	-1.956	1.963
μ_y	-2.713	-2.292
μ_z	0.0079	0.465
Total	3.3451	3.054

C=O Vibrations

The sharpest peak in the band at 1750 cm^{-1} is due to C=O stretching mode and the corresponding C=O stretching vibration is observed at 1749 cm^{-1} in DFT/B3LYP method are in good agreement with the literature values [13].

Other Molecular Properties

The thermodynamic properties calculated at HF and DFT/B3LYP/6-31 G (d,p) levels of the title compound is presented in Table 2. According to HF and B3LYP calculations, the largest dipole moment were observed for DFT and decrease in the energy were observed for DFT.

Table 2: Thermodynamical properties of 4 Butyrylbiphenyl

5 Conclusions

The present investigation thoroughly analyzed the vibrational spectra, both infrared and Raman of 4 Butyrylbiphenyl. The optimized geometries, harmonic vibrational wavenumbers and intensities of vibrational bands of 4 Butyrylbiphenyl have been carried out using the DFT/B3LYP method using the standard 6-31 G (d,p). The theoretical results were compared with the experimental vibrations and it can be seen that the values obtained from DFT levels matches well with the experimental values. Also, thermodynamical properties were tabulated. This DFT based quantum mechanical approach provides the most reliable theoretical information on the vibrational properties of 4 Butyrylbiphenyl.

References

[1] N. G.Adams and D. M. Richardson, 1953. Isolation and Identification of Biphenyls from West Edmond Crude Oil. Analytical Chemistry 25 (7): 1073-1074
[2] *"Biphenyl degradation - Streptomyces coelicolor, at GenomeNet Database".genome.jp.*
[3] W. Kohn, L. J. Sham, "Self-consistent equations including exchange and correlation effects," 140 (1965) A1133–A1138.
[4] A.D. Becke, J.Chem. Phys. 98 (1993) 5648–5652.
[5] C.Lee, W.Yang, R.G.Parr, Phys. Rev. B 37 (1988) 785–789.
[6] M. J. Frisch, G. W.Trucks, H. B. Schlegel et al., Gaussian 03, Revision A.1, Gaussian, Pittsburgh, Pa, USA, 2003.
[7] A.Frisch, A.B.Nielsen, A.J. Holder. Gaussview Users Manual, Gaussian Inc.,Pittsburgh, 2007.
[8] J. Daisy Magdaline, T. Chithambarathanu, Int. J. ChemTech Res. 8 (2015) 362-371,
[9] K Rajalakshmi, S.Gunasekaranan, S Kumaresan, Spectrochim Acta Part A 130 (2014) 466–479
[10] K Rajalakshmi, S.Gunasekaranan, S Kumaresan, Ind. J Phys DOI 10.1007/s12648-014-0468-8.
[11] G.Varsanyi, Vibrational Spectra of Benzene Derivatives, (1969) Academic Press, New York.
[12] A.Nataraj, V. Balachandran, T. Karthick, M. Karaback, A. Atac, J.Mol.Struct. 1027 (2012) 1-14.
[13] V.J.Eatch, D.Steel, J. Mol.Spectros. 48 (1973) 446-449.

DFT Computations and Spectroscopic Study of 4-Phenylbenzophenone

K. Rajalakshmi*[a] and P. Ramakrishnan [b]

[a]Department of Physics, Sri Chandrasekharendra Saraswathi Viswa MahaVidhyalaya, Kanchipuram
Corresponding author: k_rajalakshmi123@yahoo.com

Abstract

The molecular vibrations of 4-Phenylbenzophenone has been investigated at room temperature by Fourier transform infrared (FTIR) and Fourier transform Raman (FTR) spectroscopy. The solid phase FTIR and FT-Raman spectra of the title compound have been recorded in the regions 4000-400 and 4000-100 cm-^{1}. A satisfactory band assignment has been made on the fundamental modes of vibration. Employing the ab - initio Hatree –Fock (HF) and Density Function Theory (DFT) methods. The theoretical vibrational frequencies and geometry parameters like bond lengths and bond angles have been calculated and compared with the experimental values. HF and DFT calculations were performed using the standard B3LYP/6-31 G(d,p) basis set combination. Optimized geometries were obtained using the global optimization procedure. Theoretical investigations of harmonic vibrational frequencies and thermodynamic properties viz. the zero point vibrational energy (ZPVE), entropy, heat capacity have been carried out. It has been found that both methods gave consistent data for geometric parameters, but DFT yielded vibrational frequencies much closer to the experimental values.

Keywords: 4-Phenylbenzophenone; HF; DFT; FT-IR; FT-R;

1. Introduction

Phenylbenzophenone with the molecular formula $C_{19}H_{14}O$ is an organic compound insoluble in water. The benzophenone derivatives are known to be pharmacologically active in the interaction with B-DNA. The successive photo induced energy transfer is at the base of benzophenone activity as a DNA photosensitizers and may explain part of its therapeutic potentialities [1 - 2].

2. Experimental: Structure and Spectra

The sample was obtained from M/s. Sigma Aldrich Co., with a stated purity of 99% and was used as such without further purification. The Fourier transform infrared spectra are recorded using Perkin Elmer spectrometer in KBr dispersion in the range of 4000 to 400 cm^{-1}. The FT-Raman spectrum of ciprofloxacin was recorded using the 1054 line of a Nd:YAG laser as excitation wavelength in the region 4000-100 cm^{-1} on a Bruker model IFS 66 V spectrophotometer equipped with an FRA 106 FT-Raman module accessory.

3. Computational details

In the present work, the density functional method (DFT) [3] has been employed using Becke's three parameter hybrid exchange functional with the Lee-Yang –Parr correlation functional [4] to optimize the structure of the molecule and also to calculate the electronic structure of the title molecule. The entire calculations were performed at ab-initio Hartree Fock(HF) and DFT method using B3LYP levels at 6-31 G(d,p) basis sets on a Pentium V/ 1.6 GHz personal computer using Gaussian 09W program package [5-7] and applying geometry optimization Initial geometry generated was minimized at the Hartree Fock level using 6-31 G (d,p) basis set.

4. Results and Discussion

4.1 Molecular geometry

The optimized structure of 4-Phenylbenzophenone is shown in Figure 1. The FTIR and FTRaman spectra of 4-Phenylbenzophenone are shown in Figure 2 and Figure 3. The optimized geometrical bond parameters are tabulated in Table 1. From the table, it is clear that the bond length of C13 –O14 is 1.226 Å. The bond length of C10 – C13 is 1.498 Å and bond length of C4-C7 is 1.484Å where the bond length is shortened by 0.01 Å. Also the bond length of C 1 – C2 is 1.395Å where it is shortened by 0.1 Å as we move from Ring R2 to Ring R1 due to the electronegative oxygen atom attached in Ring R2 [8].

Bond Length / Å		Bond Angle / o	
C 1 – C2	1.395	C15-C13-C14	119.625
C4-C7	1.484	C10-C13-O14	119.702
C10 – C13	1.498	C9-C10-C13	117.916
C13 –O14	1.226	C13-C15-C20	117.687
C9–H27	1.084	C15-C20-H24	118.349

Table1 Optimized Bond parameters of 4-Phenylbenzophenone

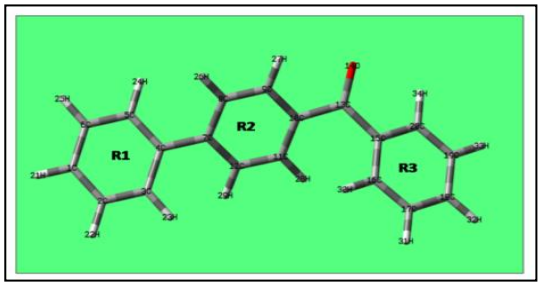

Figure 1. Optimized Structure of 4-Phenylbenzophenone

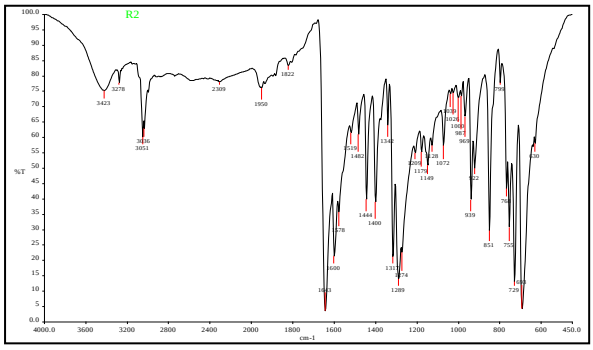

Figure 2. FTIR Spectrum of 4-Phenylbenzophenone

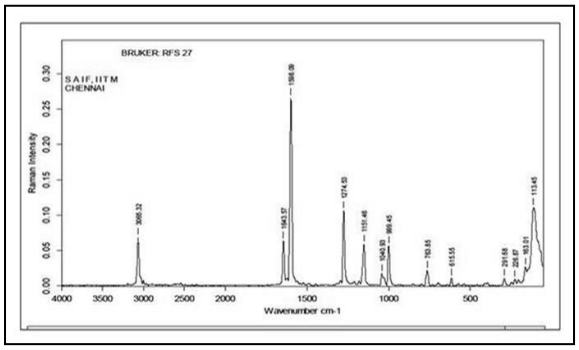

Figure 3. FT-Raman spectrum of 4-Phenylbenzophenone

4.2 Vibrational Assignments

The molecule 4-Phenylbenzophenone contains 34 atoms, and it has 96 normal modes of vibration. According to group theory the point group symmetry for the molecule is C1 symmetry and all the fundamental modes of vibrations are IR active. The harmonic vibrational frequencies calculated have been compared with the experimental frequencies and is given in Table 2.

C-H Stretching

Normally, aromatic compounds commonly exhibit multiple weak band in the region 3200-3000 cm^{-1} due to aromatic C-H stretching vibrations. In the present study, the C-H vibrations of the title compound are observed at 3205 cm^{-1} (Ring R2, R3), 3036 cm^{-1} (Ring R1, R2,) and ***3016*** cm^{-1} (Ring R1,), in the DFT/B3LYP method. A band observed at 3278,3076and ***3026*** cm^{-1} in the FT-IR and 3065 and 3015 cm^{-1} in FTRaman are assigned to C-H stretching vibrations. All the compounded bands for the C-H vibrations by DFT/B3LYP method show excellent agreement with recorded spectrum as well as with the literature values [9].

Table 2: Vibrational assignments of 4-Phenylbenzophenone

Observed Wave number		Calculated Wave number		Vibrational Assignments
FTIR cm^{-1}	FTRaman cm^{-1}	DFT	HF	
3278	-	3205	3083	C-H Stretching (R2,R3)
3036	3065	3022	3075	C-H Stretching (R1,R2,)
3026	3015	3016	3069	C-H Stretching (R1)
3008	3000	3009	3063	C-H Stretching (R3)
3000	-	3002	3055	C-H Stretching (R2)
1643	1643	1631	1779	C=O Stretching
1578	1598	1561	1653	C-C Stretching(R1,R2,)
1519	1550	1554	1642	C-C Stretching (R3)
1444	1440	1440	1512	C-H Bending (R1,R2, R3)
	350	387	401	CCCC out of plane bending

C=O stretching

The most characteristic feature of carboxylic group is a singleband observed usually in the range of 1700–1800 cm^{-1} This band is due to the C=O stretching vibration. The C=O stretching mode is observed at 1578 cm^{-1} in FT-IR spectrum and observed at 1598 cm^{-1} in FT-Raman spectrum The theoretical values of the C=O band show very good agreement with experimental results, which are predicted at 1561 cm^{-1} [10].

C-C stretching Vibrations

In the present work, the wave numbers observed in the FTIR spectrum at 1576 cm^{-1} (Ring R1,R2) and 1519 cm^{-1} (Ring R3) are assigned to C-C Stretching vibrations. A band observed at 1598 cm^{-1} (Ring R1, R2) and 1550 cm^{-1} (Ring R3) in FT-Raman are assigned to C-C Stretching vibrations. The theoretically computed values at 1561 cm^{-1} (Ring R1, R2) 1554 cm^{-1} (Ring R3) agree well with the experimental and literature values[11].

4.3 Mulliken Population analysis

The Mulliken population analysis of 4-Phenylbenzophenone was calculated using HF/6-31 G(d,p) and DFT/B3LYP/6-31 G(d,p) level and given in Figure 4. The charge distribution of the molecule in Fig.4. Shows that the carbon atoms attached to oxygen atoms are having positive charges. So, the remaining carbon atoms are negative, whereas all the hydrogen atoms have positive charges [12].

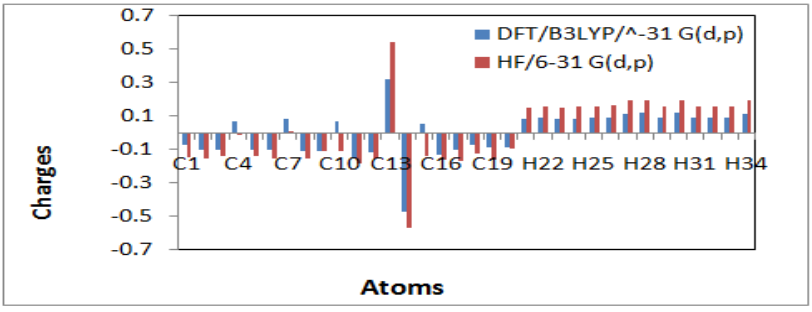

Figure 4. Mulliken atomic charges of 4-Phenylbenzophenone

Conclusion

The FT-IR and FT-Raman spectral studies of 4-Phenylbenzophenone have been carried out for the first time. A complete vibrational and molecular structure analysis has been performed based on

the quantum mechanical approach by DFT calculations. The difference between the observed and scaled wave number values of most of the fundamentals is very small. Therefore assignments made at DFT level of theory with only reasonable deviations from the experimental values seem to be correct. Mulliken analyses have also been computed.

References

1 C.S. Marvel, W.M.Sperry (1941) " Benzophenone", Org.Synth,Coll, Vol.1, P.95.

2 *M. Consuela Cuquerella, V.Lhiaubet Vallet, J.Cadet, M.A.Miranda, (2012), "Benzophenone Photosentisized DNA Damage" Acc.Chem.Res. 45: 1558-1570.*

3 W. Kohn, L. J. Sham, "Self-consistent equations including exchange and correlation effects," 140 (1965) A1133–A1138.

4 A.D. Becke, J.Chem. Phys. 98 (1993) 5648–5652.

5 C.Lee, W.Yang, R.G.Parr, Phys. Rev. B 37 (1988) 785–789.

6 M. J. Frisch, G. W.Trucks, H. B. Schlegel et al., Gaussian 03, Revision A.1, Gaussian, Pittsburgh, Pa, USA, 2003.

7 A.Frisch, A.B.Nielsen, A.J. Holder. Gaussview Users Manual, Gaussian Inc.,Pittsburgh, 2007.

8 Sethu Gunasekaran, K. Rajalakshmi, Subramanian Kumaresan, Spectrochim Acta Part A: 112 (2013) 351–363.

9 M.Arivazhagan, C.Arunagiri, A. Subashini, Indian J Pure & Appl.Phys., 51,2013, 191-201.

10 Caglar Karaca, Ahmet Atac, Mehmet Karabacak, Spectrochim Acta Part A: 136 (2015) 295–305

11 M. Karabacak, Z. Cinar, M. Kurt, S. Sudha, N. Sundaraganesan, Spectrochimica Acta Part A 85 (2012) 179– 189

12 N. Balamurugan, C. Charanya, S. SampathKrishnan, S. Muthu, Spectrochim Acta Part A: 137 (2015) 1374–1386

SYNTHESIS OF $LiCoO_2$ DOPANT Cr / Mg LAYERED OXIDE MATERIAL FOR Li –Ion BATTERIES

P.Sumathi, Simon Justin.A, P.Gomathi, P.Vickraman*

Solid State Ionics Lab, Department of physics, Gandhigram Rural Institute- Deemed University, Gandhigram-624302, Tamil Nadu.

E-mail: vrsvickraman@yahoo.com

Abstract

In the present work Lithium Cobalt Oxide $LiCo_{1-x-y}O_2$ based layered oxide material with **Chromium(Cr)$_x$/Magnesium(Mg)$_y$** as dopants in three stoichiometric ratios $LiCo_{1-x-y}Cr_xMg_yO_2$ has been prepared by sol-gel process, and as-prepared layered oxide materials (ASLOMs) are labeled as $LiCoO_2$ (OCL), $LiCo_{0.9}Mg_{.1}O_2$ (OML), $LiCo_{0.9}Cr_{.08}Mg_{.02}O_2$ (OML1), $LiCo_{0.9}Cr_{.06}Mg_{.04}O_2$,(OML2), $LiCo_{0.9}Cr_{.04}Mg_{.06}O_2$ (OML3) enroute as electrodes in Li-ion batteries. Furtherance these ASLOMs are annealed at 200, 400 and 600^{o} C to understand the structural/ stoichiometric compatability through XRD studies and the results confirms that all ASLOMs have in Rhombohedral structure (**JCPDS card no: 50-0653**). The surface morphology (SEM) on ASLOMs show that the samples which are annealed at 600^{o}C have uniform and homogeneous distribution than ASLOMs at 200 and 400^{o}C. The FTIR studies confirms molecular interaction via the vibrational bands (shifts, change in intensity and absence) between various constituents found in 400-1500 cm^{-1}.

Keywords: $LiCoO_2$, sol-gel process, XRD, Annealing.

INTRODUCTION

Materials for cathodes in rechargeable Lithium ion batteries have attracted the much concentration of research in recent years, both from the experimental and the theoretical point of view. Lithium based layered transition metal oxides $LiMO_2$ (M = Ni, Co, Mn, Fe, V) have attracted great interest worldwide and most studied for demand of high capacity energy storage devices [1]. Among this group, $LiCoO_2$ is one of the most promising materials for commercial application because of its favorable features such as good capacity, excellent electrochemical stability, good power rates, low self-discharge and excellent life cycle. $LiCoO_2$ crystals in particular have attracted attention due to their layered structure because Li^+ ions are easily removed from $LiCoO_2$ structure [2-5]. The structural stability of the $LiCoO_2$ cathode material is such that the layered cation ordering extremely preserved even after a repeated process of insertion and extraction of Li^+ ions [6]. However, due to its inherent drawbacks doping of Al, Mg, Cr and its binary stoichiometry have been attempted to promote the structural integrity and electrochemical performance. In these connections many researchers have done lot of works on the mixed doping on $LiCoO_2$. Based on these review as no one has ever reported on stoichiometry effect of Mg, Cr to the host pristine $LiCoO_2$. Thus objective of work has been designed in such way that stoichiometric effect as well as the temperature influence on as synthesized at 200◦C, 400◦C, 600◦C has been attempted and structural (XRD), molecular interaction (FTIR) and surface morphology studies have been planned on the systems.

MATERIALS AND METHODS

The $LiCH_3COO.2H_2O$, $Co(CH_3COO)_2.4H_2O$, and Mg $(CH_3COO)_2.4H_2O$ are purchased from Alfa Acer with 99% purity and used without further purification. The Cr $(NO_3)_3.9H_2O$, are purchased from Sigma Aldrich with 99% purity and used without further purification. $LiCH_3COO.2H_2O$, $Co(CH_3COO)_2.4H_2O$, $Mg(CH_3COO)_2.4H_2O$, $Cr(NO_3)_3.9H_2O$ and citric acid were used as starting

materials to synthesize $LiCo_{1-x}Cr_xMg_yO_2$ by a sol-gel method. The entire stoichiometric amounts of precursor were initially dissolved in distilled water. The amount of distilled water is 3 equal to the total molar amount of precursors. The entire solution was stirred at 60◦C with dropwise addition of the citric acid for controlling pH and avoiding the precipitation. At last, the pink color gel has obtained. The xerogel was pre-calcined at 400◦C and the black color poly crystalline powder has been obtained and grinded agate mortar. The obtained powder was calcined at 600◦C for 6 h in air, cooled at room temperature, and then the annealing was carried out at 200◦C, 400◦C and 600◦C for 6 hrs in each. The XRD, FTIR and SEM studies were carried out for as-prepared powders.

RESULT AND DISCUSSION

XRD STUDIES:

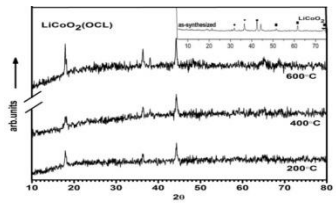

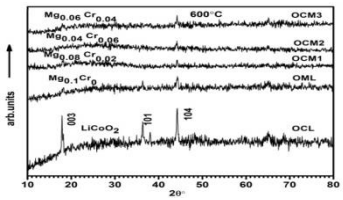

XRD diffractogram of as-synthesized sample (reported) has been taken as reference for the study as it is room temperature. A very short doublet appeared at 31◦ and 32◦, a medium peak around 36◦ and the doublet one with higher intensity and other one with lesser intensity noted at 42◦ and 44◦ and lesser intensity short peak is noted around 62◦ and prior to 80◦, a very shortest peak are noted , as per the literature and with JCPDS index, the peaks at 42 ◦and the smallest hump 52◦, the peak at 62 ◦ and the near peak at 74◦ are correspond to CoO [7]. In the present study XRD pattern of as-synthesized (reported) at 30◦C has been compared with as-synthesized sample (prepared) at 200◦C, 400◦C and 600◦C (fig.1a). Certain characteristic peaks noted in as-synthesized sample (reported) are not appeared with distinct appearance are noted at 18◦as a sharp medium peak , at 36◦as a very short peak and very enhanced sharp peak at 44◦ are noted. While comparing the as-synthesized sample with 200◦C annealed sample (prepared), it is found that the new peak appeared near 18◦and the peaks found at 36◦ and 44◦ (as-synthesized) appeared but change in FWHM and intensity. These suggest that some kind of structural orientation has taken place at 200◦C. Comparing the XRD pattern of 200◦C with the 400◦C, the peaks again appeared but change in FWHM and intensity are noted which are higher than that of 200◦C particularly the increasing intensity of peak at 44◦ while observing the 600◦C with the reference to 400 ◦C and 200◦C, the drastic increase in intensity corresponds as referred peaks at 200◦C and 400◦C. Suggest that the higher temperature in this study at 600◦C has shown the considerable temperature impact on the as-synthesized sample particularly Li and Co-O orientation. At 600◦C (fig.1b) the pristine $LiCoO_2$ where in 003 index of Lithium at 2θ = 18◦, the doublets at 101/ (102/006) at 36.8 and 38.7◦ and 104 hkl index at 44◦ have appeared with enhanced sharp intensity with increase in height and reduced FWHM suggest that the Lithium and Cobalt Oxide have improved their orderliness in the inner lattice seen very clearly. This highly orderliness of inner lattice associated with the phase of CoO_2 has not been seen in 400◦C as well as

200°C but while doping Mg, these characteristics peaks have been highly suppressed as that observed at 200°C expect the 104 hkl plane associated with the CoO_2. In this regard, it confirmed that the as-prepared powder also in Rhombohedral structure with the reference of **JCPDS card no: 50-0653**

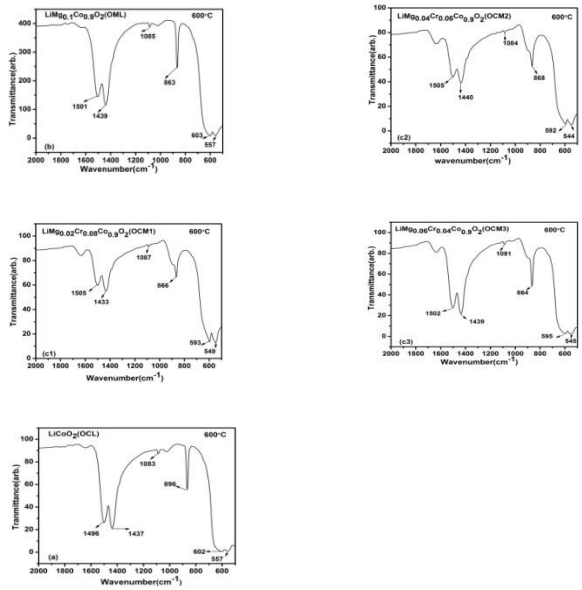

Fig.2: FTIR studies of pure and Mg,Cr doped $LiCoO_2$

FTIR STUDIES:

The following vibrational bands found in the region 400-4000cm^{-1} such as 556cm^{-1}, 599cm^{-1}, 863cm^{-1}, 1080cm^{-1} are assigned rocking vibrations. O-Co-O symmetric vibration at 1505cm^{-1}(out of plane) and asymmetric vibration at 1435cm^{-1}(out of plane) are assigned to cobalt and oxygen coordination sites [8]. The Li-O coordination site has not been traced because the vibrational band observation carried out from 400cm^{-1} instead of 200cm^{-1} wherein it has to be referred. Doping of magnesium has completely trunked off the vibrational bands found out 1435cm^{-1} and 1505cm^{-1} states that the magnesium replaces the Co sites and having coordination with oxygen [9]. Further the magnesium influence in the pristine Co-O has been distinctly made possible by the appearance of multiplets vibrational bands i.e 592cm^{-1}, 568cm^{-1} and 538cm^{-1} in the 400-600 cm^{-1} region, all correspond to the spurious effect of magnesium participation with oxygen compared to the pristine $LiCoO_2$ wherein doublet 599cm^{-1} and 556cm^{-1} are appeared (fig.2). The binary stoichiometry performance of Mg, Cr has also been observed by doping $0.04 \leq Cr \leq 0.08$ to $0.06 \leq Mg \leq 0.02$. The vibrational bands have been noted after doping Cr in the stoichiometry as mentioned earlier, and it is found that the 1642cm^{-1} RCO_3Li [10-14] which has appeared as a very smallest kink in OCL has dominantly grown and showed its vibrational bands in the same location as due to the influence of enriched Cr in OCM1 but it is returned to the same trace as found in $LiCoO_2$ (OCL) in OCM3 due to the lesser stoichiometry influence is conformed. The Cr influence has been seen irrespective of its stoichiometry in the wavenumber region 400-600cm^{-1} with the index of 599cm^{-1}. The temperature influence on these samples $LiCoO_2$(OCL), $LiMg_{0.1}Co_{0.9}O_2$ (OML), $LiMgCrO_2$ (OCM1/OCM2/OCM3) at 600°C have also been performed to understand the temperature effect on stoichiometry. The no trace of 1383cm^{-1} O-Co-O in plane at 600°C also noted.

SEM STUDIES

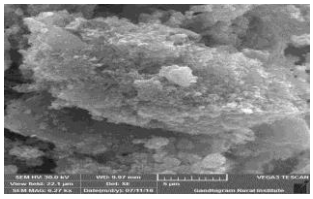

LiMg0.02Cr0.08Co0.9O2 (OCM1)

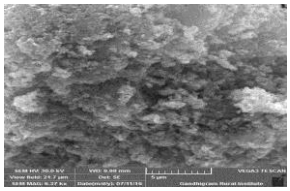

LiMg0.04Cr0.06Co0.9O2(OCM2)

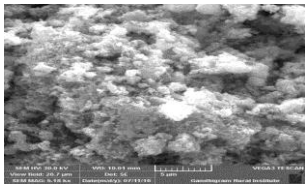

LiMg0.06Cr0.04Co0.9O2(OCM3)

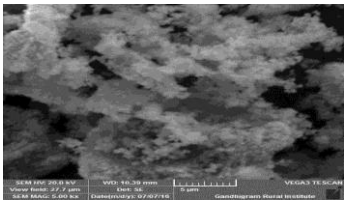

LiCoO2 (OCL)

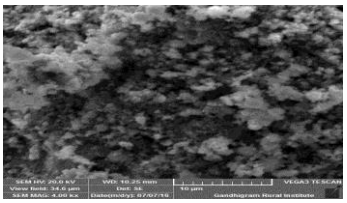

LiMg0.1Co0.9O2 (OML)

Fig.3 SEM Studies of pristine and Mg, Cr doped $LiCoO_2$ at 600 °C

The SEM surface profile of pristine $LiCoO_2$ as shown inhomogenity dispersed of it, as like that of inhomogenity distribution of dry cotton flaks. While doping, the Mg inhomogenity cotton flaks appearance has been distorted and within the distorted region, the Mg as showed its presence as shown in fig.3.The stoichiometry morphology on surface of OCM1, OCM2 and OCM3 have been closely examined and showed that the enriched Cr has not shown any appreciable effect on $LiCoO_2$ as evidenced that the inhomogenity Cobalt flaks dispersion with orientational change of Cobalt flaks. On other hand the Mg has shown its stoichiometry performance in OCM2 as Mg completely quivering the Co flaks has been seen that Mg plays a vital role than the Cr is noted.

CONCLUSION:

- The pure and Mg, Cr doped LiCoO2 materials have been prepared by conventional sol-gel process.
- The XRD studies confirmed that all the as-prepared samples were in R-3m structure with the reference of JCPDS index. Cation and anion coordination sites have been well ordered at high temperature is noted. The enriched stoichiometry Cr and enriched role of Mg have been seen in XRD.
- The Cr-O ($599cm^{-1}$) coupled with $566cm^{-1}$ through O sites have been in FTIR studies as a doublet.
- The Mg replaces certain Co-O sites have been seen in XRD and reflected in SEM morphology also.

REFERENCE:

1. T. Nagaura, K. Tozawa, Prog. Batteries Solar Cells 9 (1990) 209.
2. M. Catti, Phys. Rev. B, 61, 1795 (2000).
3. R. Koksbang, J. Barker, H. Shi, and M. Y. Saidi, Solid State Ionics 84, 1 (1996).
4. M. M. Thackeray, J. Electrochem. Soc. 142, 2558 (1995).
5. L. Predoana, A. Barau, M. Zaharescu, H. Vasilchina, N. Velinova, B. Banov, and A. Momchilov – Advanced Techniques for LiCoO2 Preparation and Testing, Proceedings of the International Workshop "Advanced Techniques for Energy Sources Investigation and Testing" 4–9 Sept. 2004, Sofia, Bulgaria.
6. S.M. Lala, L.A.Montoro, V. Lemos, M. Abbate, J.M. Rosolen, Electrochim. Acta 51, 7(2005).
7. H.Y. Xu, S. Xie, C.P. Zhang, C.H. Chen, J. Power Sources 148 (2005) 90.
8. E.I. Santiago, A.V.C. Andrade, C.O. Paiva-Santos, L.O.S. Bulhoes Solid State Ionics 158 91– 102 (2003).
9. N.K. Yabuuchi, K.Y. Yamamoto, K.H. Yoshii, I. Nakai, T.S. Nishizawa, A. Omaru,T.H. Toyooka, S.C. Komaba, J. Electrochem. Soc. 160 A39–A45 (2013).
10. Zhaoxiang Wang, Xuejie Huang, and Liquan Chen. Journal of the Electrochemical Society, 150 (2) A199-A208 (2003).
11. D. Aurbach, A. Zaban, A. Schecheter, Y. Ein-Eli, E. Zinigrad, and B. Markvsky, J.Electrochem. Soc., 142, 2873 (1995).
12. R. A. Niquist and R. O. Kagel, Infrared Spectra of Inorganic Compounds, p. 210 Academic Press, New York (1971).
13. D. Aurbach, Y. Ein-Eli, B. Markvsky, A. Zaban, S. Luski, Y. Cameli, and H. Yamin, J. Electrochem. Soc., 142, 2883 (1995).
14. A. Naji, J. Ghanbaja, P. Willmann, B. Humbert, and D. Billaud, J. Power Sources, 62, 141 (1996).

SYNTHESIS / STUDY OF ALUMINIUM AND CHROMIUM AS DOPANTS IN $LiCoO_2$ AS NOVEL LAYERED OXIDE MATERIALS FOR Li –Ion BATTERIES

P.Gomathi, Simon Justin.A, P.Sumathi, P.Vickraman*

*Solid State Ionics Lab, Department of physics, Gandhigram Rural Institute- Deemed University, Gandhigram-624302, Tamil Nadu.****E-mail: vrsvickraman@yahoo.com***

Abstract

The present work focuses on synthesis and study of new novel layered oxide materials for electrode (cathode) preparation to their end utility in Li-ion batteries i.e Lithium Cobalt Oxide material with **Aluminium and Chromium** as dopants in three stoichiometric ratios, labeled as $LiCoO_2$(OCL), $LiCo_{0.9}Al_{.1}O_2$(OAL), $LiCo_{0.9}Cr_{.08}Al_{.02}O_2$ (OAL1), $LiCo_{0.9}Cr_{.06}Al_{.04}O_2$, (OAL2),and $LiCo_{0.9}Cr_{.04}Al_{.06}O_2$ (OAL3). These as-prepared layered oxide materials (ASLOMs) have been annealed from 200-600^{o}C in steps of 200^{o}C difference in order to understand localization nature of the dopants by XRD studies. Thus study on these ALSLOMs reveal that structural domains including with pristine $LiCoO_2$ have confirmed their Rhombohedral structure with point group symmetry of α-$NaFeO_2$ (R-3m) **JCPDS card no: 89-0912**, and changes placed in their FWHMs however are not found to be varying with temperature. The surface morphology (SEM) on ASLOMs show that the samples annealed at 600^{o}C have sintered uniform disperoid than that of at 200 and 400^{o}C. The FTIR studies confirms molecular interaction via the vibrational bands (shifts, change in intensity and absence) between various constituents found in 400-1500 cm^{-1} region.

Keywords: $LiCoO_2$,sol-gel process, XRD, annealing

INTRODUCTION

Materials for cathodes in rechargeable Lithium ion batteries have attracted the much concentration of research in recent years, both from the experimental and the theoretical point of view. Lithium based layered transition metal oxides $LiMO_2$ (M = Ni, Co, Mn, Fe, V) have attracted great interest worldwide and most studied for demand of high capacity energy storage devices [1]. Among this group, $LiCoO_2$ is one of the most promising materials for commercial application because of its favorable features such as good capacity, excellent electrochemical stability, good power rates, low self-discharge and excellent life cycle. $LiCoO_2$ crystals in particular have attracted attention due to their layered structure because Li^+ ions are easily removed from $LiCoO_2$ structure [2-5]. The structural stability of the $LiCoO_2$ cathode material is such that the layered cation ordering extremely preserved even after a repeated process of insertion and extraction of Li^+ ions [6]. However, due to its inherent drawbacks doping of Al, Mg, Cr and its binary stoichiometry have been attempted to promote the structural integrity and electrochemical performance. In these connections many researchers have done lot of works on the mixed doping on $LiCoO_2$. Based on these review as no has reported on stoichiometry Al, Cr to the host pristine $LiCoO_2$. This work has been attempted and the temperature influence on the systems and the stoichiometry and their relation have been planned through some of the characterization techniques XRD, FTIR and morphology studies.

MATERIALS AND METHODS

The $LiCH_3COO.2H_2O$, $Co(CH_3COO)_2.4H_2O$, and Al $(NO_3)_3.9H_2O$, are purchased from Alfa Acer with 99% purity and used without further purification. The Cr $(NO_3)_3.9H_2O$, are purchased from Sigma Aldrich with 99% purity and used without further purification. $LiCH_3COO.2H_2O$, $Co(CH_3COO)_2.4H_2O$, $Al(NO_3)_3.9H_2O$, $Cr(NO_3)_3.9H_2O$ and citric acid were used as starting materials to

synthesize $LiCo_{1-x}Cr_xAl_yO_2$ by a sol-gel method. The entire stoichiometric amounts of precursor were initially dissolved in distilled water. The amount of distilled water is 3 equal to the total molar amount of all the precursors, for controlling pH and avoiding precipitation the citric acid was slowly added in drop wise with 60°C of continuous stirring for 6 hrs. At last, the pink colored gel has obtained. The xerogel was pre-calcined at 400°C for 6 hrs, then the black color poly crystalline powder has obtained and grinded with agate mortar. The obtained powder were calcined at 600 °C for 6 hrs in air, cooled at room temperature, and then the annealing process was carried out at 200°C, 400°C and 600°C for 6 hrs in each. The X-ray diffractometry (XRD) with Cu Kα radiation, at 2θ = 10–80°, scanning electron microscopy and FTIR studies were carried out for as-prepared powders.

RESULT AND DISCUSSION

XRD STUDIES

XRD diffractogram of as-synthesized sample (reported) has been taken as reference for the study as it is room temperature. A very short doublet appeared at 31° and 32°, a medium peak around 36° and the doublet one with higher intensity and other one with lesser intensity noted at 42° and 44° and lesser intensity short peak is noted around 62° and prior to 80°, a very shortest peak are noted , as per the literature and with JCPDS index, (fig.1a) the peaks at 42 °and the smallest hump 52° , the peak at 62 °and the near peak at 74° are correspond to CoO [7]. In the present study XRD pattern of as-synthesized (reported) at 30° C has been compared with as-synthesized sample (prepared) at 200° C, 400° C and 600° C. Certain characteristic peaks noted in as-synthesized sample(reported) are not appeared with distinct appearance are noted at 18°as a sharp medium peak , at 36°as a very short peak and very enhanced sharp peak at 44° are noted. While comparing the as-synthesized sample with 200° C annealed sample(prepared), it is found that the new peak appeared near 18° and the peaks found at 36° and 44° (as-synthesized) appeared but change in FWHM and intensity.

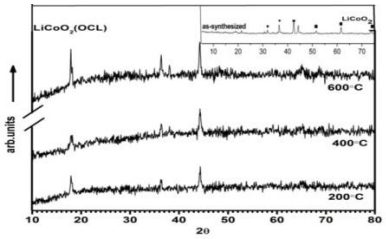

a) XRD pattern of Pristine $LiCoO_2$ for 200 -600 °C

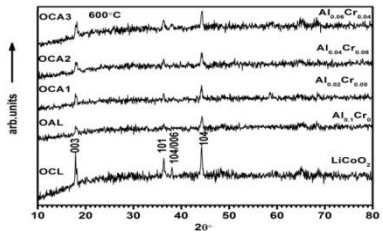

b) XRD pattern of Al doped $LiCoO_2$ at 600 °C

These suggest that some kind of structural orientation has taken place at 200°C. Comparing the XRD pattern of 200° C with the 400° C, the peaks again appeared but change in FWHM and intensity are noted which are higher than that of 200°C particularly the increasing intensity of peak at 44° while observing the 600°C with the reference to 400 °C and 200°C, the drastic increase in intensity corresponds as referred peaks at 200°C and 400°C. Suggest that the higher temperature in this study at 600°C has shown the considerable temperature impact on the as-synthesized sample

particularly Li and Co-O orientation. XRD pattern fig (1b) shows the stoichiometry effect of Al/Cr at 600°C, and which confirmed that the α- $NaFeO_2$ (R-3m) structure with the reference of **JCPDS card no: 89-0912** . The crystalline peaks how it can be distracted for the pristine host $LiCoO_2$ due to the stoichiometry influence has been seen based on their manifestations of them through change in intensity and particularly FWHM either is broaden or narrow. While observing, the 600°C XRD pattern, it could be noted that the doublets at 101 and 102/006 [8-11] have emerged in sample OCA3 suggest that high temperature exfoliates the Li_2Co_3 and Co_3O_4 phases [12-13] referring for orderliness has noted with enriched Al phase and poor Cr phase have been vacillating the structure by the temperature is noteworthy. And the sharpness mitigation of the peak ascribed to (003) is well registered at 2ɵ=18° and such a mitigation. Thus the temperature profusely showed its influence on $LiCoO_2$ sites through their respective stoichiometry.

SEM STUDIES

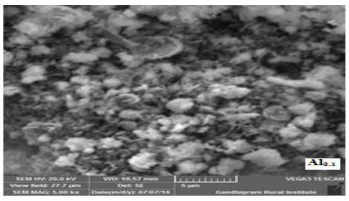

Li $Al_{0.1}Co_{0.9}O_2$

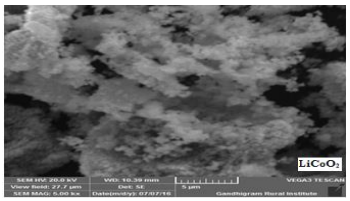

$LiCoO_2$

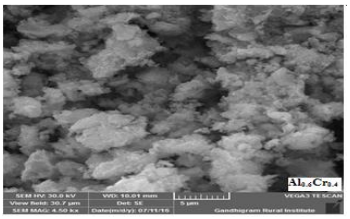

$LiAl_{0.06}Cr_{0.04}Co_{0.9}O_2$

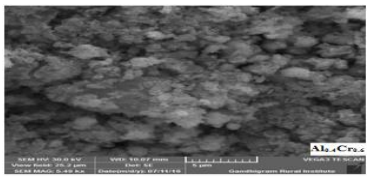

$LiAl_{0.02}Cr_{0.08}Co_{0.9}O_2$

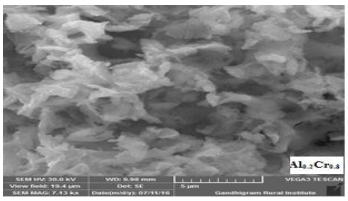

$LiAl_{0.04}Cr_{0.06}Co_{0.9}O_2$

The $LiCoO_2$ has appeared like inhomogeneous dried cotton flakes at 600 ° C. But the Al abruptly changes its dried CoO_2 surface morphology as distorted and appeared as tiny globules conglomerated that Al highly distorts the phasial appearance by localizing their presence (fig.2) With reference to the stoichiometry of further adding Cr brings back the same surface profile has noted in OCL. But it has drastically varied with a strangled spherical globules blended with CoO_2. As per the SEM $Al_{0.04}Cr_{0.06}$ this surface profile appeared as delinked bundles of Flake like appearance when Al rich presence so the stoichiometry of influence of Al and Cr on $LiCoO_2$ have shown a different surface morphology as will be understood.

FTIR STUDIES

The FTIR spectroscopy study has been carried out in order to elucidate the coordination between cations and anions comprising of Li^+ ion and CoO_2 of $LiCoO_2$ layered oxide material. As for the literature some of the IR irrational bands are reported in the wavenumber region 400 Cm^{-1}- 2000 Cm^{-1} , ie., 437 Cm^{-1} (very short) 556 Cm^{-1} (CoO_2), 865 Cm^{-1} (very sharp peak) 1087 Cm^{-1} (shortest peak) and the doublets 1443 Cm^{-1} O-Co-O (asymmetric vibration) and 1506 Cm^{-1} (symmetric vibration) are exactly matches [14]. Further while looking in to 400-700 Cm^{-1} region there are vibration bands

440Cm^{-1}, 560Cm^{-1}, 600Cm^{-1} are assigned to CoO_2 while spanning on the wavenumber region beyond 700 Cm^{-1} - 2000 Cm^{-1} one sharp singlet at 866 Cm^{-1} CoO Rocking vibration followed by 1384 Cm^{-1} O-Co-O in plane bending. While comparing the stoichiometric performance of the binary Al and Cr as shown in fig -3 respectively with increasing Al participation with reference to the corresponding increasing in Cr stoichiometric as labeled as OCA1, OCA2 and OCA3 for 0.02/0.08,0.04/0.06 and 0.06/0.04, vibrational bands have been closely differentiated with the fundamental vibrational modes of $LiCoO_2$ band position as stated earlier.

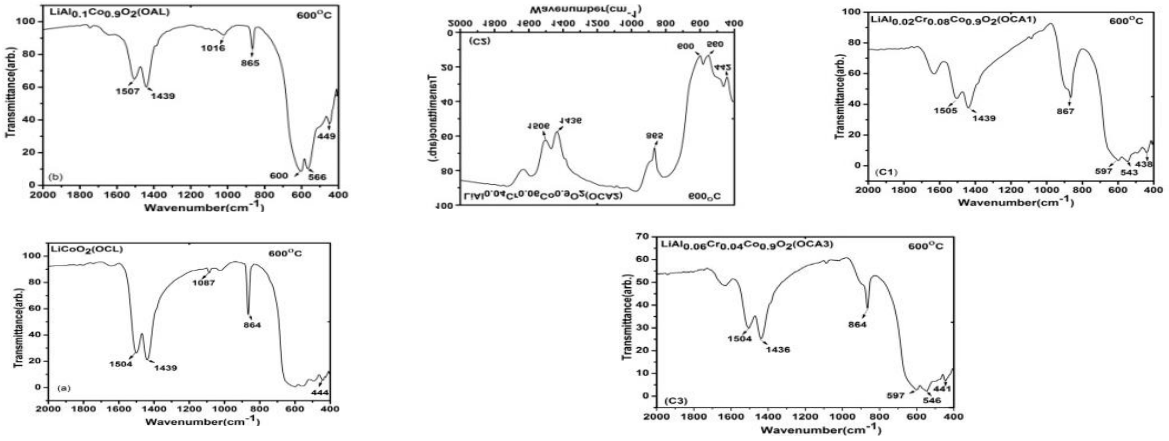

Fig.3:FTIR studies of pristine and doped $LiCoO_2$.

CONCLUSION

- The pristine and AL, Cr doped LiCoO2 have synthesized by sol-gel process.
- XRD revealed that the rhombohedral structure of the as-prepared materials, and the high order of crystallanity is noted at high temperature treated material.
- FTIR confirmed the ligand and base interaction and phase morphology confirmed the inhomogeniety of the flake like surface.

REFERENCE

1. J. M. Tarascon, M. Armand, Nature 414, 359 (2001).
2. C. H. Han, Y. S. Hong, C. M. Park, and K. Kim, J. Power Sources 92, 95 (2001).
3. T. Bak, J. Nowotny, M. Rekas, C. C. Sorrell, and S. Sugihara, Ionics 6, 92 (200).
4. T. Nagaura, K. Tozawa, Prog. Batteries Solar Cells 9 (1990) 209.
5. M. Catti, Phys. Rev. B, 61, 1795 (2000).
6. R. Koksbang, J. Barker, H. Shi, and M. Y. Saidi, Solid State Ionics 84, 1 (1996).
7. M. M. Thackeray, J. Electrochem. Soc. 142, 2558 (1995).
8. L. Predoana, A. Barau, M. Zaharescu, H. Vasilchina, N. Velinova, B. Banov, and A. Momchilov –4–9 Sept. 2004, Sofia, Bulgaria.
9. K. Teshima, S. H. Lee, Y. Mizuno, H. Inagaki, M. Hozumi, K. Kohama, K. Yubuta, T. Shishido, and S. Oishi, Cryst. Growth Design 10, 4471 (2010).
10. S.M. Lala, L.A.Montoro, V. Lemos, M. Abbate, J.M. Rosolen, Electrochim. Acta 51 7(2005).
11. Seung-Taek Myung, Naoaki Kumagai, Shinichi Komaba, Hoon-Taek Chung, Solid State Ionics 139 (2001) 47–56
12. S.M. Lala, L.A.Montoro, V. Lemos, M. Abbate, J.M. Rosolen, Electrochim. Acta 51 (2005) 7.
13. H.Y. Xu, S. Xie, C.P. Zhang, C.H. Chen, J. Power Sources 148 (2005) 90.

GROWTH AND CHARACTERISATION OF PURE AND HIPPURIC ACID DOPED ZINC THIOUREA SULPHATE (ZTS) SINGLE CRYSTAL

M. Selvapandiyan[a], J. Arumugam[b]

[a]*Department of Physics, Periyar University, PG Extension center, Dharmapuri- 636 705*

[b]*Department of Physics, Sri Vidya Mandir Arts & Science College, Uthangarai- 636 902*

Abstract

Zinc tris-thiourea sulphate (ZTS) is promising semiorganic nonlinear optical material in the field of photonics and optoelectronics. Pure and hippuric acid doped Zinc tris thiourea sulphate single crystals were grown from aqueous solution by slow evaporation method at room temperature. The grown crystals are subjected to various characterisations such as single crystal X- ray diffraction studies to know that the crystal structure. Grown crystals have low cut off wavelength it is confirmed by UV- visible absorption studies. The mechanical strength of the grown crystals was tested by Vicker's micro hardness tester. The nonlinear optical property of the grown crystals was confirmed by Kurtz powder technique.

Keywords: Slow evaporation, nonlinear optical material, second harmonic generation, single crystal X-ray diffraction, micro hardness.

1. Introduction

Nonlinear optics is playing a major role in the emerging photonics and optoelectronics technologies. New non linear optical frequency conversion materials have a significant impact on laser technology, optical communication and data storage.Recent interest in quantum electronics has centered on finding a new materials for efficient second harmonic generation[1-2]. Due to poor mechanical and thermal properties most of the organic materials are susceptible to damage, hence in last several years many researchers mainly concentrated on new types of NLO materials which combine the advantages of organic and inorganic materials called semiorganic materials.The organic materials exhibit high nonlinearity compared to inorganic material. A close literature survey shows that the various amino acids exhibit enhanced NLO properties[3]. Hence in this present study an attempt has been made to grow pure and dopedZinc-tris thiourea sulphate crystal (ZTS). ZTS crystal having 1.2 times more nonlinear than that of KDP and ZTS possesses orthorhombic structure with $Pca2_1$ space group [4].In the present work hippuric acid was added in molar percent in saturated ZTS solution to enhance second harmonic generation property.

2. Experimental

The Zinc tris-thiourea sulphate salt was synthesised by dissolving high purity AR grade zinc sulphate and thiourea in molar ratio 1:3[5] in deionized water. The solution was stirred by magnetic stirrer. White crystalline ZTS salt was obtained immediately.

$$ZnSO_4 .10H_2O + 3[CS(NH_2)_2] \longrightarrow Zn[CS(NH_2)_2]_3 SO_4 \quad [1]$$

The salt was purified by repeated recrystallization. Then the saturated solution of ZTS was prepared at room temperature and then filtered by whattman filter paper. The obtained saturated ZTS solution was kept in a glass vessel covered with polythene paper for slow evaporation. The good quality transparent ZTS crystal was harvested at the end of 10 days. The saturated homogeneous pure ZTS solution was kept in a beaker and then 1 mol % of hippuric acid solution was added to the ZTS solution and same procedure was followed as in case of pure ZTS crystal. After 20 days, optical good

quality of transparent crystals were harvested. Fig. 1 and 2 shows that the photograph of as grown pure and 1 mol % hippuric acid doped ZTS single crystals.

Fig.1 As grown pure ZTS single crystal

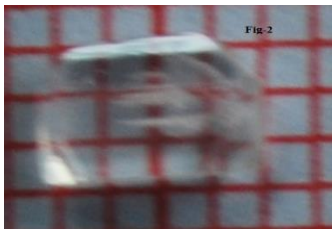

Fig.2 As grown hippuric acid doped ZTS single crystal

3. Result and discussion

3.1 Single crystal X-ray diffraction analysis

Single crystal X- ray diffraction analysis of grown pure and hippuric acid doped ZTS single crystal was carried out using Enraf Nonius CAD4 X-ray diffractometer with Mokα radiation of wavelength of 0.71073 Å. The obtained lattice parameter values and volume of grown crystals are tabulated in Table-1.The grown pure and hippuric aciddoped ZTS crystals belong to orthorhombiccrystal system[5].

Table-1 Lattice parameters of pure and 1 mol % hippuric acid dopedZTS single crystals

Grown crystal	**a (Å)**	**b (Å)**	**c (Å)**	**V ($Å^3$)**
Pure ZTS	11.166	7.792	15.491	1347.8
1 mol % hippuric acid doped ZTS	11.131	7.791	15.485	1343.0

3.2 UV- visible spectral analysis

The UV- visible absorption studies of pure and 1mol % hippuric acid doped ZTS single crystals were carried out by using Lambda 35 model. UV-visible spectrometer in the range of 190 to 1100 nm. The optical absorption spectra of grown pure and hippuric aciddoped ZTS single crystals shown in fig.3. From the spectra, it is evident that the grown crystals have low UV cut-off wavelengths about 279nm and 296 nm along with a large transmission window in the entire visible region [7]. The optical band gap of the grown crystals was determined from the absorption spectra using the relation $E_g=hc/\lambda$, where h is Planck's constant, c is speed of light and λ is the wavelength. The calculated band gap of the grown pure and hippuric acid dopedZTS single crystals are 4.4eV and 4.1 eV from this band gap results the grown pure and hippuric acid dopedZTS crystals belongs to the insulating material [7].

3.3 Micro hardness Studies

The mechanical behavior of the grownpure and hippuric acid doped ZTS single crystalswas analysed by using Vicker's microhardness tester HMV-2T model.The hardness values of grown crystals were measured by applying different loads like 25 gm, 50gm, and 100gm. This is shows that the hardness values of grown crystal are increased with increasing of load. The graph was plotted between load P and hardness number (Hv) which is a straight line (Fig.4). If we increase the load beyond 100 gm the crystal will be breaked. The graph is also plotted between log P and log d and is

also a straight line (Fig.5). The slope of the straight line gives the work hardening co-efficient (n) value. The calculated work hardening coefficient of pure and hippuric aciddoped ZTS crystals are 2.5 and 2.2[8]. The obtained values of n confirmed that the grown both pure and hippuric aciddoped ZTS single crystals belong to categories of soft in nature.

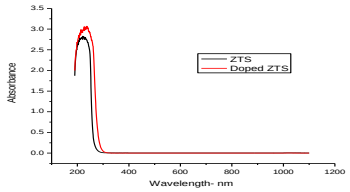

Fig 3. Optical Absorption spectra of pure and 1 mol % hippuric acid doped ZTS crystals

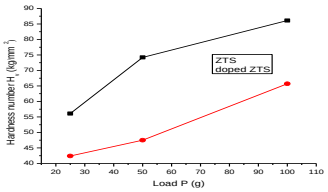

Fig.4 Load Vs Hardness number for pure and doped ZTS single crystals

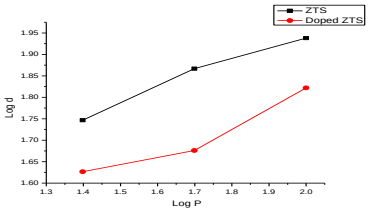

Fig.5 Log P Vs Log d for pure and doped ZTS single crystals

3.4 SHG test

The second harmonic generation studies of the grown crystals were carried out by using Kurtz powder technique. The grown pure and hippuric acid doped ZTS crystals were illuminated using Q – switched Nd-YAG laser with wavelength of 1064 nm as a input and power input as 0.70J.The NLO property of the sample was confirmed by the sample was emission of bright green radiation as output with wavelength of 532 nm. The relative second harmonic generation efficiency of the both pure and hippuric acid doped materials was calculated which are around 1.2 and 1.23 times higher than that of KDP [9-10]. These results confirmed that the grown materials are well suitable one for nonlinear optical applications.

4. Conclusion

Optical quality single crystals of pure and hippuric acid doped ZTS crystals were grown by slow evaporation technique. Single crystal X ray diffraction confirms that there is no change in basic structure of ZTS while doping. The unit cell parameters show that the grown crystals are belong to orthorhombic structure.The UV-Vis-NIR absorption spectra of the grown pure and hippuric acid doped crystals shows that the crystals have lower cut-off wavelengths less than 300 nm.The calculated work hardening coefficient of pure and hippuric aciddoped ZTS crystals are 2.5 and 2.2. The obtained values of n confirmed that the growncrystals belong to categories of soft in nature. The relative second harmonic generation efficiency of the both pure and doped materials wascalculated which are around 1.2 and 1.23 times higher than that of KDP.

References

[1] A.S. Haja Hameed, G.Ravi, P.Ramasamy, J.Cryst.Growth 212 (2000) 227-232
[2] S.Selvakumar, S.M.Ravikumar, G.P.Joseph, K.Rajarajan, J.Madhavan, S.A. Rajasekar, P.Sagayaraj, Mater.Chem.Phys.103 (2007) 153
[3] P.M.Ushasree, R.Jayavel, C.Subramanian, P.Ramasamy, J.Cryst.Growth 197 (1999) 216
[4] K.Kanagasabapathy, R.Rajasekaran, Opt. 124 (2013) 4240
[5] M.Selvapandiyan, J.Arumugam. P.Sundramoorthi, S.Sudhakar, J. Alloys and Comp. 580 (2013) 270
[6] C.Krishnan, P.Selvarajan, T.Freeda Materials Letters 62 (2008) 4414
[7] N.R.Dhumane, S.S.Hussaini.V.G.Dongre, M.D.Shirsat, Opt.Mater. 3(2008) 328-332
[8] E.M. Onitsch, Strain rate dependence of the hardness of glass and Meyer's Law, Mikroskopie 2 (1947) 131
[9] S.K.Kurtz, T.T.Perry, J.Apply. Phys 39 (1968) 3798-3813
[10] M.Selvapandiyan, J.Arumugam. P.Sundramoorthi, S.Sudhakar, J. Alloys and Comp. 558 (2013) 34.

STRUCTURAL AND OPTICAL PROPERTIES OF THIN FILMS GROWN BY SILAR TECHNIQUE

Balaji R and Seenuvasakumaran Perumal

PG and Research Department of Physics,Muthurangam Government Arts College (Auto) Vellore-02

ABSTRACT

Nanostructured thin films have engrossed the research community all over the world. This is because of the properties of thin films are quite different from the bulk materials and they show impending application in semiconductor industry, microelectronic devices, telecommunication devices, optical coatings, sensors, photo conductors, catalysts and IR detectors etc. Successive Ionic Layer Adsorption and Reaction (SILAR) technique is well suited for producing large area deposition and multilayer thin films especially for solar cell like Dipping time, precursor concentration and number of process cycle. In the present investigation lead Sulphide (PbS), cadmium and strontium doped PbS thin films are deposited on a glass substrate by SILAR process at room temperature to study the various structural and optical properties of them. The crystalline nature of the nanofilms is confirmed from X-ray diffraction analysis and they exhibit tetragonal structure. From Scherer formula the average particle size is found to be 18nm to 30nm. The lattice parameters, strain (ε and dislocation density (δ of the materials are also calculated from XRD data. The different molecular vibrations are confirmed through FTIR vibrational spectra. From the UV-VIS spectroscopic data using the Tauc relation the energy gap (*Eg*) at the edge of absorbance band is calculated as 2.53eV, 2.15eV and 2.33eV for PbS, PbCdS and PbSrS respectively. The refractive index (*n*) and thickness of the thin films are calculated by using Swanpoel method. The morphological studies are done through SEM microscope.

I.INTRODUCTION

Thin films studies have advanced in many new areas of research in solid state physics because of it's uniquely characteristics of the thickness, geometry and structure of the thin films [1]. In the last few years, nano crystalline thin film materials find significant interest due to their various applications. Lead Sulphide (PbS) is an important direct band gap semiconductor material with a narrow band gap of 0.4 eV at 300K and a relatively large excitation Bohr radius of 18nm [2] . Due to their suitable band gaps, PbS thin films are extensively used in infrared detection application [3], photography [4], Pb^{2+} ion selective sensors [5], and solar absorption [6]. In addition, PbS has been utilized as photo resistors, diode lasers, humidity & temperature sensors, decorative and solar control coatings [6, 7]. These applications depends on selection of materials, mostly from II and IV semiconductors such as Sr, Ba, and Cd. These properties have been correlated with the growth conditions and the nature of the substrate. High quality thin films are produced by different techniques such as electro deposition[8], spray Pyrolysis[9], microwave heating[10] and chemical bath deposition[11], Successive Ionic Layer Adsorption And Reaction (SILAR)[12] etc.

Successive Ionic Layer Adsorption and Reaction (SILAR) is a simplest method to produce larger area deposition, easy control of thin film thickness, economically inexpensive and capable of yielding good quality thin films. In the present work PbS, Cd doped Lead Sulphide (PbCdS) and Sr doped Lead Sulphide (PbSrS) are synthesized by SILAR [12] Method at room temperature under atmospheric pressure. First time an attempt is made for preparation of these thin films (PbS, PbCdS and PbSrS) has been attempted for the improvement of IR detective sensor performance and

optoelectronic device applications. The coated thin films properties are studied various different types of characterization techniques are reported below.

II. MATERIALS AND METHODS

(a) Cleaning of the substrate:

The microscope glass slides of the dimension 75mm X 25mm X 1.35mm substrate was cleaned as in the following steps (1) Boiling in concentrated chromic acid for 1 Hour, (2) Rinsed with acetone for 10 Minutes (3) Rinsed with double Deionized water for few seconds (4) Dry the substrate for few seconds in air[13].

(b) Deposition of thin films:

Lead nitrate ($Pb(NO_3)_2.\ 4H_2O$), Cadmium nitrate ($Cd(NO_3)_2.\ 4H_2O$) and Strontium chloride ($SrCl_2$) are taken as a cationic precursors. The Sodium Sulphide ($Na_2S.\ XH_2O$) is taken as anionic precursor. The Cationic and Anionic precursors are taken with definite molar ratio of 1:1. The cleaned substrates are used to deposit the desired thin films with SILAR technique of predetermined program for deposition, rinsing and drying time.

Reaction mechanism,

The reaction mechanism observed to be [14],

$$Pb(NO_3)_2.4H_2O + H_2O \longrightarrow Pb^{2+} + 2NO_2 + 5H_2O + O_2 \quad (1)$$
$$Cd(NO_3)_2.4H_2O + H_2O \longrightarrow Cd^{2+} + 2NO_2 + 5H_2O + O_2 \quad (2)$$
$$SrCl_2.6H_2O + H_2O \longrightarrow Sr^{2+} + Cl_2 + 7H_2O \quad (3)$$
$$Na_2S + H_2O \longrightarrow S^{2-} + SH^- + OH^- \quad (4)$$
$$Pb^{2+} + Cd^{2+} \longrightarrow Pb^{2+}Cd^{2+} \quad (5)$$
$$Pb^{2+} + Sr^{2+} \longrightarrow Pb^{2+}Sr^{2+} \quad (6)$$
$$Pb^{2+} + S^{2-} \longrightarrow PbS \quad (7)$$
$$Pb^{2+}Cd^{2+} + 2\,S^{2-} \longrightarrow PbCdS_2 \quad (8)$$
$$Pb^{2+}Sr^{2+} + 2\,S^{2-} \longrightarrow PbSrS_2 \quad (9)$$

The deposited films are calcinated at 120^0C to remove impurities of any. The deposited thin films are subjected to different characterization.

III. RESULT AND DISCUSSION

A. Structural Characterization

The deposited PbS, Sr doped PbS and Cd doped PbS thin films are analyzed using X-Ray Diffraction technique. The broadened peak in XRD indicates that the synthesized thin

films has very small crystalline size they exhibit tetragonal structure for all deposited thin films (PbS, $PbCdS_2$ and $PbSrS_2$). Using XRD data the average particle size [15] and Dislocation Density [16] are calculated from below Debye- Scherrer formula. The Strain [17] are found using Williamson- Hall plot, they are tabulated. $D = k\,\lambda/\beta\cos\theta$ (10)

Where k is a constant taken to be 0.94, D is average particle size, λ wavelength of X-ray source (λ= 1.5418), β full width half maximum, θ diffraction angle.

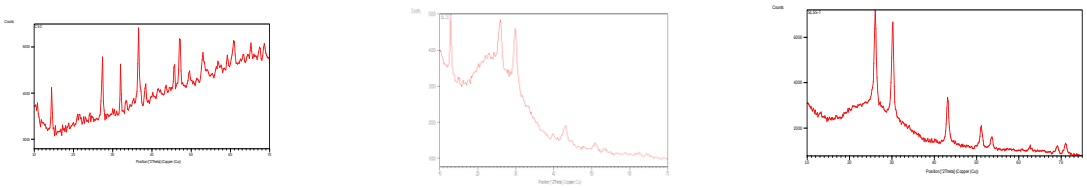

Fig.1 XRD analysis of PbS, $PbCdS_2$ and $PbSrS_2$ thin films

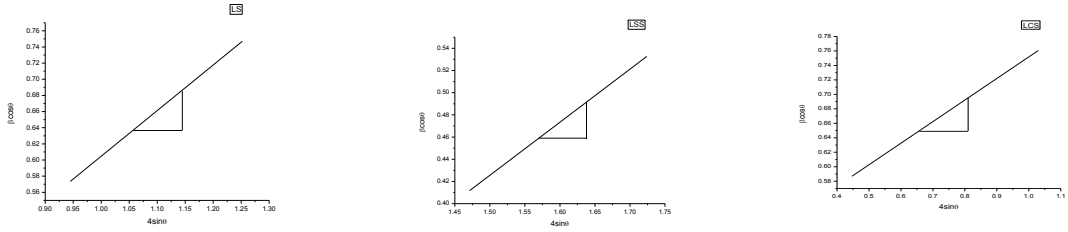

Fig.2 Williamson-Hall plot for PbS, $PbCdS_2$ and $PbSrS_2$

TABLE 1

S. No	PROPERTIES	PbS	Cd doped PbS	Sr doped PbS
1.	Crystal structure	Tetragonal	Tetragonal	Tetragonal
2.	Lattice parameters	a=4.437Å b=4.437Å c=24.48Å	a=13.815Å b=13.815Å c=4.79Å	a=11.867Å b=11.867Å c=4.476Å
3.	Particle size (D)	18nm	18nm	24nm
4.	Strain (ε)	0.3012	0.2269	0.2000
5.	Dislocation density (δ	$2.832X10^{-17}m^{-2}$	$2.935X10^{-17}m^{-2}$	$1.684X10^{-17}m^{-2}$
6.	Volume	$482.75m^3$	$914.27m^3$	$630.36m^3$

B. Fourier transforms infrared spectroscopy (FTIR)

FTIR is a powerful tool for identifying types of chemical bonds in a molecule by producing an infrared absorption spectrum. The FTIR spectra are recorded in region of 400 - 4000 cm^{-1}. The various transmittance peaks of deposited thin films as shown in the fig.2 which reveals the conformation analysis of functional groups and metal sulphide groups.

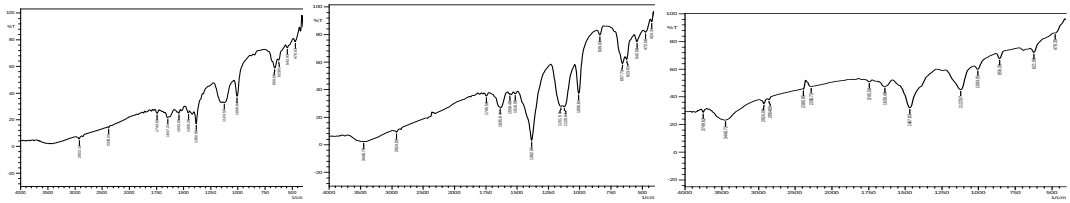

Fig.2 FTIR vibrational spectra of PbS, PbCdS and PbSrS thin films

The transmittance peaks at the observed frequencies $470cm^{-1}$, $424cm^{-1}$ and $478cm^{-1}$ for PbS, $PbCdS_2$ and $PbSrS_2$ exhibits the presence of metal groups. The frequencies $623cm^{-1}$, $621.08cm^{-1}$, $621.01cm^{-1}$, $839cm^{-1}$ and $856cm^{-1}$ are conform the Sulphide groups presence in the region [18]. The stretching vibration of Cd-S is observed $659cm^{-1}$[19]. The well defined S=O stretching vibrations are presence in the region of $1554cm^{-1}$, $1543cm^{-1}$[20]. The strong O-H stretching vibration $2922cm^{-1}$ and $2924cm^{-1}$ are present in the deposited thin films respectively.

C. Optical study

The UV-VIS absorbance spectra are recorded in the range of 200-800 nm. The study of optical absorption is to calculate the cutoff wavelength (λ), absorption co-efficient (α) and energy band gap (*Eg*) of semiconductors. The cutoff wavelengths are calculated for PbS, $PbCdS_2$ and $PbSrS_2$ are shown in below figure 3.

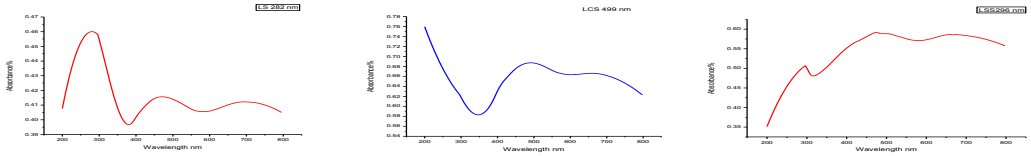

Fig.3(a) for PbS Fig.3(b) for $PbCdS_2$ Fig.3c absorption spectra $PbSrS_2$

From Fig.3a and 3b shows the PbS and $PbCdS_2$ thin film exhibit the less absorption in the range of 290-800nm respectively. Fig.3c PbSrS molecules more absorption in visible region comparing with other deposited films. The variation of the optical absorption coefficient with wavelength is analyzed to find out the nature of the electronic transition across the optical band gap (*Eg*). The nature of the transition is determined by using the Tauc relation,

$$\alpha h\nu = B(h\nu - Eg)^n \qquad (13)$$

Where *B* is a constant, *h* is the planks constant, *v* is the frequency of incident photon and n half integer for direct band gap and integer values for indirect band gap. Band gap energy of PbS, Cd and Sr doped PbS thin films obtained from $(\alpha h\nu)^n$ *vs. hv* graph as shown in below Fig.4.

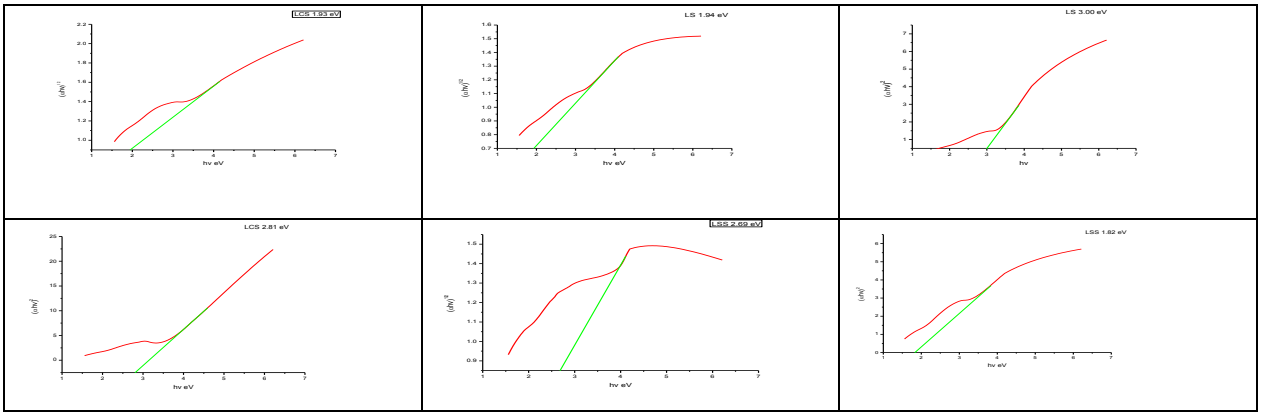

Fig.4 Tauc plot for the deposited PbS, $PbCdS_2$ and $PbCdS_2$ thin films

The thin films extrapolating the straight line of $(\alpha h\nu)1/2$ *vs. hv* curve intercept the horizontal h*v* axis as show in above figure. It can be seen that the direct band gap of the films determined as 1.94eV, 1.93eV and 2.69eV for PbS, $PbCdS_2$and $PbCdS_2$ respectively. The high values of band gap can be attributed to the quantum confinement effect, due to small grain size in nanocrystalline thin films [21, 22]. For $(\alpha h\nu)^2$ *vs. hv* curve the straight line nature of the plots over a wide range of photon energy suggested allowed indirect type of transition. It was found that the optical band gap to be about 3.00eV, 2.81eV and 1.82eV for thin films PbS, $PbCdS_2$ and $PbSrS_2$ respectively. So they are widely used in the fields of optoelectronic devices in IR region and solar cell applications.

The refractive index (n) and thickness (d) of a thin film can be calculated from a simple transmittance spectrum using the Swanpoel method [23]. According to Swanpoel method, the

refractive index (n) of the deposited thin films is 2.043, 1.960 and 1.880 for PbS, $PbCdS_2$ and $PbSrS_2$ respectively. Calculated thin film thickness is 0.00234μm for PbS, 0.00202 μm for $PbCdS_2$ and 0.00230 μm for $PbSrS_2$. Thickness of the films are plays a major role in yielding good quality thin films.

IV CONCLUSION

Thin films of Lead Sulphide (PbS), Cadmium doped PbS and Strontium doped PbS were prepared on glass substrate at room temperature under atmospheric pressure by SILAR method. XRD results show that the obtained films have tetragonal structure. From the XRD data the lattice parameters, the average particle size of PbS, $PbCdS_2$ and $PbSrS_2$ are 18nm, 18nm & 24nm and Strain (ε) is found to be 0.3012, 0.2269 and 0.2000 respectively. The dislocation densities (δ have been calculated 2.832X$10^{-17}$$m^{-2}$ for PbS, 2.935X$10^{-17}$$m^{-2}$ for $PbCdS_2$ and 1.684X$10^{-17}$$m^{-2}$ for $PbSrS_2$ thin films. FTIR vibrational spectra shows different types of functional groups are present in the deposited thin films are verified. Optical properties of the thin films are studied by UV-Visible spectroscopy. The optical band gap (*Eg*) was found 1.94 eV, 2.69 eV and 1.93eV from Tauc relation. So this band gap (*Eg*) materials are widely used in IR detection sensors and Solar cell applications because of low cost of precursor and good quality, large area deposition is possible.

Reference

1. A.R. West , 'Solid State Chemistry' John Willey & Sons, Singapore
2. P. Gadenne, Y. Yagil, G. Deutcher, J. Appl. Phys. 66 (1989) 3019.
3. P.K. Nair, O. Gomezdaza, M.T.S. Nair, Adv. Mater. Opt. Electron.1 (1992) 139
4. H. Hirata, K. Higashiyama, Bull. Chem. Soc. Jpn. 44 (1971) 2420.
5. T.K. Chaudhuri, S. Chatterjes, Proceedings of the International Conference on Thermoelectronics, Vol. 11, 1992, p. 40
6. P. K. Nair, V.M. Garcia, A.B. Hernandez, M.T.S. Nair, Nair, J. Phys. D: Appl. Phys. 24 (1991) 1466-1472.
7. Ileana pop, Cristina Nacasu, Violeta Ionescu, E.Indrea, I. Bratu, Thin Solid Films 307 (1997) 240-244.
8. Maheswar Sharon,K.S. Ramaiah, Mukul Kumar, M. Neumann Spallart, C. Levy- clement, Electroanal. Chem. 436 (1997) 49-52.
9. B. Thangaraju, P. Kaliannan, Semicond. Sci. Technol. 15 (2000) 849-853.
10. Yonghong, Ni, Fei Wang, Hongjiang Liu, Gui Yin, Jianming Hong, Xiang Ma, Zheng Xu, Growth 262 (2004) 399-402
11. Cristina Nacasu, Valentina Vomir, Ileana Pop, Violeta Ionescu, Rodica Grecu, Mater. Sci. Eng. B 41 (1991) 235-240.
12. S Lindross, J Puiso, S Tamulevicius and M Leskela *Solid state Phenom*. 99-100 (2004).
13. P. Gadenne, Y. Yagil, G. Deutscher, J. Appl. Phys. **66,** 3019 (1989)
14. Ramphal sharma, *Adv. Apply. Sci. Res*., 2011, 2(4): 417-425.
15. A.U. Ubale, D.K. Kulkarni, *Indian J. Pure Appl. Phys 44, 254 (2006)*
16. Theivasanthi T and Alagar M, *Int. J. Of the phys. Sci.,* 2011, 3726, 6 (15)
17. T Banarjee M. Chongad L. And Sharma A. *Research journal of recent sciences* Vol.2(ISC-2012), 326-329 (2013)
18. Silverstein, Basster and Morril, '*spectrometric identification of organic compounds*', John wiley and sons, USA, 91 (1991)
19. Jag Mohan, *Organic spectroscopy*, Narosa publishing house, 61-62 (2000).
20. A. Sabah, S.A. Siddiqi, and S. Ali, 'world academy of science, and engineering and technology', Vol.70, pp, 82-89 (2010).
21. S. Kaci, A. Keffous, L. Guerbous, M. Trari, T*hin solid films* 520, 79 (2011).
22. S. Kaci, A. Keffous, M.Trari, H. Menari, A.Manseri, J.Alloys comp. 496, 628 (2010).
23. R. Swanapoel, J. Phys. E: Sci.Instr, 16, 1214 (1983).

SECOND HARMANONIC GENERATION OF DYE DOPED ZTS CRYSTALS FOR LASER APPLICATIONS

G.SURESH[1], M.LENIN[1], P.DAMODARAN [1] , P.AMBALAVANAN [2] & P.KUMARESAN[1*]

[1]P.G & Research Department of Physics, Thiru.A.Govindasamy Government Arts College, Tindivanam - 604 002.

[2] P.G &Research Department of Physics, Arignar Anna Government Arts College, Villupuram-605 602

e-mail : logeshkumaresan@yahoo.com

Abstract

Zinc Thiourea Sulphate (ZTS), crystal is an excellent metal organic compound, which combines the advantages of both organic and inorganic materials when compared with other conventional non-linear optical materials, and therefore can be used in a wider range of applications. Recent efforts at producing new frequency conversion materials have focused primarily on increasing the magnitude of the NLO properties that can frequency double low peak power sources, such as diode lasers. The UV – Vis spectral studies were carried out using double beam spectrometer in the range 100–1200 nm. The thermo gravimetric analysis (TGA) and differential thermal analysis (DTA) were carried out using Seiko thermal analyzer at heating rate 20°C/min in air to determine the thermal stability of the compound. ZTS crystals were grown by slow cooling technique.The growth rate of ZTS crystals for different pH values has been discussed. This enables the growth of bulk crystals along all the three directions at an optimum pH. FTIR studies show that in the spectra of ZTS there is a shift in the frequency band in the low-frequency region which reveals that thiourea forms sulfur-to-zinc bonds in the ZTS crystal. The growth experiment in large scale with this optimized pH values is expected to yield bulk crystals suitable for laser fusion experiments and SHG device application.

1. INTRODUCTION

Non-linear optical (NLO) materials have a significant impact on laser technology, optical communication, optical storage technology and electro optic modulation. The search for new frequency conversion materials over the past decade has led to the discovery of many semi organic materials. These materials posses large nonlinearity, high resistance laser induced damage and low angular sensitivity. The semi organic NLO materials gain importance over organic and inorganic NLO materials because of their large polarizability and wide transmission window. Extensive investigation in this direction resulted in the discovery of a new phase match inorganic material like ZTS crystals.

2. EXPERIMENTAL PROCEDURE

2.1 Crystal Growth

Pure ZTS crystals were grown from aqueous solution by slow evaporation and also by slow cooling method (0.5^0 C/Day). The same method is followed for doped Thiourea crystals (0.1 mole % of Xylenol Orange). The solubility of doped ZTS in the solvent was measured for each dopant, it was found to be 31.5-gms/100 ml at 42^oC for Xylenol Orange. The seed crystals are prepared at low temperature by spontaneous nucleation. The seed crystals (Fig. 1) with perfect shape and free from macro defects were used for growth experiments. Large single crystals of ZTS and doped ZTS were grown using constant temperature bath (CTB) controlled with an accuracy of 0.01^0C. The mother solution was saturated with the initial pH value, 4.2 for Xylenol Orange. The growth was carried out for more than 22 days by keeping the bath at a temperature of 39^0C.

Figure 1. Xylenol Orange doped ZTS Crystal

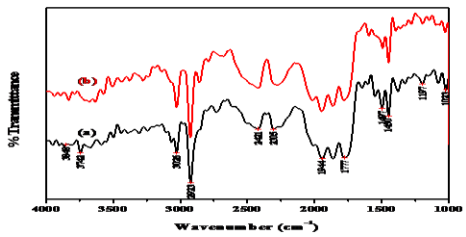

Figure 2. FT-IR spectra of (a) pure and (b) Xylenol Orange doped ZTS crystal

2.2 FT-IR Analysis

The FT-IR spectrum was recorded between 1000 cm^{-1} and 4000 cm^{-1}, using BRUKER IFS 66V FT-IR spectrometer. The FT-IR Spectra of both the pure and doped ZTS crystals are shown in Figure 2. The FT-IR spectra of pure and doped ZTS appear almost similar to each other. N-H stretching frequencies of amino group are found between 3026cm^{-1} and 2923 cm^{-1} for both pure and doped crystals. Both the pure and doped compounds show absorption at 1620 cm^{-1} indicating the presence of primary amino group. The characteristic absorption for the -NH group in the aromatic ring is observed at 2421 cm^{-1} for ZTS. The broad absorption around 3000 cm^{-1} indicates the co presence of C=O stretching and O-H stretching.

The FT-IR spectra of both the pure and doped ZTS confirm the structural aspects. Doping of metal ion into the crystal lattices does not show any significance change in absorption pattern. Some of the absorptions show a marked difference in percentage transmittance. The percentage change of transmittance especially, at 950 cm^{-1} and 690 cm^{-1} are worth noting. It is inferred that the metal ion, form weak linkages in the interstices of the corresponding crystals.

2.3 MICROHARDNESS STUDIES

Microhardness is one of the important mechanical properties of the ZTS crystals. It can be suitably used to measure the plastic properties and strength of a material. Microhardness measurements were carried out using Leitz Weitzler hardness tester fitted with a diamond indenter(Fig.3). The well-polished doped ZTS crystal was placed on the platform of the Vickers micro hardness tester and the loads of different magnitudes were applied over a tester at a fixed interval of time. The indentation time was kept as 8 sec for all the loads. The microhardness value was calculated using the relation $H_v = 1.8544 \text{ X } P/d^2$ kg/mm^2, where P is the applied load in kg and d is the diagonal length of the indentation impression in mm. Dye doping improves the mechanical strength of ZTS.

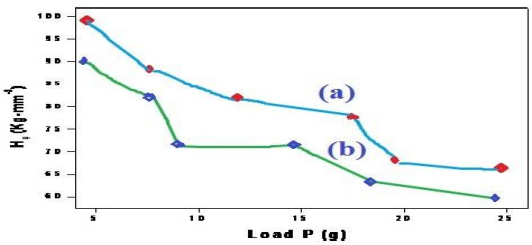

Figure3. Microhardness studies of (a) Xylenol Orange doped ZTS and (b) Pure ZTS crystals

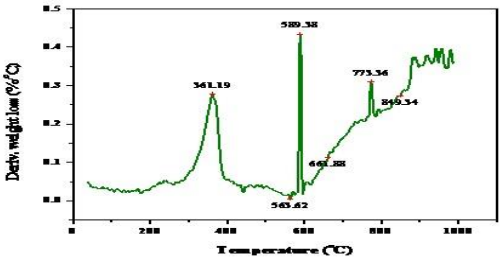

Figure 4. TGA curves of Xylenol Orange doped ZTS Crystal

2.4 THERMAL STUDIES

Figure 4. illustrates the Differential Thermal Analysis (DTA) and Thermo-Gravimetric Analysis (TGA) curves for the grown Coumarine doped ZTS crystal. The DTA curve implies that the material undergoes an irreversible endothermic transition at 200°C where the melting begins. This peak was endothermic peak, represents the temperature at which the melting terminates which corresponds to its melting point at 210°C. Ideally, the melting point of the trace corresponds to a vertical line. The sharpness of the endothermic peak shows good degree of crystallinity of the grown ingot. The exothermic peak at 290°C indicates a phase change from liquid to vapour state as evident from the loss of weight of about 87% in TG curve.

CONCLUSION

The dye doped GLS crystals are used for the generation of second harmonics of Nd-based near-infrared solid-state lasers. The fundamental of an Nd:YAG laser (1064 nm) can be converted to 532 nm of second harmonic or its 355 nm of third harmonic or its 266 nm of fourth harmonic by using ZTS crystals. In order to confirm the suitability of the doped GLS crystal, the non-linear application, harmonic generation was tested using the Nd-YAG laser. A small crystal was placed on the sample holder and the YAG laser beam was made to pass through the crystal and the output conversion of input as green light SHG was analyzed. The efficiency of doped ZTS crystals were compared with pure ZTS and also show that dye doped ZTS crystal has higher efficiency. A sample of ZTS, also powdered was used for the same experiment as a reference material in the SHG measurement. It was found that the frequency doubling efficiency of the doped ZTS was better than KDP.

ACKNOWLEDGEMENT

We gratefully acknowledge financial supports from the Department of Science & Technology-Science and Engineering Research Board **[**Dr.P.Kumaresan, Young Scientist Award, DST-SERB-FAST TRACK, PS-20/2009(SR)] and University Grants Commission- [Dr.P.Kumaresan, Major Research Scheme-F.No.38-18/2009 (SR)], New Delhi, India

REFERENCES

[1] V. Venkataramanan, G. Dhanaraj, V. K. Wadhawan, J. N. Sherwood, and H. L. Bhat, J. Cryst. Growth 154, 92(1995).
[2] A. V. Alex and J. Philip, J. Appl. Phys. 90, 720 (2001)
[3] K. Vasantha and S. Dhanuskodi, Spectrochemica Acta Part A 58, 311 (2002).
[4] S. Selvasekarapandian, K. Vivekanandian, P. Kolandaivel, and T. K. Gundurao, Cryst. Res. Technol. 32, 299(1997).
[5] R. M. Silverstein, G. Clayton Basseler, and T. C. Morrill, Spectrometric Identification of Organic Compounds, VEdn.John Wiley & Sons, Inc. New York 1998.
[6] H. O. Marcy, M. J. Rosker, L. F. Warren, P. H. Cunningham, C. A. Thomas, L. A. Deloach, S. P. Velsko, C. A. Ebbers, J. H. Liao, and M. G. Kanatzidis, Opt. Lett. 20, 252 (1995).
[7] N. J. Long, Angew. Chem. 34, 21 (1995).

SOL- GEL ROUTE TO ANATASE TiO_2 NANO POWDER AND ITS CHARACTERIZATION

V. Maria Vinosel*, M. Asisi Janifer, A.Persis Amaliya, S. Pauline

Department of Physics, Loyola College, University of Madras, Chennai – 34, India

**Corresponding author: vinovincent90@gmail.com*

Abstract

Titanium dioxide (TiO_2) nanoparticles were synthesized by Sol-Gel route using Titanium Tetraisopropoxide (TTIP) as the precursor. The synthesized product was characterized by Powder X-Ray diffraction. The X-Ray diffraction pattern indicates the presence of pure crystalline anatase phase of TiO_2. The microstructure and phase composition were analyzed by High Resolution Scanning Electron Microscope (HR-SEM) and Energy Dispersive X-ray Analysis (EDAX). Fourier Transform Infrared Spectroscopy (FTIR) spectra showed the vibrational bands of Ti-O metal oxygen bonds. From Ultraviolet visible (UV-Vis) spectra the optical properties of TiO_2 were studied.

Keywords: TiO_2, XRD, SEM, FTIR, UV-Vis.

INTRODUCTION

Titanium dioxide (TiO_2) exists in three different phases, i.e., anatase, rutile, and Brookite. Anatase and rutile are the active crystallite phases of titanium dioxide [1]. TiO_2 is the promising material as semiconductor having high photochemical stability with low cost. Titania nanoparticles with very fine sizes are promising in many applications such as pigments, adsorbents, catalytic supports, paints, toothpaste, UV protection, photocatalysis, photovoltaics, electrochromics, and photochromics [2]. TiO_2 has been studied extensively as photocatalyst to deal with environmental pollutions such as water purification, wastewater treatment, hazardous waste control and air purification. Photocatalytic oxidation reactions are initiated when a photon of higher energy level or equal to the band gap energy is absorbed by a TiO_2 catalyst promoting an electron (e^-) from the valence band to the conduction band with simultaneous generation of a positive hole (h+) in the valence band [3]. The enhancement of optical properties of TiO_2 has been the center of study in the recent years. The use of large surface area semiconductor materials in dye sensitized solar cells (DSSC) is necessary to provide sufficient light absorption and charge separations which are the two critical stages in the solar electric energy conversion [4]. TiO_2 can be synthesized by various techniques such as chemical precipitation, chemical vapour deposition, sol-gel technique, micro emulsion method, spray deposition, hydrothermal method and solvothermal method. Among these sol-gel technique is a simple method to synthesis TiO_2 nanoparticles. The sol-gel synthesis of metal oxides offers advantages such as high purity, good homogeneity, and low processing temperature [5].

In the current study, a simple Sol-gel route is used for the synthesis of TiO_2 nanoparticles, which are analyzed for their crystallinity, crystallite size, band gap and structural properties.

EXPERIMENTAL PROCEDURE

Stotaw Talbachew Hayle et al [2] have reported Sol-gel method to prepare highly crystalline phase of anatase TiO_2 for different calcination temperatures. Here also TiO_2 nanopowder was prepared by Sol-gel route. The synthesized product TiO_2 was obtained from Titanium (IV) isopropoxide (TTIP) and Isopropyl alcohol as precursors. In a typical process, 100 ml of isopropyl alcohol was added to 15 ml of TTIP. The whole mixture was stirred for 25 min using magnetic stirrer. 10 ml of deionised water was added drop by drop to the above solution for hydrolysis reaction. Then

the mixture was continuously stirred for 2hrs and it gets transformed to gel. After an aging period of 24 hrs the gel is filtered and dried in vaccum oven at 80°C for 3 hrs. The obtained TiO_2 was calcinated at 550°C for 4 hrs. Finally the TiO_2 nanoparticles were obtained.

RESULT AND DISCUSSION

X-ray diffraction (XRD) analysis

The XRD pattern of the as synthesized TiO_2 is shown in fig.1. The XRD pattern of TiO_2 nanoparticles with 2Θ peak at 25.4° confirm pure TiO_2 anatase phase. The crystal structure with peaks at 25.4°, 37.9°, 48.1°, 53.9°, 62.8° correspond to (101), (004), (200), (105), (204) planes respectively. The lattice parameter of TiO_2 nanoparticles were a=b= 3.785 Å c=9.513 Å. This is in accordance with the reported value (JCPDS card 21-1272 [6]). The intense sharp peak indicates the crystalline phase of anatase TiO_2. The intensity of the diffraction signal increases with the increasing calcination temperature. Using the Scherrer equation, the average crystalline size was estimated to be 24 nm for anatase TiO_2 nanoparticles.

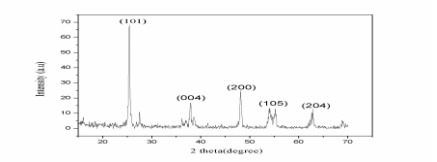

Fig.1 XRD spectrum of TiO_2 nanoparticles

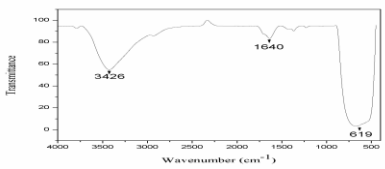

Fig.2. FTIR spectrum of TiO_2 nanoparticles

Fourier Transform Infrared (FT-IR) Analysis

The FTIR transmission spectra of TiO_2 nanoparticles are shown in fig 2. FTIR analysis was used to determine the functional groups of titanium dioxide nanoparticles. It can be observed apparently that the strong band in the range of 580 to 660 cm^{-1} was assigned to be Ti-O stretching bands. The absorption at around 3426 cm^{-1} indicates the presence of hydroxyl group (stretching). The 1630 cm^{-1} absorption peak may be related to hydroxyl (bending) representing the water as moisture in the sample. There is no peak at 2900 cm-^{1} which means all organic compounds are removed from the sample after calcination. S. Perumal et al [1] have reported similar absorption peaks observed in the synthesis of TiO_2 nanopowders.

Scanning electron microscopy (SEM) studies

Using High Resolution Scanning electron microscope the surface structure of the as prepared sample was probed. Fig 3 shows SEM images for different magnification. The morphology of the as synthesized nanoparticles was spherical in shape with strong agglomeration. Sample shows uniform morphology in the form of TiO_2 nano clusters. In general the morphology, shape and particle size of TiO_2 depend on the calcination temperatures.

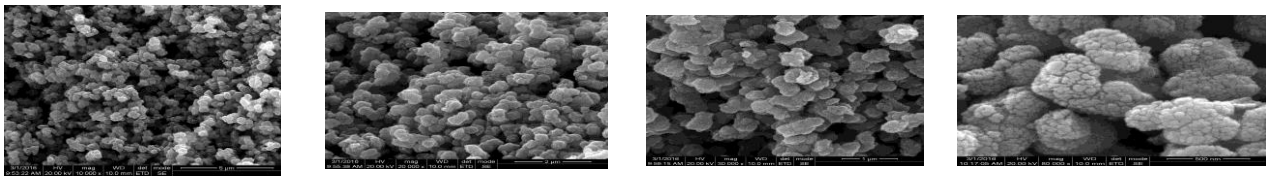

Fig.3. SEM micrograph of TiO_2 nanoparticles

Energy dispersive X-ray (EDX) analysis

Energy dispersive X-ray (EDX) spectra revealed the presence of stoichiometric proportion of Ti and O elements without extra signals. This confirms the pure phase of antase TiO_2.

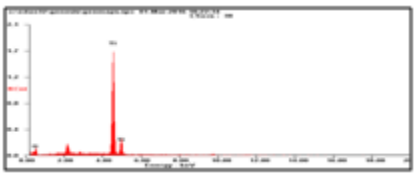

Fig.4 EDX analysis of TiO_2 nanoparticles

UV- Visible Spectroscopy

UV-Visible absorption and band gap spectra for TiO_2 nanoparticles are shown in fig 5. The spectrum shows the band edge-absorption peak which is found to be at 410 nm. In UV-Vis, high energy electromagnetic radiation in the wavelength range of 100-2000 nm is utilized to promote electrons to higher energy orbitals. From the UV spectra, it is clear that the absorbance decreases with increase in wavelength. This decrease in absorption indicates the presence of optical band gap in the material. The band gap energy (Eg) of the synthesized TiO_2 nanomaterials was obtained using the equation, $E_g = 1240/\lambda$ eV. Where Eg the band gap in electron volt (eV) and λ is is the wavelength of the absorption edges in nanometer (nm). Using equation the calculated value for the band gap energy of the synthesized TiO_2 nanoparticle is 3.025 eV. The band gap increases with the decrease in the particle size. The direct energy band gap is calculated from the $(\alpha h\nu)^{1/n}$ Vs hν plot. The value of bulk TiO_2 nanoparticle is 3.2 eV. Smaller crystallite size will have larger band gap and larger crystallite size will have smaller band gap.

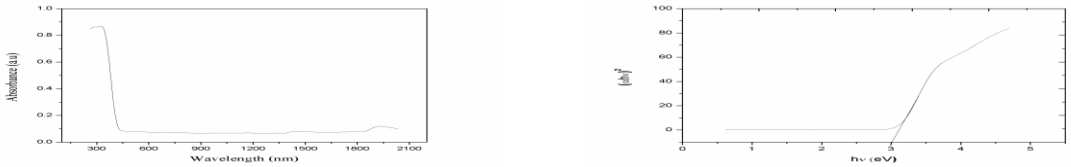

Fig.5 UV-Vis spectrum and hν Vs $(\alpha h\nu)^2$

CONCLUSION

TiO_2 nanopowder synthesized by Sol-gel method was annealed at 550°C for 4 hrs. The X-ray diffraction confirms the pure anatase of TiO_2 nanoparticles. The FTIR spectra of TiO_2 with absorption peaks at 619 cm^{-1} is for Ti-O stretching vibration mode and the presence of O-H groups at 3426 and 1640 cm^{-1} are in conformation with that of the literature reports. The SEM image confirms the morphology of TiO_2 nanoparticles as spherical in shape. The agglomeration may be because of the higher calcination temperature as reported by Muneer M. Ba-Abbad et al [3]. The crystallites develop in size as the calcination temperature is increased and move towards the bulk crystalline material. EDAX confirms the pure form of the sample. From UV-Vis Tauc plot the band gap of TiO_2 is estimated to be 3.025 eV which is a blue shift.

REFERENCES

1. S.Perumal, C.Gnana Sambandam, K.Monikanda prabu, S.Ananthakumar International Journal of Research in Engineering and Technology Volume: 03 Issue: 04 Apr-2014.
2. Stotaw Talbachew Hayle, Girma Goro Gonfa American Journal of Nanoscience and Nanotechnology2014; 2(1): 7.
3. Muneer M. Ba-Abbad1, Abdul Amir H. Kadhum, Abu Bakar Mohamad , Mohd S.Takriff , Kamaruzzaman Sopian Int. J. Electrochem. Sci., 7 **(2012)** 4871 – 4888.
4. D. Arun Kumar, J. Merline Shyla, Francis P. Xavier Appl Nanosci (2012) 2:429–436.
5. Chi-Hwan Han, Hak-Soo Lee, and Sang-Do Han Bull. Korean Chem. Soc. 2008, Vol. 29, No.8 1495.

GROWTH AND CHARACTERIZATION OF L-MALIC ACID DOPED KDP SINGLE CRYSTALS

A.Venkatesan[1,2], S. Arulmani[3], E. Chinnasamy[3], S.Senthil[3] and M.E. Rajasaravanan[2]

[1]Department of Physics, Arignar Anna Govt. Arts College, Villuppuram – 605 602.

[2]Department of Physics, Government Arts College, Salem – 636 007.

[3]Department of Physics, Govt. Arts College for Men (Autonomous), Nandanam, Chennai - 600 035.

Corresponding Author: ssatoms@yahoo.co.in

Abstract

Potassium Dihydrogen Phosphate (KDP) is a popular nonlinear optical materials that is widely used in the field of nonlinear optics for the frequency conversion processes. Optically good quality L-Malic acid doped KDP (LMKDP) crystals have been grown by slow evaporation method at room temperature. The crystallinity of the LMKDP crystals has been studied. The presence of the functional group for LMKDP crystals are qualitatively analyzed from FTIR and FT-RAMAN spectra. The second harmonic generation (SHG) efficiency was measured by using Kurtz powder technique. The dielectric behavior of grown crystals has been studied in the frequency range from 50 Hz to 50 MHz.

KEYWORDS: PXRD, FT-IR, FT-RAMAN, NLO studies, Dielectric studies.

1. INTRODUCTION

Nonlinear optical (NLO) single crystals have been wide applications in high energy lasers for inertial confinement fusion research, color displays, electro-optic switches, frequency conversion etc. In this modern era of information and technology with fast and high data storage capacity, data retrieving, processing, and transmission demands the search of new NLO materials with unique physical properties. Hence there is a great demand for synthesize the new NLO materials and grow their single crystals. KDP is among the most widely used NLO material. Many methods have been tried to improve the NLO properties of KDP crystal. The rapid growth of good quality KDP crystals and the addition of the doped organic and inorganic KDP crystals are newly developed and have been reported by several researchers [1-6]. With the aim of improving the second harmonic generation (SHG) efficiency of KDP, researchers have attempted to modify KDP crystals by doping different types of impurities. L-Malic acid of 0.2 molar percentages has been doped with KDP material. The grown L-Malic acid doped KDP (LMKDP) crystals were characterized by PXRD, FTIR, FT-RAMAN, NLO, Dielectric studies.

2. EXPERIMENTAL METHOD

2.1 CRYSTAL GROWTH

In the present study, L-Malic acid of 0.2 molar percentages has been doped with KDP material. The solution was thoroughly stirred for homogenization and then filtered into a borosil beaker using whatmann filter paper. It was porously sealed and placed in a dust free atmosphere for slow evaporation technique at room temperature. Single colorless and optically transparent crystals were harvested within 30 days.

3. RESULT AND DISCUSSION

3.1 POWDER X-RAY DIFFRACTION ANALYSIS

Powder X-ray diffraction technique is a powerful tool to analyze the crystalline nature of materials. Powder X-ray diffraction analysis was carried out by using XPERTPRO X-Ray diffractometer with CuKα radiation (λ=1.5406 Å). The cell parameter values for LMADP are

a=b=0.634Å, c=0.524Å with the angles $\alpha = \beta = \gamma = 90°$. The samples were scanned over the range 10-70°. The sharp and well defined peaks at specific 2Θ values indicate the high crystalline nature of the crystal. Powder XRD graph has been shown in the Figure 1.

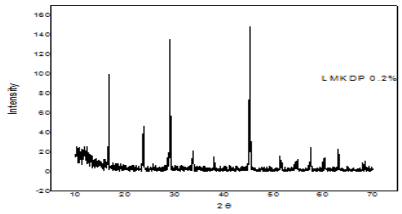

Figure 1. Powder XRD pattern of LMKDP

3.2 FT-IR AND FT-RAMAN ANALYSIS

FT-IR and FT-Raman spectra of LMKDP crystal were recorded and the spectrums of LMKDP crystals are shown in Figure 2 and Figure 3. The functional groups of the LMKDP crystals have been identified by the spectrum. In the high frequency region of IR spectra, the sharp peaks observed at 546 cm^{-1} are described to PO_4 stretching vibration in the crystal. The O-H deformation and P=O stretching will be observed in the frequency of 1320 cm^{-1}. In FTIR the absorption band at 914 cm^{-1} is due to P-O-H bending vibration in the LMKDP. In Raman studies the sharp peak will be observed at 914.08 cm^{-1} are described to P-O-H stretching molecule in the LMKDP crystals.

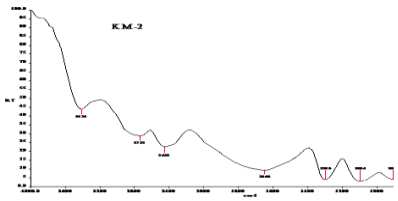

Figure 2. FT-IR studies of LMKDP

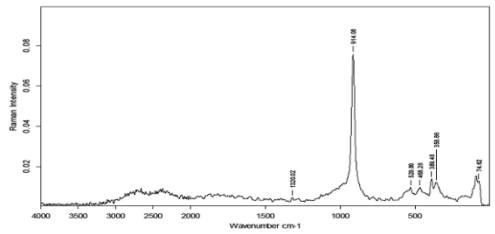

Figure 3. FT-RAMAN studies of LMKDP

3.3 KURTZ AND PERRY POWDER TEST

Kurtz and Perry second harmonic generation efficiency test (SHG) was performed for the comprehensive analysis of second order nonlinearity. Nonlinear optical measurements were carried out by using Kurtz powder technique. A Q-switched Nd:YAG laser beam of 1064 nm wavelength with 1.9 mJ/pulse input power, 8 ns pulse width and repetition rate 10Hz was used to estimate SHG efficiency of the grown LMKDP crystals. KDP crystalline powder was the reference material, the output of SHG range was compared and found that the SHG conversion efficiency of LMKDP is 1.4 times greater than that of reference KDP.

3.4 DIELECTRIC STUDIES

Every material has a unique set of electrical characteristics that are dependent on its dielectric properties. The variation of dielectric constant and dielectric loss of the sample with frequency is studied at room temperature by H10K1 3532 LCR HITESTER in the frequency range 50 Hz to 50 MHz and is shown in Figure 4 and Figure 5. The high value of dielectric constant at high frequency may be due to the presence of all the four polarizations namely space charge, orientation, electronic and ionic. The dielectric characteristic of a crystal are determined by the dielectric constant and

dielectric loss. The low value of dielectric loss indicates that crystal posses the good quality. These parameters have vital importance for NLO application.

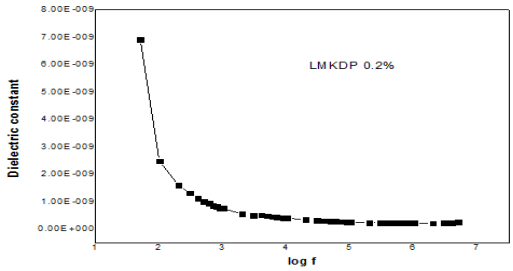

Figure 4. Dielectric constant Vs Log f

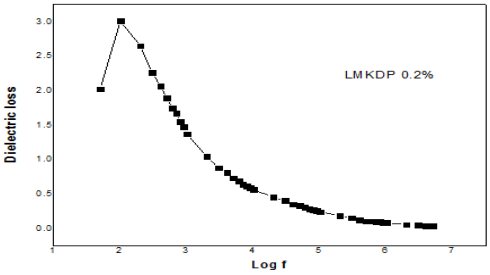

Figure 5. Dielectric loss Vs Log

4. CONCLUTION

High quality stable and transparent L-Malic acid doped potassium dihydrogen phosphate (LMKDP) has been grown by slow evaporation method at room temperature. Powder XRD studies shows that the grown crystals are crystalline in nature and tetragonal in structure. The vibrational frequencies were assigned from FT-IR and FT RAMAN spectral analysis which confirms the presence of functional groups. The SHG efficiency of the grown crystal was measured by Kurtz and Perry power test and its efficiency was found to be 1.4 times that of the standard KDP crystal. The dielectric properties of the grown samples have been studied.

REFERENCES

[1] B. Suresh Kumar, K. Rajendra Babu, Indian Journal of Pure & Applied Physics, 46, 2008, 123.

[2] K. D. Parikh, B. B. Parekh, D. J. Dave, M. J. Joshi, Crystal Research and Technology, 45(6), 2010, 603.

[3] Ferdousi Akhtar and Jiban Podder, Journal of Crystallization Process and Technology, 3, 2011, 55.

[4] P. Jagadish and N. P. Rajesh, J. Optoele. and Adv. Mat.,13, 2011, 962.

[5] G. G. Muley, Journal of Science and Technology, 2(5), 2012, 109.

[6] R. Ananda Kumari and R. Chandramani, Bull. Mater. Sci., 26, 2003, 255.

Structural, Optical and Morphological studies of CdSe Nanoparticles by Hydrothermal Method

K.Deepa[1], P.Sanjay[2], M. Victor Antony Raj[1], S.Senthil[2] and J. Madhavan[1,*]

[1]*Department of Physics, Loyola College, Chennai - 34.*

[2]*Department of Physics, Government Arts College For Men, Nandanam, Chennai - 35.*

[*]*-Corresponding Author: jmadhavang@yahoo.com*

Abstract

Cadmium selenide nanoparticle [CdSe] is an important chemical substance gaining great importance and widely used as an additive in the production of various, industrial products like rubber, cosmetics, catalyst, optical materials solar cells etc. CdSe being a wide band gap material and with better lattice matching properties made it suitable option for solar cell applications, Nano crystalline samples of cadmium Selenide were prepared by hydrothermal method. The morphological, structural, and optical properties of prepared samples were characterized by Transmission electron microscopy [TEM], X-ray diffraction [XRD] analysis and UV-Vis absorption spectroscopy studies. The crystalline size of the synthesized CdSe nanoparticles was calculated from XRD pattern and it was also confirmed through TEM. The broadened XRD peaks revealed that the formation of nanorods with Wurtzite structure. The low-resolution TEM images confirm the formation of CdSe nanorods, and also the agglomeration of nanoparticles and the presence of few spherical nanoparticles.

Keywords: CdSe nanorods, XRD, TEM, UV-Vis, etc

1. Introduction

Semiconductor nano crystals have attracted impressive attention, because of their novel optical and electronic properties [1]. One of the most important II – VI group semiconductors and nano crystalline Wurtzite structured Cadmium Selenide has attracted great interest in their various promising optoelectronic applications owing to its excellent optical conductivity such as photoelectron – chemicals, photoconductors , thin film transistor [2-4].

Many strategies have been utilized to prepare 1-D nano structural materials, where wet chemical method is considered as a practical and effective method for the synthesis of 1-D nano materials because it is more convenient and facile to be compared with most physical methods and need little expensive equipment by which CdSe nanorods, nanowires and nanotubes have been prepared successfully. Recently, many wet chemical methods have been applied to synthesize CdSe, and most noticeable hydrothermal or solvothermal technique [5-8]. Hydrothermal synthesis is becoming popular for environmental reason, since water is used as reaction solvent than organics. This method has been widely used to prepare nanostructures due to its simplicity, high efficiency and low cost. The prepared samples were characterized structurally and optically using powder X – ray diffraction, UV-visible spectroscopy, Transmission Electron Microscopy (TEM).

2. Experimental Procedure

2.1. Synthesis of cdse nanoparticles

All the chemicals were used of highest purity analytical grade, Cadmium nitrate ($Cd(NO_3)_2$ $4H_2O$, Merck 99%) and Sodium selenite (Na_2SeO_3, Merck 90%), no need to undergo any post treatment after the reactions with excess of ($N_2H_4.H_2O$) and ammonia (NH_3 H_2O). During the synthesis, the molar ratio of $Cd(NO_3)_2$ $4H_2O$ and Na_2SeO_3 was kept at 2:1. Cadmium nitrate $Cd(NO_3)_2$ $4H_2O$ (0.01 mol) was dissolved in 10 ml of Milli Q – water and then $NH_3.H_2O$ was slowly added into the solution,

which initially led to the formation of white precipitate, however with further addition of ammonia, a clear solution was formed. This indicates the conversion of Cd^{2+} into $Cd(NH_3)_4^{2+}$. The Se source, Na_2SeO_3 (0.005 mol) was stirred for 5 min with 15 ml of hydrazine hydrate (N_2H_4 H_2O) and it was mixed with the previously prepared solution (Cd source), this resulted in colorless and transparent solution. The final solution was transferred into Teflon – coated autoclave and then filled with Milli Q – water up to 70% of filling capacity. The pH of the solution was found to be 11 before heating. The autoclave was sealed and heated at 180°C for a reaction time of 4 hr. After the completion of the reaction, the autoclave was allowed to cool up to room temperature. Finally, the deep dark red product was collected, washed repeatedly with Milli Q – water, ethanol and then dried at 80°C.

3. Results & Discussions

3.1. XRD studies

The structural properties of the prepared nanoparticles were studied using X – ray diffraction. Fig.1 shows the XRD pattern of CdSe nanoparticles. All the peaks correspond to the Wurtzite phase of CdSe the lattice parameter values a, b and c have been calculated and are found to be a = 4.218 A° b = 4.218 A° and c = 6.887 A° which are in good agreement with the JCPDS 77 – 2307. The presence of small and broad peaks in the X – ray diffractogram reveals that the formation of nanoparticles. The average size of particles has been obtained from the X – ray diffraction pattern using the Scherrer formula, $D = 0.89\lambda/\beta\cos\theta$, where D is the grain size, β is the full width at half maximum (FWHM) and λ is the wavelength of X - ray (1.5466 A°). The obtained average particle size of the prepared CdSe nanorods is 35 nm.

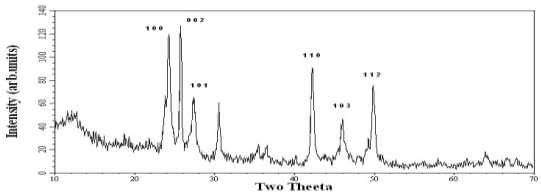

Fig. 1. XRD pattern of CdSe nanorods

3.2. Optical analysis

In order to determine the band gap of CdSe nanoparticles the optical properties of the nano materials depend on the size and shape of the particles. UV – Visible absorption spectrum of CdSe nanorods is shown in Fig. 2. The absorption edge of CdSe nanorods is 645 nm. The excitonic absorptions are very sharp. The absorption edge of CdSe nanorods at 645nm to be blue shifted. The blue shift of the absorption curves is a reduction of the band gap energy. The band gap energy of the material is calculated using the formula, $Eg = h\frac{C}{\lambda} \times 6.2415 \times 10^{18}$ eV. Where h = Planks constant = 6.626×10^{-34} Js, C = Speed of light = 3.0×10^{8} m/s, λ = Cut-off wavelength = 645×10^{-9} m. The calculated band gap energy of the CdSe nanorods is 1.9235 eV.

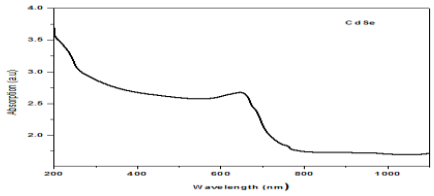

Fig. 2. UV-vis absorption spectra of CdSe nanorods

3.3. TEM analysis

The structure and morphologies of the CdSe nanoparticles were characterized using transmission electron microscopy. The TEM images of CdSe shown in Fig. 3 confirm the uniform size and shape distribution of CdSe nanorods. The morphologies of the CdSe nanorods were mainly affected by the amount of hydrazine hydrate and the reaction temperature. The CdSe nanorods synthesized in this method are in good shape with less pronounced stacking faults with their measured values of mean diameter and length 25 nm and 82 nm respectively.

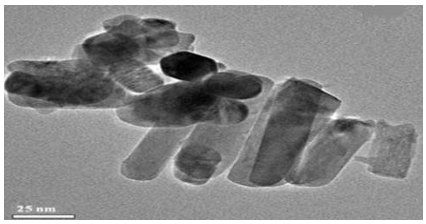

Conclusion

CdSe nanoparticles have been synthesized by the hydrothermal method with better control over the morphology and crystalline quality. The particle size and morphology were verified by powder XRD and transmission electron microscopy (TEM). The optical properties were studied by UV-Visible spectrum and the band gap value was found to be 1.9235 eV. This study opens up new avenues for research to find suitable experimental conditions and the possibilities of using different reaction mechanisms to bring out better control over the size/morphology of the semi conducting nano particles.

References

[1] D. Mohanta, G. A. Ahmed, A. Choudhury, F. Singh and D. K. Avasthi, Journal of Nanoparticle Research, 2006, 8, 645 ‑ 652.
[2] S.J. Lade, M.D. Uplane and C.D. Lokhande: Mater. Chem. Phys., 2001, 68, 36.
[3] M.T.S. Nair, P.K. Nair, R.A. Zingaro and E.A. Meyers, J. Appl. Phys., 1993, 74, 1879.
[4] A.V. Claster, A. Veraet, I.D. Rycke and J.D. Bates, J. Cryst. Growth, 1988, 86, 624.
[5] K. Deepa, S. Senthil, S. ShriPrasad and J. Madhavan, International Journal of ChemTech Research, 2014, 6, 1956-1958.
[6]G.Ramalingam and J. Madhavan, Archives of Applied Science Research, 2011,3(3), 217-224
[7] K.B. Tang, Y.T. Qian, J.H. Zeng and X.G. Yang: Adv. Mater., 2003, 15, 448.
[8] Q. Yang, K.B. Tang and C.R. Wang: J. Mater. Res., 2002, 17, 114.

OPTICAL AND ELECTRICAL CHARACTERIZATION OF NON LINEAR OPTICAL SINGLE CRYSTALS OF UREA PHTHALIC ACID

N. Indumathi[1,*], P. Sanjay[1], A. Venkatesan[2] and S. Senthil[1]

[1] *Department of physics, Government Arts College, Nandanam, Chennai-600035.*

[2]*Department of Physics, Arignar Anna Govt. Arts College, Villuppuram-605 602.*

*-Corresponding Author: indumathy.phy@gmail.com

ABSTRACT

Single crystals of a novel organic Urea Phthalic acid (UPA) were grown by slow solvent evaporation method. The triclinic structure of UPA was confirmed by single crystal X-ray diffraction (XRD). The presences of various functional groups in the crystal are confirmed by FT-IR analysis. An ultraviolet - visible (UV–vis) absorption spectrum was obtained to investigate the optical properties. The response of dielectric constant and dielectric loss has been investigated and results are discussed.

Keywords: Organic NLO crystal, FTIR, Optical and Dielectric studies.

Introduction

The nonlinear organic materials have attracted great attention and are gaining enormous demand due to their wide application in the recent technologies like opto-electronics, area of optical switching, optical data storage for the developing technologies in telecommunication and signal processing [1,2]. Organic crystals are found to possess high nonlinear optical efficiencies and additionally offer large number of design possibilities [3]. Urea is one of the most promising materials for nonlinear optical application in UV region and it has a high birefringence and a high laser-damage threshold. However, the growth of high quality and large-sized urea crystals is difficult due to unfavourable growth habits, and it also serves a better crystal compared to KDP for its NLO efficiency. The combination of both organic materials such as urea with tartaric acid and urea with L-malic acid form non-centrosymmetric crystal structure, because the interesting nonlinear optical properties. With this reported background, we have ventured into growth and characterization of Urea Phthalic acid (UPA) crystal. In this paper, the grown UPA crystal was subjected to various characterizations such as Single crystal XRD, FT-IR studies, linear optical studies and dielectric studies are reported and discussed.

2. Experimental

2.1 Crystal growth

In the present study UPA crystals were grown by slow evaporation solution growth technique. Urea and Phthalic acid were taken in the stiochiometric ratio of 1:1 in methanol and stirred separately for about half an hour using a magnetic stirrer. After that these solutions were mixed together and stirred well for about 1h and the saturated solution was filtered. A colourless transparent crystal was obtained and is shown in Fig.1.

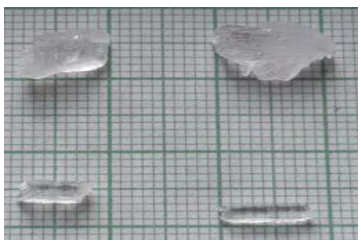

Fig.1. Photograph of as grown crystal of UPA by slow evaporation method

3. Result and discussions

3.1 Single crystal XRD analysis

The single crystal X-ray diffraction analysis for the grown UPA crystal has been carried out using an ENRAF NONIUS CAD4 automatic X-ray diffractometer. The UPA crystal retained its triclinic structure with lattice parameter values are a=7.402 Å, b=7.654 Å, c=10.052 Å and α=85.92°, β=81.94°, γ=65.20° and the volume of the crystal V=511.9 Å ^{3}. The lattice parameters are in good agreement with the reported values [4].

3.2 FTIR studies

Fig. 2 shows the FTIR spectrum of UPA crystal. In the high energy region between 3458 and 2511cm^{-1}, the appearance of broad absorption band is attributed to (NH_2) hydrogen bond symmetric and asymmetric vibrations. Moreover, the absorption band appears at 1687 cm^{-1}, which is attributed to NH_2 deformation. Bands above 2000 cm–1 correspond to absorption due to –CH_2 grouping. The band at ~922 and 1014 cm^{-1} corresponds to CCN stretching vibrations. The absorption peaks at ~705, 550 and 495 cm^{-1} can be assigned to COO– rock, wag and bend vibrations, respectively.

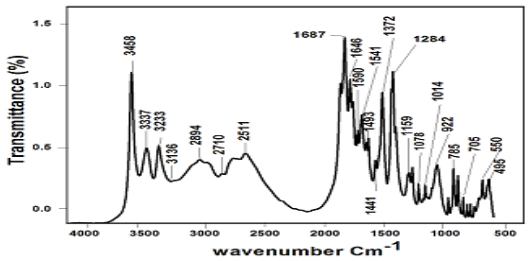

Fig. 2. FT-IR spectrum of UPA crystal

3.3 UV- Visible spectral absorption studies

Optical transmission spectrum was recorded for UPA is shown in the Fig. 3. From the UV absorption spectrum, it is evident that UPA crystal has UV cut-off wavelength occurs at 258 nm. The material is found to be transparent to all radiation in the wavelength range 300-900 nm. The large transmittance in the entire visible region makes the crystals good optical window materials. This is one of the most desirable properties of the crystals for the device fabrication [5].

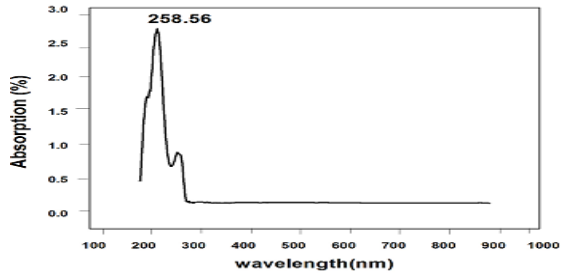

Fig. 3. UV Absorption spectrum for UPA crystal

3.4 Dielectrics studies

The study of dielectric parameters such as dielectric constant and dielectric loss as a function of temperature and frequency are shown in the Fig 4a and 4b. The low value of dielectric constant at higher frequencies could be attributed to the contribution of the electronic, ionic, orientation and space charge polarizations which depend on the frequencies [6]. The dielectric constant is low at

lower temperature and it increases with the increase of temperature sharply up to the Curie point. The dielectric constant of the crystal can be calculated using the equation, $\varepsilon_r = Cd/A\varepsilon_o$, Where d is the thickness of the sample, A is the area of the sample, C is the capacitance of the sample, ε_o is the permittivity of free space and ε_r is the dielectric constant of the sample. The low value of dielectric loss with increasing frequency indicates that the UPA crystal possesses the good quality and lesser number of electrically active defects. These parameters have vital importance for NLO applications.

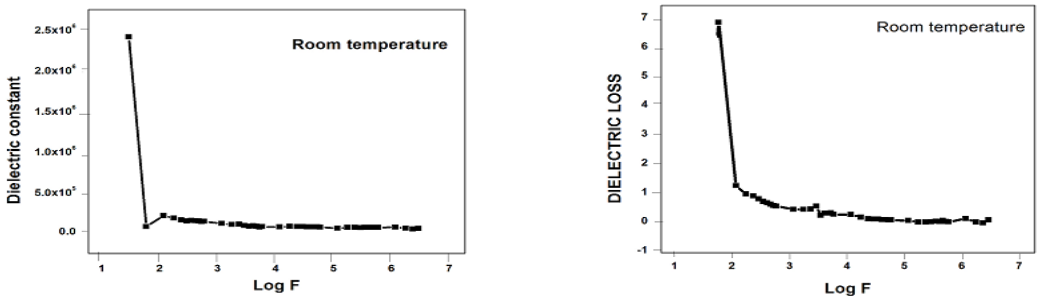

Fig. 4a and 4b Dielectric studies of UPA single crystal

4. Conclusion

The novel organic single crystal of was grown from the methanol solvent by slow evaporation technique. The crystal structure has been confirmed and the lattice parameters have been calculated by single crystal X-ray diffraction studies. The vibration spectral of FT-IR analyses confirms the different functional groups in UPA. The absence of significant absorption in the entire visible region and lower cut-off wavelength indicates the suitability of UPA for optical applications. The dielectric constant and dielectric loss of the grown UPA crystal decreases with increase in frequency and these low values at high frequencies reveal the desirable property of the crystal for NLO device applications.

References

[1] A. M. Petrosyan, J. Cryst. Phys. Chem. 1, 33-56 (2010).

[2] P. Vivek, P. Murugakoothan, Opt. Laser Technol. 49, 288-295 (2013).

[3] L. Dalton, Adv. in polymer Science, Springer-Verlag, Germany. 158, 1-8, (2002).

[4] V. Videnova, Adrabinska, J. Mol. Struct. 374, 199 (1996).

[5] K.V. Rajendran, D. Jayaraman, R. Jayavel, R. Mohan Kumar, P. Ramasamy, J. Cryst. Growth. 224, 122, (2001).

[6] S.O. Pillai, Solid State Physics, New Age International Ltd, New Delhi, p. 618 (2001).

SYNTHESIS AND CHARACTERIZATION OF Nd^{3+} DOPED TiO_2 NANO PARTICLES BY SOL GEL METHOD

P.Sanjay[1], K.Deepa[2], J. Madhavan[2] and S.Senthil[1,*]

[1]*Department of physics, Government Arts College For Men (Autonomous), Nandanam, Chennai - 35.*
[2]*Department of Physics, Loyola College, Chennai - 34.*
[*]*-Corresponding Author: ssatoms@yahoo.co.in*

Abstract

Nano structured materials are currently receiving wide attention due their optical, electronic, magnetic, chemical physical and mechanical properties. Semiconductor nano crystals have been widely studied for their fundamental properties. The Nd^{3+} doped titanium dioxide nano powder were successfully synthesized by sol-gel method. The structural and optical properties of as-prepared samples were characterized by X-ray diffraction (XRD), UV-Vis spectroscopy. The structure and elemental presence of the synthesized nanoparticles were studied by HRSEM and EDX analyses.

Keywords: Titanium dioxide, sol -gel method, Nd^{3+} doped TiO_2, XRD, HRSEM, etc

1. Introduction

Titanium dioxide (Tio_2) has been extensively studied oxide as a pigment and in sunscreens, paints, ointments and toothpaste and as a photo catalytic material for self cleaning coatings. Semiconductors nano crystals have been widely studied for their fundamental properties especially titanium dioxide (Tio_2). Nano sized titanium dioxide materials have been the focus of great interest because the exhibit modified physical-chemical properties in comparison with its bulk. a wide band gap and high refractive index of Tio_2 make it attractive for practical applications [1]. The use and performance for a given application are strongly influenced by the crystalline structure, the morphology and the size of the particles. The Tio_2 has been improved by optimizing the nanostructure size using various synthetic methods such as sol-gel, hydrothermal, solvothermal, co-precipitation etc.

The optical and electronic properties of nano structured Tio_2 can be tailored by a variety measures including thermal treatments, supported film growth, and metal-ion doping [2,3]. It is critical to assess the effects of lanthanide-ion doping on the structure of titania which will allow greater control over the desired properties. Doping of Tio_2 with neodymium ion would introduce a distortion in Tio_2 lattice. In this study, Nd^{3+} doped Tio_2 nanoparticels were obtained by sol-gel method. The prepared samples were characterized by X-ray diffraction (XRD), High resolution scanning electron microscope (HRSEM), the energy dispersive X -ray (EDX, and ultraviolet visible spectroscopy (UV-vis).

2. Experimental Details

2.1 Synthesis procedure

The doped titania nano particles were synthesized by sol-gel method from titanium(IV)-Iso-propoxide (TTIP, Aldrich 98), isoproponal (IPA), neodymium (III) acetylacetanate hydrate (Nd^{3+}) and certain amount of de-ionized water was added to the solution in molar ratio of 1:1. The mixed solution was stirred and ammonia was added drop-wise under magnetic stirring. The white precipitations were formed. The final solution was vigorously stirred for 12 hrs. The obtained precipitate was washed for several times with de-ionized water and ethanol and dried at 100^0C for 1

hr to remove the water and organic material. The dried precipitate powder was calcined at 400^0Cfor 3 hrs in high temperature furnace, finally the Nd^{3+} doped Tio_2 nano particles were obtained.

3. RESULT AND DISCUSSION

3.1. XRD analysis

The crystalline phase of Nd^{3+} doped Tio_2 nanoparticles were analyzed by X-ray diffraction [XRD]. Fig. 1 shows the powder XRD pattern of as- prepared Nd^{3+} doped Tio_2 nano particles. The presence of sharp diffraction peaks in the XRD confirm that products are highly crystalline and the crystalline size was calculated by the Debye Scherrer formula D =0.89λ/β cosθ, [4-6]. It was found that the average crystalline size of Nd^{3+} doped Tio_2 surface were 20 nm.

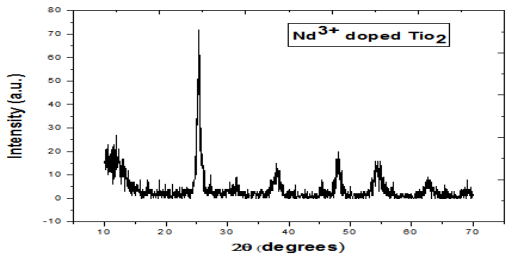

Fig.1 : XRD pattern of Nd^{3+} doped Tio_2 nanoparticles

3.2. UV-Vis spectroscopy

Optical properties were observed by UV – Vis spectroscopy. Fig. 2 demonstrates the optical absorption spectra of Nd^{3+} doped Tio_2 nano particles. The absorption edge of Nd^{3+} (0.5%) doping Tio_2 nano particles at 386 nm respectively. The doping with Nd^{3+} the response of Tio_2 nanoparticles to visible light was increased and showed red shift (towards increased wavelength). The band gap energy of the materials calculated using the formula, Eg = $h\frac{C}{\lambda} \times 6.2415 \times 10^{18}$ eV. The calculated band gap energy of the Nd^{3+} doped Tio_2 nano particles is 3.02eV.

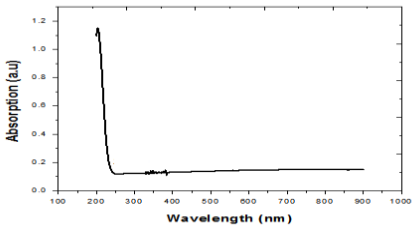

Fig. 2: UV-vis absorption spectra of the Nd^{3+} Tio2 nanoparticles

3.3. High Resolution Scanning Electron Microscopy (HRSEM)

High resolution Scanning electron microscope (HRSEM; Model, Jsm - 6360) was used to examine the surface morphology of prepared sample. As it can be seen, nano particles are uniformly distributed throughout the samples with rough surface, and the particles sizes are fairly small. Under the low temperature in sol-gel method Fig.3 shows HRSEM images of the Nd^{3+} doped $Tio_{2.}$. The HRSEM investigations of all the nano Tio_2samples reval that the crystallites are nanometer size all samples shown uniform morphology in the form of Tio_2 nano clusters.

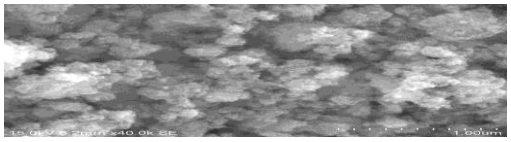

Fig.3 HRSEM image of the Nd^{3+} doped Tio_2 nanoparticles

3.4. Energy Dispersive X-Ray (EDX) analysis

To identify the type of elements present in the sample, Energy X-ray spectroscopy (EDX) was used. The EDX spectra of the synthesis of Nd^{3+} doped Tio_2 nano particles were recorded and they are displayed in Fig. 4 From the result, it is confirmed that such Tio_2 and Nd^{3+} ions are present in the sample, the presence of Nd^{3+} is confirmed which indicates the doping has entered into the sample.

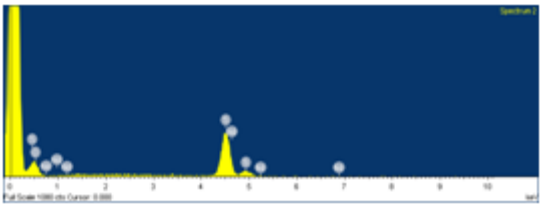

Fig. 4 : EDX spectra of the Nd^{3+} doped Tio_2 nanoparticles

```
S
1*       32   600         20     0   0.5
```

Conclusion

The rare earth Nd^{3+} doped Tio_2 nanoparticles were synthesized via low temperature sol-gel method. The crystal structure and grain size of the particles are determined using XRD studies. The morphology of the Nd^{3+} doped Tio_2 nanoparticle were characterized using High resolution scanning electron microscopy (HRSEM). The presences of various elements were analyzed by EDX analysis. . The optical properties were studied by UV-Visible spectrum and the band gap value was found to be 3.02 eV.

REFERENCES

[1]` WU. Xue-wei, WU Da-jian, and LIU Xiao-jun, "silver- doping induced lattic istortion in Tio_2 nanoparticles", chin.phys.Lett. 26(7), 077809 (2009).

[2] B. Keerthana, J. Madhavan and M. Arul Thalapathi, "Optical Properties of Pure and Gd3+ Doped Titanium Dioxide", International Journal of Engineering Development and Research. 3(2), 726-731 (2015).

[3] B. Keerthana, J. Madhavan and M. Victor Antony Raj, "Structural and Dielectric Observation of Gd3+ Doped Titanium Di Oxide", International Journal of ChemTech Research. 7(4), 1867-1872 (2015)

[4] J.Xu, Y.Ao, D.Fu, and C.Yuan, "A simple route forth preparation of Eu, N-codoped Tio_2 nanoparticles with enhanced visible light- induced photo catalytic activity", Journal of Colloid and Interfacial Science. 328, 447–451(2008)

[5] C.Chi, J.Choi, Y.Jeong, O.Y.Lee and H.J.Oh, Nitrogen and europium doped Tio_2 anodized films with application sin photo- catalysis, ThinSolidFilms. 519, 4676–4680 (2011)

[6] S.Ramya, R.P.George, R.V.SubbaRao, R.K.Dayal, Effect of biofouling on anodized and sol–gel treated titanium surfaces: a comparative study, Biofouling. 26, 883–891(2010)

GROWTH AND CHARACTERIZATION OF UREA DOPED SULPHAMIC ACID SINGLE CRYSTALS.

E. Chinnasamy[1], A.Venkatesan[2,3], N.Indumathi[1], M.E.Rajasaravanan[3] and S.Senthil[1,*]

[1]*Department of Physics, Govt Arts College for Men, Nandanam, Chennai - 600 035*

[2]*Department of Physics, Aringnar Anna Arts College, Villuppurm - 605 602*

[3]*Department of Physics, Government Arts College, Salem – 636 007.*

**-Corresponding Author: ssatoms@yahoo.co.in*

ABSTRACT

In this present work we are interested in investigating the effects of the crystal structure and general characterization of Urea Doped Sulphamic Acid (USA) single crystal. Urea doped Sulphamic acid single crystal was grown by slow evaporation technique at room temperature. The cell parameters of the grown crystal were determined by single crystal X-ray diffraction analysis. The band gap energies of the USA single crystals have been calculated and their cut off wavelength was determined from UV-visible spectral analysis. Thermo gravimetric and differential thermo gravimetric analysis (TG/DTA) indicates the thermal stability of the grown crystal. The dielectric properties of the grown crystal have been studied.

Key words: Single crystal XRD, UV-visible spectral analysis, TG/DTA, dielectric studies.

INTRODUCTION

Organic single crystal growth has greatly increased due to their applications in optoelectronics, nonlinear optics etc. Organic materials lead to growth related problems because of their intrinsic properties such as low thermal conductivity, ease of super cooling, low melting point and weaker mechanical properties [1]. Inorganic crystals are extensively used in the applications of optical modulation, fiber optical modulation and optoelectronics [2]. Sulphamic acid is an important industrial chemical compound, which is strongly soluble in water. Apart from its catalytic and electrometallurgical uses, salts of Sulphamic acid have wide applications as anticorrosive agent (or) cross linking agent for polymer [3]. Hence in the present work, a systematic study on the growth and characterization of Urea doped Sulphamic acid (USA) is reported. The single crystals have been subjected to single crystal XRD, UV-visible-, TG/DTA and dielectric studies respectively.

1. EXPERIMENTAL PROCEDURE

Urea and Sulphamic acid were taken in equimolar ratio and dissolved in Millipore water. The solution was stirred up to saturation state. The solution was filtered by using watt men filter paper and covered with dust free polyethylene sheet then placed at room temperature. After a period of 5 to 6 days good transparent Urea Sulphamic acid (USA) single crystal with dimension of about 16 x 11 x5 mm^3 was harvested. The photograph of the grown single crystal is shown in Fig.1.

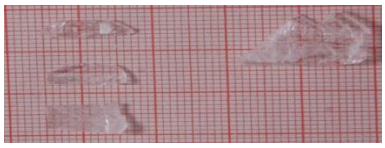

Fig. 1: USA single crystal

3. RESULTS AND DISCUSSION

3.1 SINGLE CRYSTAL X-RAY DIFFRACTION

Single crystal X-ray diffraction analysis of USA crystal was carried using an Enraf Nonius CAD4 single crystal X-ray diffractometer with an incident CuKα radiation, and the calculated lattice parameter values are a= 8.076 Å, b= 8.098 Å, c= 9.218 Å, α=β=γ=90° and V = 602.8 (A^3). The lattice parameter values show that the grown USA crystal belongs to orthorhombic structure which is confirmed with the reported values.

3.2 UV-VISIBLE ABSORPTION SPECTRUM

The optical absorption spectrum of USA is shown in Fig.2. From the UV absorption spectrum, it is evident that USA crystal has the cut off wavelength at 235 nm. The band gap energy is calculated to be 4.74eV. This indicates that USA is a higher band-gap energy material. This shows that the crystal has a wide transparency range, which starts in the UV region and extends up to the near-infrared region through the visible region. The large transmittance in the visible region makes the crystals good optical window materials [4].

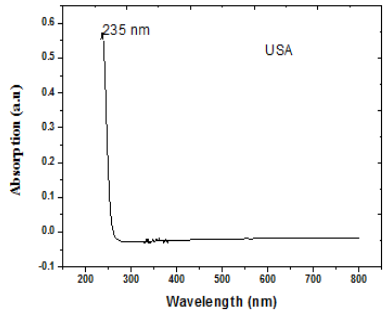

Fig 2: UV absorption spectrum for USA

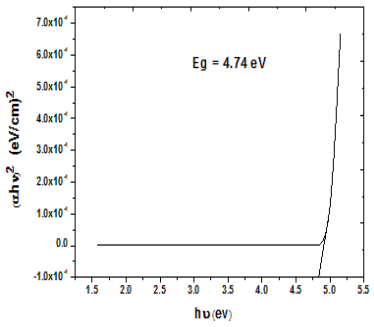

Fig 3: Band gap spectrum for USA.

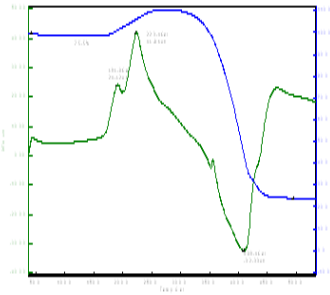

Figure 4: TG-DTA spectrum of USA single crystal.

3.3 THERMAL ANALYSIS

The thermal stability and physiochemical changes of USA crystal were analyzed by recording the TG–DTA spectrum as shown in Figure 4. It reveals that USA is thermally stable upto 191.0°C and after this the sample undergoes appreciable weight loss. The change in weight loss confirms the decomposing nature of USA sample. The DTA spectrum confirms the melting point of the sample through a sharp exothermic peak at 191.0°C. Moreover, the endothermic peak at 409.4°C reveals the volatile nature of the sample. After that no sharp peak was observed, which confirms that the material is thermally stable up to 409.4°C.

3.5. DIELECTRIC STUDIES

Variations in dielectric constant and dielectric loss as a function of room temperature and frequency are shown in Fig. 5a and 5b. In Fig.5a, it is seen that the value of dielectric constant is found to increase with temperature and it becomes independent of frequency at higher frequency region. The decrease in dielectric constant of USA crystal at low frequencies may be attributed to the contribution of the electronic, ionic, orientation and space charge polarizations which depend on the frequencies. The low value of dielectric loss at high frequencies suggests that the sample possess

enhanced optical quality with lesser defects and this parameter is of vital importance for NLO applications [5].

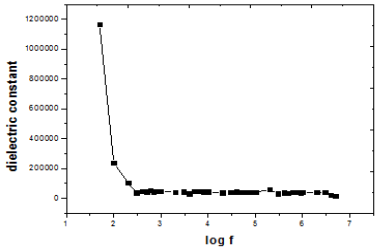

Figure 5a: Dielectric constant for USA

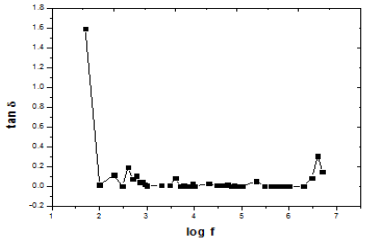

Figure 5b: Dielectric loss for USA

CONCLUSION

An organic single crystal of USA was grown from aqueous solution by the slow evaporation method. The crystal structure was confirmed by single crystal XRD analysis. In UV There is good optical transmittance in the entire visible region, which makes the USA crystal for optoelectronic applications. Thermal stability has been observed by TG/DTA analysis. The low dielectric constant and dielectric loss of USA at higher frequencies show that the material is a more suitable candidate of nonlinear optical application.

REFERENCES

[1] X.J. Liu, Z.Y. Wang, X.Q. Wang, G.H. Zhang, S.X. Xu, A.D. Duan, S.J. Zhang, Z.H. Sun, D. Xu, Cryst. Growth Des. 8, 2270–2274, (2008).

[2] D.Yu and D.Xue Acta Cryst.B 62,702, (2006).

[3] B.Kannan[1],P.R.Seshadri[1*],P.Murugaakoothan and K.llangovan, Indian Journal of Science and Technology,6,4357-4361,(2013)

[4] V. Siva shankar, R. Siddheswaran, T. Bharthasarathi, P. Murugakoothan, *J. Cryst Growth*, , 311, 2709, (2009**)**.

[5] C. Balarew, R. Duhlew, J. Solid Sate Chem., 1, 55, (1984).

GROWTH AND OPTICAL STUDIES ON L-MALIC ACID DOPED ADP SINGLE CRYSTALS FOR NON LINEAR OPTICAL APPLICATIONS

S. Arulmani[1], N. Indumathi[1], M. Victor Antony Raj[2] and S.Senthil[1,*]

[1]Department of Physics, Govt. Arts College for Men (Autonomous), Nandanam, Chennai - 600 035.
[2]Department of Physics, Loyola College, Chennai -600034
[*]-Corresponding Author: ssatoms@yahoo.co.in

Abstract

Ammonium dihydrogen phosphate (ADP) is one of the most popular crystals used for non linear optical (NLO) applications. ADP crystal is of more appeal due to its piezo-electric property. ADP crystals attract more interest because of their unique non linear optical, dielectric and anti-ferroelectric properties. The L-Malic acid doped ADP (LMADP) single crystals were grown by slow evaporation method at room temperature. The Crystalline nature of the grown LMADP crystal has been studied by powder XRD analysis. Fourier transform infrared (FT-IR) studies confirm the functional groups of the crystals. The UV-visible study confirms the wide optical transmittance window for the doped crystals imperative for optoelectronics applications. The second harmonic generation efficiency of the crystals was determined.

KEY WORDS: PXRD, FT-IR, NLO, UV-visible.

1. INTRODUCTION

Ammonium dihydrogen phosphate (ADP) is a well known anti-ferroelectric crystal. The study of ADP crystal is very interesting in view of the dielectric, piezo-electric and optical properties. Most important application of ADP crystals are that they are used as electro-optical modulator, harmonic generators, parametric generator and as monochromotors for X-ray fluorescence analysis [1]. ADP was belongs to scalenohedral (twelve faced) class of tetragonal crystal system [2]. The rapid development of optical communication system has led to the search for more sufficient compounds for the processing of optical signals. Organic crystals in terms of NLO properties posses advantages when compared with inorganic counter parts [3]. Organic materials allow their fine tuning of their chemical structure and properties for the desired NLO properties [4]. ADP is an excellent inorganic NLO material has a considerable interest amongst several research workers because of its wide frequency, high frequency of frequency conversion.

One of the earliest applications of ADP was used in design of hydrophone for acoustically active mines, due its zero aging characteristic because, ADP remains stable during many year of storage [5]. It was also reported that the addition of some of the amino acids as dopants has enhances the non linear optical and piezoelectric properties of inorganic materials [6]. L-Malic acid doped with ADP will be of special interest as a fundamental building block to develop complex crystal with improved NLO properties. The grown crystals were characterized by PXRD, FTIR, UV-vis spectroscopy and NLO Studies.

2. EXPERIMENTAL METHOD

2.1 CRYSTAL GROWTH

L- Malic acid of 0.3% has been doped with pure ADP (Ammonium dihydrogen phosphate) along with double distilled water was used for the growth of single crystals. The solution was stirred for 3-4 hours and then filtered. The pH value of the reaction mixture was monitored. It was porously sealed and placed in a dust free atmosphere for slow evaporation at room temperature. Optically transparent crystals were harvested within 30 days.

3. RESULT AND DISCUSSION

3.1 POWDER X-RAY DIFFRACTION ANALYSIS

X-ray diffraction technique is a powerful tool to analyze the crystalline nature of materials. Powder X-ray diffraction analysis was carried out by using XPERTPRO X-Ray diffractometer with CuKα radiation (λ=1.5406 Å). The samples were scanned over the range 10-70° as shown in the Figure 1. The cell parameter values for LMADP are a=b=0.744Å, c=0.697Å with the angles $\alpha = \beta = \gamma = 90°$. The structure of LMADP is tetragonal it can be analyzed by the cell parameter. The sharp and well defined peaks at specific 2Θ values indicate the high crystalline nature of the crystal.

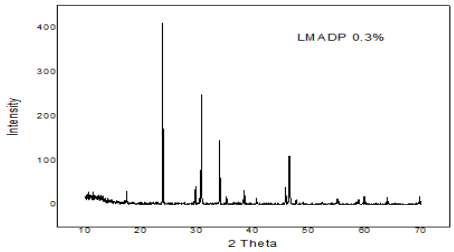

Figure 1. Powder XRD pattern of LMADP single crystals

3.2 FT-IR ANALYSIS

FT-IR spectra of LMADP crystal were recorded in range of 450-4000cm^{-1} by KBr PELLET technique. The functional groups of L-Malic acid doped with ADP crystals have been identified and it was shown in Figure 2. The broad band in the high energy regions is due to the O-H vibration of water, P-O-H group and N-H vibration of ammonia. The peaks at 1101 and 908 cm^{-1} represent P-O-H vibrations. The PO_4 vibration gives their peaks at 547 and 499 cm^{-1}. The bending vibration of water gives it peak at 1646 cm^{-1} in IR. The peak at 1402cm^{-1} is due to bending vibrations of ammonium. The vibrational band at 3245 cm^{-1} was also assigned to the vibration of N-H band. The PO_4 vibration of the parent is shifted from 499 to 481 cm^{-1}, which was confirmed by the presence of L-Malic acid on the lattice of ADP crystals.

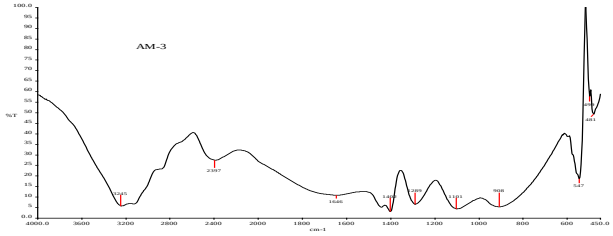

Figure 2. FT-IR spectral analysis of LMKDP

3.3 SHG ANALYSIS

Quantitative measurement of the conversion efficiency of the crystal was determined by using the powder technique developed by Kurtz and Perry techniques. Kurtz and Perry techniques were employed to measure the SHG efficiency of the grown crystals in reference with the pure KDP. In the measurement, Q-switched Nd:YAG laser of wavelength 1064nm of peak power 2.35 mJ, pulse duration 8 ns and repetition rate 10Hz was used. Output intensity of SHG gives relative values of NLO efficiency of the material. The output energies from the grown sample and reference KDP are found to be 21.2 mW and 19.6 mW respectively. It is found that the SHG efficiency is 1.6 times greater than that of standard KDP.

3.4 OPTICAL ABSORPTION STUDIES

The UV-Vis spectrum of LMADP crystals were recorded by using Perkin Elmer UV-Vis spectrometer (Model: Lambda 35) in the wavelength range of 200-900 nm. Optically polished single crystals of thickness 3mm were used for this study. Figure 3. Shows that the absorption spectrum of the grown crystals and the lower cut-off wavelength is found to be 220 nm. The presence of low cut off wavelength and the wide optical transmission window range of the materials possessing NLO activity. Figure 4. Shows that the optical band gap energy value is found to be 4.68 eV.

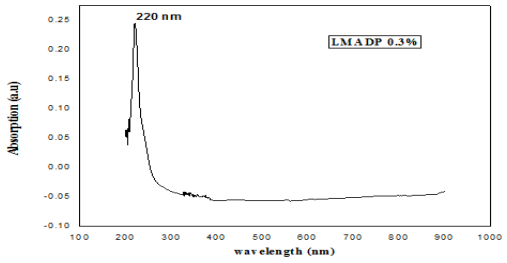

Figure 3. UV-vis absorption

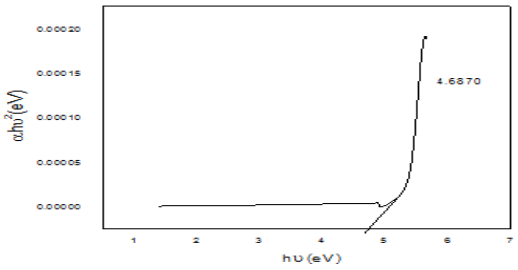

Figure 4. UV-vis band gab

CONCLUTION

The L-Malic acid doped with ADP (LMADP) single crystals were grown by slow evaporation method at room temperature. The crystalline nature of the grown LMADP crystal has been studied by powder XRD analysis. Fourier transform infrared (FT-IR) studies observed that the functional groups of the LMADP crystal. The UV-visible study confirms the wide optical transmittance window for the doped LMADP crystals imperative for optoelectronics applications. The second harmonic generation efficiency of the crystals was determined. All the above strongly attributes the L-malic acid doped with ADP improves the non linear optical properties of the pure ADP crystals.

REFERENCES

[1] P. **S**henoy, K.V. Bangera, J.Cryst. Growth 45 (2010)825-829.
[2] P.Rajesh, K.Boopathi, P.Ramasamy, J.Cryst. Growth 318 (2011) 751-756.
[3] G.Bhagavannarayanna, S.Parthiban, S.P.Meenakshisundram, J.Appl.Crystallogr. 39 (2006)784-790.
[4] .P. Ramasamy, P. Santhana Raghavan, J. Cryst. Growth 20 (1999) 191-203.
[5]. P.V. Dhanaraj, Santheep K. Mathew, N.P. Rajesh, J. Cryst. Growth 310 (2008) 2532–2536.
[6]. M.Meena, C.K. Mahadevan, Cryst. Res. Technol. 43 (2008) 166.

GROWTH AND CHARACTERIZATION OF PURE AND NEODYMIUM DOPED L-THREONINE ACETATE CRYSTALS

[1]A.SENTHAMIZHAN, [2]T.PANCHATSARAM, [3]T.THAMIZHARASAN, [4]A.MADHAVAN

[1]Department of Physics, VRS college of Engineering & Technology,Arasur-607 107
[2]Department of Physics,TKGA, college
[3]Department of Physics. Sir Theayagaraya college,Chennai
[4]GHSS,Kammapuram, Tamil Nadu. India
senthamizhan_pa@yahoo.co.in

ABSTRACT

The work deals with synthesis, growth and characterization of pure and neodymium doped NLO active L-Threonine acetate single crystals. The crystals were grown by slow evaporation technique at room temperature. The grown crystals were characterized by XRD, FTIR and other studies. The results will be discussed in detail.

INTRODUCTION

The emergence of new materials with superior quality is often responsible for major advances in new technologies. The high speed, high degree of parallelism of optics will lead gradually to optoelectronic systems where an increasing number of functions will be implemented optically. However, the development of photonic technology relies largely on the progress achieved in fabricating new optical materials with better performance. In that respect, materials with a nonlinear optical (NLO) response are expected to play a major role in enabling optoelectronic and photonic technologies. Many NLO single crystals have been identified as potential candidates in optical and electro-optical devices. Nonlinear optical materials have acquired new significance with the advent of a large number of devices utilizing solid-state laser sources.

NLO materials are essential for the fabrication of electro-optic modulators, which convert an electric signal to an optic one for transmission on a fiber optic cable. The exchange and processing of information is growing rapidly and more powerful data-systems including larger networks, faster processors and mass storage devices are under intensive research and development.

1.1 MATERIAL PREPARATION

LTA single crystals (pure and doped) were grown by slow evaporation technique at room temperature. Good quality, transparent and defect free tiny crystals formed due to spontaneous nucleation were used as seeds to grow bulk crystals shown in fig 1.

1.2 SYNTHESIS AND SOLUBILITY

The L-threonine acetate was synthesized by the stoichiometric incorporation of pure L-threonine and acetic acid in the ratio (1:1). The calculated amount of salts were dissolved in double distilled water and kept for slow evaporation at room temperature. The reaction is as follows:

$$C_4H_9NO_3 + CH_3COOH \longrightarrow C_4H_{10}NO_3^+CH_3COO^-$$

The resultant product L-threonine acetate was found to be homogeneous and the purity of the same was increased by successive recrystallization. The solubility diagram for both pure and doped crystals is shown in Figure1.0 Transparent good quality seed crystals free from macro defects were used for

growth experiments. The crystal size obtained was 10 x 4 x 5 mm^3 in 28 days. Neodymiun Nd (2 mole %) doped L-threonine was also synthesized separately at room temperature and purified by recrystallization. The Nd- LTA was grown at the size of 13x8x6 mm^3. Figure 1.0 shows the photographs of as grown crystals.

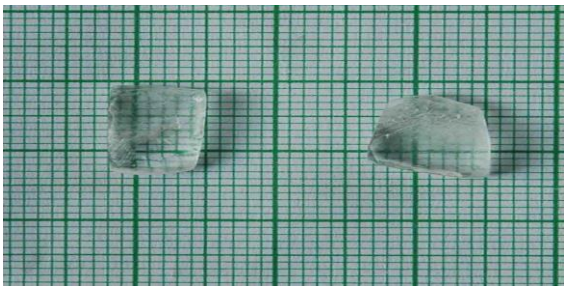

Figure 1.0Photograph of pure & Nd^{3+} doped LTA crystal

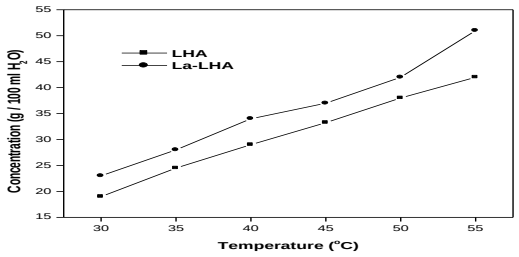

Figure 2 Solubility curves for pure & Nd 3^+ doped LTA crystal

1.3 CHARACTERIZATION TECHNIQUES & DISCUSSION

The lattice parameters (Shown in Table:1.1)values for the pure and doped LTA crystals have been calculated, from the powder X-ray diffraction pattern (shown in fig: 3) Both the pure and doped LTA crystals crystallize in triclinic P1 space group. The FT-IR Spectra of both the pure and doped LTA confirm the structural aspects of pure compounds. The FT-Raman spectra were recorded for the pure and doped LTA in order to qualitatively analyze the presence of functional groups in LTA. FT-Raman analysis of doped crystals confirmed the presence of metal dopants in the crystal lattice. Optical absorption spectra were recorded on these polished crystal samples between 200–2500nm. Kurtz SHG tests were carried out on the pure and doped LTA samples. The SHG efficiency of doped crystal is found to be higher than that of pure crystal and KDP. The TGA and DTG analysis of pure and doped LTA crystals were done at a heating rate of 20 K/min. There is a reduction in the decomposition temperature for doped crystals. The values of work hardening coefficient of the pure and doped crystals were found. Dielectric studies were carried out for the pure and doped LTA crystals. The dielectric nature of the pure LTA is marginally altered by the presence of dopant metals. Photoconductivity studies confirm that these materials exhibit positive photoconductivity.

Table 1.1 Lattice parameters for the pure and Nd^{3+} doped LTA crystal

Lattice parameters	Pure LTA	Nd^{3+}-LTA	LTA (Madhavan et al)
a (Å)	8.611	8.810	8.520
b (Å)	9.101	9.712	9.059
c (Å)	9.011	9.891	9.023
α(°)	62.01	61.72	61.70
β(°)	86.78	86.91	86.60
γ(°)	86.13	85.99	86.30
Crystal System	triclinic	triclinic	triclinic
Space group	P1	P1	P1
Volume ($Å^3$)	611.6	613.4	611.6

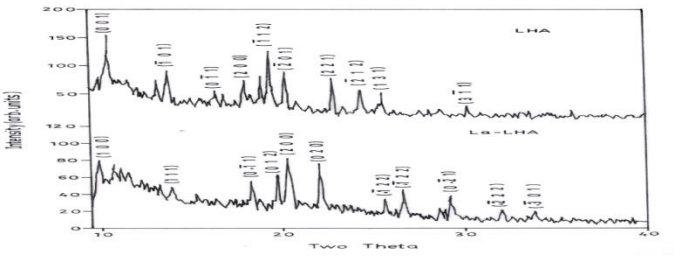

Figure 3: Powder XRD pattern of pure and Nd^{3+} doped LTA crystal

1.3.1 FT- IR analysis

FT-IR spectra of the pure and Nd doped LTA crystals were recorded in the range 400 cm^{-1} to 4000 cm^{-1}, using KBr pellet on BRUKER IFS FT-IR Spectrometer. The presence of functional groups in pure and doped LTA is qualitatively analyzed. The FT-IR Spectra of the LTA crystals are shown in Figure 4. The FT-IR spectra of doped LTA appear almost similar to that of pure LTA N-H stretching frequencies of amino group are found between 3168 and 2874 cm^{-1} for both pure and doped crystals. The absorption at 3026 cm^{-1} is due to O-H stretching vibration of carboxylic group. Both the pure and metal doped compounds show strong absorption at 1626 cm^{-1} indicating the presence of. Primary amino group. The characteristic absorption at 1479 cm^{-1} is due to symmetric N-H deformation. The peak at 1418 cm^{-1} corresponds to the symmetric COO^- stretch. The CH deformation is found by the peak at 1319 cm^{-1}. An absorption band at 935 cm^{-1} is due to the CC stretching. The wagging of COO^- gives rise to a band at 702 cm^{-1}. Doping of metal ions into the crystal lattices does not show any significant change in absorption pattern. The frequency assignments of these crystals are presented in Table 1.2.

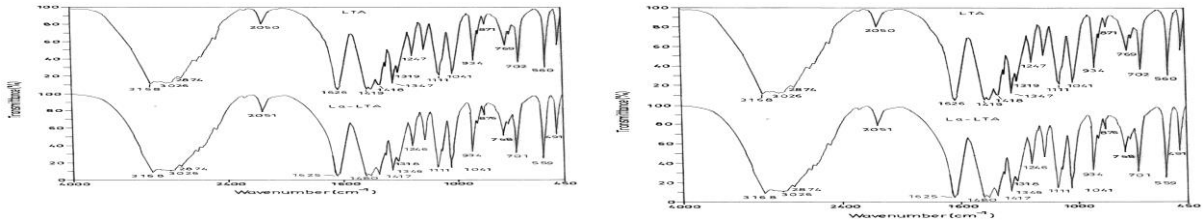

1.3.2 FT- Raman spectra

Table 1.2 FT-IR spectral assignments of pure and Nd doped LHA crystal

Wave number (cm^{-1})		Assignments
Pure LTA	Nd - LTA	
3168 - 2874	3168 - 2874	N-H stretching frequencies
3026	3026	O-H stretching vibration
1626	1626	Presence of primary amino group
1479	1479	symmetric NH_2 deformation
1418	1418	symmetric COO^- stretch
1319	1319	C-H deformation
935	934	C-C stretching
702	702	Wagging of COO^-

In order to qualitatively analyze the presence of functional groups in LTA, polarized FT-Raman spectra were recorded for the pure and doped LTA in the range 50 cm^{-1} – 3500 cm^{-1}. Figure 5 shows the recorded spectra of the pure and doped LTA. The O-H stretching gives a peak at 2988.9 cm^{-1}. The bands at 2938.4 cm^{-1} and 2873.5 cm^{-1} are due to aliphatic CH_2 and CH_3 stretching. The less intense peak at 1481.2 is due to the CH_2 deformation. The peak at 1337.9 cm^{-1} is due to the C=O

stretching. The weak absorption at 3100 cm^{-1} is due to the N-H stretching of amino group. The absence of peaks at 3019.2 cm^{-1}, 2938.6 cm^{-1}, 1450.2 cm^{-1} and 698.2 cm^{-1} in the La-LTA spectrum which are present in the pure LTA, indicates the probable metal linkage with the N of amino group. The FT-Raman frequency assignments of these crystals are presented in Table 1.3.

1.3.4 UV-Vis-NIR spectrum

Optical absorption data were taken on the polished pure and doped LHA crystals of about 4mm thickness using a Varian carry 5E model dual beam spectro- photometer between 200nm – 2500nm. The spectra (Figure 5) indicates that the pure and doped LTA crystals have minimum absorption in the region between 250 nm – 1588nm and 260nm - 1580nm. The required key properties for NLO activity are minimum absorption and low cut-off wavelengths for pure and doped LTA are 250nm and 260nm respectively. LTA crystals are found to posses these properties.

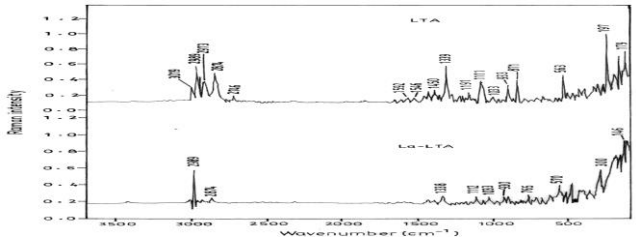

Table 1.3 FT-Raman spectral assignments of pure and Nd^{3+} doped LTA crystal

Wave number (cm^{-1})		Assignments
Pure LTA	**Nd^{3+} - LTA**	
3019	-	Asymmetric NH stretching
2989	2988	O-H stretching
2938	2938	CH_2 stretching
2874	2873	CH_3 stretching
1481	1481	CH_2 deformation
1450	-	NH_2 deformation
1339	1337	C=O stretching

1.3.5 Microhardness studies

Microhardness studies have been carried out in (1 0 0) plane on pure and doped LTA single crystals using HMV SHIMADZU microhardness tester filled with diamond Vickers pyramidal indenter to estimate the mechanical properties. The static indentations were made at room temperature with a constant indentation time of 15 seconds for all indentations. Measurements were taken by varying the applied loads from 10g to 50g only.

1.3.6 Thermal Studies

Single crystals of pure and doped LTA crystals were subjected to thermo gravimetric analysis (TGA) and differential thermogravimetric analysis (DTG) simultaneously using STA 409C instrument, in the nitrogen atmosphere at a heating rate of 10 K/min. Figure 6 shows the resulting TGA and DTG traces of the pure and doped crystals. The decomposition of the material starts at 262^o C. The material is found to be thermally stable up to 230^o C. There is a reduction in the decomposition temperature of the doped crystals compared to the pure LTA crystals, which is attributed to the presence of the metal dopant Nd.

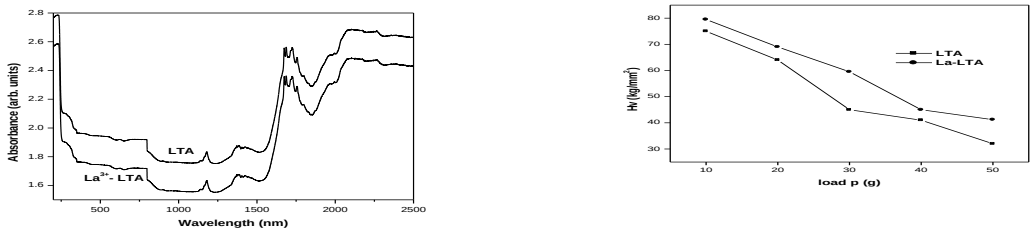

Figure 6 Absorption spectrum of pure and Nd^{3+} doped LTA crystal

CONCLUSION

Good quality single crystals of pure and doped L-Threonine acetate (LTA) were grown successfully by slow evaporation technique. Powder X-ray diffraction studies were carried out, and the lattice parameters are calculated. Inductively coupled plasma studies shows that the amount of dopant incorporated into the doped crystal is less than the concentration of the dopant in the corresponding solution. The pure and doped LTA crystals are transparent in the entire visible region, and have minimum absorption. The TGA and DTG studies show that the metal dopants have not altered the thermal stability of the molecules. From the dielectric studies it is seen that the dielectric constant and dielectric loss decreases with frequency. Photoconductivity studies reveal that the pure and doped LTA have positive photoconductivity. Hardness studies show that pure and doped LTA crystals are soft materials. NLO studies proved that the metal dopant have increased the efficiency of pure LTA. The presence of dopant has improved the Nonlinear optical (NLO) properties of the grown crystals and these crystals can be promising material for nonlinear device fabrication.

References:

1. Aoki K., Kozo Nagano and Yiochi Iitaka (1971), 'The crystal structure of L-arginine phosphate monohydrate', Acta Crystallogr. B, Vol. 27, pp. 11–25.
2. Arunmozhi G. and E.de Gomes M., (2004), 'Metastability and crystal growth kinetics on L-arginine phosphate', Cryst. Res. Tech., Vol. 39, No.1, pp. 34-39.
3. Balarew C. and Duhlew R., (1984), 'Application of the hard and soft acids and bases concept to explain ligand coordination in double salt structures', J. Solid Sate Chem., Vol. 55, No.1, pp. 1-6.
4. Batta Calleja F.J., Rueda D.R., Poster R.S. and Mead W.T. (1980), 'New aspects of the microhardness of ultra oriented polyetheline', J. Mater. Science, Vol. 15, pp. 762–765.
5. Brice J. C.(1972), 'The growth of crystals from liquids', Wiley, New York.
6. Brice J. C.(1986), 'Crystal Growth Process' , Wiley, New York.
7. Brice J.C. (1973), 'The growth of crystals from liquids', North Holland publishing company, Amsterdam.
8. Brzozowski L, Sargent E H, (2000) 'Optical Signal Processing Using Nonlinear distributed Feedback Structures', IEEE Journal of QuantumElectronics, vol. 36, no. 5, pp. 550-555.
9. Buckley H.E. (1951), 'Crystal Growth', John Wiley and Sons, New York.
10. Bunget and M. Popescu, (1984), "Physics of Solid Dielectrics", Elsevier, New York,
11. Chemla D.S. and Zyss J. (1987), 'Nonlinear optical properties of organic molecules and crystals', Vol.1-2, Academic Press, Orlando, New York.
12. Cheng L.K., Bosenberg W, and Tang C.L. (1990), 'Growth and characterization of nonlinear optical crystals suitable for frequency conversion' Prog. Crystal Growth and Charact., Vol.20, pp. 9-57.
13. Chernov A.A. (1984), 'Modern Crystallography III-Crystal Growth', Springer-Verlag, Solid State Series, Vol. 36, Berlin.
14. Colthup.N.B, Daly.L.H, Wilberley.S.E, (1975), 'Introduction to Infrared and Raman Spectroscopy', Academic Press, New York.
15. Dmitriev V.G., Gurzadyan G.G. and Nikogosyam D.N. (1991), Hand book of Nonlinear optical crystals, Springer-Verlag, Berlin-Heidelberg

GROWTH AND CHARACTERIZATION OF DYES DOPED BIS THIOUREA CADMIUM CHLORIDE (BTCC) CRYSTALS

M.KALAISELVAN[1], S.RAJESH KUMAR[2], G.SURESH[3] ,P.AMBALAVANAN[4], P.DAMODARAN[5] & P.KUMARESAN[6]

[1, 2, 3,4,5,6] *Department of Physics, Thiru.A.Govindasamy Government Arts College, Tindivanam- 02*
[1]*Government Higher Secondary School, Melmalaiyanur-604210, Gingee Tk, Villupram*
[2]*P.G Department of physics, King Nandhivarman College of Arts and Science, Thellar-604 406*
E.mail : logeshkumaresan@yahoo.com

Abstract

Crystal growth is an inter disciplinary subject covering engineering, metallurgy, crystallography, mineralogy, etc. In the past few decades, there has been a growing interest on crystal growth processes, particularly in view of the increasing demand of materials for technological applications. Good optical quality single crystals of Rhodamine B doped Bis Thiourea Cadmium Chloride (BTCC) have been grown from solution by slow solvent evaporation technique. Experiments were allowed to run for considerably larger duration of the time (20 days) can grow large crystals. Single crystal X-ray diffraction study was carried out to measure the unit cell dimension of both the crystals. The FTIR studies ascertained the metal co ordination. To ensure the purity and thermal stability of the materials thermo gravimetric study was carried out. The second harmonic generation (SHG) nature of crystals was identified by Kurtz method. These studies shows that Rhodamine B dye doped BTCC crystals were formed to exhibit enhanced optical, thermal, electrical, mechanical and second harmonic generation properties compared to the pure BTCC.

1 INTRODUCTION

The strong influence of single crystals in the present day technology is evident from the resent advancements of the fields of semiconductors, polarizer's, transducers, infrared detectors, ultrasonic amplifiers, solid state lasers, non-linear optic, piezoelectric, Acosta-optic, photosensitive materials and crystalline thin films for microelectronics and computer industries. Hence to achieve high performance from the device, good quality single crystals are needed. The growth of single crystals and their characterization towards device fabrication has assumed great impetus due to their importance for both academic research and applied research.In recent years more emphasis is given to inorganic materials due to their much matured NLO applications than organic materials and owing to their good transparency, chemical stability, and mechanical properties. Also research into the growth of large single crystals from aqueous solution is currently serving as the important avenue to general progress in understanding many fundamental concepts of crystallization.

2. EXPERIMENTAL PROCEDURE

2.1 CRYSTAL GROWTH

A solution of BTCC was prepared by dissolving in the ratio (2:1) of Thiourea and Cadmium Chloride. The solution was continuously stirrer using a magnetic stirrer of room temperature. The prepared solution was filtered and kept undisturbed in a constant temperature bath maintained at a temperature of 38°C. When evaporation taken place slowly, supersaturation is activated. BTCC crystals were grown from aqueous solution by slow evaporation method. The solubility of Rhodamine –B doped BTCC was measured. It was found to be 17.5 g/100 ml at 40^{o}C for Rhodamine –B doped BTCC. The solution was stirred long enough to ensure complete dissolution of the solute,

and filtered. Subsequently the solution was cooled at a rate of 0.1°C/day. The amount of BTCC salt to be dissolved was determined from its solubility curve at an average temperature of 37°C. As a result, crystals with dimensions 6.2 × 3.5 × 2.5 mm^3 were harvested in a period of 20 days.

Figure1. Rhodamine-B doped BTCC Crystal

3. CHARACTERIZATION STUDIES

3.1 UV-Visible studies

The transmission spectra were taken at room temperature using UV-Vis double beam spectro photometer-Systronics. The transmission spectra were recorded in the range 200-1200 nm for 1 mm thick c-cut plates of pure and Rhodamine-B doped BTCC was shown in Figure 2. All the crystals irrespective of the dopants are transparent in the entire visible region. The UV-Visible spectrum of rhodamine-B doped BTCC crystal, maximum wavelength of absorption (λ_{max}) appeared at 780 cm^{-1}.Therefore, it reveals that after incorporation of rhodamine-B dye, the UV absorption was shifted to Red region. The Bathochromic shift (Red shift) increases in accordance of mole fractions of dopants. The pure BTCC crystal has about 75 % of transmission. The dye doped BTCC crystal is invariably has higher transmission percentage compared to pure BTCC crystal. From the UV-Visible spectrum, transmission percentage increases due to addition of doped in BTCC crystal, which would enhances the optical property of BTCC crystal.

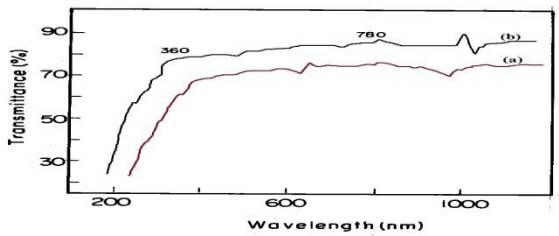

Figure 2. UV-Visible spectra of (a) Pure BTCC and (b) Rhodamine-B doped BTCC crystal

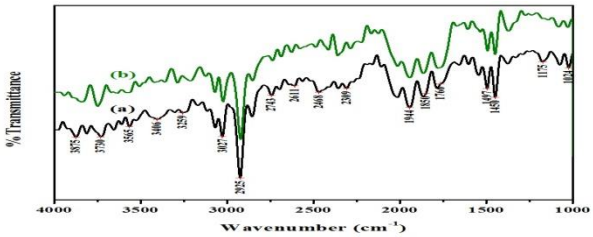

Figure 3. FTIR Spectra of (a) Pure and (b)Rhodamine-B doped BTCC crystal

The FT-IR spectrum was recorded between 1000 cm^{-1} and 4000 cm^{-1}, using BRUKER Alpha FT-IR spectrometer. The FT-IR Spectra of both the pure and doped BTCC crystals are shown in Figure 3. The FT-IR spectra of pure and doped BTCC appear almost similar to each other.Fig. 4 show the TGA thermograms of doped BTCC. The first weight loss of about 35% observed in KDP starts at 115°C could be attributed to the loss of lattice water. The next stage between 115.5°C with a total loss of 65% is assigned to the decomposition of BTCC. The resulting residue gives a weight loss for a wider range of temperature between 220°C and 570°C. TG analysis of the doped BTCC shows that the softening starts at 114.9˚C due to loss of water. The compound is stable and there is no phase

transition till it is melting. However, thermogravimetric analysis indicates that on melting, the compound decomposes and loses weight.

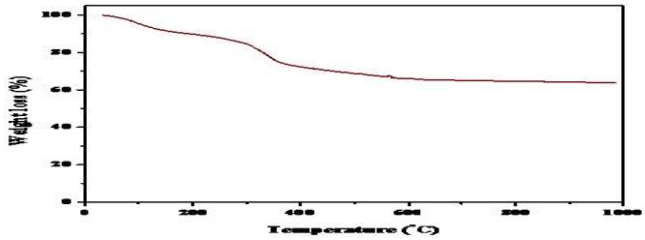

Figure 4. TGA Curve of BTCC

Conclusion

The powder SHG measurement shows that the grown doped BTCC crystal has 1.85 times higher SHG efficiency than KDP. Vickers micro hardness was calculated in order to understand the mechanical stability of the grown crystals. Each type of constituent chemical bond is regarded as one part of the whole crystal that has contributions to the total nonlinearity. The distribution of valence electrons of the metallic elements is an important factor that strongly affects the linear and nonlinear properties of each type of constituent chemical bond. The fundamental beam of 1064 nm from Q-switched Nd:YAG laser was used to test the SHG property of the grown crystal.

Acknowledgements

We gratefully acknowledge financial supports from the Department of Science & Technology-Science and Engineering Research Board **[**Dr.P.Kumaresan, Young Scientist Award, DST-SERB-FAST TRACK, PS-20/2009(SR)] and University Grants Commission-[Dr.P.Kumaresan, Major Research Scheme-F.No.38-18/2009 (SR)], New Delhi, India.

References

1. Bordui P. (1987) 'Growth of large single crystals from aqueous solution: a review' Journal of Crystal Growth, Vol.85, pp.199-205.
2. Buckley H.E. (1951), In: 'Crystal Growth', John Wiley & Sons Inc., New York, London. Chemla D.S. and Zyss J. (1987), 'Nonlinear optical properties of organic molecules and crystals', Vol.1-2, Academic Press, Orlando.
3. Chernov A.A. (1990), 'Secondary nucleation induced by the cracking of a growing crystal KDP and DKDP', Journal of Crystal Growth, Vol.102, pp.793-800.
4. Munn R.W.and Ironside C.N. (1994), 'Principles and Applications of Nonlinear Optical Materials', CRC press, Inc., USA.
5. Robey H.F, Journal of Crystal Growth 259(2003) pp.388-392.
6. Eaton D.F. (1991), 'Nonlinear optical materials', Science, Vol.253, pp.402-406.

LATENT HEAT OF VAPORIZATION OF ORGANIC LIQUIDS FROM ULTRASONIC VELOCITY

P.Ramadoss* and K.Aruna Devi

PG & Research Department o Physics, Government Arts College,Tiruvannamalai-606 603

E-mail: dossrpg@yahoo.co.in

ABSTRACT

A simple method of estimating Latent heat of vaporization is described. $H_v = Au^2 + B$ where A & B are constants. The values of A and B are determined by using least square fitting for alcohols,alkanes and cyclic hydrocarbons. In results, the found values are compared with literature values.

Keywords: latent heat of vaporization, ultrasonic velocity, organic liquids, alcohols.

Introduction

Measurement of velocity in liquids is great interest of researchers as it brings out physical, thermal and optical properties of the medium such as compressibility, internal pressure, volume viscosity, gibbs free energy, Debye's temperature and optical refractive index(1-7).

Latent heat of vaporization of organic liquids is one of the important properties as it is related with phase change(8). Investigation of various liquid mixtures and solution of organic and inorganic compounds and polymers are made by ultrasonic studies(9-13).

In excess acoustic and thermodynamic parameters such as adiabatic compressibility, free length, free volume, internal pressure, relaxation time and acoustic impedance of binary liquids have been used to study interactions(14). Further, these parameter studies give the information about ion-solvent interactions(15).

In the present work, latent heat of vaporization is calculated using ultrasonic velocity data in alcohol, alkane and cyclic hydrocarbons.

Theory

Latent heat of vaporization of a liquid varies with temperature and pressure(16-17) and Enthalpy of vaporization of both liquids & solids particularly for homologous series have been reported by the method of correlation gas chromatography(18-20).

Heat of vaporization was also explained by additivity relationships(21). In hydrocarbons, there are many methods have been developed for estimating heats of vaporization of liquids(22,23). Still, there is space to correlate latent heat of vaporization with other pro perty such as sound velocity.

Surface phenomena and viscosity play important role in processes connected with transition from one aggregate state to another(24). Compressional wave propagation is influenced by surface and viscous property(25,26). This leads to relate latent heat of vaporization to ultrasonic velocity as,

$$H_v = Au^2 + B$$

Where A and B are constant which are determined by least square fitting method.

Results and Discussion

Tables 1,2 and 3 give, the ultrasonic velocity and latent heat of vaporization for alcohols, alkanes and cyclic hydrocarbons respectively. The values of A and are presented in Table-4.

The calculated and literature values of latent heat of vaporization for alcohols and alkanes are in good agreement. In the case of cyclic system, found values are much deviated from literature because

of their different functional group. It has been shown in the figures 1-3. The authors hope that more experimental work support this approach.

TABLE 1: Latent heat of vaporization of alcohols

System	Velocity [a,b] u/ms^{-1}	H_V X10^5 J/Kg	
		LIT [a,b]	CAL
Propane	253	4.3273	4.1154
Butane	216	3.8689	4.1279
Pentane	1008	3.5819	3.4289
Hexane	1203	3.3546	3.1182
Heptane	1138	3.177	3.2279
Octane	1192	2.98	3.1371
Nonane	1248	2.9046	3.0386

TABLE 2: Latent heat of vaporization of alkanes

System	Velocity [a,b] u/ms^{-1}	H_V X10^5 J/Kg	
		LIT [a,b]	CAL
Methanol	1143	11	9.8514
Ethanol	1156	8.46	9.36
1 Propanol	1205	6.9066	7.474
1Butanol	1258	5.85	5.3419
1Pentanol	1253	4.9273	5.5476
1Hexanol	1289	4.3627	4.0536

TABLE 3: Latent heat of vaporization of cyclic hydrocarbons

System	Velocity [a,b] u/ms^{-1}	H_V X10^5 J/Kg	
		LIT [b]	CAL
Benzene	1321	3.9	3.9869
Toluene	1275	3.51	3.9343
O-Xylene	1352	3.4188	4.023
Phenol	1274	4.9068	3.933
Aniline	1614	4.5	4.3653

TABLE 4: Constant values of various system

System	A X10^5 J/Kg	B
Alcohols	31.1812	-1.6327
Alkanes	4.1616	-0.0721
Cyclic Hydrocarbons	3.2191	0.0440

[a] Values taken from Reference[27]

[b] Values taken from Reference[28]

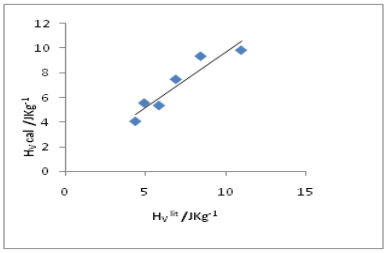

Fig 1: Latent Heat of Vaporization of Alcohol: H_V lit Vs H_V cal

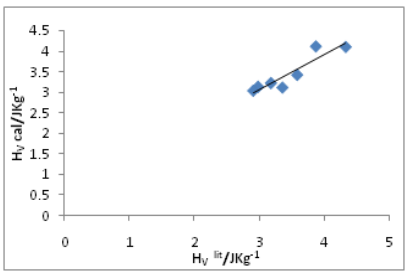

Fig 2: Latent Heat of Vaporization of Alkanes: H_V lit Vs H_V cal

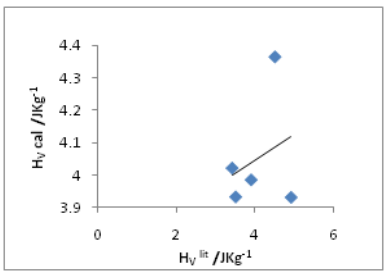

Fig 3: Latent Heat of Vaporization of Cyclic Hydrocarbons: H_V lit Vs H_V cal

Reference

[1] O.Namoto. J.Phys.Soc.Japan.13(1958)1528- 1533.
[2] S.Durai,P.Ramadoss,Acta Acoustica.89(2003)173-175
[3] S.Barnat. J.Chem.Phys.20(1952)278-279.
[4] Rama Rao. Curr.Sci.23(1954)325-326.
[5] S.K.Kor,N.D.Tripathi.J.Phys.Soc.Japan.23(1967) 476.
[6] D.Geetha,C.Rakkappan.J.Mol.Liq.121(2005)102-104.
[7]R.Kubendran,F.LiakathAliKhan,J.Asghar,M.Aravinthraj,J.Udayaseelan.Arch.Appl.Sci.Res.3(2)(2011)568-576.
[8] J.S.Chickos,D.G.Hesse.J.Org.Chem.53(1988)3424-3429.
[9] V.Rajendran. Indian J.Pure & Appl.Phys.34(1996)52-56.
[10] A.Ali,A.K.Nain, Pramana.58(2002)695-701v.
[11] P.S.Nikam,B.S.Jagdale,A.B.Sawant,Medical Hassan. Indian J.Pure & Appl.Phys. 39(2001)433.
[12] P.S.Agarwal. Eur.J.Sci.Res.45(3)(2010)470.,
[13] G.Ravichandran,T.K.Nambinarayanan,Acous.Let.19(1996)245-253.
[14] V.Pandiyan,S.L.Oswal,N.I.Malek, P.Vasandharani. Thermodyn.Acta.524(2011)
[15] Li Yu,Xin-Gen Hu,Rui-Sen Lin.J.Mol.Liq.135(2007)96-104.
[16] J.J.Martin,J.B.Edwards.A.I.Ch.E.J.11(1965) 331-333.
[17] K.M.Watson.Ind.Eng.Chem.35(1943)398-406.
[18] J.S.Chickos,W.Hanshaw.J.Chem.Eng.Data.49(2004)77-85.
[19] J.Chickos,D.Lipkind.J.Chem.Eng.Data.53(2008) 2432-2440.
[20] J.S.Chickos,H.Zhao,G.Nichols. Thermochim.Acta.424(2004)111-121.
[21] J.PeterGuthrie,K.F.Taylor. Can.J.Chem.61(1983)602-607.
[22] K.J.Laidler. Can.J.Chem.34(1956)626-648.
[23] J.S.Chickos,A.S.Hyman,L.H.London, J.F.Liebman.J.Org.Chem.46(1981)4294-4296.
[24] J.Frenkel,Kinetic Theory of Liquids,Dover Publications,New York.1955.
[25] V.L.Rykov,Russian J.Phys.Chem.39(1965)494.
[26] S.Durai,P.Ramadoss.Ind.J.Pure&Appl.Phys. 42(2004)334-337.
[27] G.W.C.Kaye & T.H.Laby, Physical and Chemical costants,13th. Ed., Longmans,London, 1966.
[28]D.R.Lide, Hand Book of Chemistry and Physics,CRC Press,80th Ed.,London,1999. 150.

SHG MEASUREMENTS ON L-GLUTAMIC ACID AND L-VALINE DOPED OXALIC ACID CRYSTALS FOR NLO APPLICATIONS

M.RAJASEKARAN[1], B.LATHA[2], & P.KUMARESAN[3]

[1,4]Department of Physics, Thiru.A.Govindasamy Government Arts College, Tindivanam- 604 002, Tamil Nadu
[2] Department of Physics, Rajalakshmi Engineering College, Thandalum, Chennai.
e-mail : logeshkumaresan@yahoo.com

Abstract

Nonlinear optical (NLO) crystals have come upon the materials science scene and are being studied by many research groups around the world. Oxalic acid single crystals of were synthesized by a slow evaporation technique. Single crystal and powder XRD analyses confirmed the orthorhombic crystal structure. On the other hand, ion beam irradiation effects have rarely been studied. The structural, chemical, optical, mechanical and non-linear optical properties of the doped crystals were analysed with the characterization studies such as powder XRD, FT-IR, UV-Visible, SEM and SHG measurements respectively. The results for L-Glutamic acid and L-Valine doped oxalic acid crystal are compared with the results of the pure oxalic acid crystals. The TGA, DTA shows that the material has good thermal stability; the UV-Vis spectrum shows the transmitting ability of the crystal in the entire visible region.

1. INTRODUCTION

The search for nonlinear optical (NLO) materials has been of great interest because of their significant impact on laser technology, optical communication and data storage technology. The synthesis of new and efficient frequency conversion materials has resulted in the development of new semi organic materials. Semi organic system provides many structure and bonding schemes for the molecular engineering of new materials. Semi organic nonlinear optical (NLO) crystals are attracting a great deal of attention due to their high NLO coefficient, high damage threshold and high mechanical strength compared to organic NLO crystals. Non-linear optical (NLO) materials have a significant impact on laser technology, optical communication, optical storage technology and electro optic modulation. The search for new frequency conversion materials over the past decade has led to the discovery of many semi organic materials. These materials posses large nonlinearity, high resistance laser induced damage and low angular sensitivity. The semi organic NLO materials gain importance over organic and inorganic NLO materials because of their large polarizability and wide transmission window. Extensive investigation in this direction resulted in the discovery of a new phase match semi organic NLO crystals.

To analyze the influence of dye based dopant on the non-linear optical property of oxalic acid crystals; efforts were made to dope oxalic acid crystals. The effects of impurity atoms on the quality and performance of the crystals were analysed. Bulk crystals of oxalic acid crystals and L-Glutamic acid and L-Valine doped oxalic acid crystals were grown by solution growth technique.

2. EXPERIMENTAL PROCEDURE

2.1. Crystal Growth

The recrystallised salt was used for the preparation of saturated solution at room temperature (32^oC). The solution was filtered by filtration pump and Whatman filter paper of pore size 11 μm. The solvent evaporates slowly leading to super saturation which in turn initiates the nucleation and the crystal grows. Pure oxalic acid crystals were grown from aqueous solution by slow evaporation and also by slow cooling method (0.5^0 C/Day). The same method is followed for L-Glutamic acid doped oxalic acid crystals (0.1 mole % of L-Glutamic acid). The solubility of doped oxalic acid crystals in the solvent was measured for each dopant, it was found to be 14.5 gms/100 ml at 35^oC for L-Glutamic acid.

Figure: 1 L-Glutamic acid doped Oxalic Acid Crystal

3. CHARACTERIZATION STUDIES

3.1. X-Ray Diffraction Studies

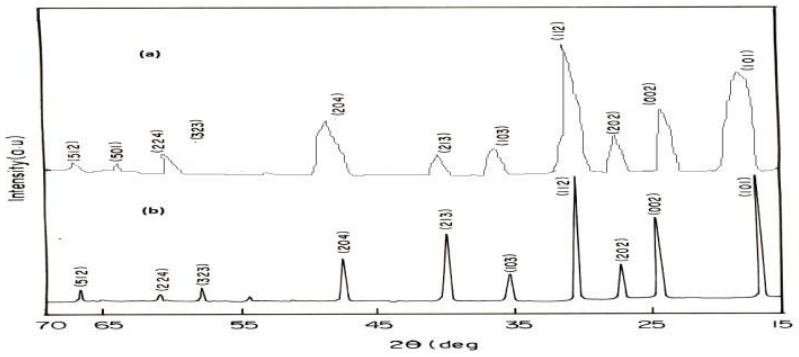

Figure: 2 XRD of (a) pure Oxalic Acid Crystal and (**b) L-Glutamic acid Oxalic Acid**

Powder XRD spectra (Fig.2) for the pure and L-Glutamic acid and L-Valine doped oxalic acid crystals revealed that the structures of the doped crystals are slightly distorted compared to the pure oxalic acid crystal. This may be attributed to strains on the lattice by the absorption. It is observed that the reflection lines of the doped oxalic acid crystal correlate well with those observed in the individual parent compound with a slight shift in the Bragg angle. The crystallinity of the grown sample was confirmed by X-ray diffraction analysis.

3.2 FTIR Studies

The FTIR [Fig.3] of all of them were recorded from solid phase samples on a bruker IFS 66V model spectrophotometer using 1064nm output of a cw diode pumped Nd:YAG laser as a source of excitation in the region 400 – 4000 cm^{-1} operating at 200mW power at the samples with a spectral resolution of $2cm^{-1}$. The IR spectra were also recorded on Shimadzu–800, FTIR spectrometer series of Japan in the region 400 – 4000 cm^{-1}. The frequencies for all sharp bands are accurate to ± 1 $cm^{-1.}$ The observed spectra of single and doped coumarin shown in Fig: 2.

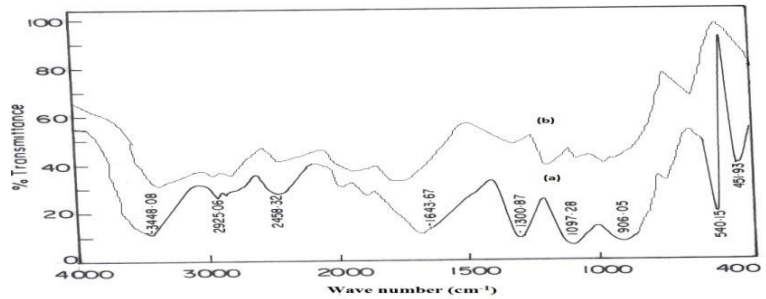

Figure: 3 FT-IR spectra of (a) Pure Oxalic (b) L-Glutamic acid doped Oxalic Acid Crystal

The FTIR spectral analysis for the grown crystal has been recorded in the range 400-4000 cm-1 using KBr pellet technique and the resultant spectrum is shown in Fig.3. The carbonyl stretching C=O is found to be near 1083 cm-1.A peak at 2694 cm-1 corresponds to NH2 deformation. The C-N stretching and the O-H stretching bands are found to be near 1125 and 3186 cm-1 respectively. A peak at 2694 cm-1 corresponds to CH2 stretching. The band at 1580cm-1 indicates the presence of symmetric stretching of carboxylate (COO-) ion. It was confirmed that broad envelope positioned in between 2750-3500 cm^{-1} corresponds to symmetric and asymmetric stretching modes of NH_2 grouping of L-Glutamic acid and L-Valine coordinated oxalic acid. The NH and N-C-N stretching vibrations were also seen in these crystals.

3.3 NLO Properties

Their NLO figures of merit can be of orders of magnitude higher compared to inorganics, and their long-term orientation and photochemical stability orders of magnitude better as in conventional electro optic polymers. In the last few years there have been several promising structuring techniques developed for the highly NLO organic crystal-oxalic acid, which open a wide spectrum of new possibilities and functionalities in guided wave photonic technology. Nd:YAG laser using the first harmonics output of 1064 nm with pulse width of 8 ns and repetition rate10 Hz was passed through the sample. The second harmonics signal, generated in the crystal was confirmed to form the emission of green radiation by the crystal. It shows that amino acids doped oxalic acid crystals have higher

efficiency. It was observed that the irradiation process enhance the NLO property of doped oxalic acid crystals.

4. RESULTS AND DISCUSSIONS

We have grown single crystals of oxalic acid crystals and organic dyes doped oxalic acid crystals and characterized them by employing FT-IR and X-Ray diffraction methods. The doped crystals show good second harmonic generation efficiency. There is a different class of non-linear optical materials, which possess important optoelectronic properties. However, to fabricate optical devices using these materials, a detailed study of ion induced stoichiometric and structural changes occurring in them are necessary.The optical transmittance of the crystal confirms the transparency of the crystal. The band gap energy value (4.25eV) predicted from UV studies confirms the dielectric behaviour of the material. Hence, the material is confirmed as a dielectric material to induce polarization for second harmonic generation when a powerful laser beam is incident on the material. The dielectric studies prove that the sample has low dielectric constant and dielectric loss values at high frequency.

5. CONCLUSION

Single crystals of oxalic acid crystals were grown from aqueous solution by slow evaporation technique under room temperature. The grown crystals were characterized by single crystal XRD and it is confirmed that the crystal belongs to the orthorhombic system. The functional group values were predicted by using FTIR analysis. Dielectric measurements were carried to analyze the dielectric constant and dielectric loss at different frequencies and temperatures. Doping organic dyes, the stability of oxalic acid crystals is strong enough and such effect is likely to be reduced. Irradiation effects diffuse the dyes uniformly in the crystal. The nano-islands of dyes in oxalic acid crystals are likely to be dissolved and enhance the nonlinear optical properties of these materials.

References

[1]. H. F.Robey, J.Crystal Growth 259, 388 (2003).

[2]. Sonal S .Gupte, Ranjit D.Pradhan, J.Appl.Phys. 91, 3125 (2002)

[3]. Shukin Lin, Liting Li, J. Cryst. Growth 249, 341 (2003).

[4]. K. Muthu, S.P. Meenakshisundaram, J. Phy. and Chem. of Solids 73, 1146 (2012).

[5]. J. Thomas Joseph Prakash, M. Lawrence, Int. J. of Comp. Appl. 8, 37 (2010).

[6]. N.R. Dhumane, S.S. Hussaini, V.G. Dongre, M.D. Shirsat, Opt. Mat. 31, 328 (2008).
P. Ramasamy, Mat. Chem.Phys. 82, 273 (2003).

[7]. H. V.Alexandru, S. Antohe, J. Crystal Growth 258, 149 (2003).

[8]. P. Angeli Mary and S. Dhanuskodi, Cryst. Res. Technol. 36, 1231 (2001).

[9].R. Mohan Kumar, D. Rajan Babu, D. Jayaraman, R. Jayavel, and K. Kitamura, J. Cryst. Growth 275.

GROWTH AND CHARACTERIZATION OF DYES DOPED KDP CRYSTALS FOR LASER APPLICATIONS

S.Rajeshkumar[1], M.Kalaiselvan[2], P.Damodaran [3] , P.Ambalavanan[4] and P.Kumaresan[5*]

[1]P.G Department of physics, King Nandhivarman College of Arts and Science, Thellar-604 406.
[2]Govt.Hr.Sec.School, Melmalaiyanur-604 210, Gingee,Villpuram Dt.
[3,5]P.G & Research Department of Physics, Thiru.A.Govindasamy Government Arts College, Tindivanam - 604 002.
[4] P.G & Research Department of Physics, Arignar Anna Govt. Arts College, Villupuram-605 602.
Email : logeshkumaresan@yahoo.com

Abstract

Potassium Dihydrogen phosphate (KDP) crystals are one of the most popular crystals used for Non-linear optical (NLO) applications. Pure and dyes (Coumarin, Methyl Red) doped KDP crystals were grown by slow evaporation technique at room temperature. Grown crystals have been characterized using power X-ray diffraction and Fourier Transform Infrared Spectroscopy (FTIR). The presences of dyes were confirmed by FTIR and EDX spectra. Dye molecules possess π electron similar to conjugated polymers, but the molecules themselves are not very big. Their energy level structure shows the presence of bands containing many closely spaced levels corresponding to vibrational and rotational states. A variety of dyes for many laser operating wavelengths were employed in the past. Dyes embedded in KDP crystal and dye doped crystal were also reported as useful non-linear optical media.

1. INTRODUCTION

Potassium Dihydrogen phosphate (KDP) crystals are one of the most popular crystals used for Non-linear optical (NLO) applications. An increasing demand of crystal in scientific media is because of high nonlinear transparence property. KDP dominates all other inorganic crystal by having this kind of properties. In the present investigation the organic Coumarin and Methyl red were doped with KDP in 0.1 % ratio and grow by slow evaporation Technique at room temperature. The grown pure and Coumarin and Methyl red dye doped KDP crystal has been subjected to Powder X-ray diffraction and FTIR. The presences of dyes were confirmed by FTIR and EDX spectra.

2. EXPERIMENT

2.1 CRYSTAL GROWTH

The method of growing crystals varies widely; it is mainly dictated by the characteristics of the material and its size. Crystal growth techniques are generally classified in to three categories; they are growth from solution, growth from vapor and growth from melt. Each growth techniques has numerous variations, all materials cannot be grown by all the above three methods. In my investigation the organic Coumarin and Methyl red were doped with KDP in 0.1 % ratio and grow by slow evaporation technique at room temperature.

In this technique, an excess of a given solute is established by utilizing the difference between rates of evaporation of the solvent and the solute. A solution of the compound in a suitable solvent is

prepared. The water is mainly used as a natural solvent. If the compound is not dissolved in water then organic solvents such as acetone, ethanol, methanol etc are used.Unlike the cooling method, in which the total mass of the system remains constant, the solvent evaporation technique; the solution loses particles, which are weakly bound to other components and therefore the volume of the solution decreases. In almost all cases, the vapor pressure of the solvent above the solution is higher than the vapor pressure of the solute and therefore the solvent evaporates more rapidly and the solution becomes supersaturated. Usually, it is sufficient to allow the vapor formed above the solution to escape freely into the atmosphere. This is the oldest technique of crystal growth and technically, it is very simple.

The KDP salt was purified by repeated recrystallization using the method of dissolving in distilled water. Then the solution of KDP salt was prepared in a slightly under saturation condition. The solution was stirred well for three hours constantly using magnetic stirrer still the salt has been dissolved in water. Then the prepared solution were transferred into two clean Petri dishes and kept for crystallization at room temperature in a quiet place.

Figure 1(a).Coumarin doped KDP Crystal and 1(b).Methyl Red doped KDP Crystal

A supersaturated solution of pure KDP and 0.1% of Coumarin and Methyl red doped KDP at room temperature was obtained by constant stirring up to three hours and then filter into beakers. The good quality seeds were suspended in respective beakers using the nylon thread. Slow evaporation method was employed for the growth. After completion of growth run, the crystal was harvested. The photograph of grown Coumarin and Methyl Red doped KDP crystal is shown in figures 1(a) and1 (b).

3. CHARACTERIZATION

The powder X-ray diffraction and Fourier Transform Infrared Spectroscopy analysis has been carried out on the grown crystal.The structural properties of single crystals of pure and Coumarin doped KDP have been studied by X-ray powder diffraction technique. Powder X-ray diffraction studies of pure and methyl red doped KDP crystals were carried out, using Rich Seifert XRD 3000P, X-ray diffractometer with Cu K_α (λ=1.54056Å) radiation. The samples were scanned for 2θ values from 10˚ to 40˚ at a rate of 2˚ /min. Figure 2. shows the powder XRD pattern of the pure , Coumarin and methyl red B doped KDP crystal. The diffraction patterns of the pure and Coumarin doped KDP have been indexed by least square fit method. It is seen that both the pure and doped crystals

crystallizes variations in the lattice parameters which are due to the incorporation of the dopant in the KDP crystal lattice.

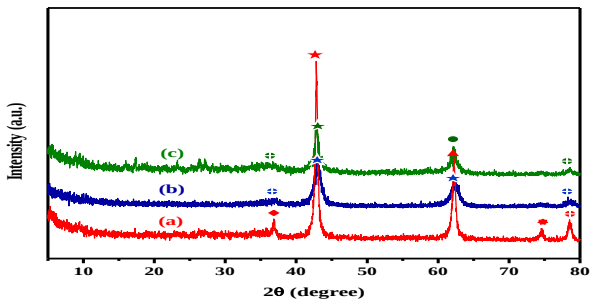

Figure 2. XRD of (a) Pure KDP (b) Coumarin doped KDP and (c) Methyl Red doped KDP Crystal

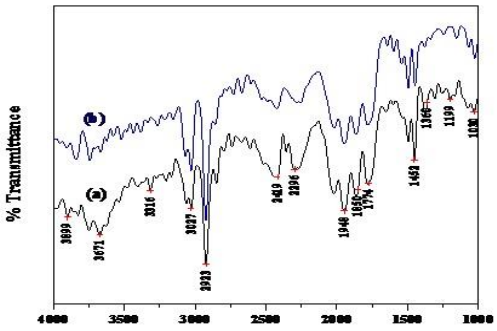

Figure 3. FTIR Spectra of (a) Coumarin doped KDP and (b) Methyl Red doped KDP Crystal

The FTIR (Fig.2) of all of them were recorded from solid phase samples on a bruker IFS 66V model spectrophotometer using 1064nm output of a cw diode pumped Nd:YAG laser as a source of excitation in the region 400 – 4000 cm^{-1} operating at 200mW power at the samples with a spectral resolution of $2cm^{-1}$. The IR spectra were also recorded on Shimadzu–800, FTIR spectrometer series of Japan in the region 400 – 4000 cm^{-1}. A peak at 2296 cm^{-1} corresponds to CH2 stretching. The band at 1580cm-1 indicates the presence of symmetric stretching of carboxylate (COO-) ion. It was confirmed that broad envelope positioned in between 2750-3500 cm^{-1} corresponds to symmetric and asymmetric stretching modes of NH_2 grouping of methyl red coordinated KDP. The NH and N-C-N stretching vibrations were also seen in these crystals.

4. RESULTS AND DISCUSSION

When Coumarin and Methyl red dye has been doped in KDP crystal it has some changes in its character. By comparing pure KDP crystal the characteristic changes in Coumarin and Methyl red dyes doped KDP crystal has been studied by using XRD and FTIR analysis.The excitation of X-ray in KDP and Coumarin, Methyl red dye doped KDP crystal has been found. While comparing the XRD pattern of coumarin and methyl red dye doped KDP crystal with pure KDP crystal structure the 2 theta values slightly shifted towards left i.e. the 2 theta values decreased in fraction and hence the d-spacing range increased in fraction. The pyramidal plane (110) and (101) has been dominated heavily whereas the basal plane (200) is unaffected. From FTIR pattern it was found that a strong absorption peak near the wavelength of 280nm in pure KDP crystal. Whereas in Coumarin and methyl red dye doped KDP crystal the absorbance range is shifted towards the higher wavelength side around 480nm. This implies that coumarin and methyl red dye finely incorporated in KDP crystal.

CONCLUSION

Using FTIR and XRD analysis, the data coumarin and methyl red dye doped KDP crystal has some changes in its structure. The shift of absorption and excellent transmission in entire visible region makes this crystal a good candidate for electronic applications. The characteristics study of grown coumarin and methyl red dye doped KDP crystal indicated that this crystal can be a high NLO crystal than a pure KDP crystal.

ACKNOWLEDGEMENTS

We gratefully acknowledge financial supports from the Department of Science & Technology-Science and Engineering Research Board **[**Dr.P.Kumaresan, Young Scientist Award, DST-SERB-FAST TRACK, PS-20/2009(SR)] and University Grants Commission-[Dr.P.Kumaresan, Major Research Scheme-F.No.38-18/2009 (SR)], New Delhi, India.

REFERENCES

1.G. Ramasamy and G. Bhagavannanarayanana, , Ind. J. Pure Appl. Phys. 52, 255(2014).

2. G. G.Muley, Sci. Technol. 2, 109 (2012).

3. G. G. Muley, M. N. Rode, and B. H. Pawar, Acta Polonica A 116, 1033 (2009).

4. B. S. Kumar and K. R. Babu, Indian J. Pure Appl. Phys.46, 123 (2008).

5. P. Kumaresan and S. Moorthy Babu J. Optoelectron. Advc. Mater. 9, 1299 (2007).

6. P. Rajesh, P. Ramasamy, J. Cryst. Growth 311, 3491(2009).

7. P. Rajesh and P. Ramasamy, Phys. B 404, 1611(2009).

STRUCTURAL AND OPTICAL STUDIES OF SILAR DEPOSITED CdS THIN FILM WITH SWANEPOEL METHOD

GUNASEKARAN M[1], JAYAPRIYA J[2] AND SEENUVASAKUMARN P[1]

1Department of Physics, Muthurangam Government Arts College (Aut), Vellore-2, Tamil Nadu.

2Department of Physics, Arinjar Anna Government Arts College, Walajapet, Tamil Nadu.

***Corresponding author**: rpyeskay@gmail.com*

1. Introduction

Any solid or liquid system possesses at most two-dimensional order of periodicity called "thin film". Thin film is a layer of materials ranging from nanometer to several micrometer ranges. CdS thin films have received considerable attention during recent years because of their excellent properties in optoelectronic fields, heterojunction solar cell considered to be a promising alternative to the more widely used silicon devices [1-2], electronic devices including light emitting diodes [3], large screen liquid crystal devices [4], gas sensors [5], single electron transistors and field effect transistor [6, 7] etc.

Efforts have been devoted in preparation of high quality CdS thin film are synthesized and its different chemical techniques such as chemical bath deposition (CBD) [8, 9], spray pyrolysis (SP) [10], electro deposition [11], SILAR etc have been used to obtain thin films. In all these experimental methods there is wastage of chemicals and time. Moreover films can't uget deposited uniformly on the substrate. SILAR is one of the newest solution methods used for the deposition of thin film, which is also known as a modified version of chemical bath deposition. SILAR method is a step-wise process of chemical deposition of thin films from aqueous precursor solutions. It is a unique method in which thin films of compound semiconductor can be deposited by alternate dipping of a substrate into the aqueous solutions containing ions of each component. The relative simplicity of the successive ionic layer adsorption and reaction (SILAR) method and its potential application for large area deposition make it very attractive. Easy control of thin film thickness by adjusting number of deposition cycles is the beauty of this method. In this method the substrate can be separately immersed in cationic and anionic solutions for the formation of thin films. In this work, we report the fabrication of CdS thin films havin appropriate properties for application like photo voltaic etc has been confirmed using different characterization techniques are reported below.

2. Experimemtal Details

2.1. CdS Thin Film Formation

Cadmium Sulphide films were deposited on glass substrates. It is Note worthy that any substrates can be used where main criteria in the selection is that the selected substrates do not react with the bath precursor solutions [12]. In order to remove the moisture from the surface, substrates were cleaned with double distilled water for few minutes. In the present case, Cadmium Sulphide films have been deposited by alternate immersion of substrates in Cadmium nitrate (Cd $(No_3)_2$ $4H_2O$) as a cationic precursor with the pH maintained at 4 and in Sodium Sulphide (Na_2S H_2O) as anionic precursor with

the pH at 12. The reaction occurred at the substrate surface to form CdS. The adsorption time of cations, anions, rinsing time, dry time and number of cycles are already programmed for desired period of time. After dried for enough time, the formed thin films are subjected to characterizations like X-ray diffraction for identification of crystal structure, particle size, strain and dislocation density of synthesized film. The spectroscopic studied like UV-VIS, PL & FTIR are performed to analyze the band gap excitation wavelengths and molecular vibrations respectively. The morphological studies are studied from SEM micrograph and the different elements present in the films are identified form EDAX studies.

Reaction mechanism

The reaction mechanism is

$Cd(NO_3)2\ 4H_2O + H_2O \rightarrow Cd_2+ + 2NO_2\uparrow + 5H_2O + O_2\uparrow$ → 1

$Na_2S + H_2O \rightarrow 2Na+ + SH- + OH-$ → 2

$SH- + OH- \rightarrow S2- + H2O$ → 3

$Cd_2+ + S_2- \rightarrow CdS$ → 4

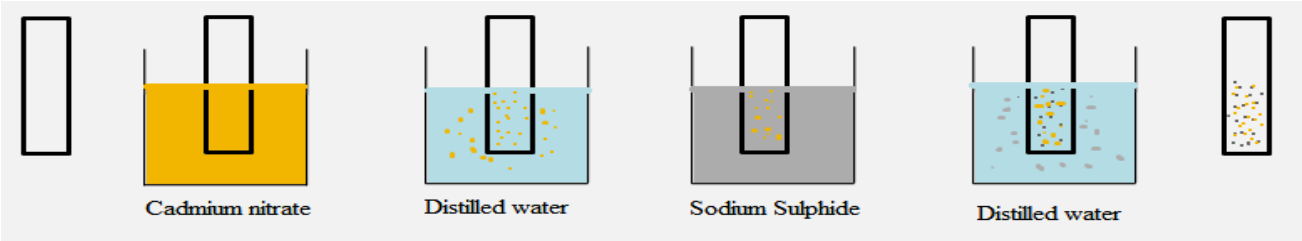

Figure 1. SILAR technique for CdS thin film

3. RESULTS AND DISCUSSION

3.1. X-Ray Diffraction Analysis

Film crystallinity was analyzed using X-ray diffraction and diffraction peaks are shown in figure 2. The presence of peaks confirms the crystalline nature of thin film. The XRD pattern of a typical CdS thin film exhibits prominent broad peaks and the lattice parameter values are a=b=8.578 Å & c= 5.872 Å with α = β = γ= 90°. This suggests that deposited thin film is to have tetragonal structure.

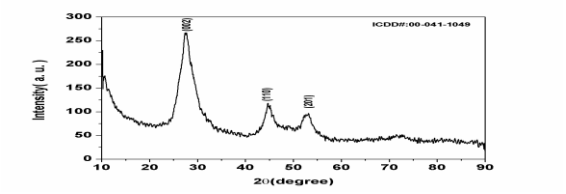

Figure 2 X-Ray Diffraction Analyses

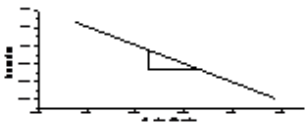

Figure 3 βcos θ vs 4sin θ Strain plot form XRD

The average particle size was calculated by using Debye Scherrer's formula by knowing the Full Width at Half Maximum (FWHM) for the corresponding maximum intensity peak (2θ=27.6811°) [13]. The particle size is found to be 10.9568nm. Moreover from the graph as the base width of the 100% peak is broadened one indicates that the particle size is less than 100nm range. The dislocation

density $\delta = 8.32976 \times 10^{-14}$ m^{-2} is calculated using crystallite size and the strain is found to be $1.3224 \times 10^{-3} m^3$ from the figure 3 [14].

3.2. Optical studies

The optical absorption spectra of as-deposited CdS film are shown in figure 4. The absorption spectrum was studied in the region 200-1200 nm for the deposited thin film at room temperature. The cut of wave length for CdS thin film is found to be in visible region. This indicates that grown thin film can used for any optoelectronic applications.

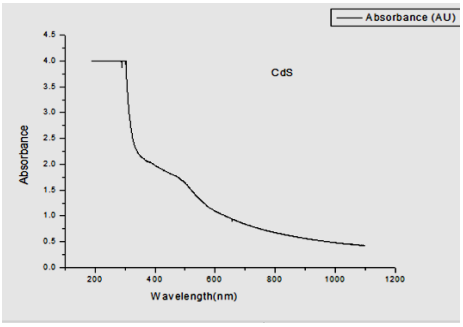

Figure 4 Absorbance spectra of CdS thin film

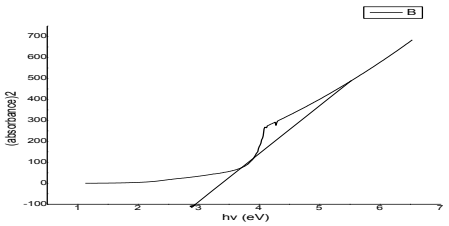

Figure 5 Plot of $(\alpha h\upsilon)^2$ vs. hυ for CdS thin film

The energy band gap for a deposited thin film was calculated using the Tauc equation $(ah\upsilon)^2 = \alpha_0^2 (h\upsilon - E_g)^n$ .Here α_0 is a constant and E_g is band gap energy [14]. Figure 5 shows the plot of $(\alpha h\upsilon)^2$ vs. hυ for CdS thin film. It has been observed that the plot of $(\alpha h\upsilon)^2$ vs hυ is linear over a wide range of photon energies indicating a direct type of transition [15]. The X-intercept on the graph gives the transition band gap energy gap to be 2.92 eV.

Refractive index and film thickness

The refractive index and thickness of the thin film can be calculated from a simple transmittance spectrum using the Swanepoel method [16, 17]. Practical application of this method entails, as a first step, the calculation of the maximum and minimum transmittance envelope functions, *TM* (λ) and *Tm* (λ), *M m* respectively. From these functions the refractive index *n* (λ) found to be 1.532.The film thickness, *d*, a number of thicknesses are calculated using Swanepoel equation and then the average of *d* is calculated which is about 1315 nm[18, 19].

3.3. Photoluminescence

Light emission from compound semiconductors has been an important phenomenon due to its technological applications [20]. Most of the optoelectronic component devices such as light emitter or photo detectors are being fabricated using semiconductors having a direct band gap with high efficiency like CdS thin films. These films are also used in solar cells as light absorbing panels. PL analysis of the CdS thin film over glass substrate was performed to analyze the purity of deposition [21]. The photoluminescence spectral ranges between 300-800nm for both emission and excitation peaks shown in figure 6. The PL spectra of CdS exhibits many lower energy emission peaks for certain excitation wavelengths are tabulated in table 1.

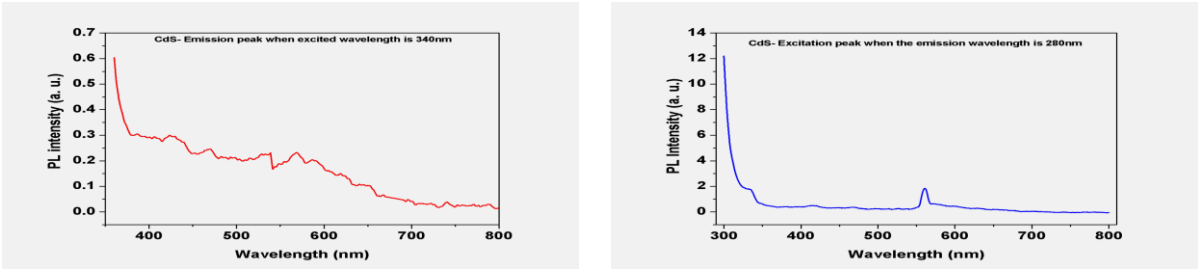

Figure 6 Excitation peak for CdS thin film & Emission peak for CdS thin film

Table 1. Excitation wavelength, Emission wavelength, Colour and Reported Energy

COLOUR	EMISSION nm	EXICATION nm	REPORTED ENERGY eV
Blue	450	340	2.76
Green	560	340	2.33
Ultraviolet	280	400	2.28
Green	555	480	2.33

` 3.4. Surface Morphology

The surface morphological studies of the CdS thin film have been carried out from Scanning Electron Micrographs (SEM). Figure 7 shows the SEM images of CdS film for three different scale regions. Among these three images 10 µm range shows the film is deposited on glass substrate is homogeneous and the CdS nanoparticles can occupy the glass substrate without any space in the grown film [21].

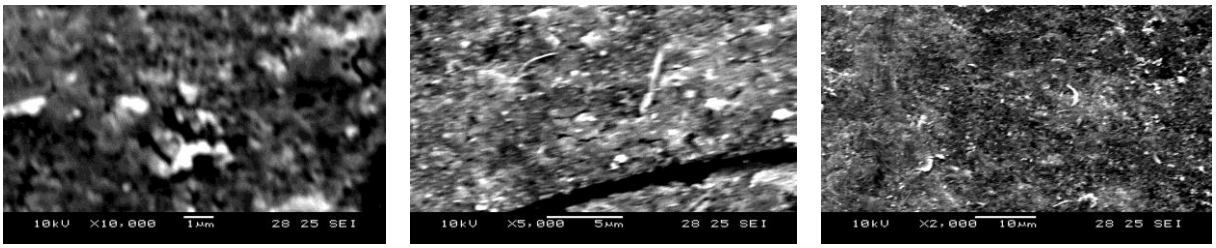

Figure 7. SEM images of grown CdS thin film for as 1 µm range, 5 µm range, 10 µm range

3.5 Energy Dispersive X-Ray Analysis Spectra

Figure 8 shows typical EDAX patterns and details of relative analysis for this thin film. This spectra show the expected elements (Cd and S) and absence of impurities detected in the thin film. The elemental analysis was carried out only for CdS, Cd and S the average atomic percentage was found to be 51.4:48.6.

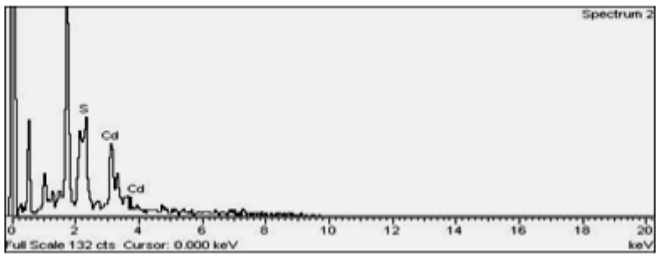

Figure.8. EDAX spectrum of CdS thin film deposited on glass substrate

4. Conclusion

In this study, the SILAR method was used to deposit CdS thin film on a clean glass substrate. The structural property of this thin film was investigated by XRD which confirms its crystalline nature and tetragonal structure. The average particle size is found to be 10.9568nm, strain (ε) found to be 1.3224 x $10^{-3}m^3$, dislocation density (δ) 8.32976 X 10^{-14} m^{-2} of the materials is calculated from XRD data using Scherrer formula. The refractive index *n* (λ) of the film is found to be 1.532.The average film thickness, is calculated to be about 1315nm. The energy dispersive X-ray analysis spectra showed that the expected elements exist in the thin films. Using UV-VIS spectroscopical data the optical band energy gap (E*g*) at the edge of absorption band has been found 2.92 eV by the Tauc relation. CdS has a bandgap of 2.92 eV which corresponds to a light wavelength of 300 nm at 300 K. It is a good material to study the photoluminescence properties.The grown thin films are subjected to different excitation wave lengths and their corresponding emission wave lengths are observed from photoluminescence spectroscopy. CdS is a direct band gap material and has been of interest due to its high efficiency in the solar cells. It is also known as an efficient light emitter of green light resulting from the band-to-band transition. Recently, it has attracted a great deal of attention for the production of nanocrystals for biomedical applications.

References

1. H.R. Motinho, D. Albin, Y. Yaan, R.G. Dheo, X. Li, C. Perkis, C.S. Jiang, *Thin Solid Films* 436, 175 (2003).H. Metin, R. Esen, *Semicond. Sci. Technol.* 18, 647 (2003).J.
2. J. Barman, J. P. Borach and K. C. Sarma, "Effect of pH Variation on Size and Structure of CdS Nanocrystalline Thin Films," Chalcoginide Letters, Vol. 11, No. 5, 2008, pp. 265-266.
3. G.S. Vorobjov, V.O. Zhurba, A.S. Krivets, *J. Nano- Electron. Phys.* 2 No4, 47 (2010).
4. N. I. Achuko and C. C. Ugwuegbu, "Optical Properties of CdS Thin Films Obtained by Chemical Bath Deposition," International Journal of Academic Research, Vol. 6, 2011, pp. 368-374.
5. J. Levinson, F.R. Shepherd, P.J. Scanlon, W.D. Westwood, G. Este, M. Rider, *J. Appl. Phys.* 53, 1193 (1982).
6. U. Pal, R. Silva-Gonzalez, G. Martinez-Montes, M. Gracia- Jimenez, M.A. Vidal, S. Torres, *Thin Solid Films* 305, 345 (1997).
7. J.H. Schon, O. Schenker, B. Batlogg, *Thin Solid Films* 385, 271 (2001).
8. S.S. Kale, C.D. Lokhande, *Mater. Chem. Phys.* 62,103 (2000).
9. S.D.Sartale,C.D.Lokhande,. Growth of copper sulphide thin films by successive ionic layer adsorption and reaction method. Matter.Chem.Phys.1999,64
10. **T**Banerjee M. Chongad L. and Sharma A. "Structural and Optical Properties of Pure and Copper Doped NiS Nanoparticles" *Research Journal of Recent Sciences* Vol. **2**(ISC-2012), 326-329 (2013)
11. J. Sa´nchez-Gonza´lez, A. Dı´az-Parralejo, A.L. Ortiz , F. Guiberteau, "Determination of optical properties in nanostructuredthin films using the Swanepoel method",

12. .B.R.Sankapal,R.S.Mane, and C.D.Lokhande, "Photoluminescence Specroscopy Of CdS and GaSe" *Mater.Res.Bull*.,2000,35,177-184.
13. Linhtowlers R. A. Stradling and P.C.Klippstein Growth and characterization of semiconductors, *Bristol* 1990, p. 135.
14. R Swanepoel, "Determination of the Thickness and Optical Constants of Amorphous Silicon". *J. Phys*. E 16, 1214–1224 (1983).
15. R.J. Swanepoel "Optical Properties of Solids", *J. Phys. E: Sci. Instrum*. 16 (1980) 1214.M. Fox, Oxford University Press, 2002.
16. Ramphal Sharma, "Effect of annealing on structural and optoelectronic properties of CdS thin film by SILAR method" *Adv.Appl.Sci.Res*.,2011, 2(4):417-425.
17. S.Patra,S.Mondal, and P.Mitra "Preparation of ZnS and SnS Nanopowders by Modified SILAR Technique" *Jour.Phys.Sci*.Vol.13,2009,229-234.
18. C.B. Collins, R. O. Carlson and C.J. Gallagher, "Negative-U properties for substitutional Au in Si''Phys.Rev. EPL 105, 1168, (1957).
19. R M Sangshetti, V A Hiremath and V M Jali, "Combustion synthesis and structural characterization of Li–Ti mixed nanoferrites" *Bull. Mater. Sci*, vol 34, No. 5 August 2011 pp. 1027–1031 Indian Academy of Sciences.
20. T Theivasanthi, N Kartheeswari and M Alagar**, "**Chemical Precipitation Synthesis of Ferric Chloride Doped Zinc Sulphide Nanoparticles and Their Characterization Studies" *Research gate*, 03/2013, DOI 10, 7598/cst 2013.207.
21. P. Mitra and S. Mondal," Structural and Morphological Characterization of ZnO thin Films Synthesized by SILAR" *Theoretical and Applied Physics* Vol. 1, 2013, 17-31.

PYRO ELECTRIC STUDIES ON DYES DOPED TGS CRYSTALS FOR IR DETECTOR APPLICATIONS

D.Narayanasamy [1], P.Kumaresan [2] J.Logeswari [3] & P.M.Anbarasan [4]

[1] Department of Physics, S.K.P Engineering College, Tiruvannamamala-606611

[2]Department of Physics, Thiru.A.Govindasamy Government Arts College, Tindivanam-604 002

[3]Department of Chemistry, Adhiparasakthi Engineering College, Melmaruvathur-603 319

[4] Department of Physics, Periyar University , Salem-636 011

e.mail ID : nsamyrd10@gmail.com

Abstract

This crystal has the most rectangular hysteresis loop and it has high pyroelectric coefficient and low dielectric constant. These properties make it a ferroelectric of great interest. TGS has a complex chemical and crystallographic structure. Triglycine sulphate (TGS) crystals were grown by slow evaporation process. The stability of TGS single crystal was improved by doping organic dyes. To determine the lattice parameters, powder X-ray diffraction analysis was performed by X-ray diffractometer system with Cu-K_α (λ = 1.54178Å) radiation at room temperature with an operating voltage 40 kV and the tube current was 30 mA. In the present work, optical transmission and absorption spectra were recorded by Systronics UV-Double beam spectrometer in the wavelength range 190 to 1100 nm. The FTIR spectra of all grown crystals have been recorded in the range of 400 - 4000 cm^{-1} using Bruker FT-IR 8400 spectrophotometer by KBr pellet technique. The results for doped TGS crystal are compared with the results of the pure TGS crystals. The structural, optical properties, pyroelectric properties and dielectric properties of the doped crystals were analyzed.

1. Introduction

The study of Ferro electricity has been closely linked with device applications [1]. The pyroelectric properties of ferroelectrics make them very suitable for thermal detection. This can be used to detect any radiation that results in a temperature change of the crystal [2]. They also have useful features at room temperature operation TGS has been the most extensively studied material for thermal detector applications. Triglycine sulphate $(NH_2CH_2COOH)_3.H_2SO_4$ crystals are very important because of their application as room temperature IR detectors and imaging systems[8].

Triglycine sulphate $(NH_2CH_2COOH)_3.H_2SO_4$ crystals are very important because of their application as room temperature IR detectors and imaging systems[3].

1. CRYSTAL STRUCTURE AND PROPERTIES OF TGS

TGS [$(NH_2CH_2COOH)_3.H_2SO_4$] is a colourless, odourless and acidic salt[4]; it is synthesized by Glycine acid with sulphuric acid in the molar ratio of 3:1[5].

2.1 Synthesis of the salt

TGS was synthesized by taking the analar grade glycine (CH_2NH_2COOH) and concentrated sulphuric acid (H_2SO_4) Glycine and sulphuric acid were taken in the ratio 3:1 respectively. The required volume of concentrated sulphuric acid was diluted with millipore water.

The reaction between glycine and sulphuric acid is given below

$$3\ (CH_2NH_2COOH) + H_2SO_4 \text{ --------> } (NH_2CH_2COOH)_3.H_2SO_4$$

2.2 Experiment

Recrystallized salt was used to study the solubility of pure and xylenol orange doped TGS for three different temperatures 35, 40 and 45°C. A sealed container charged with Millipore water and the

solute, maintained at a constant temperature, was used to determine the equilibrium concentration. The solution was stirred continuously for 24 hours.

3. FTIR STUDIES

The presence of dopants in the crystal was qualitatively investigated by the FTIR studies. The infrared spectra were obtained with a BRUKER IFS 66V FTIR spectrometer using the KB_r pellet technique. The FTIR data for pure and dye doped TGS.

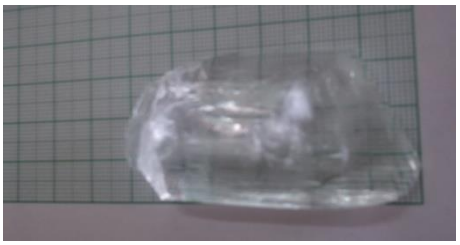

Figure 1. Xylenol dye doped TGS crystal

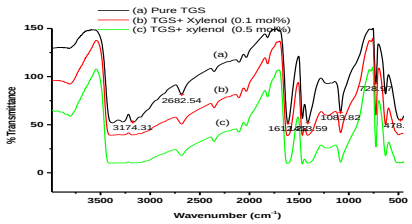

Figure 2.FT-IR Spectra of pure and Xylenol doped TGS Crystals

The strong absorption in the 1015 - 1175 cm region is evidently due to the sulphate part of the molecule.

4. ANALYSIS OF PYROELECTRIC STUDIES

The doping of TGS with Xylenol orange has shifted the ferroelectric transition temperature (T_c) to a higher value. The shift observed at Curie temperature may be due to simultaneous change in macroscopic polarization and increase in the electrical conductivity. The dipolar strength of Xylenol orange is larger compared to pure TGS as a result of large electron repulsion from $(CH_3)_2CH$ group. So, Xylenol orange doped TGS is found to have maximum pyroelectric coefficient compared to pure TGS.

5. Conclusion

In the present investigation, the molecules of dye such as xylenol orange, whose molecular structures are CH_3 (CH) (NH_2) COOH, have been introduced in the TGS crystal. The pyroelectric studies it was found that doping the crystals with xylenol orange enhanced the pyroelectric coefficient and the ferroelectric transition temperature (T_c). The FTIR studies reveal a broadening of peaks for the doped samples confirming the presence of dopants in the crystal. The substitution of dye - in the place of glycine has been found to improve the crystal properties by the way of contributing to effective internal bias in these crystals which, in turn, inhibits ferroelectric switching giving permanently poled single domain crystal. This improved the device characteristics and hence xylenol orange crystals. The spontaneous polarization of ferroelectric crystal originates from the dipole moment of each dipole within the crystal.

References

[1] Tiffany N.Thomas,Terry A Land, Michael Johnson, William H Casey, Journal of Colloid and Interace Science ,280 (2004)18-26.
[2] H.F.Robey, J.Crystal Growth, 259(2003)388-403
[3] N.Zaitseva, L.Carman and I.Smolsky, J. Cryst. Growth, 241 (2002) 363.
[4] P.M.Ushasree, R.Jayavel, P.Ramasamy , Mater. Chem. Phys. 61 (1999) 270.
[5] Silverstein, Bassler and Morrill, Spectrometric identification of organic compounds: by John Wiley & Sons, Inc., Fourth Edition, (1981), Page176.

CRYSTAL GROWTH AND CHARACTERISATION OF PURE AND METAL DOPED AMINO ACID FOR NLO CRYSTALS

P. Sakthi[1] and R. Rajasekaran[2]*

[1]P.G & Research Department of Physics, Government Arts college, Thiruvannamalai-606603
*[2]*Aruna Vidhya Arts & Science College, Kannakurukkai - 606 704*
Email: sakthiperumalphd@gmail.com

ABSTRACT

A new organic non linear optical material pure maleic acid, L-Tartaric acid and $CoSo_4$, KCl doped maleic acid and L-Tartaric acid MA, CMA, TA and KTA crystals have been synthesized and grown from its aqueous solution by slow evaporation method at room temperature. Crystalline nature of the grown crystals were identified by using powder X-ray diffraction studies. The different modes of vibration presents in the crystals are identified by the FTIR analysis. The optical transmittance spectra were carried out UV-Visible spectrometer. The second harmonic generation were measured by Kurtz and Perry technique.

1.1 Introduction

Great efforts have been devoted to the research and design of highly efficient nonlinear optical (NLO) materials due to their widespread applications such as high-speed information processing, optical communications, and optical data storage [1-2]. It is well known that the deliberate election of reaction reagents is crucial to produce more efficient NLO materials of good quality. Amino acids are widely utilized because they not only contain chiral carbon atoms directing the crystallization in noncentrosymmetric space group, but also possess zwitterionic nature favoring crystal hardness [2–4]. Here we first discuss the grown MA, CMA, TA and KTA crystals together with various characteristic studies such as powder X-ray diffraction, FT-IR spectra and optical property

2.2 Experimental details

The calculated amounts of the AR grade starting materials pure and copper sulphate, potassium chloride doped L-maleic and L-tartaric acid MA, CMA, TA and KTA are taken 2:1 and 1:1 molar ratio were dissolved in double distilled water and thoroughly mixed for about 8 hours using a magnetic stirrer to ensure homogeneous temperature and concentration throughout the volume of the solution. The chemical reaction are given bellow,

$$C_4H_4O_4 + 2CuSo_4 \longrightarrow Cu\,[C_4H_3O_4] + H_2So_4 \uparrow$$

$$C_6H_6O_6 + KCl \longrightarrow K\,[C_4H_3O_4] + HCl$$

The saturated solutions were filtered twice with whattman filter paper before it was subjected to evaporation. The solutions were covered to avoid dust and kept undistributed for days together. Crystal of appreciable size of pure L-maleic and L-tartaric acids were obtained with in 20 and 15 days. The $CoSo_4$ and KCl doped L-maleic and L-tartaric acids single crystals were obtained at the end of 18 and 12^{th} days. The dimensions of the grown pure and $CoSo_4$ and KCl doped L-maleic and L-tartaric acids crystals are 9× 5.2 × 1.5, 75× 45 × 3, 2×13×2 and 19×13×3 mm^3 respectively.

3.1. Powder XRD Studies

The grown MA, CMA, TA and KTA crystals were subjected to powder X–ray diffraction analysis using βRigaku Minifix II-C, CuKα radiation of wavelength (1.5406 Å) (Fig.2). The results indicate that that planes gives the strongest reflection and the sharp XRD peaks of grwon crystals without any broadending reflects the MA, CMA, TA and KTA crystals in good rystalline nature.

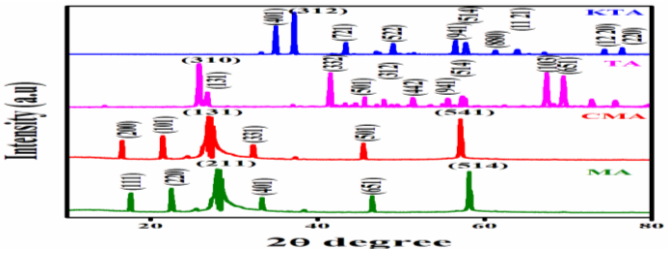

Fig. 1 Powder XRD pattern of MA andCMA grown crystals

3.2. FTIR spectroscopic study

The FTIR absorption spectra were recorded in the range of 4000-500 cm^{-1} by using Perkin Elmer Spectrum two FTIR/ATR Spectrometer ATR technique is shown in Fig. 3. The funtional groups of grown MA, CMA, TA and KTA crystals were identified and tabulated in Table. 1.

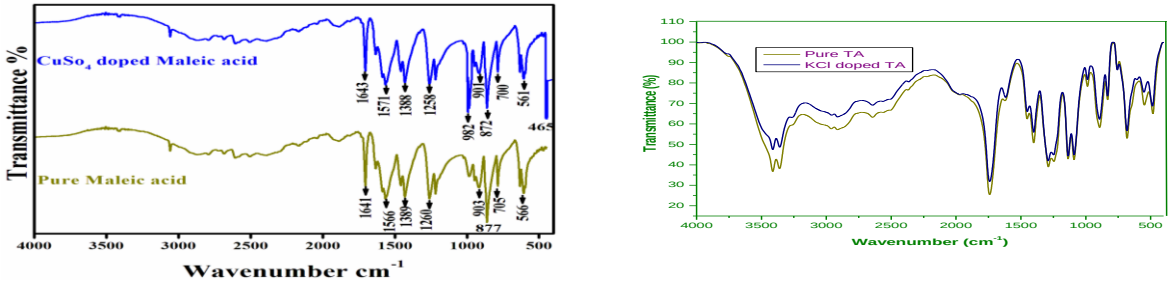

Fig. 2(a&b) FTIR spectra of MA, CMA, TA and KTA grown crystals

Table. 1. Wavenumbers and assignments of pure maleic acid and $CoSo_4$ doped maleic acid

MA (cm^{-1})	CMA (cm^{-1})	Assignments
1641	1643	Asymmetric-carboxylate anion
1566	1571	Symmetric-carboxylate anion
1389	1388	C-C stretching vibration (medium)
1260	1258	C-C stretching vibration (strong)
903	982	O-H stretching vibration
877	901	O-C=O stretching vibration
705	872	C=O stretching vibration
566	700	Asymmetric-carboxylate anion
	561	Symmetric-carboxylate anion
	465	C-C stretching vibration (medium)

TA (cm^{-1})	KTA (cm^{-1})	Assignments
3359	3412	N-H stretching vibration
1799	1741	NH_2 asymmetric vibration
1689	1617	N-C-N symmetric stretching vibration
1586	1402	C=S asymmetric stretching vibration
502	486	N-C-N symmetric bending vibration

3.3. Optical transmission analysis

The UV-Visible spectrumn recorded for a transparent and defect free single crystal of MCTD using LABINDIA UV 3092, UV-Visible spectrophotometer in the wavelength range of 190-900 nm is shown in Fig. 5 MA, CMA, TA and KTA crystals shows the UV cut-off wavelength of 212, 218, 300 and 303 nm. They are well known that an efficient nonlinear optical crystal has an optical transparency and lower cut-off wavelength between 200 and 400 nm. Thus, good transparency

combined with low cut-off wavelength makes MA, CMA, TA and KTA crystals are suitable for the NLO applications. The bandgap of the crystal (E_g) was estimated from the following

$$E_g = 1.243 \times 10^3 / \lambda_{max}$$

Where λ_{max} is the maximum wavelength. This was found to be 5.8 eV, 5.6 eV, 4.1 eV, and 4.0 eV which are thypical property of the dielectric materials. This high value of bandgap shows the crystal possesses dielectric behavior to induce polarization when powerful radiation is incident on the material. The suitability of the grown crystals for photonic and optical applications is confirmed by the absence of absorption bands in the visible region. The large energy bandgap also confirms that the defect concentration in the grown crystal is very low.

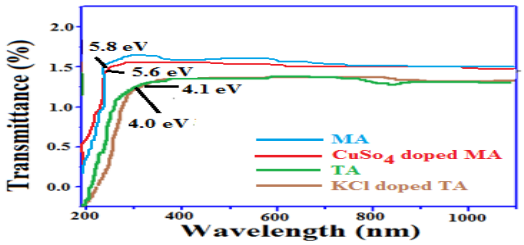

Fig 4. UV-visible transmission spectra of grown MA, CMA, TA and KTA crystals

3.7. Second Harmonic Generation Test

The SHG efficiency of MA, CMA, TA and KTA crystals were evaluated by the Kurtz and Perry powder technique using a Q- switched, mode locked Nd^{3+}: YAG laser emitting 1.06 μm, 8 ns laser pulses with spot radius of 1 mm**.** The input laser beam was passed through an IR reflector and then directed on the powdered sample. The light emitted by the sample was measured by the photo-diode detector and oscilloscope assembly. Microcrystalline material of KDP was used for comparison with MA, CMA, TA and KTA for the SHG experiments. For a laser input pulse of 0.68 mJ, the second harmonic generation of grown crystals are higher than that of KDP. Thus, MA, CMA, TA and KTA grown crystals are relatively a good candidate for SHG applications.

4. Conclusion

The crystalline nature of the grown ZTC, NTC, NCTC and MCTD single crystals have been identified by using Powder X– ray diffraction study. The FTIR spectra revealed that the coordination in the crystals occurs through the sulphur and nitrogen. From the powder SHG measurement, it can be concluded that the grown ZTC, NTC, NCTC and MCTD crystals single crystals generate second harmonic frequency which are 1.1, 3.7, 4.5 and 6.6 times higher than that of pure KDP. The grown single crystals of ZTC, NTC, NCTC and MCTD have shown in lower cut-off wavelength of 341, 327, 318 and 247 nm by using Uv-visible spectrometer. Due to their excellent optical and NLO properties of these crystals can be used for NLO applications.

References

[1] P.N. Prasad, D.J. Williams, Introduction to Nonlinear Optical Effects in Organic Molecules and Polymers, Wiley, New York, 1991.
[2] T. Pal, T. Kar, G. Bocelli, L. Rigi, Cryst. Growth Design 3 (2003) 13.
[3] M.K. Marchewka, S. Debrus, A. Pietraszko, A.J. Barnes, H. Ratajczak, J. Molec. Struct. 656 (2003) 265.
[4] E. de Matos Gomes, V.H. Rodrigues, M.M.R. Costa, M.S. Belsley, P.J.M. Cardoso, C.F. Gonc¸alves, F. Proenc¸a, J. Solid State Chem. 179 (2006) 2521.
[5] G. Ramesh Kumar, S. Gokul Raj, R. Mohan, R. Jayavel, J. Cryst. Growth 275 (2005) e1947.

SYNTHESIS AND CHARACTERIZATION OF PURE AND Ni DOPED TIN OXIDE NANOPARTICLES

K.PRABHA 1*, T.AMUTHA[2], M.VIDHYA[3] AND M. RAMESHBABU[4]

[1, 2]Department of Physics, Mother Teresa Women's University, Kodaikanal.*

[3]Fathima College (Autonomous), Madurai.

[4]Department of Physics, Palani Andavar College for Arts and Culture, Palani

***Corresponding author:** Dr.K.Prabha, Department of Physics, Mother Teresa Women's University, Kodaikanal. 624101, India, Mob: 09787891603;*

E.mail: mtwprabha@gmail.com

ABSTRACT

Pure and Ni–doped Tin Oxide (SnO_2) nanoparticles were synthesized by simple co-precipitation method. The structural, morphological and optical properties of these nanoparticles were investigated by using X-ray diffraction, UV-Vis spectroscopy, FTIR and Photo Luminescence Studies. The X-ray diffraction revealed that all samples are pure tetragonal rutile- structure with crystalline space ($P4_2/mnm$) and the nickel doping did not change the tetragonal structure of tin oxide. The optical band energies of pure and Ni doped SnO_2 nanoparticle were evaluated from UV-Vis-NIR studied and found to be ~2.16 eV and ~1.75 eV respectively.

Key Words: Tin Oxide, X-ray Diffraction, UV-Absorption, FTIR, PL Studies

1. INTRODUCTION

Nanomaterials have attracted great interest due to their intriguing properties, which are different from those of their corresponding bulk state. In the past few years, SnO_2 is an important n-type wide-energy-gap semiconductor (Eg = 3.64 eV, 330 K) which has a wide range of applications such as in solid-state gas sensors [1], transparent conducting electrodes [2], rechargeable Li batteries [3], and optical electronic devices [4]. During the past decade, SnO_2 nanostructures have been one of the most important oxide nanostructures due to their properties and potential applications [5, 6].In present study pure and Ni doped tin oxide nanoparticles were synthesized by co-precipitation method. The effect of Ni doping has been studied using and Powder XRD, optical and FT-IR.

2. EXPERIMENTAL PROCEDURE

For preparation of Ni doped SnO_2, the appropriate amounts (1M of Ni ($Ni(NO_3)2.9H_2O$ and 99M of Tin ($SnCl_2.2H_2O$) of two precursors of Tin chloride (Tin ($SnCl_2.2H_2O$) and Nickel nitrate (Ni ($Ni(NO_3)2.9H_2O$) were dissolved in de-ionized water, stirred for 2 hours hot using plate with a magnetic stirrer. Then, Ammonium Hydroxide (NH_4OH) was added into the solution (drop by drop), with stirring, until the white precipitates were obtained. After 30 minutes of stirring the resultant mixtures were rinsed, several times, with de-ionized water to remove chlorine and other ionic impurities, which may formed during the synthesis process. Then, washed precipitates were dried in air at 40^0C for 20 hours followed by natural cooling up to the room temperature and then final powder products were collected carefully. These precursors were ground in an agate mortar pestle for 30 minutes to obtain fine powder. These powders placed in a Al_2O_3 crucible for sintering in furnace at 450 °C for 5 hrs followed by furnace cooling at room temperature. To get the annealed powdered sample of Nickel doped SnO_2.

3. RESULTS AND DISCUSSION

Fig.1(a) shows the XRD patterns of pure and nickel doped tin oxide nanoparticles synthesized by co-precipitation method.

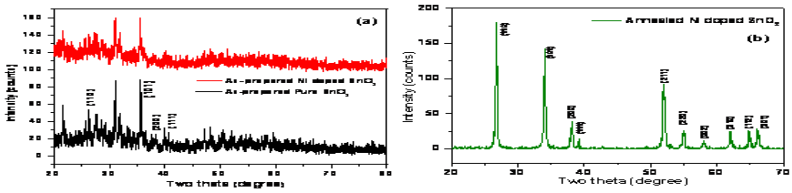

Fig.1 Shows the XRD patterns of (a) as-prepared pure SnO_2 and Ni doped SnO_2, (b) shows the Ni doped SnO_2 annealed for 400°C for 2h sample

Fig.1(b) shows the XRD spectrum of Ni doped SnO_2 nanoparticles annealed at 400°C for 2 hr which showing well defined characteristics peaks. The observed values of 2θ and d-spacing's are in good agreement with the standard values of the JCPDS file no. 21-1250. The diffraction angle 2θ with corresponding diffraction planes (h k l) was observed at 26.81° (1 1 0), 34.04° (1 0 1), 38.07° (2 0 0), 39.13° (1 1 1), 51.93° (2 1 1), 54.90° (2 2 0), 57.98° (0 0 2), 62.01° (3 1 0), 64.82° (1 1 2) and 66.18° (3 0 1) correspond to tetragonal SnO_2 rutile structure with crystalline space group ($P4_2/mnm$). Ni doped SnO_2 samples structure also a comparable similar pattern of pure-SnO_2 was observed except that the diffraction peak shifts slightly to the lower angle. Ni doping does not affect the original tetragonal unit cell of SnO_2. The diffraction planes are broadened. The peak position also shifts towards lower angle indicating the expansion of lattice. The crystalline size of the Ni doped SnO_2 samples were calculated by the Debye-Scherrer's equation which is given by $d = k\lambda/\beta \cos\theta$, where 'k' is the shape factor, 'λ' is the wavelength of x-rays used, β is the full width half maximum of the peak and θ is the glancing angle. The annealed sample of Ni doped SnO_2 determined the Crystalline size is about 23 nm of lattice constant a=4.738 and c=3.188 (Tetragonal).

3.1. PHOTOLUMINESENCE SPECTROSCOPY (PL) STUDIES

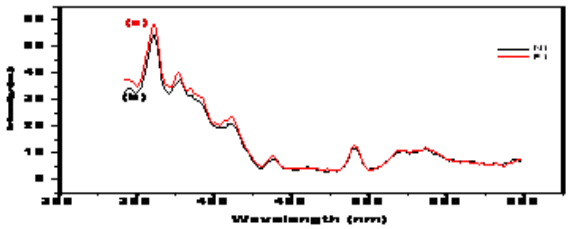

Figure 2. shows PL spectrum of (a) as-prepared pure SnO_2 sample, and (b) as-

The PL spectra of pure and Ni doped SnO_2 nanas emission bands at 361nm, 377nm, 412 nm, 438.71 nm, 491.73 nm, 521nm, and 537 nm excited at a wave length of 439 nm at room temperature are shown in Fig.(a). Figure (b) shows the photoluminescence spectra of samples with Ni doped SnO_2 annealed at 400 °C for 2 hour. The PL emission is directly related to the recombination of excited electrons and holes, so the higher PL intensity indicates a faster in recombination rate which in turn increase in the conductivity of the material.

3.2. UV-VISIBLE SPECTROSCOPY STUDIES: Ni doped SnO_2

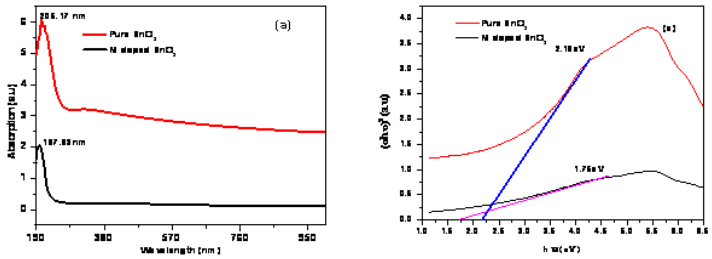

Figure 3. shows the (a) absorption spectrum of annealed Pure and Ni doped SnO_2 (b) energy band gap of annealed Pure and Ni doped SnO_2

Absorption spectra shows an ultraviolet cut-off around 190–250 nm Fig. 3(a) which can be attributed to the photo-excitation of electrons from valence band to conduction band. Generally, high absorption value is observed in the UV region and it becomes low at visible region. Optical transmittance spectra of pure SnO_2 and Ni-doped SnO_2 nanoparticles at annealed samples from 200 to 1000 nm are shown in Fig. 3(b). It is observed that the values of transmittance are high in the visible region and minimum at wavelength ~200 nm. The inset of the figure shows 3(c) the Tauc's plot for determining the band gap energy of nanoparticles. The estimated band gap energy of un‐doped SnO_2 is ~2.16 eV, while, the band gap energy of the Ni doped compound found to almost same and is ~1.75 eV. The observed band gap energy of un‐doped SnO_2 nanoparticles is quite higher than the band gap energy of bulk SnO_2 (3.6 eV). The decrease in the band gap energy may be due to the accumulation of donor energy levels of TM ions in the actual band gap of SnO_2.

3.3. FTIR- Studies

Fig shows that the FTIR spectra of tin oxide nanoparticles as prepared and annealing temperature at 450^0C by using deionized water as a solvent. As-prepared SnO_2 powders exhibit an intense, very broad peak ranging from ca. 3565.58 to 3406 cm^{-1}, which may be due to the adsorbed water and NH_3. After annealing, the peaks shift to higher wave numbers such as 3931.52 to 3416.28 cm^{-1}. The band centered at 1622.26 cm-1 may also be related to water for without annealing temperature. After heating at 450^oC, other bands present are H-O-H stretching of water at 1629.89 cm^{-1}, which is present in the environment or as impurity in the structure and at 2918.48 cm^{-1}, corresponding to a C-H bond, possibly impurities of organic compounds involved in the washing process like ethylene. The band at 613.18 cm^{-1} confirmed purity of tin metal. After annealing the band was shifted to 625-630 cm-1. The absence of peaks such as 1189, 1125, and 1080 cm^{-1} were observed after annealing at 450^oC indicated the absence of inorganic carbonates [7]. The FT-IR spectra of of Ni doped SnO_2 as prepared and annealing temperatures at 450oC. The particle are given in Figure, in which the band located at 3404.94 cm^{-1} is owing to the vibration of O-H and the band located at 1699.32 cm^{-1} is due to the H-O-H vibrating mode of the absorbed water. After annealing at 450^oC indicated that vibrational mode observed at 2921.17 cm^{-1} is due to C-H stretching vibration. The characteristic band at 3415.28 cm^{-1}

corresponds to the stretching vibration of O–H groups. No additional absorption peaks were observed with Ni addition after annealing at 450^{o}C, indicating its homogeneous dispersion in the support material [8].

CONCLUSION

Pure and Ni-doped Tin Oxide nanoparticles have been synthesized by using co-precipitation method. The nanoparticles were synthesized without any requirements of special atmosphere and high pressure. Structural study reveals that the prepared samples have tetragonal structure. The band gap energy of doped SnO_2 nanoparticles was found to be lesser than the pure. This may due to the accumulation of donor energy levels of Ni ions in the bandgap of tin oxide.

REFERENCES

1. Z.Ying, Q.Wan, Q.T Song, S.L Feng: SnO_2 nanowhiskers and their ethanol sensing characteristics. Nanotechnology 15, 1682 (2004)
2. K.L Chopra, S.Major, D.K Pandya,: Transparent conductors–a status review. Thin Solid Films 102, 1 (1983)
3. Z.Peng, Z.Shi, M.Liu,: Mesoporous Sn–TiO_2 composite electrodes for lithium batteries. Chem. Commun. 21, 25 (2000)
4. A.Aoki, H.Sasakura: Tin oxide thin film transistors. Japan J. Appl. Phys. 9,582 (1970)
5. F.Paraguay-Delgado, W.Antúnez-Flores, M.Miki-Yoshida, A.Aguilar-Elguezabal, P.Santiago, R.Diaz, R.Ascencio, Structural analysis and growing mechanisms for long SnO_2 nanorods synthesized by spray pyrolysis. Nanotechnology 16, 688 (2005)
6. B.Cheng, J.M. Russell, W.Shi, L.Zhang, E.T Samulski: Large-scale, solutionphase growth of single-crystalline SnO_2 nanorods. J. Am. Chem. Soc. 126,5972 (2004)
7. K.Nakamato, "Infrared and Raman spectra of inorganic and coordination compounds, "New York: John Wiley and Sons, 1, 978-226, 1986.
8. L. S. Chuah, M. Y. Yaacob, M. S. Fan, S. S. Tneha, Z. Hassana: Optoelectronics and Advanced Materials- Rapid Communication Vol. 4, No. 10, October 2010, p. 1542 – 1545.

LUMINESCENCE PROPERTIES AND ENERGY TRANSFER IN THE KBr : Sm^{3+} Tb^{3+} SINGLE CRYSTALS

S.Bangaru[1*], K.Saradha[2]

Associate Professor of Physics, Arignar Anna Govt. Arts College, Namakkal.

Ph. D Research Scholar in Physics, Arignar Anna Govt. Arts College, Namakkal.

Abstract

KBr: $Sm^{3+}Tb^{3+}$ crystals were grown by Bridgemann Stockbarger technique. The crystallinity and photoluminescence properties of these crystals were investigated. KCl crystals co-doped with Sm^{3+} and Tb^{3+} exhibit green and orange emission under excitation by UV light. The green emission is due to the 5d-4f transition of Tb^{3+} and the orange emission is ascribed to the $^4G_{5/2} \rightarrow {}^6H_{7/2}$ transition of Sm^{3+}. The spectral overlap between the excitation band of Sm^{3+} and emission band of Tb^{3+} supports the occurrence of energy transfer from Tb^{3+} to Sm^{3+} and energy transfer process were investigated.

Key words: KBr, Sm^{3+}, Tb^{3+}, Photoluminescence

1. Introduction

The study of optical properties of rare earth metals in ionic solids can be very conveniently carried out on the simplest compound alkali halides AX,Where A denotes an alkali cation and X denotes a halogen anion. They offer a number of advantages such as simple structure,high degree of chemical purity, easy manipulation and wide range of possible doping impurities with different concentrations. On the other hand, their high band gap energy (~10ev) provides a large window for doping the impurities and optical spectroscopy studies. The rare earth ions being used as dopants since 1975. Nowadays rare earth doped/co-doped materials are among hot topics of research in the development of new full colour emitting phosphor materials. Of many rare earth ions, Sm^{3+} ion is well known as an important activator for many different inorganic lattices producing reddish orange light emitting due to its $^4G_{5/2} \rightarrow {}^6H_J$ (J=5/2,7/2,9/2) transitions [1]. From the view point of practical applications, the light which emitting wavelength located at the longer side (red or orange) is the most suitable source for illuminating light and is appropriate for various displays. Most of the work on samarium doped materials is on powder and glasses. Not much work could be traced to Sm^{3+} in the crystalline structure. However no attempts have been made so far to investigate the emission and structural properties of Potassium Bromide (KBr) doped Sm^{3+}/Tb^{3+} single crystals. In the present work, terbium transfer energy to samarium in KBr host. So terbium ion act as sensitizer (i.e) energy donors and samarium ion act as activators (i.e) energy acceptors. This energy transfer may be due to the reason that low energy region of broad 4f band of Tb^{3+} lies close to higher vibrational level of Sm^{3+} from which the electrons undergo non-radiative relaxation to lower vibrational level of $^4G_{5/2}$ state.

2. Experimental details

Single crystals of pure KBr, samarium doped and terbium codoped KBr (99.99% purity) were grown using Bridgemann Stockbarger technique.Samarium was added in the form of samarium fluoride (Aldrich 99.99% purity) and terbium in the form of terbium fluoride. The crystal grown with three different impurity concentrations 1%, 3% and 5% by weight. The results due to three

concentrations were similar except high luminescence yield for crystals with a high concentration.Hence only the results pertaining to terbium and samarium concentration of 5% by weight are presented and discussed. X-ray diffraction spectrum of the prepared sample by using (Rigaku) X-ray diffractometer (CuK_α, λ=1.5443Å) at the rate of 2°/min and the variation of 2θ is from 10° to 90°. PL spectra were recorded at room temperature using Perkin Elmer LS 55 fluorescence spectrophotometer from 200nm to 900nm with spectral with of 5nm.

3. Powder X-ray Diffraction (XRD)

The crystallization behaviour of the studied sample were investigated representatively by applying XRD on KBr: Sm Tb single crystals. The phase purity of of grown crystal was checked by means of X-ray powder diffraction. The results of KBr: Sm^{3+} Tb^{3+} are most probable similar to those of pure KBr. Fig.1(a) and 1(b) shows the representative X-ray diffraction pattern for pure KBr and KBr: Sm^{3+} Tb^{3+} crystals respectively . It can be seen that all diffraction peak of KBr: Sm^{3+} Tb^{3+} sample can be well assigned to the pure KBr except two peaks with low intensity at higher angles. The smaller intensity peaks observed at higher diffraction angles (88.6°,82.48°) which is also evidence of the incorporation of the dopant in crystal lattice. The high intensity of diffraction peaks indicates good crystallinity of the prepared sample. The crystallite size of the samples can be estimated from Scherrer equation,$D=0.9\lambda/\beta\text{Cos}\theta$, Where,D is the average grain size, λ is the X-ray wavelength(0.15405nm) ,θ and β are the diffraction angle and full width at half maximum of an observed peak respectively[2]. The strongest peak (200) at 2θ=26.88 was used to calculate the average crystallite size (D) of KBr : Sm Tb single crystals. The XRD pattern reveals the crystalline nature of the crystals. The estimated average crystallite size is about 1.642μm.

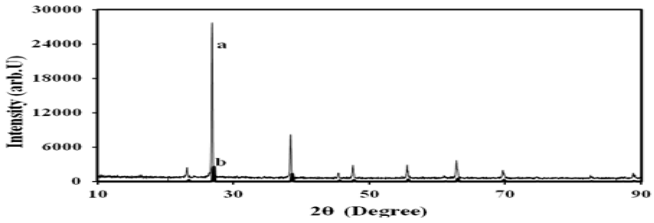

Fig.1 Powder X-ray Diffraction pattern of (a) pure KBr, (b) KBr: Sm Tb single crystals(normal line)

4. Photoluminescence(PL)

Fig.2(a) and 2(b) shows the PL excitation and emission spectra of KBr: Sm^{3+} Tb^{3+} single crystals respectively. The involvement of Sm^{3+} and Tb^{3+} ions in the luminescence process was studied using PL spectra. The excitation spectrum consists of broad band with maximum at 430nm which is the emission wavelength of terbium. Selecting 430nm excitation wavelengths, we recorded the emission spectrum of KBr: Sm^{3+} Tb^{3+} crystals. As with the emission spectrum, the emission of Tb^{3+} and Sm^{3+} in this host is observed at 430nm and 601nm respectively. This in turn will excite Sm^{3+} ion again, leading to more excitations of Sm^{3+} ions and then in emission enhancement. The same trend has been observed in the previous reported work [3]. If the energy transfer occurs from Tb^{3+} to Sm^{3+}, the

emission band of Tb^{3+} should overlap well with the absorption of Sm^{3+} in the KBr host. Fig. 2 reveals that significant overlap between the emission band of Tb^{3+} with the excitation band of Sm^{3+}. Transfer of excitation energy from Tb^{3+} to Sm^{3+} ions brings Tb^{3+} to ground state and Sm^{3+} to excited state followed by radiative transition of samarium ions. Similar energy transfer has been reported in Tb^{3+}/Ce^{3+} co doped KCl crystals [4]. One key factor in the probability of total energy transfer is the energy overlap between the emission of sensitizer and absorption of activator [5]. It shows that the terbium co-doping of KBr:Sm^{3+} sample become more efficient due to matching energy levels of the emission band of terbium (430nm band) and the excitation band of samarium ion (432nm band). Consequently, an efficient energy transfer can occur and be responsible for band emission in KBr host under the excitation at 430nm. In view of the result, it is obvious and worth mentioning here that the process of energy transfer from Tb^{3+} to Sm^{3+} ion takes place in this crystal is the main cause for improvement incase of PL emissions. Therefore we conclude that the KCl crystals co-doped with Sm^{3+} and Tb^{3+} exhibit green and orange emission under excitation by UV light. The green emission is due to the 5d-4f transition of Tb^{3+} and the orange emission is ascribed to the $^4G_{5/2} \rightarrow {}^6H_{7/2}$ transition of Sm^{3+}ions. The PL of studied sample shows emission at the longer wavelength side (orange) which is the most suitable source for illuminating light and is appropriate for various displays.

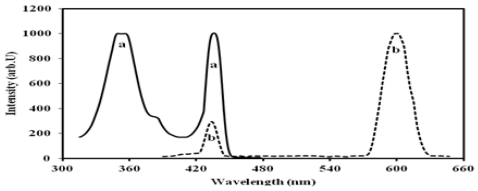

Fig. 2 Photoluminescence (a) Excitation spectrum, (b) Emission spectrum of KBr:Sm Tb single crystals

5. Conclusions

The phase purity of of grown crystal was checked by means of X-ray powder diffraction. The high intensity of diffraction peaks in studied sample indicates good crystallinity of the prepared sample. The XRD pattern reveals the crystalline nature of the crystals. The estimated average crystallite size is about 1.642μm. an efficient energy transfer can occur from Tb^{3+} to Sm^{3+} ions and be responsible for band emission in KBr host under the excitation at 430nm. The PL of studied sample shows emission at the longer wavelength side (orange) which is the most suitable source for illuminating light and is appropriate for various displays.

References

[1]. B.Lei,Y.Liu, J.Liu, Z.Ye, C.Shi, Journal of Solid State Chemistry, 177, 2004, 1333.
[2]. C.G.Hu,Z.W.Zhang, H.Liu, P.X.Gao and Z.L.Wang, Nanotechnology,17,2006,5983.
[3]. N.Salah,P.D.Sahare, Radiation Measurements, 41, 2006, 665.
[4]. S.Bangaru,K.Saradha,G.Muralidharan, Journal of Biological and Chemical Luminescence,31, 2016,649.
[5]. P.Dorenbos, Journal of Luminescence,104,2003,239.

Optimization of N doped ZnO Crystalline Thin Films Prepared by Pulsed Laser Deposition

R. K. Kalaiezhily[1], G. Saravanan[1], V. Asvini[1] and K. Ravichandran*[1]

[1]Department of Nuclear Physics, University of Madras, Chennai 600 025,
**E-Mail: ravi21068@unom.ac.in*

ABSTRACT

ZnO is a direct band gap (3.37 eV) material with a large excitonic binding energy of 60meV compared with GaN (21meV) which could find potential applications in UV LEDs/LASER sources with higher brightness, lower threshold current and better performance at high temperatures. Here, we made an attempt to deposit pure and N doped ZnO thin films on sapphire substrates by pulsed laser deposition technique. X- ray diffraction studies confirm that all the films formed in single phase wurtzite structure. UV- visible studies show an appreciable band gap change in the doped ZnO compared with undoped ZnO. The results of photoluminescence and Raman spectroscopy studies on samples will be presented in detail.

Introduction

Semiconductors are the foundation of modern solid state electronics, including transistors, solar cells, light-emitting diodes (LEDs), digital and analog integrated circuits. ZnO is a direct band gap (3.37 eV) semiconductor with a large excitonic binding energy of 60meV compared with GaN (21meV) which could find potential applications in UV LEDs/LASER sources [1]. ZnO doped with different dopant like Al, Ga and In have improved electrical, optical, and catalytic properties [2]. Here, we made an attempt to deposit pure and N doped ZnO thin films on sapphire substrates by pulsed laser deposition technique.

Experimental Procedure

Sigma Aldrich 99.9% Pure ZnO is used as precursor. A drop of binder Poly Vinyl alcohol (PVA) was added with it and ground till it become fine powder. The powder was compacted as pellet by applying pressure of 10 MPa using uniaxial press. Pellet was sintered at 1200°C for 48 hours. This pellet is used as target in Pulsed Laser Deposition (PLD). C-axis sapphire is used as substrate. For cleaning, the substrates were ultrasonicated with ethanol and heated in hot plate till ethanol was evaporated.

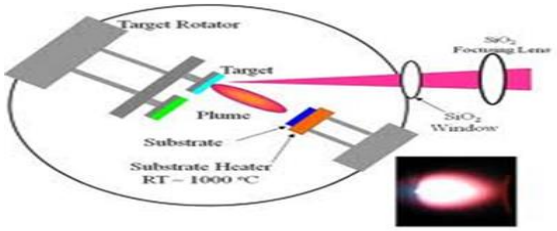

Undoped ZnO and N doped ZnO were deposited on C-axis sapphire substrate in the presence of O_2 and N_2O gas respectively with partial pressures in order of 10^{-3} mbar and also in different substrate temperatures (200°C and 400°C). The laser deposition was carried out using a "Quantel Brilliant B" Nd-YAG excimer laser model with energy of 82 mJ/ pulse. The films were characterised by X-ray diffraction analysis and the deposition parameters were optimised.

Results and Discussion

X-Ray Diffraction Analysis

X-ray diffraction analysis for undoped and N doped ZnO thin films deposited at partial pressures in order of 10^{-3} mbar were done using analytical X-ray diffractometer with Cu K_α radiation (λ = 1.5406 Å). The data was collected from $2\theta = 10°$ to 90°. From the XRD patterns, it is confirmed that all sample corresponds to hexagonal wurtzite structure. It is clearly observed that, in the case of ZnO (without annealing) two main peaks appeared in the directions (002) and (100). As the substrate temperature was fixed to 400°C, we got good crystalline single phase. There was no secondary peak observed in the X-ray diffraction pattern. This confirms that N is well doped in ZnO.

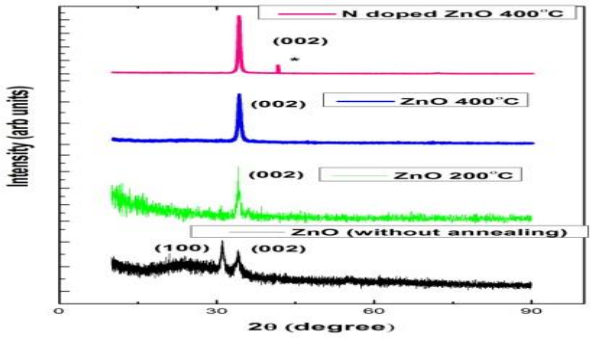

The peak of N doped ZnO thin film shifted towards the lower diffracting angles compared with undoped ZnO thin films. Nitrogen (1.71Å) is higher ionic radii element compared to zinc (0.74 Å) or oxygen (1.38Å). So, while doping N in ZnO, the lattice parameters get increased due to the increase in bond length and inducing the lattice strain. And hence, the diffraction peaks were shifted towards lower diffracting angle in doped ZnO thin films.

Conclusion

Undoped ZnO and N doped ZnO thin films were deposited on C-axis sapphire substrate in the presence of O_2 and N_2O gas respectively, with partial pressure in order of 10^{-3} mbar and also in different substrate temperature (without annealing, 200°C and 400°C) by PLD.

X-ray diffraction analysis was done for all samples. From the XRD patterns, it is confirmed that all sample corresponds to hexagonal wurtzite structure. It was optimised that films deposited with substrate temperature 400°C got sharp intense single phase peak with good crystallinity.

Reference

[1] U. Ozgur., et al., A comprehensive review of ZnO materials and devices, J. Appl. Phy. 98 (4), (2005).

[2] Janotti and Van de Walle., Fundamentals of zinc oxide as a semiconductor, Rep. Prog. Phys.72 (2009).

[3] Pulsed laser deposition of thin films applications- LED growth of functional materials by Robert Eason., Wiley-interscience (2007).

Liner and nonlinear optical and spectroscopic properties of an Inorganic nonlinear optical crystal: sodium manganese tetra chloride (SMTC)

M. Packiyaraj[1], S. M. Ravi Kumar[2*], S.Selvakumar[3] and T. Kubendiran[2]

[1]*Department of Physics, S.K.P. Engineering College, Tiruvannamalai 606 611*

[2] *Department of Physics, Government Arts College , Tiruvannamalai 606 603*

[3]*Department of Physics, Government Arts and Science College, Nandanam, Chennai 606 603*

**corresponding author: smravi78@rediffmail.com; ravism23@gmail.com*

Mobile: 09884473709; 08608953139

Abstract

Single crystal of sodium manganese tetra chloride (SMTC) has been successfully grown form aqueous solution by the slow evaporation technique at room temperature. The crystalline nature of the grown crystal of SMTC was analyzed by powder X-ray diffraction. Single crystal X-ray diffraction study reveals that the crystal belongs to orthorhombic system with non-centrosymmetric space group Pban. Optical transmission study on SMTC crystal shows high transmittance in the entire UV–Vis region and the lower cutoff wavelength is found to be 240 nm. The second harmonic generation (SHG) efficiency of the crystal was measured by Kurtz's powder technique infers that the crystal has nonlinear optical (NLO) efficiency 1.32 times that of KDP.

1.0 INTRODUCTION

The well known properties of laser radiation are important for a wide variety of applications. Laser radiation could be converted into one form of frequency to another through the nonlinear optics, hence the application of nonlinear optics is increased significantly in various fields in science and technology. Generally, nonlinear optical (NLO) interaction is made by one or two laser beam incident on a suitable material in which an output beam of the desired frequency is produced [1-2]. Harmonic generation, sum and difference frequency generation and parametric oscillation are included in the NLO interaction [3]. A Lower frequency pair of tunable output beam can be produced only by suitable material when it is interact (NLO) with high input laser beam. Mostly, NLO interaction imposes several demands on potential NLO materials. The field of nonlinear optics is one of the most attractive fields of current research because of its vital applications in various areas like optical switching, optical data storage for developing technologies in telecommunication and signal processing [4-6].

Inorganic materials have advantages over organic materials, such as architectural flexibility for molecular design and morphology, high mechanical strength and good environmental stability with non toxicity andusability in high power applications. Historically, inorganic NLO materials have been chronicled more extensively inorganic oxide crystal, $LiNbO_3$, $KNbO_3$, KDP and KTP, etc., have been studied for device application like piezoelectric, ferroelectric and Electro-optics [7]. This material has also been formed successful usage in commercial frequency doublers, mixers and paramedic generators to provide coherent laser radiation with high frequency conversion efficiency in the new region of the spectrum, inaccessible by other nonlinear crystal conventional sources.

The aim of this research work is to survey the processing and properties of inorganic nonlinear optical crystal sodium manganese tetrachloride (SMTC) with molecular formula Na_2MnCl_4

used in NLO frequency conversion. Hence, an attempt hasbeen made on growth of sodium manganese tetra chloride (SMTC) single crystals by slow evaporation solution growth technique and its physical-chemical properties have been investigated.

2.0 EXPERIMENTAL PROCEDURE

2.1. Synthesis

SMTC salt was synthesized by taking analytical reagent (AR) grade manganese chloride and sodium chloride in stoichiometric ratio 1:2 with double distilled water as a solvent. The synthesized SMTC salt has been obtained by the following chemical reaction.

$$MnCl_2 + 2NaCl \longrightarrow Na_2MnCl_4$$

Manganese chloride + sodium Chloride ⟶ Sodium manganese tetra chloride.

The scheme of the molecular structure of SMTC is as shown below.

2.2 Crystal Growth

The prepared solutions were stirred vigorously at RT for 4 h. Continuous stirring with slightly rise in temperature ensures homogeneity and avoids co-precipitation of motives. Purification of synthesized salt was achieved by successive recrystallization process. The saturated mixture of solution was filtered two times with micron pore size Wattmann filter paper. This synthesized clean solution was poured into a Petri dish and covered by polythene paper with pores, and allowed for slow evaporation of the water solvent. After a time span of 35 days, the solvent was evaporated and good quality SMTC crystal of dimensions 2 ×2 ×1 mm^3 were harvested from the Petri dish. The grown crystal was defect less, optically transparent and with no inclusions. As-grown crystal of SMTC is shown in the figure 1.

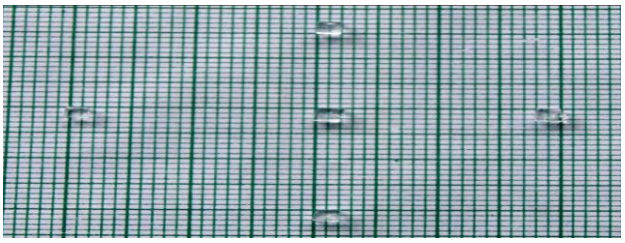

Figure.1 Photograph of as grown crystals of SMTC

3.1 RESULTS AND DISCUSSION

3.1.1 Single crystal XRD studies.

The grown crystal of SMTC was subjected to single crystal and powder XRD analysis using ENRAF NONIOUS CAD4 X-ray diffraction meter and BRUKER, Germany (model D8 advance) X-ray diffractometer.The Single crystal XRD study confirms the unit cell parameters of as grown SMTC crystals a=6.93 Å, b=11. 82 Å, c=3. 86 Å,$\alpha = \beta = \gamma = 90°$ and volume of the cell is found to be, 316.182 $Å^3$. Hence the SMTC crystal is Orthorhombic in structure and in thespace group Pbam. The lattice parameters are well coincide with a reported value [8].

3.1.3 Fourier Transform Infrared Analysis.

The FTIR analysis of SMTC was carried out by the Wily KB pellet technique in the wavelength between 3500 and 500 cm^{-1} . The recorded spectrum is shown in figure 3. The table .1 shows the frequency of absorption and their assignments of various functional groups present in the as-grown SMTC crystal.

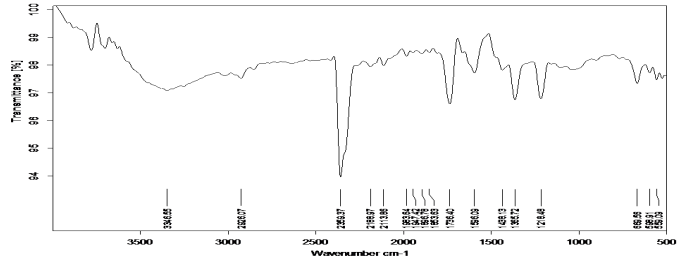

Figure 3 FTIR spectrum of as grown crystal of SMTC

3.1.4 UV-vis-NIR studies

Transmission behavior of the grown crystal was studied by using LAMBDA-35 UV-visible spectrophotometer. The transmission range of SMTC crystal was determined by recording the optical transmission spectrum in the wavelength region of 200 - 900 nm. The optical transmission spectrum of SMTC crystal is shown in the figure 4. The transmission spectrum shows that the grown crystal has a lower cutoff wavelength at 240 nm,which attributes the electronic transmission in the SMTC crystal. Absence of absorbance in the region between 240 nm and 900 nm is an essential property of the nonlinear optical crystals.

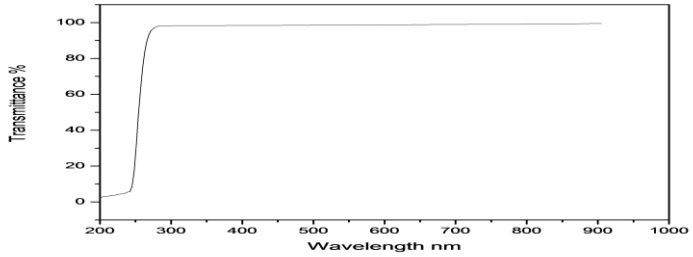

Figure 4 UV-Visible spectrum of SMTC crystal

3.1.5. Second harmonic generation efficiency measurement

In order to confirm the nonlinear optical property, powdered sample of SMTC was subjected to Kurtz and Perry techniques, which remains a powerful tool for initial screening of materials for SHG [14]. The SHG signal generated in the sample was confirmed from emission of bright green (532 nm) radiation from the sample. The measured amplitude of second harmonic generation for SMTC crystal is 11.32 mJ and 8.8 mJ for KDP (KDP crystal was powdered to the identical size of SMTC and used as reference materials). It shows a powder SHG efficiency of SMTC crystal is about 1.3 times of KDP.

4.0 Conclusion

A potential inorganic nonlinear optical single crystal of sodium manganese tetra chloride was prepared at room temperature by slow evaporation of aqueous solutions. The well defined external appearance with bright, transparent and colourless crystals is obtained. The unit cell parameters and the space group were found using single crystal data. The good crystalline nature of the SMTC was confirmed by well defined peaks of powder X-ray diffraction studies. The FT-IR spectrum reveals the functional groups of the grown crystals. The grown crystal shows 99 % transmission with UV cut-off at 240 nm hence suitable for frequency conversion applications. The SHG efficiency of the SMTC was measured to be higher than that of KDP. The above experimental results, viz., bulk size, extremely good crystalline perfection, optical transparency, SHG efficiency and mechanical strength may have possible NLO applications.

References

[1] A. H. Reshak, H. Kamarudin, and S. Auluck, Acentric Nonlinear Optical 2,4-Dihydroxyl Hydrazone Isomorphic Crystals with Large Linear, Nonlinear Optical Susceptibilities and Hyperpolarizability, J. Phys. Chem. B 116, 4677 **(2012)**.

[2] Ali Hussain Reshak , I. V. Kityk , and S. Auluck, Investigation of the Linear and Non- linear Optical Susceptibilities of $KTiOPO_4$ Single Crystals: Theory and Experiment, J. Phys. Chem. B 114, 16705 **(2010)**.

[3] F. Peter, M.Bordui and Martin,Fejer.Annu. Rev. Mater. Sci. 23, 321 **(1993)**.

[4] P.N. Prasad, D.J. Williams. Introduction to nonlinear optical effects in organic molecules and polymers, John Wiley & Sons, Inc., New York, USA **(1991)**.

[5] H.O. Marcy, L.F. Warren, M.S. Webb, C.A. Ebbers, S.P. Velsko, G.C. Kennedy, G.C. Catella, Second harmonic generation in zinc tris(thiourea) sulfate, Appl. Opt. 31, 5051 **(1992)**.

[6] X.Q. Wang, D. Xu, D.R. Yuan, Y.P. Tian, W.T. Yu, S.Y. Sun, Z.H. Yang, Q. Fang, M.K. Lu, Y.X. Yan, F.Q. Meng, S.Y. Guo, G.H. Zhang, M.G. Jiang, Synthesis, structure and properties of a new nonlinear optical material: Zinc cadmium tetrathiocyanate, Mater. Res. Bull. 34, 2003 **(1999)**.

[7] D.S. Chemla, J. Zyss, Nonlinear optical properties of organic molecules and crystals. 01-02, Academic Press, Orlando, New York **(1987)**.

[8] S.K. Kurtz, New nonlinear optical materials, IEEE, J. Quantum Electron. 4, 578 **(1968)**.

Synthesis, Growth and Physicochemical Properties of Seminorganic NLO Crystal Bis (Thiourea) Ammonium Nitrate

A.Anbarasi[1], S.M. Ravi Kumar[2]*, M. Prabhakar[2], and G.J.Shanmuga Sundar[3]

[1]*Department of Physics, Periyar Government Arts College Cuddalore – 607 001*

[2]*Department of Physics, Government Arts College, Tiruvannamalai-606 603*

[3]*Department of Physics, Arignar Anna Government Arts College, Cheyyar-604 407*

**Corresponding Author: ravism23@gmail.com, smravi78@rediffmail.com*

Abstract

Nowadays, the fast developing fields like photonics and optoelectronics are mainly focusing on nonlinear optical (NLO) crystals. Most of semiorganic materials are able to produce the nonlinear optical properties because they are having the nonlinear optical function bonds. Particularly, thiourea complex semiorganic crystals are shows good second harmonic generation (SHG) efficiency. Hence, in this work concentrated on (bis)thiourea ammonium nitrate (BTAN) crystal was grown from aqueous solution by slow evaporation technique. The grown crystal has been subjected to single crystal X-ray diffraction to determine the unit cell dimensions. The Fourier Transform Infrared (FT-IR) spectra have been recorded in the range 400–4500 cm^{-1}. Second harmonic generation (SHG) for the materials of this work was confirmed using Nd:YAG laser. The UV–visible spectra show that the grown crystals have wide optical transparency in the entire visible region. The Thermo gravimetric/Differential Thermal Analyses (TG/DTA) thermograms reveal that the materials have good thermal stability.

1 Introduction

Photonics and optoelectronics are fast developing fields and are mainly focusing on nonlinear optical (NLO) materials. NLO materials are widely used in various fields of optics and optoelectronics such as second harmonic generation, optical bi-stability, laser remote sensing, optical disk data storage, laser driven fusion, medical and spectroscopic laser, photonic integrated circuitry, optical parametric oscillations and THz wave generation [1-4]. Materials exhibiting large non linearity remains very active in research both basic and applied sciences [5]. In recent years, to achieve large charge transfer and the optical transparency with fewer dislocations density extensive efforts have been made to develop new inorganic, organic and semi-organic NLO crystals [6-8]. The selection of material may depend not only on laser conditions but also on the physiochemical properties such as molecular nonlinearity, transparency, and conversion efficiency and laser damage threshold [9, 10]. The strong delocalization of π electron in the organic back bone of semi-organic establishes higher molecular polarizability and hence electron density takes place. This functionalizes both the ends of the π bond system with suitable electron donor and acceptor groups and enhances the asymmetric electronic distribution in both ground and excited states of semi-organics. This enables an increased optical nonlinearity by means of such as π delocalization length and donor acceptor groups with nonlinear optical function bonds [11]. Hence, the synthesis of novel efficient frequency conversion materials has resulted in the development of semiorganic materials, which possess efficient physicochemical properties, such as large nonlinearity over a broad frequency range, high optical damage threshold, low angular sensitivity, low dielectric constant, mechanical stability and inherent synthetic flexibility

[12-14]. Semi-organic crystals possess both the good qualities of organic and inorganic, it is used in device fabrication technology due to their enhanced physiochemical properties such as thermal stability, wide range of transparency and excellent NLO coefficient [15, 16].

The NLO properties of semiorganic crystals have attracted significant attention in the last few years, because both organic and inorganic components in it contribute specifically to process of second harmonic generation (SHG). Particularly, thiourea complex semiorganic crystals are shows good second harmonic generation (SHG) efficiency. Thiourea molecules are an interesting in organic matrix modifier due to its large dipole moment and its ability to form and extensive network of hydrogen bonds [17]. The centrosymmetric thiourea molecule, when combined with inorganic salt yield non-centrosymmetric complex, which has the nonlinear optical properties [18]. Hence, in the present study concentrated on synthesis, growth, structural, optical, SHG and thermal properties of thiourea complex semiorganic crystal namely bis(thiourea) ammonium nitrate (BTAN) and the results are reporting for the first time.

2 EXPERIMENTAL PROCEDURES

2.1 Synthesis

Thiourea and ammonium nitrate supplied by Merck, India, were used without further purification. Thiourea mixed with ammonium nitrate in molar ratio 2:1. The saturated solution of ammonium nitrate was slowly added to the saturated solution of thiourea at room temperature and it has been stirred well for nearly 8 hours to obtain the homogenous solution. The solution of title compound was synthesis by the following chemical reaction.

$$2[CH_4N_2S] + NH_4NO_3 \rightarrow NH_4(CH_4N_2S)_2\,NO_3$$

2.2 Growth of BTAN

The saturated solution was filtered using Wattman filter paper. The filtered solution was taken in a beaker and covered with good quality perforated polythene cover to restrict the fast evaporation and it's kept at room temperature in a dust free compartment for slow evaporation. After the period of 40-60 days, colorless crystals with dimension 10mm x 6mm x 3mm were harvested. The grown crystals are non-hygroscopic and optically good transparent in nature. Well-faced good quality crystals of BTAN are shown in the figure 1.

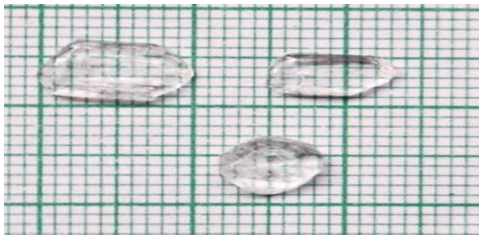

Fig. 1 photograph of as grown crystals of BTAN

3. Results and Discussion

3.1. Single crystal XRD analysis:

The title compound was analysed by single crystal XRD by ENRAF NONIUS CAD4-F single X-ray diffractometer with $M_OK_\alpha(\lambda=0.717Å)$ radiation. It is observed that the grown crystal crystallizes in orthorhombic system.. The calculated lattice parameter for BTAN was found to be a = 8.73Å, b = 9.90Å, c=12.64Å and volume, V=1092Å^3.

3.3 FTIR study

The FTIR spectroscopy studies are effectively used to identify the presence of functional groups in BTAN. The FTIR spectrum was recorded using thermo Nicolect V-200 FTIR spectrometer by KBr pellet method in the range of wave number 4000-500 cm^{-1} as shown in figure 3. The observed peak at 3410 cm^{-1}and 3183 cm^{-1} belongs to NH_2 stretching and N-H symmetric stretches respectively. This peak defines that presence of thiourea in the grown crystal. The peaks at 2977 cm^{-1} is due to C-H stretching vibration. The NH_2 bending is observed at 1620cm^{-1}. The peaks at 1383 cm^{-1} is observed as C=S stretching. The C-H deformation was observed at 666 cm^{-1}. The peak at 588 cm^{-1} is due to N-C-N stretching.

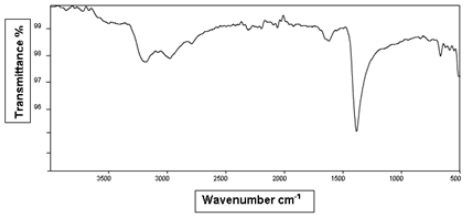

Fig. 3 FTIR Spectrum of BTAN Crystal

3.5 NLO TEST

Kurtz-Perry Powder second harmonic generation (SHG) measurements [25] was carried on grown crystal of BTAN using a a spectra-physics quanta-ray prolab 170 Nd:YAG laser with the first harmonics input at 1064nm and a pulse width of 10ns at repetition rate of 10Hz. This measurement offers possibility of assessing the nonlinearity of new materials. The grown crystal was indentified as a NLO crystal due to the emission of high intense green radiation. Also the SHG efficiency was found to be 11.82 mJ. This value is compare with known NLO crystal of KDP which has the SHG efficiency 7.80 mJ. Hence, the SHG efficiency of BTAN is 1.52 times greater than that of KDP crystal. Therefore, BTAN crystal is a suitable candidate for device and various technological applications.

3.6 Thermal study

Information regarding phase transition and different stages of decomposition of the grown crystal BTAN crystal were identified by DTA and TGA thermal studies. BTAN crystal was weighed in an Al_2O_3 crucible with microprocessor temperature control system. DTA and TG curve of grown crystals were plotted in nitrogen atmospheres between ambient temperatures 100 to 1232 ºC shown in the figure 6. There is no weight loss upto 184.05 ºC indicating that there is no inclusion of water in the

crystal lattice. The recorded thermogram reveals that the major weight loss starts at 184 ºC and continures upto 1232 ºC. It is further observed that the DTA curve shown that first endo thermionic peak at 184 ºC is assigned to melting point of the BTAN compound and the remains exo thermionic peaks at 221 ºC, 232 ºC, 235 ºC, 266 ºC and 290 ºC are indicate the changes in the physical state of the crystal. The nature of the weight loss and sharpness of the peak ensure the decomposition and purity with crystalline nature of the material respectively. The observed decomposition point of BTAN crystal 184 ºC indicates that BTAN crystal is thermally stable up to 184 ^{o}C.

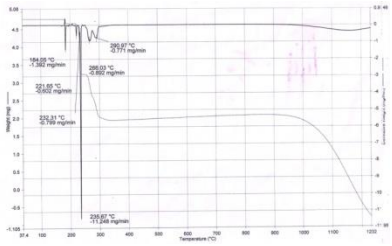

Fig. 6 DTA and TG curve of BTAN crystal

Conclusion

Optically good crystals of (bis)thiourea ammonium nitrate has been grown from aqueous solution by slow evaporation technique under room temperature. Single crystal XRD analysis confirmed that the BTAN crystallize in orthorhombic system. Powder X-ray diffraction study revealed the crystalline nature of grown crystal. The optical quality of the grown crystal was justified by optical absorption studies. The sharp absorption on set at 280 nm and high absorption values of the grown crystal at wavelength above 380 nm, exhibit the optical quality. The powder SHG measurement shows the grown BTAN crystal having SHG efficiency of about 1.52 times that of KDP crystal. Thermal stability of grown sample was studied by TGA and DTA analyses which reveal that the BTAN crystal thermally stable up to 184 ºC.

References

1. Santhanu Bhattacharya, Parthasarathi, Dustidar, T.N. Guru Row, Chem. Mater. 61, 531 **(1994)**.
2. T.Kaino, B.Cai, T.Takayama, Adv. Funct. Mater. 12, 599 **(2002)**.
3. M.Thakur, J.Xu, A.Bhowmilk, L.Zhou, Appl. Phys. Lett. 74, 635 **(1999)**.
4. A. Schneider, M.Neis, M.Stillhart, B.Ruiz, R.U.A.Khan, P.Gunter, J.Opt. Soc. Am. B23, 1822 **(2006)**.
5. R.J.Collins, D.F.Nelson, A.L.Schawlow, W.Bond, C.G.B.Garrett, W.Kaiser, Phys. Rev. Lett. 5, 303 **(1960)**.
6. Xiue Ren, Dongli Xu, Dongfeng Xue, J.Crystal Growth 310, 2005 **(2008)**.
7. Dongfeng Xue, Henryk Ratajczak, Chem. Phys. Lett. 371, 601 **(2003)**.
8. Dongfeng Xue, Siyuan Zhang, Chem. Phys. Lett. 301, 449 **(1999)**.
9. F.Zernike, J.E.Midwinter, in:Applied nonlinear optics, Wiley, Newyork, **(1973)**.
10. P.N.Prasad, D.J.Willams, in:Introduction to nonlinear efforts in molecules and polymers, Wiley, New York **(1991)**.
11. Daqiu Yu, Dong feng Xue, Henryk Ratajczak, J.Mol. Stuct. 792 (2006) 280-285.
12. Y.R.Shen, The principles of nonlinear optics, Wiley, New York **(1984)**.
13. H.O. Marcy, L.F. Warren, M.S.Webb, C.A.Ebbers, S.P.Velsko, G.C.Kenndy, Appl. Opt. 31, 5051 **(1992).**
14. S.Ledoux, J.Zyss, J. Int. Nonlinear opt. Phys. 3, 287 **(1994)**.
15. S.M. Ravi Kumar, N. Melikechi, S. Selvakumar, P. Sagayaraj, Physica B: Condensed Matter 403, 4160 **(2008)**.
16. S. Selvakumar, S.M. Ravi Kumar, Ginson P. Joseph, K. Rajarajan, J. Madhavan, S.A. Rajasekar, P. Sagayaraj, Materials Chemistry and Physics 103 (1), 153 **(2007).**
17. Hellwege, K.H,. Hellwage, A.M. Landolt-Bornstein Group II 14, 584 **(1982)**.
18. M.Lawrence, J.Thomas Joseph Prakash, Spectrochim. Acta Part A, 91, 30 **(2012)**.

An Insight into the Conformal Preferences of 2-Nitroso-1-Napthol: A DFT Approach

V Ragavendran[a*], S Muthunatesan[b]

[a]*Department of Physics, Sri Chandrasekharendra Saraswathi Viswa Mahavidyalaya, Kanchipuram-61*
[b]*Department of Physics, Government Arts College (Autonomous), Kumbakonam-01*
**Corresponding author, Email: ragav910@gmail.com*

Abstract

The conformational stability of 2-Nitrosol-1-napthol was elucidated using potential energy surface scan studies. In order to carry out a detailed vibrational spectroscopic analysis of 2-Nitrosol-1-napthol, Fourier Transform Infrared and Fourier Transform Raman spectra have been recorded in condensed phase. To determine the optimized geometry and vibrational wavenumber, Density functional theory calculations in the B3LYP/6-31G** level have been carried out followed by scaling using the **s**caled quantum mechanical methodology. Substitution of nitroso group into the 1-napthol has produced remarkable changes in the structural parameters.

Keywords*:* DFT, Conformational analysis, SQM, UV-Visible, NBO

Introduction:

Nitroso-napthols have greater ability to form metal chelates and it is sensitive for fluorimetric determinations of tyrosine residues in proteins and peptides.[1,2] Napthol has an enhanced solubility in nature due to the presence of hydroxyl group. 1-napthol is found to be an urinary metabolite of both carbaryl and naphthalene. In the present study, the analysis of Fourier Transform Infrared(FT-IR), Fourier Transform Raman(FT-Raman), Ultraviolet-Visible spectra and Density functional theory(DFT) analysis of 2-Nitroso-1-napthol (2N1N) are presented**.**

Materials and methods:

A fine sample of 2-nitroso-1-naphthol(2N1N) was obtained from M/s. Sigma Aldrich chemicals and used without any further purifications for spectral measurements. The Fourier transform infrared spectrum(FTIR) of the title compound was recorded in the region 4000–400 cm^{-1} and the Fourier transform Raman(FT–Raman) spectrum of 2N1N was recorded in 3500-50 cm^{-1} range with a Nicolet model 950 FT–Raman spectrometer at 4 cm^{-1} spectral resolution using the 1064 nm line of a Nd:YAG laser for excitation at a 200 mW output power. Density Functional Theory calculations of 2N1N were performed by using Gaussian 09 software package[3] at B3LYP functional[4,5] combined with 6-31G** basis set to obtain the optimized geometry and energy of the title compound.

RESULTS AND DISCUSSION

The optimized structure of 2N1N along with numbering of atoms is shown in Fig.1. Different conformers were tried by changing the angles of nitroso group and the most stable conformer was obtained when nitroso group turned away from the napthol group. This is also confirmed from the PES scan analysis. The global minimum energy obtained by DFT structure optimization and PES scan analysis of 2N1N was found to be -370500.5 Kcal/mol. All the calculated vibrational wavenumber using the optimized geometry obtained were found to be positive for the title compound.

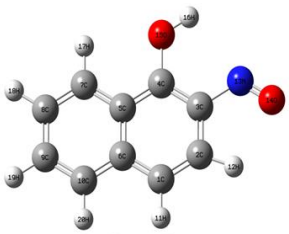

Fig.1 Optimized structure of 2N1N

Conclusion

The most stable conformer of 2-nitroso-1-napthol have been identified using DFT optimization procedure and potential energy scan analysis. A weighted RMS deviation of 9.6 cm^{-1} between experimental and calculated wavenumber for the title compound has been achieved by employing the SQM methodology. Substitution of nitroso group into the 1-napthol has produced remarkable changes in the structural parameters. A satisfactory assignment of most of the fundamentals was provided using the scaling procedure. The vibrational wavenumber, IR intensities and Raman intensities were calculated using B3LYP/6-31G** method and they were found to be in good agreement with the experimental values.

References:

1. Sundler, F.; Larsson, L.J.; Hakanson, R. Fluorescence histochemistry of peptide harmome producing cells observations on the nitrosonaphthol method for the determination of tyrosine residues. Histochemistry **1976,** 50**,** 39-46.
2. Portela, M.P.M.; Villamil, S.H.F.; Perissinotti, L.J.; Stoppani, A.O.M. Redox cycling of o-naphthoquinones in trypanosomatids – superoxide and hydrogen peroxide production. Biochemical Pharmacology **1996,** 52**,** 1875-1882.
3. Frisch, M. J.; Trucks, G. W.; Schlegel, H. B.; Scuseria, G. E.; Robb, M. A.; Cheeseman, J. R.; Scalmani, G.; Barone, V.; Mennucci, B.; Petersson, G. A.; Nakatsuji, H.; Caricato, M.; Li, X.; Hratchian, H. P.; Izmaylov, A. F.; Bloino, J.; Zheng, G.; Sonnenberg, J. L.; Hada, M.; Ehara, M.; Toyota, K.; Fukuda, R.; Hasegawa, J.; Ishida, M.; Nakajima, T.; Honda, Y.; Kitao, O.; Nakai, H.; Vreven, T.; Montgomery, J. A., Jr.; Peralta, J. E.; Ogliaro, F.; Bearpark, M.; Heyd, J. J.; Brothers, E.; Kudin, K. N.; Staroverov, V. N.; Kobayashi, R.; Normand, J.; Raghavachari, K.; Rendell, A.; Burant, J. C.; Iyengar, S. S.; Tomasi, J.; Cossi, M.; Rega, N.; Millam, J. M.; Klene, M.; Knox, J. E.; Cross, J. B.; Bakken, V.; Adamo, C.; Jaramillo, J.; Gomperts, R.; Stratmann, R. E.; Yazyev, O.; Austin, A. J.; Cammi, R.; Pomelli, C.; Ochterski, J. W.; Martin, R. L.; Morokuma, K.; Zakrzewski, V. G.; Voth, G. A.; Salvador, P.; Dannenberg, J. J.; Dapprich, S.; Daniels, A. D.; Farkas, Ö.; Foresman, J. B.; Ortiz, J. V.; Cioslowski, J.; Fox, D. J. Gaussian, Inc., Wallingford CT, 2009.
4. Lee, C.; Yang, W.; Parr, P.G. Development of the Colle-Salvetti correlation-energy formula into a functional of the electron density. Physical Review B B **1988,** 37**,** 785.
5. A. D. Becke,. Density-functional thermochemistry. III. The role of exact exchange. The Journal of Physical Chemistry A **1993**, 98, 5648.

Structural, optical, morphological and antibacterial studies of bullet shaped Cadmium Oxide nanoparticles synthesized by Chemical precipitation method

K. Mohanraj[1], D. Balasubramanian*[1]

[1]Raman Research Laboratory, PG & Research Department of Physics, Government Arts College, Tiruvannamalai-606603

**Corresponding author: dr.d.balu@gmail.com Mobile: +91 9443990556*

Abstract

The Cadmium Oxide (CdO) nanoparticles were synthesized by chemical precipitation method. The synthesized sample was characterized with X-ray diffraction (XRD), diffuse reflectance spectroscopy (UV-Vis DRS), transmission electron microscopy (TEM) and high resolution transmission electron microscopy (HRTEM), energy dispersive X-ray analysis and antibacterial study. The XRD result shows the cubic structure and average particle size is about 18nm. The bullet shape morphology and lattice fringes have been identified from TEM and HRTEM. The chemical composition is confirmed by EDX. UV-Vis DRS gives the bandgap value. The antibacterial activities of the synthesized CdO nanoparticles against Gram-negative bacteria have also been studied.

Keywords: Chemical precipitation, Bullet shape, TEM, HRTEM, Antibacterial.

1. Introduction

In the present decay nanotechnology has become a fast emerging field. Moreover inorganic semiconductor materials find wide range of applications in optoelectronics, telecommunications and photocatalytic activities [1-4]. Semiconductor nanoparticles possess interesting unique chemical and physical properties, which are different from bulk structure [5]. Their high specific surface area results in high chemical reactivity. The surface to volume ratio of atoms play vital role in quantum confinement effect [6].Cadmium oxide (CdO) is a II–VI n-type semiconductor with a cubic crystal structure and possesses a band gap of 2.2 eV. In the present study, CdO has been chosen because of its potential important applications, chemical stability and wide spread availability [7-8].CdS nanoparticles have been synthesized and characterized by several methods and their important technological applications are explored [9-12]. Monte et al. [13] prepared CdS nanoparticles embedded in polymeric microsphere templates and characterized their optical properties. Nanosized CdS particles were also synthesized by melting nucleation method within a hosting glass template [14]. In this work, we report the synthesis of CdO nanoparticles by chemical precipitation method. The structural, morphological, optical and antibacterial properties of the synthesized CdO nanoparticles have been discussed in detail.

2. Materials and methods

2.1 Chemicals

Cadmium chloride and ammonia hydroxyl solution were purchased from Merck and were used as-received since they were of analytical reagent grade with 99.9% purity. Further, the sample preparation and dilution were done using deionized water.

2.2 Synthesis of CdO nanoparticles

The CdO nanoparticles are synthesized by chemical precipitation method as follows. 0.1M of cadmium hydroxyl solution was prepared by dissolving cadmium chloride in double distilled water

and stirred for 4h. The pH of cadmium hydroxyl is maintained at 8 by drop wise addition of ammonia hydroxyl solution. Then white precipitate of CdO was obtained**.** Thereafter, the precipitate was filtered by using Whatman filter paper and washed several times using deionized water and ethanol. Then, the precipitate was dried at 110^{o}C in hot air oven. Further, the products were heated at 400^{o}C for 2 h in Muffle furnace. White color powder was formed. Finally, the dried powder was grained in an agate mortar to avoid agglomeration.

2.3 Characterization techniques

The crystalline structure and crystallites size of the samples were studied by X-ray Diffractometer (X' PERT PRO-PANalytical, PHILIPS) using CuK radiation in steps of 0.05^{0} and a time/step of 10.16 s. The band gap energies of samples were recorded using UV–Vis-DRS study (UV140404B). Transmission Electron Microscopy (TEM), high resolution transmission electron microscopy (HR-TEM) and selected area electron diffraction (SAED) images were collected on a Philips (Mod.CM 200) electron microscope with an acceleration voltage of 80 kV. The Energy dispersive X-ray (EDX) analysis was recorded on a JEOL Mod.JSM-6390LV instrument.

3.Results and discussion

3.1 Powder X-ray diffraction analysis (XRD)

Powder X-ray diffraction pattern of CdO nanoparticles with miller indices is shown in Fig. 1. In the synthesized product, several diffraction peaks were observed and all peaks well matched with cubic phase (JCPDS ICDD: 39-1221). The diffraction peaks were observed at 2θ values of 29.27^{o}, 33.82 ^{o}, 36. 72 ^{o}, 43.17 ^{o}, 48.32 ^{o}, 57.17 ^{o}, 61.02 ^{o}, and 70.17 ^{o}and corresponding planes are (111), (200), (210), (211), (220), (311), (222), and (400), with typical face centered cubic (fcc) crystal structure. The crystalline size of crystallites was determined using the Scherrer's formula,

$$d = \frac{K\lambda}{\beta\cos\theta}$$

where d is the average crystalline size, K is a constant (0.9), λ is the wavelength of the incident beam, θ is a Bragg reflection angle, and β is the full width at half maximum (FWHM) of the main diffraction peak. The average crystallite size of CdO nanoparticles was calculated and found to be 18nm and lattice constant was calculated as a=5.3028Å, which coincides with standard lattice values.

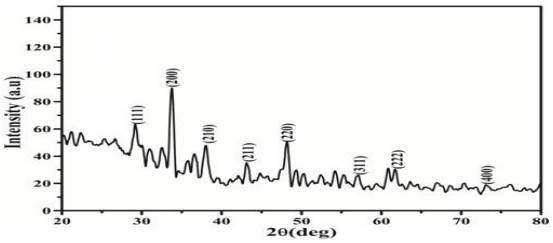

Fig1. XRD pattern of CdO nanoparticles

3.2 Ultraviolet visible diffuse reflectance spectroscopic analysis

The linear optical properties were recorded using UV-Vis DRS technique. The diffuse reflectance technique is capable of collecting the reflected flux of light after interacting with the CdO nanoparticles. The reflectance spectrum shown in Fig. 2 is for reflectance recorded at 200-1100nm range. The optical band gap value of synthesized CdO nanoparticles has been calculated from reflectance spectra using the Kubelka-Munk function,

$$K = \frac{(1 - \mathrm{R})^2}{2R}$$

where K is the absorption co-efficient and R is the reflectance (%). Fig. 3 shows Energy Vs $(k_{*}h\upsilon)^{1/2}$ which is used to calculate the band gap value and is found to be 4.52eV.

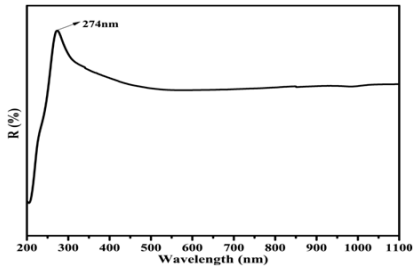

Fig2. UV/Vis DRS spectra of CdO nanoparticles

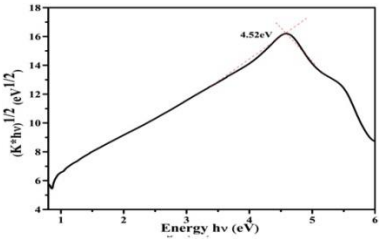

Fig3. Energy Vs $(K_{*}h\upsilon)^{1/2}$ spectra of CdO nanoparticles

3.3 Transmission electron microscope and Energy dispersive X-ray spectroscopic analysis

The captured TEM morphology of the CdO nanoparticles is shown in Fig. 4(a-b). Fig. 4(a) shows the bullet shape morphology and particles are in agglomerated state having size from 10 to 50nm. The high resolution transmission electron microscope (HRTEM) image (Fig. 4(b)) clearly shows the small crystallites and lattice fringes, and provides good evidence of the crystalline structure of the CdO nanoparticles. The measured d-spacing value from HRTEM is 1.61Å (311) which coincided with XRD result. The inset Fig. 4(b) shows the selected area diffraction (SAED) pattern of CdO nanoparticles. The SAED shows the diffraction planes (220), (311), and (111) which correspond to the cubic phase (JCPDS ICDD: 39-1221). Fig. 4(C) shows the energy dispersive X-ray analysis (EDX) of CdO nanoparticles. EDX analysis shows the presence of the Cd and O chemical composition. The Cd and O atomic percentages are is 82.92% and 17.08% .

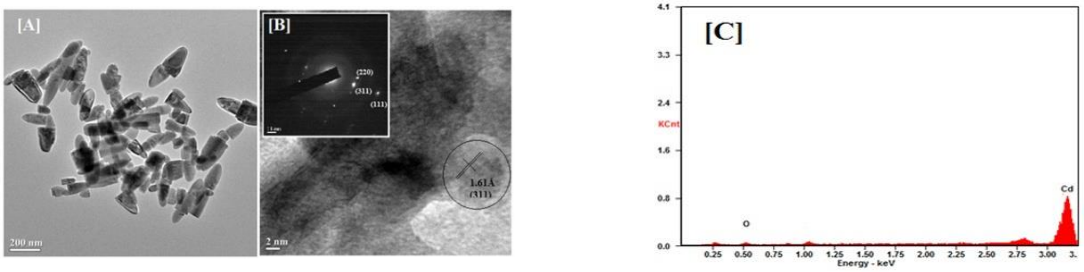

Fig. 4 (a) TEM micrograph, (b) HRTEM and corresponding SAED (inset of (b)), (C) EDX spectra of CdO nanoparticles

3.4 Antibacterial activity

The antibacterial activity of CdO nanoparticles displayed a level of inhibitory effects against the tested pathogenic organisms in disc diffusion method. Maximum zone of inhibitory action (ZOI) appeared in the test organisms for gram negative (Escherichia coli*)* bacteria. In the present study CdO nanoparticles have shown more prominent cell inhibition of 16 mm for Escherichia coli when compared to the standard antibiotics (Ampicillin). The zone of inhibition is found to be gram negative bacteria because CdO nanoparticles damages the structure of bacteria cell membrane and depresses the activity of some membranous enzymes which cause gram negative bacteria to die eventually [15].The commonly accepted mechanism of antibacterial action of the material states that the production of reactive oxygen species (ROS) on the surface of these nanoparticles in light causes oxidative stress in bacterial cells, eventually leading to their death. ROS contain the most reactive hydroxyl radical (OH), the less toxic super oxide anion radical (O2-). This can damage DNA, cell membranes etc., leading to cell death. The attachment of the nanoparticles to the bacteria has also been demonstrated. This is attributed to the electrostatic attraction between the negatively charged bacteria and the positively charged nanoparticles. Such a contact may not only inhibit bacterial growth, but the generated ROS may also kill the cell [16]. The zone of inhibition has shown Fig. 5.

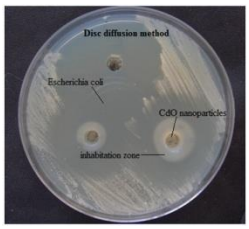

Fig 5.Antibacterial activities for Gram negative bacteria (Escherichia coli)

4. Conclusion

The CdO nanoparticles were synthesized by chemical precipitation method. The synthesized CdO nanoparticles are found to have cubic structure and their particles size are calculated to be about 18nm. The optical bandgap is found to be 4.52eV from UV-Vis DRS analysis. The TEM result shows the bullet shape morphology and particle size of 10-50nm and is in good agreement with XRD result. The EDX confirmed the chemical composition of CdO. The synthesized CdO nanoparticles show faster and stronger antibacterial activity against pathogenic organisms than the standard antibiotics.

Reference

[1] E.W. Wong, P.E. Sheeshan, C.M. Lieber, Science 277 (1971) 1997.
[2] X. Peng, L. Manna, W. Yang, J. Wickham, E. Scher, A. Kadavanich, A.P. Alivastons, Nature 404 (2000) 59.
[3] S.J. Park, S. Kim, S. Lee, Z.G. Khim, K. Char, T. Hyeon, J. Am. Chem. Soc. 122 (2000) 8581.
[4] Lopez-Serrano, R. Munoz-Olivas, J. Sanz-Landaluze, M. Olasagasti, S. Rainieri, C. Camara, Environ. Pollut. 191 (2014) 207–214.
[5] Y. Xiong, J. Zhang, F. Huang, G. Ren, W. Liu, D. Li, C. Wang, Z. Lin, J. Phys. Chem. C 112(2008)9229.
[6] Y. Wang, N. Herron, J.Phys.Chem.95(1991)525.
[7] M. Ortega, G. Santana, A. Morales, Solid State Electron. 44 (2000) 1765–1769.
[8] T.P. Gujar, V.R. Shinde, W.Y. Kim, K.D. Jung, C.D. Lokhande, O.S. Joo, Appl. Surf. Sci. 254 (2008) 3813–3820.
[9] Y.W. Jun, S.M. Lee, N.J. Kang, J. Cheon, J. Am. Chem. Soc. 123 (2001) 5150.
[10] Z.A. Peng, X.G. Peng, J. Am. Chem. Soc. 123 (2001) 183.
[11] X.F. Duan, C.M. Lieber, Adv. Mater. 12 (2000) 298.
[12] K. Murakoshi, H. Hosokawa, M. Saitoh, Y. Wada, T. Sakata, H. Mori, M. Satoh, S. Yanagida, J. Chem. Soc. Faraday Trans. 94 (1998) 579.
[13] A.F.G. Monte, D. Rabelo, P.C. Morais, J. Alloys Comp. 495 (2010) 436.
[14] E.S. Freitas Neto, N.O. Dantas, S.W. da Silva, P.C. Morais, M.A. Pereira-da-Silva, A.J.D. Moreno, V. López-Richard, G.E. Marques, C. Trallero-Giner, Nanotechnology 23 (2012) 125701.
[15] Sumeet Kumar, K. Animesh, Ojha, AIP Advances 3 (2013) 052109 1-6.

Conformal Stability And Vibrational Behavior Of 1-Nitroso-2-Napthol: A DFT Approach

V Ragavendran[a*], S Muthunatesan[b]

[a]*Department of Physics, Sri Chandrasekharendra Saraswathi Viswa Mahavidyalaya, Kanchipuram-61*

[b]*Department of Physics, Government Arts College (Autonomous), Kumbakonam-01*

**Corresponding author, Email: ragav910@gmail.com*

Abstract

The conformational analysis of the title compound was studied using potential energy surface scan studies and Density Functional Theory (DFT) optimization. In order to carry out a detailed vibrational spectroscopic analysis of 1-Nitrosol-2-napthol, Fourier Transform Infrared and Fourier Transform Raman spectra have been recorded in condensed phase. The optimized geometry and vibrational wavenumber of the title compound, Density functional theory calculations in the B3LYP/6-31G** level have been carried out followed by scaling using the **s**caled quantum mechanical methodology. Substitution of nitroso group into the 1-napthol has produced remarkable changes in the structural parameters.

Keywords*:* DFT, Conformational analysis, SQM, UV-Visible, NBO

Introduction:

1-Nitroso-2-naphthol is the chelating ion-exchanger in the synthesis of alumina adsorbents that are of acidic, basic and neutral nature. It is used for the removal and pre concentration of Pb(II), Cu(II), Cr(III) from waste, as well as drinking water. Both isomers are soluble in simple alcohols, ether, and chloroform. 2-Naphthol is a widely used intermediate for the production of dyes and other compounds.[1,2] In the present study, the Fourier Transform Infrared (FT-IR), Fourier Transform Raman(FT-Raman) spectra and Density functional theory(DFT) analysis of 1-Nitroso-2-napthol (1N2N) were presented**.**

Materials and methods:

A fine sample of 1-nitroso-2-naphthol (1N2N) was obtained from M/s. Sigma Aldrich chemicals and used without any further purifications for spectral measurements. The Fourier transform infrared spectrum(FTIR) of the title compound was recorded in the region 4000–400 cm^{-1} and the Fourier transform Raman(FT–Raman) spectrum of 2N1N was recorded in 3500-50 cm^{-1} range with a Nicolet model 950 FT–Raman spectrometer at 4 cm^{-1} spectral resolution using the 1064 nm line of a Nd:YAG laser for excitation at a 200 mW output power. Density Functional Theory calculations of 1N2N were performed by using Gaussian 09 software package [3] at B3LYP functional [4,5] combined with 6-31G** basis set to obtain the optimized geometry and energy of the title compound.

RESULTS AND DISCUSSION

The structure of 1-nitroso-naphthalen-2-ol was optimized using B3LYP/6 -31G** method and the optimized structure was shown in fig. 1. The optimized parameters like bond length and bond angles obtained from the DFT optimization were suitably tabulated. The global minimum energy obtained for the title compound was observed to be -1226.662164 a.u. and the titlecompound belongs

to Cs symmetry. All the calculated vibrational wavenumber using the optimized geometry obtained were found to be positive for the title compound.

4.1 optimized structure

Conclusion

The most stable conformer of 1-nitroso-2-napthol have been identified using DFT optimization procedure and potential energy scan analysis. The Vibrational assignments has been done based on the TED got from the VEDA 4.0 program package [6] and it was found to be in good agreement with the experimentally observed values [24]. Substitution of nitroso group into the 2-napthol has produced remarkable changes in the structural parameters. Thermo dynamical parameters such as the zero point vibrational energy, entropy, heat capacity rotational constants have been computed out. The Mullikan Atomic Charges have been calculated and the charges corresponding to each atoms were properly tabulated.

References:

1. Mohamed E. Mahmoud, Maher M. Osman, Osama F. Hafez, EssamElmelegy, Journal of Hazardous Materials, Volume 173, Issues 1–3, 15 January 2010, Pages 349-357.
2. Mohammad Ali Taher, Ali MostafaviDehzoei, Bal Krishan Puri, Swati Puri, AnalyticaChimicaActa, Volume 367, Issues 1–3, 3 July 1998, Pages 55-61.
3. Frisch, M. J.; Trucks, G. W.; Schlegel, H. B.; Scuseria, G. E.; Robb, M. A.; Cheeseman, J. R.; Scalmani, G.; Barone, V.; Mennucci, B.; Petersson, G. A.; Nakatsuji, H.; Caricato, M.; Li, X.; Hratchian, H. P.; Izmaylov, A. F.; Bloino, J.; Zheng, G.; Sonnenberg, J. L.; Hada, M.; Ehara, M.; Toyota, K.; Fukuda, R.; Hasegawa, J.; Ishida, M.; Nakajima, T.; Honda, Y.; Kitao, O.; Nakai, H.; Vreven, T.; Montgomery, J. A., Jr.; Peralta, J. E.; Ogliaro, F.; Bearpark, M.; Heyd, J. J.; Brothers, E.; Kudin, K. N.; Staroverov, V. N.; Kobayashi, R.; Normand, J.; Raghavachari, K.; Rendell, A.; Burant, J. C.; Iyengar, S. S.; Tomasi, J.; Cossi, M.; Rega, N.; Millam, J. M.; Klene, M.; Knox, J. E.; Cross, J. B.; Bakken, V.; Adamo, C.; Jaramillo, J.; Gomperts, R.; Stratmann, R. E.; Yazyev, O.; Austin, A. J.; Cammi, R.; Pomelli, C.; Ochterski, J. W.; Martin, R. L.; Morokuma, K.; Zakrzewski, V. G.; Voth, G. A.; Salvador, P.; Dannenberg, J. J.; Dapprich, S.; Daniels, A. D.; Farkas, Ö.; Foresman, J. B.; Ortiz, J. V.; Cioslowski, J.; Fox, D. J. Gaussian, Inc., Wallingford CT, 2009.
4. Lee, C.; Yang, W.; Parr, P.G. Development of the Colle-Salvetti correlation-energy formula into a functional of the electron density. Physical Review B B **1988,** 37**,** 785.
5. A. D. Becke,. Density-functional thermochemistry. III. The role of exact exchange. The Journal of Physical Chemistry A **1993**, 98, 5648.
6. Jamroz, M. H. Vibrational Energy Distribution Analysis VEDA 4 program Drug Institute Warsaw, Poland 2004.

SYNTHESIS AND CHARACTERIZATION OF SILVER NANOPARTICLES PREPARED BY GREEN ROUTE

M. Sudha*, S. Dinesh Kumar, B. Murugan and A. Balamurugan

Department of Physics, Government Arts College, Udhagamandalam- 643002.

*Mobile: *9786773495, 9865372315*

Abstract

The development of reliable, eco friendly production of nanoscale materials is significant feature of Nanoscience and nano technology. Silver nanoparticles are well known as inhibitory and antibacterial materials. The present study focus on the production of silvernanoparticles (AgNps) using citrus sinensis seed aqueous extract by green route. Green synthesized AgNps were characterized by UV-Vis spectrum, , X-Ray Diffraction(XRD), Scanning Electron Microscope(SEM), Energy Dispersive X-Ray (EDX) and Fourier Transform Infrared(FTIR). The results emphasized the potent application of citrus sinensis seed in the synthesize of nano silver with economic viability and ease in scaling up for mass production. Duly characterized AgNps tested for antibacterial activity against Escherichia Coli(E.Coli) and Staphylococcus aures(S.aures)

Key Words: Silver Nano particles(AgNps), green route, Citrus Sinensis seed

1.Introduction

Nanotechnology concerns with the development of experimental processes for the synthesis of nanoparticles of different sizes, shapes and controlled dispersity. Nanoparticles are particles between 1 -100 nm in size. Nanoparticle research is currently an area of intense scientific interest due to wide variety of potential applications in biomedical, optical and electronic files. Silver Nanoparticles (AgNps) are the most applicable and interesting nanoparticles between researchers. AgNps have been reported in various applications as sensors(Chandrakani k.T. et al 2013) DNA deduction, Catalyst(Bharat. B et al., 2013) , from a therapeutic point of view biosynthesized AgNps use as antifungal agent batteries to increase the efficiency (Ganesh kumar et al 2015) , electronics , photovoltaic, nano heaters . AgNps prepared by various physical and chemical methods irradiation and but the use of toxic chemicals as reducing agents in many of these routes is potentially dangerous to the environment and biological systems. Green routes for synthesis of AgNps by biological process using plant extract containing phytochemical agents have attracted considerable interest in recent years. Such green process can lead the formation of nanoparticles to more biocompatible environmental begin and cost effective products. On the basis of the available literature , we hypothesize that Citrus Sinensis seed could be used in the synthesis of AgNps. The nanoparticles were characterized by UV-Vis spectroscopy, XRD, SEM, EDX , FTIR analysis.

2.Materials and methods

The chemical silver nitrate($AgNo_3$) was purchased from SD fine chemical Pvt . Ltd and antibiotic and Muller Hinton agar were purchased from Hi Media – Mumbai for this study. The seed

of Citrus Sinensis was collected from local market ooty . The seed of Citrus Sinensis washed with water followed by rinsed with distilled water , dried at room temperature for 10 days and dried seed obtain in powder. 10gms of dried powdered Citrus Sinensis seed was weighted and boiled for 20min in 100ml distilled water in 250ml Erlenmeyer flask and cooled for room temperature. Then the aqueous extract was then filtered through normal filter paper followed by whatman filter paper no.1. This extract was used as reducing as well as stabilizing agent. 500ml of aqueous solution of 1mM concentration silver nitrate solution was added 25ml of Citrus Sinensis seed extract while stirring for reduction into silver ions and the reaction mixture was kept at room temperature for 24 - 48 hours . The formation of dark brown colour indicating the formation of AgNps.

3.Characterization Technique

The reduction of pure silver ions Ag^{+} ions into silver nanoparticles can be identified by. UV-Visible spectrometer (JASCO, V-670) from 300-800 nm at resolution of 1nm. The crystalline nature of AgNps were measured by X-Ray diffraction studies by using X'pert Pro X-Ray diffractometer (Pan analytical BV, Netherlands) operated at 30Kv/ 30mA equipped with Cu/kα radiation source and all the XRD Patterns were recorded.

The silver nanoparticles solution thus purified by centrifugation at 5000rpm for 30mins. The supernatants were discarded and the final pellets were dissolved in 1ml of deionized water. After air drying of AgNps with cover slip was used during SEM analysis along with Energy – Dispersive X-Ray analysis to identify the composition of materials. the images of silver nanoparticles were obtained in a SEM (Model:FB quanta 200 SEM) machine at different masgnification level. Finally AgNps were characterized by fourier transform infrared spectra for was obtained in the range 4000 to 400 cm-1 with an IRA-Prestige-21 shimadzu FTIR spectrometer by KBr pellet method to identify chemical compounds based on the way infrared radiation is absorbed by the compound.

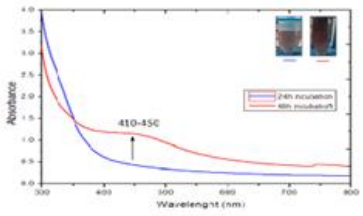

Figure 1: UV-Vis absorption sprectum of AgNps

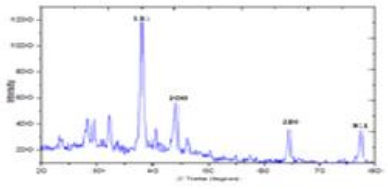

Figure 2 : XRD analysis of AgNps

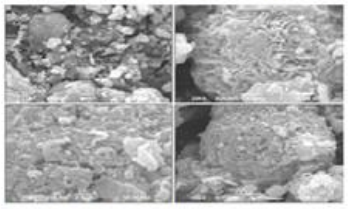

Figure. 3: SEM image of AgNPs

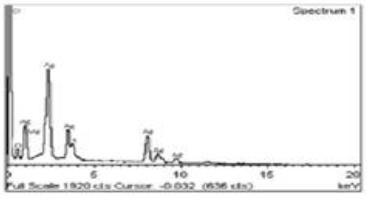

Figure 4: EDX analaysis of AgNps

4. Result and Discussion

Reduction of silver ions present in the aqueous solution of silver complex during the reaction with the ingredients present in the citrus sinensis seed extract observed by the UV-Vis spectroscopy revealed the presence of silver nanoparticles and it shows the Plasmon resonance peak at 442 .The xrd and sem analysis showed the particle size between 13-50 nm as well as spherical in shape and face center cubic structure of the nanoparticles. FTIR analysis confirmed that the bioreduction of Ag+ ions to silver nanoparticles due to the reduction by capping material of plant extract. EDX analysis peaks showed the purity of silver. The silver nanoparticles synthesized via green route are highly toxic to multidrug resistant bacteria hence has a great potential applications.

Conclusion

In conclusion , the biuo-reduction of aqueous Ag+ ions by the seed ectract of the citrus sinensis has been demonstrated. The reduction of the metal ions through seed extract leading to the formation of silver nanoparticles of fairly well defined dimensions -. But the capabilities of the other plant part such as seed as a capping and reducing agent is not tested and not well defined. The present study we found that seed can be also good source for synthesis of silver nanoparticles. The biological approach toward the synthesis of silver nanoparticles has advantageous such as ease with which the process can be scaled up, economic viability etc.applications of such eco-friendly nanoparticles in bactricidial wound healing and other textile coating makes this method potentially exciting for the large-scale synthesis of other inorganic materials. Toxicity studies of silver nanoparticles on human pathogen opens a door for a new range of antibacterial agents.

Reference

1. Bharat, B.; Gabriel, G J.; Akbashev, M. J.; Booher, M E. Langmuir, 2013; 29: 4225−4234.
2. Ganesh Kumar, C.; Poornachandra, Y.; Colloids and Surfaces B: Biointerfaces, 2015; 125: 110-119.
3. Krishnaraj C, Jagan EG, Rajasekar S, Selvakumar P, Kalaichelvan PT, Mohan N, Synthesis of silver nanoparticles using Acalypha indica leaf extracts and its antibacterial activity against water borne pathogens. Colloids Surf B: Biointerfaces 76:50–56, (2010)
4. Kumar, A.; Praveen kumar, V.; Ajayan, P, M.; John, G.; Nature materials, 2008; 7: 230-241. Holtz, R, D.; Lima, B, A.; Souza Filho, A, G., Marcelo, B.; Alves, O. L.; Nanomedicine: Nanotechnology, Biology, and Medicine, 2012; 8: 935–940.
5. Usha. C and D. Gladys Angelin Rachel. Biogenic synthesis of silvenanoparticles by *Acacia nilotica* and their antibacterial activity. *Int. J. Scientific Res*., 3(6), 27-29.(2014).

GROWTH, SPECTRAL, OPTICAL AND NLO STUDIES ON PURE AND Hg^{2+} DOPED L-PHENYLALANINE FUMARIC ACID SINGLE CRYSTALS

P. Jayaprakash [a], M. Nageshwari [a], S. Sudha [a], M. Lydia Caroline [a]*,

[a] *PG & Research Department of Physics, Arignar Anna Govt. Arts College, Cheyyar - 604 407, TamilNadu, India*

Corresponding author : lydiacaroline2006@yahoo.co.in

ABSTRACT

The influence of doping the metal Hg^{2+}on the growth of L-Phenylalanine fumaric acid (LPFA) crystals grown by slow evaporation method have been investigated. The concentrations of metal dopants in the mother solution with 3wt % for mercury were carried out individually and crystals were obtained with well-defined morphology. Structural characterizations of the grown crystals were carried out by single crystal X-ray diffraction analysis and it shows slight structural changes as a result of doping. The FT-IR spectral study reveals the presence of various functional groups in pure and doped LPFA. The UV–Vis spectral study was carried out to analyze the optical transmittance of the grown crystals and was found that the transmittance is very high in the visible and UV regions for both pure and doped crystals. The second harmonic generation (SHG) for the pure and doped LPFA crystals was confirmed by Nd: YAG laser.

1. INTRODUCTION

Nonlinear optics (NLO) is one of the new modern scientific frontiers where the interest is not only for understanding of new physical phenomena, but also to realize the technological applications [1]. NLO has emerged as one of the most attractive fields of current research in view of its vital application in areas like optical modulation, optical switching, optical logic, frequency shifting and optical data storage for the developing technologies in telecommunications and signal processing [2]. The newly emerging technology of photonics utilizes photons instead of electrons to acquire, store, transmit and process information. Organic nonlinear crystals have played an important role in nonlinear applications due to their large nonlinear optical (NLO) coefficient and structural diversity or flexibility when compared to other inorganic counterparts. They have their intrinsic weakness due to poor physicochemical stability and low mechanical strength. Materials with large second order nonlinear optical (SONLO) properties, short transparency cut off wavelengths and stable physicochemical performance are needed to realize many of the above applications, other advantages of organic compound apart from the above include accessibility for synthesis, multifunctional substitutions, higher resistance to optical damage, and maneuverability for device applications**.** Organic crystals with large order nonlinear optical susceptibilities attract great interest because of their potential application in second harmonic generation [3]. Crystal growth from solution is very important process that is used in many applications from the laboratory to industrial scale. These molecular organic compounds with one or more aromatic systems in conjugated positions, leading to charge transfer systems have been intensely studied for the past two decades, these compounds must crystallize in a non-centrosymmetric class in view of applications making use of quadratic optically nonlinear effects. Thus organic NLO materials play an important role in second-harmonic generation

(SHG), frequency mixing, electro-optic modulation, optical parametric oscillation, optical bistability, etc. Amino acid based crystals exhibit excellent nonlinear and electroptic properties. Recently amino acid L-phenylalanine mixed with fumaric acid is reported in the literature exhibits good NLO effect**,** L-phenylalanine, an aromatic and hydrophobic α-amino acid mixed with fumaric acid, an organic compound widely found in nature, and is a key intermediate in the biosynthesis of organic acids are mixed in the ratio 1:1. Several new complexes incorporating the amino acid have been recently crystallized and their structural, optical and thermal properties have been investigated [4]. In LPFA structure of two molecules of fumaric acid are in the asymmetric unit, which are related to each other through a pseudo-inversion centre, and are essentially planar.

2. Synthesis and Crystal growth of LPFA

Single crystals of LPFA and mercuric chloride doped LPFA were synthesized by separately dissolving stoichiometric amount of L-phenylalanine (AR grade) and fumaric acid (AR grade) (pure LPFA) in deionized water and 3 wt% (doped LPFA) with the reactants. The chemical reaction that takes place in the process is as follows:

The calculated amounts of the reactants were thoroughly dissolved separately in solvent of deionized water using a magnetic stirrer and filtered twice to remove the suspended impurities in the solution. The filtered solution was transferred to two crystal growth vessels and crystallization was allowed to take place by slow evaporation under room temperature. Single crystals of both pure and doped LPFA were obtained in a period of 7 days by slow evaporation. The photograph of pure LPFA and doped LPFA crystals are shown as inset in Fig.1 and Fig. 2 respectively.

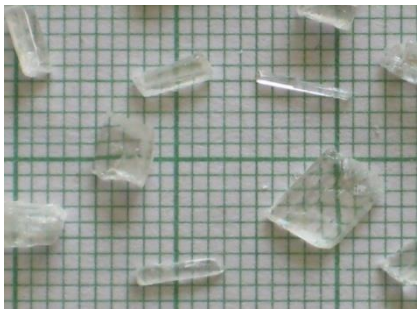

Fig. 1 Photograph of pure LPFA single crystals.

Fig. 2 Photograph of doped (Hg^{2+}) LPFA single crystals.

3. Characterization techniques

The grown pure and doped LPFA single crystal were subjected to various characterization techniques like single crystal X-ray diffraction, Fourier transform infrared (FTIR), UV–vis-NIR, and nonlinear optical studies**.** Single crystal X-ray diffraction studies have been carried out using Enraf Nonius CAD4 diffract meter with MoKα (λ = 0.7170 Å) to determine the cell parameters. The optical transmission spectra of pure and doped Hg^{2+}LPFA single crystals have been reported in the region 200-1100nm using a Shimadzu UV-1061 UV–vis spectrometer. An FTIR study was performed

using BRUKER 66V FT-IT spectrometer in the range 4000-400 cm^{-1} following KBr pellet technique. The NLO properties of the grown crystals were confirmed by Kurtz powder second harmonic generation (SHG) test. The crystals were illuminated using Spectra Physics Quanta Ray DHS2. The SHG radiations of 532 nm green light was collected by a photomultiplier tube(PMT- Hamasu R2059) after being monochromated (monochromotor-Czerny-Turner) to collect only the 532 nm radiation. The optical signal incident on the PMT was converted into voltage output at the CRO (Tektronix-TDS 3052B). The input laser energy incident on the powdered samples was chosen to be 4.45 mJ/pulse.

4. Results and discussion

4. 1 Single crystal XRD analysis

Single crystal X-ray diffraction studies were carried out on the pure and doped Hg^{2+}LPFA single crystals. Reflections from a finite number of planes were collected. It is observed that the crystal belongs to triclinic system and space group p1.The pure and doped Hg^{2+}LPFA singlecrystals retained their monoclinic structure with the lattice parameter a = 5.78Å, b=11.64 Å, c=11.67 Å, α=68.22º, β=80.60º, γ=79.14. The volume of the material is found to be 712 $Å^3$.The crystallographic data of the crystal are compared with that of [5] and are in accordance with literature.

4. 2 FTIR spectral analysis

The characteristics of the vibrational spectra for the various functional groups present in the compound consisting of pure and doped Hg^{2+}LPFA single crystals were recorded in the range of 400 to 4000cm^{-1},form hydrogen-bonded double layers, linked together by N-H…O and O-H…O is depicted in Fig. 3 and Fig. 4. The presence of zwitter ionic groups is observed at 3066cm^{-1} for pure and 3080$cm^{-1}$for (doped LPFA) are due to NH_3^+asymmetric stretching vibration. The band at 3413cm^{-1} for pure and 3441cm^{-1} for doped LPFA are attributed due to O-H stretching mode and at 2926$cm^{-1}$for pure and 2860cm^{-1} for doped LPFA due to aromatic C-H asymmetric stretching mode. The symmetric stretching mode of the carboxyl anion, $CO2^-$is located at 1422$cm^{-1}$for pure and 1421cm^{-1} for doped LPFA aromatic C=C symmetric vibrations are assigned at 1663$cm^{-1}$for pure and 1661cm^{-1} for doped LPFA. The protonation of carboxyl group COO^- deformation absorption bands appears around 1373 and 1422 cm^{-1}. The peak around 1132cm^{-1} is due to the presence of C-C stretching. The in-plane deformation occurs at 1316 $cm^{-1}$for pure and 1318 cm^{-1}confirms the presence of phenylalanine ions and at 1275cm^{-1} (very weak) for and 1272 cm^{-1} . At 925 cm^{-1} O-H out of plane deformation wave number is observed. The benzene ring deformation is due to band at 1080 cm^{-1} and presence of benzene ring is confirmed at the absorption band at 703cm^{-1} (phenyl and benzene ring out of plane ring deformation) and at 745 $cm^{-1}$for pure and 748 cm^{-1} for doped LPFA(phenyl ring out of plane CH deformation). The band at 642 $cm^{-1}$for pure and 643 $cm^{-1}$for doped LPFA illustrates the presence of substituted ring 1, 4 distributions. The bands at 581cm^{-1} for pure and 483 $cm^{-1}$for doped LPFA may be attributed due to C-C deformation. The observed shift in vibrational wave numbers of pure L-

phenylalanine fumaric acid [LPFA], and metal doped (mercuric chloride) LPFA confirms the incorporation of metal dopants in the pure L-phenylalanine fumaric acid crystal structure.

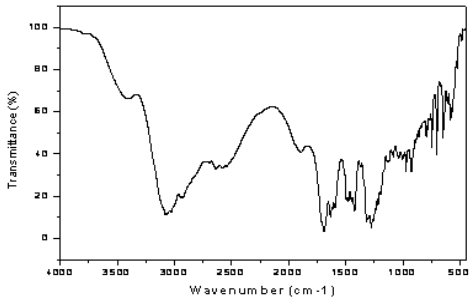

Fig. 3 FTIR spectrum of LPFA

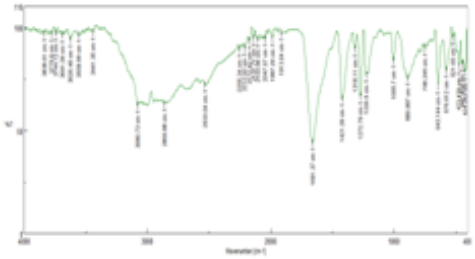

Fig. 4 FTIR Spectrum of Hg^{2+}doped with LPFA

Table 1.COMPARISON OF FTIR BANDS OF PURE LPFA AND DOPED Hg^{2+} LPFA

PURE LPFA	DOPED Hg^{2+} LPFA	Assignment
581	576	C-C Deformation
745	748	CH Deformation
1316-1275	1318-1272	Confirms The presence of phenylalanine
1421	1422	CO_2^- Symmetric
3066	3080	NH_3^+ Asymmetric

4. 3 UV-VIS-NIR spectral studies

To determine the transmission range and hence to know the suitability of pure and doped L-phenylalanine fumaric acid with mercuric chloride single crystals for optical applications, UV-vis-NIR analysis was made in the wavelength range from 200 to 1100 nm using Shimadzu model UV-1061 UV–visible spectrometer. The plot of absorption vs. wavelength is shown in Fig. 5 andFig.6. For optical fabrications, the crystal should be highly transparent in the considerable region of wavelength [6]. There is no appreciable absorption of light in the entire visible range, as in the case for all amino acids. The UV absorption edge for the grown crystals of pure LPFA and doped LPFA were observed to be around240 nm and 233.6 nm respectively, is an essential parameter for frequency doubling process using diode and solid-state lasers [7].

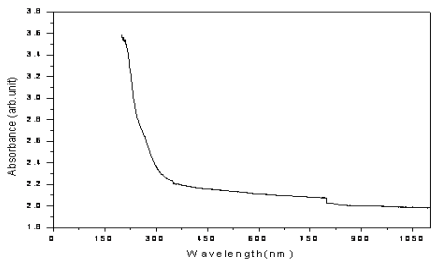

Fig. 5 UV-VIS-NIR Spectrum of LPFA

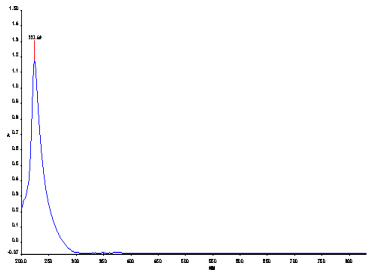

Fig. 6 UV-VIS-NIR spectrum of Hg^{2+} doped LPFA

4. 4 NLO study

The first and the most widely used technique for confirming the SHG from prospective second order NLO materials is the Kurtz powder technique [8]. To test the second harmonic generation property of the LPFA crystal, Nd: YAG laser using the first harmonics output of 1064 nm with pulse width of 10 ns and repetition rate10 Hz with beam energy 0.70 mJ/pulse was passed through the sample. The second harmonic green signal (λ = 532 nm) was generated by the pure and mercury doped LPFA confirmed that the samples exhibit good NLO property.

CONCLUSION

Single crystals of pure and Hg^{2+} doped LPFA, were successfully grown by slow evaporation technique at room temperature. The grown crystals were confirmed by X-ray diffraction analysis and it is found that the crystals belong to the triclinic system with space group P1. FTIR analysis confirms the functional groups present in the pure and Hg^{2+} doped LPFA crystals. Optical transmission studies showed that crystals were optically transparent in the entire visible region with a lower cut-off below 300 nm. NLO behaviour of the pure and Hg^{2+} doped LPFA crystal were observed by Kurtz-Perry powder technique. With the presence of wide transparency range and good SHG efficiency, both pure and Hg^{2+} doped LPFA single crystals could be potential materials for NLO application.

REFERENCES

[1] P.N. Prasad, D.J. Williams, John Wiley & Sons, Inc.: New York 1991.

[2] K. Ambujam, C. Preena Thomas, S. Aruna, D. Prem Anand, P. Sagayaraj, Mat& Man. Pro. 23, 2007,346-350 .

[3] D.S. Chemla, J. Zyss, Academic Press: New York 1987.

[4] M. Lydia Caroline, S. Vasudevan, Mat. Lett. 63, 2009, 41-44.

[5] M. Alagar, R.V. Krishna Kumar, K. Rajagopal, M. Subha Nandhini, S. Natarajan, Acta E, 59, 2000, 952-954.

[6] V. Krishnakumar, R.J. Xavier, Spectrochimi. Acta A, 60, 2004, 709-714.

[7] N. Vijayan, R. Ramesh Babu, R.Gopalakrishnan, S. Dhanuskodi, P. Ramasamy, J.Cryst. Growth 265, 2004, 290-295.

[8]S.K. Kurtz, T.T. Perry, J. Appl. Phys. 39, 1968, 3798-3813.

A STUDY ON GROWTH, SPECTRAL, LINEAR AND NONLINEAR OPTICAL STUDIES ON PURE AND Zn^{2+} DOPED L-PHENYLALANINE 4-NITROPHENOL SINGLE CRYSTALS

P. Sangeetha [a] ,M. Peer Mohamed [a,b], C. Rathika Thaya Kumari [a],

M. Lydia Caroline[a]*

[a] *PG & Research Department of Physics, Arignar Anna Govt. Arts College, Cheyyar - 604 407, TamilNadu, India*

[b] *Department of Physics, C. Abdul Hakeem College,Melvisharam-632 509, TamilNadu ,India*

Corresponding author:lydiacaroline2006@yahoo.co.in

ABSTRACT

Single crystals of pure and Zn^{2+} doped L-phenylalanine-4-nitrophenol (LP4NP) have been successfully grown by slow evaporation technique. The lattice parameters of the grown crystals have been determined by X-ray diffraction studies. FT-IR spectrum was recorded to identify the presence of functional group. The grown pure and doped crystals were found to be transparent in the entire visible region. The existence of second harmonic generation signals was observed using Nd:YAG laser with fundamental wavelength of 1064 nm for pure and Zn^{2+}doped LP4NP.

1. Introduction

The field of molecular nonlinear optics has benefited from both upstream rejuvenation and downstream application oriented breakthroughs, aiding to bring the field closer to industrial developments [1]. Engineering of new nonlinear optical (NLO) materials, structures, and devices with enhanced figures of merit has developed over the last two decades as a major force to help drive nonlinear optics from the laboratory to real applications. The NLO process requires materials that manipulate the amplitude, phase, polarizations and frequency of optical beam. The intellectual construction of structurally controlled supramolecular assemblies (e.g., acentric and chiral solids) remains a great challenge even though the art of chemical synthesis of discrete molecules has significantly advanced in recent decades. The relevance of organic materials in this interesting context is because the delocalized electronic structure of p-conjugated organic compound offers a number of tempting opportunities in applications as NLO materials. In continuation of our work, we report in this present investigation growth, structural, spectral, optical and thermal studies on L-phenylalanine-4-nitrophenol (LP4NP) single crystals. The crystal structure title compound has already been reported [2].

2. Synthesis and Crystal growth of LP4NP

Pure and zinc doped L-Phenylalanine (LP4NP) crystals were grow by a slow evaporation techniques by dissolving separately in double distilled water. The solutions were then mixed in a 1:1 M ratio and stirred to ensure homogenous temperature and concentration over entire of the solution. The solutions were transferred to crystal growth vessels followed by slow evaporation at room temperature. The seed crystals were obtained in a period of 2 weeks. The photograph of as grown crystals of pure and metal doped LP4NP is shown are Fig. 1 & Fig. 2 respectively.

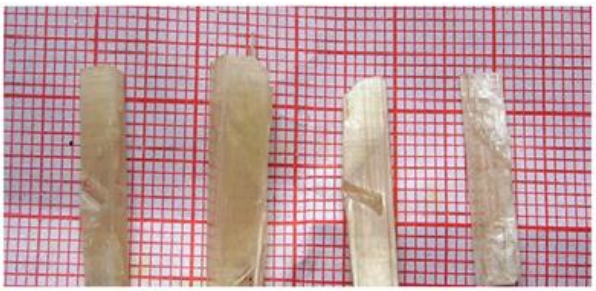

Fig.1 Photograph of pure LP4NP Single Crystal

Fig. 2 Photograph of LP4NP Doped Zn^{2+} single crystal

3. Characterization techniques

The grown LP4NP single crystal was subjected to various characterization techniques like single crystal X-ray diffraction, Fourier transform infrared (FTIR), UV–vis-NIR and nonlinear optical studies**.** Single crystal X-ray diffraction studies have been carried out using Enraf Nonius CAD4 diffractometer with MoKα (λ= 0.7170 Å) to determine the cell parameters. The transmission property of the materials was analysed using a Shimadzu UV-1061 UV–vis spectrometer between the region 200 -1100 nm. The coordination of L-phenylalanine with 4-nitropheol was confirmed by FTIR studies using BRUKER 66V FT-IT spectrometer in the range 4000-400 cm^{-1} following KBr pellet technique. The NLO property of the crystal was confirmed by Kurtz powder second harmonic generation (SHG) test. The crystal was illuminated using Spectra Physics Quanta Ray DHS2. The SHG radiations of 532 nm green light was collected by a photomultiplier tube(PMT- Hamasu R2059) after being monochromated (monochromator - Czerny - Turner) to collect only the 532 nm radiation. The optical signal incident on the PMT was converted into voltage output at the CRO (Tektronix-TDS 3052B). The input laser energy incident on the powdered sample was chosen to be 4.45 mJ/pulse.

4. Results and discussion

4. 1 Single crystal XRD analysis

Single crystal X-ray diffraction study was carried to demonstrate the crystallinity of the compound crystals using EnrafNonius CAD4 diffractometer at room temperature. Reflections from a finite number of planes were collected. It is observed that the crystal LP4NP belongs to triclinic system and space group P1: the lattice parameters are a = 5.78 Å, b=11.64 Å, c=11.67 Å, mα=68.22º, β=80.60º, *γ*=79.14. The volume of the material is found to be 712 $Å^3$. Fordoped LP4NP,a = 5.79 Å, b=11.69 Å, c=11.70 Å, α=68.22º, β=80.59º, *γ*=79.18, v=714.2 $Å^3$respectively. The crystallographic data of the crystal are compared and are in accordance with literature [2].

4. 2 FTIR spectral analysis

The recorded FTIR spectrum is shown in Fig. 3 and Fig. 4. A broad strong absorption in the region 3300–2300 cm^{-1} corresponds to the NH_3^+ ion of the amino acid [3]. The band that appears at 2700– 1800 cm^{-1} signifies the overtone combinations. The peak at 1742 cm^{-1} is assigned to COO^- stretching vibration. The bands at 1586$cm^{-1}$for pure and 1581 $cm^{-1}$for doped LP4NP, established the presence of NH_3 deformations. The bands at 1496 cm^{-1}(pure) and 1496 cm^{-1}(doped LP4NP) which

confirms the presence of NH3 symmetric stretching and rocking respectively. The bands at 1457 cm^{-1} (pure) and 1455 cm^{-1}(doped LP4NP) established the presence of COO^- stretching. The bands at 645 cm^{-1} pure and 647 cm^{-1}doped LP4NP signifies the presence of COO^- wagging and rocking respectively. The bands at 1353 cm^{-1} ,1331cm^{-1} ,1109 cm^{-1} (pure)and 1348 cm^{-1}, 1329 cm^{-1}, 1113 cm^{-1}(doped LP4NP)established the presence of CAH deformation. The OH and COH out of plane deformation vibrations produces sharp intense peaks at 923 and 845 cm^{-1} respectively. The bands at 1586cm^{-1}(pure) and 1581 cm^{-1}(doped LP4NP) was due to the presence of NO2 symmetric stretching. The peak at 706 cm^{-1} established the presence of benzene ring. The presence of CACO deformation is clearly illustrated by the peak at 530 cm^{-1}. The bands at 1079 cm^{-1}(pure) and 1079 cm^{-1}(doped) LP4NP, signifies the deformation benzene ring. The CH_2 wagging and stretching shows the characteristic vibration at 1244 $cm^{-1}$for pure and 1243 cm^{-1}(doped LP4NP)respectively. The stretching vibrations of CH2 and CHO presence the peak at 1165 cm^{-1}. The bands at 1110$cm^{-1}$and 1005 cm^{-1} established the presence of COH out of plane deformation and CACAN bending respectively. From this FTIR spectrum clear that both L-phenylalanine and 4-nitrophenol functional group present in the grown crystal. The influence and incorporation of the metal dopants is usually ascertained from the wavelength assignments at low frequency regions. The observed shift in vibrational wave numbers pure LP4NPmetaldoped L-phenylalanine 4-nitrophenol doped with zinc chloride confirms the incorporation of metal dopants in the pure L-phenylalanine 4-nitrophenol crystal structure.

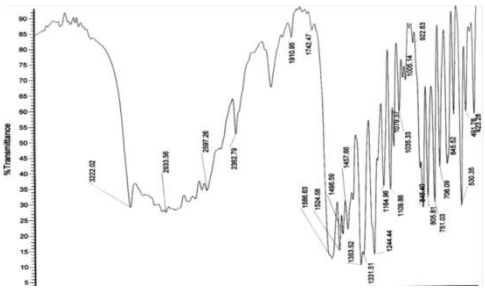

Fig. 3 FT-IR spectrum of LP4NP

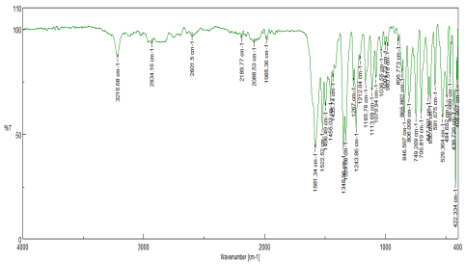

Fig. 4 FTIR Spectrum of LP4NPdoped with Zn^{2+}

4. 3 Optical absorption studies

The UV–Vis–NIR analysis of LP4NP crystal was carried out between 200 and 2000 nm, covering the entire near ultra violet, visible and near infrared regions. There is no appreciable absorption of light in the entire visible range as in the case for all amino acid [4]. Fig. 5 and Fig. 6, shows the UV–Vis–NIR optical absorption spectra of LP4NP crystal. The lower cut-off wavelength of 218.35 nm and 401.55 nm for pure LP4NP and Zn^{2+} doped LP4NP respectively. Which is sufficient for SHG laser radiation of 1064 nm or other application in the blue region. Interestingly, in the entire visible region starting from 218.35 to 900nm, the crystal has almost no absorption. The wide optical

transmission window is an encouraging optical property seen in LP4NP crystal and is of vital importance for NLO materials.

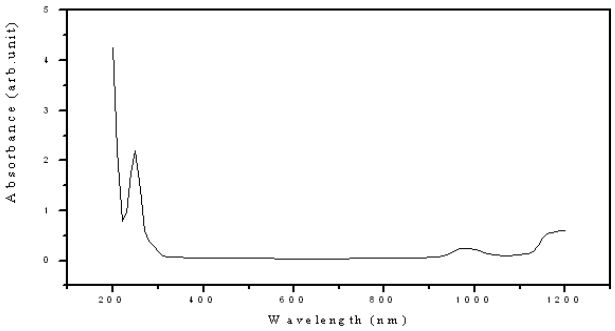

Fig. 5 UV-visible spectrum of pure LP4NP

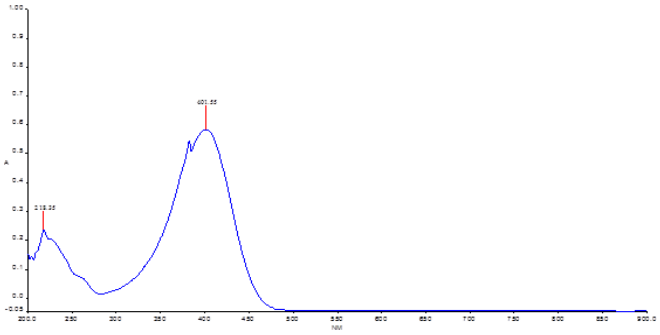

Fig. 6 UV-visible spectrum of LP4NP doped with Zn^{2+}

4.4 NLO studies

In order to confirm the NLO property, the grown crystals was subjected to a Kurtz powder test [5] using a Q-switched, mode locked Nd:YAG laser of 1064 nm and a pulse width of 8 ns (spot radius of 1 mm) on the powder sample of LP4NP. The input laser beam was directed on the as-grown crystals powder to get maximum powder SHG. The emitted light passed through an IR filter was measured by means of a photomultiplier tube and oscilloscope assembly. The SHG efficiency of the Zn^{2+} doped LP4NP and pure LP4NP crystal were evaluated by taking the microcrystalline powder of KDP as the reference material. The SHG efficiency of pure LP4NP results show a high signal output of 15.25 mV with input laser power of 0.70 J/pulse when compared to 22.1 mV of KDP.SHG efficiency of pure LP4NP is 0.687 times that of KDP crystal. The SHG output of Zn^{2+} doped LP4NP is slightly higher than the pure LP4NP.

CONCLUSION

Single crystals of pure LP4NP and Zn^{2+} doped LP4NP, were successfully grown by slow evaporation technique at room temperature. X-ray diffraction analysis of both pure LP4NP and Zn^{2+} doped LP4NP revealed the structure of the crystal as monoclinic system with space group $P2_1$. The presence of functional group was confirmed by FT-IR. Both pure LP4NP and Zn^{2+} doped LP4NP were optically transparent in the entire visible region with a lower cut-off wavelength of 218.35 nm and 401.55nm for pure LP4NP and Zn^{2+} doped LP4NP respectively. The optical and SHG efficiency studies show the suitability of the crystals for NLO application.

References

[1] J. Zyss, F. Nicoud, Curr. Opin. Solid State Mater. Sci. 1 (1996) 533–546.
[2] V.H. Rodrigues, M.M.R.R. Costa, E. De Matos Gomes, E. Nogueirab, M.S. Belslsey, Acta Cryst. E 62 (2006) 0699–0701.
[3] P. Srinivasan, Y. Vidyalakshmi, R. Gopalakrishnan, Crystal Growth Des. 8 (2008), 2329–2334.
[4] J.J. Rodrigues Jr, L. Misoguti, F.D. Nuns', C.R. Mendonca, S.C. Zilio, Opt. Mater. 22 (2003) 35–240.
[5] S.K. Kurtz, T.T. Perry, J. Appl. Phys. 39, 1968, 3798-3813.

SURFACE ANALYSIS ON GREEN ALGAE CHARCOAL ADSORBENT USING HR-SEM STUDY

M. Sundarrajan, S. Jayaprakash

Department of Physics, Sri ChandrasekharendraSaraswathiViswaMahavidyalaya, Enathur, Kanchipuram 631561, Tamilnadu, India
rajan_sugi@yahoo.com

ABSTRACT

This study aims at surface characteristics of charcoal prepared from fresh water green algae. Algae samples were collected from 10 locations in and around Kancheepuram district from running water streams like river sides and canal sides. The algae were cleaned, dried and burnt to charcoal. The charcoal micrographs were recorded by High Resolution Scanning Electron Microscopy (HRSEM) and surface characteristics were discussed.

INTRODUCTION

Our environment is continuously polluted by our everyday activities. The pollutants mixed to water channels like river, lakes and canals attribute for water contamination. The major pollutants are organic, inorganic and oil pollutants.Among various sources of organic and inorganic pollutants, heavy metals are common and are continuously contributing to major levels of pollution in water bodies[(1)].The surface water in industrial areas gets more polluted [(2)] and when living things get interacted with the above water resources, they are prone to harmful health effects. In this scenario water treatment is to be done to remove these contaminants. Adsorption is one among the various treatment processes and adsorption using natural cost effective adsorbents is under research.

The waste water treatment is carried out in various sequences of processes such as primary, secondary and tertiary treatments. In primary treatment wastes are removed as settled debris. In secondary treatment, the wastes are removed by decomposition. In tertiary treatment, wastes are removed by chemical coagulation and sedimentation [(4, 5, and 6)]. Metallic ions can be removed through various processes like precipitation, adsorption, ion exchange, membrane processes, eletrodialysis, and reverse osmosis [(7, 8, 9, and 10)]. In water treatment processes, adsorption processes are mainly achieved using charcoal and activated carbons prepared from various precursors. This is mainly due to the reason that activated carbons and charcoal are having high surface area and hence achieve higher adsorption. The sequential processes such as carbonizing and subsequent activation make the charcoal to have porous structure with higher surface area [(11, 12)]. The adsorption process is the result of adhesion of atoms, ions or molecules from liquid, gas or dissolved solid over the surface of adsorbent material and forms a thin layer of adsorbate.

SCOPE OF THE STUDY

The main objective of this study is to analyze the porous surface structure of the charcoal prepared from the fresh water green algae.

MATERIALS AND METHODS

Algae are certain group of organisms which occur in various shapes and sizes and have different ecological roles. The algae occur widely as fresh and marine water algae. Freshwater algae float in the water, but others are in submerged condition and they are attached to rocks or aquatic plants.

Study Area

Fresh water green algae were collected from fresh water regions like running canals and river sides situated in and around Kancheepuram district, Tamilnadu, India.

Sample Collection

Fresh water green algae were collected from running canals and river sides from 10 places in and around Kancheepuram district. The samples were collected using plastic wire mesh. The trapped algae were then washed with distilled water 5 times to remove other impurities. The washed algae were then spreaded in glass plates and dried fully under hot sun in semi air permeable containers.

Sample preparation

Algae were collected from various fresh water zone The selected algae sampled were taken in a container with closed lid. The top of the lid is perforated. The closed lid is kept inside a firing pot. The pot is ignited and the algae in lid are allowed to burn in the firing atmosphere. As the flame heats the lid, the algae burn with fumes which are coming through the perforation. The firing pot is flamed until the fumes through the perforation stops. After the lid is taken out from the pot, it is cooled in atmosphere to room temperature. The algae burnt in to charcoal is taken out and ground to fine powder and packed in polyethylene bags.

HRSEM analysis

The powdered charcoal was then subjected to HRSEM analysis at SAIF, IITM, Chennai for surface area porous structure characterization.

RESULTS AND DISCUSSION

HRSEM micrographs of charcoal samples of fresh water green algae were presented and analyzed for their porous structure. Pore size has been determined from the scaling of micrographs.

Pore size analysis from HRSEM Micrographs

The micrograph of charcoal samples of fresh water green algae are shown in fig.1 and 2. The surface morphology may be well observed from the micrographs.

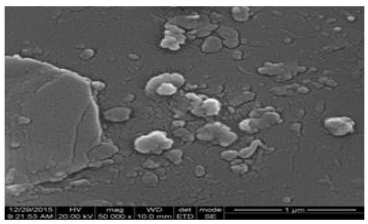

Fig.1 Micrograph of Algae Charcoal

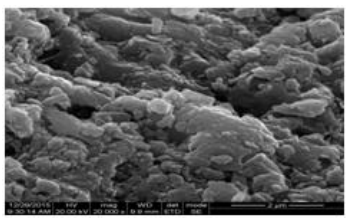

Fig. 2 Micrograph of Algae Charcoal

From the figure1, using the scale bar information on the micrograph, the following results are observed.

1. The surface consists of porous boundaries and pores are not well formed.
2. Usingthe scale bar information thelinear sizeof the intra poroussurface is approximately calculated andit liesbetween 13.8 to 55.2 nm.
3. The thickness of porous boundary is approximately calculated and lies between2.7 to13.8 nm.

Since the above results are concentrated on a particular region on the sample, it may approximately suit with other regions. The above porous surface area attributes for better adsorption.

REFERENCES

1. Vennilamani, N., Kadirvelu, K., Sameena, Y. and Pattabhi,S. (2005). 'Utilization of activated carbon prepared from industrial solid waste for the removal of chromium(VI) ions from synthetic solution and industrial effluent', Adsorption Science and Technology, vol. 23, no. 2, pp. 145–160.
2. Trivedy, R. K. (1995). 'Environmental pollution and control', I. Karad, Enviro-media, Maharastra, India.
3. Tchobanoglous G. (1987). 'Aquatic plant systems for wastewater treatment; Engineering considerations. In': Smith W.H., Reddy K.R., editors. Aquatic Plants for Waste Treatment and Resource Recovery. Springer; pp. 27.
4. Kiff, R. S. (1987) "General inorganic effluents: In survey in industrial waste water treatment manufacturing and chemical industries", Vol. 31, Longman, Newyork.
5. Bowers, A. R. and Huang, C. P. (1980). "Progress in water technology", Vol. 12, pp. 629-650, Tata McGraw hill, New Delhi, India.
6. Lalvani, S.B., Wiltowski, T., Hubner, A.H., Weston, A., Mandich, N. (1998). 'Removal of hexavalent chromium and metal cations by a selective and novel carbon adsorbent', Carbon 36 , pp1219–1226.
7. Kobya, M. (2004). 'Removal of Cr(VI) from aqueous solutions by adsorption onto hazelnut shell activated carbon: kinetic and equilibrium studies', Bioresour. Technol. 91, pp 317–321.
8. Sulaymon, A.H., Abid, B.A., Al-Najar, J.A. (2009). 'Removal of lead copper chromium and cobalt ions onto granular activated carbon in batch and fixed-bed adsorbers', Chem. Eng. J. 155, pp 647–653.
9. Gosh, P.K. (2009). 'Hexavalent chromium [Cr(VI)] removal by acid modified waste activated carbons', J. Hazard. Mater. 171, pp 116–122.
10. John Hassler, W.(1974). 'Purification with activated carbon: Industrial Commercial environmental', Chemical Publishing Co., Inc., Newyork.
11. Monser, L., Adhoum, N. (2002). 'Modified activated carbon for the removal of copper, zinc, chromium and cyanid from wastewater', Sep. Purif. Technol. 26, pp 137–146.
12. Trivedy, R. K. (1995). 'Environmental pollution and control', I. Karad, Enviro-media, Maharastra, India.

HEAVY METAL ADSORPTION (Cu) OF FRESH WATER GREEN ALGAE CHARCOAL- ICP OES STUDY

M.Sundarrajan, C.Pari

Department of Physics, Sri ChandrasekharendraSaraswathiViswaMahavidyalaya, Enathur, Kanchipuram 631561, Tamilnadu, India

rajan_sugi@yahoo.com

ABSTRACT

The present study was aimed to study the heavy metal (Copper Cu) adsorption characteristics of charcoal prepared from fresh water green algae. Fresh water green algae samples were collected from 10 locations in and around Kancheepuram district from running water streams like river sides and canal sides. The algae were cleaned, dried and burnt to get charcoal. This charcoal is chosen as adsorbent material and the same is subjected for heavy metal (Cu) adsorption at various concentrations of heavy metal solution. The amount of heavy metal (Cu) ion adsorbed was analyzed by Inductively Coupled Plasma Optical Emission Spectroscopy (ICP-OES) technique and the results are plotted and discussed.

INTRODUCTION

Our environment is continuously polluted by our everyday activities. The industrial smoke, effluents, road side transportation, emission activities and domestic waste discharge are some of the sources that contaminate the environment heavily.The land contaminants go deep to the ground and contaminate the ground water system.The surface water in industrial areas gets more polluted due to the toxic gaseous substances in atmosphere, exhaust from vehicles and factory emissions to atmosphere [(1)].All the above contaminations bring lots of ill effects to all living things of the earth. Among all the organic and inorganic pollutants from various sources, heavy metals are common and are continuously contributing to major levels of pollution in waterbodies [(2)].Metals which have atomic density greater than 4 g/cm^3 or 5 times more than water are grouped as heavy metals. Metals like cadmium (Cd) , chromium (Cr), Nickel (Ni) , Arsenic (As), Manganese (Mn), and lead (Pb) have no nutritious value rather they are carcinogenic and bio-accumulate into toxic level to damage human and animal organs.Water treatment refers to the removal of the pollutants from waste water and makes the water usable for industrial and domestic purposes. The various waste water treatment processes are done by physical, chemical and biological methods [(3)]. The waste water treatment is carried out in various sequences of processes such as primary, secondary and tertiary treatments [(4, 5, and 6)]. The metallic ions can be removed throughvarious processes like precipitation, adsorption,ion exchange, membrane processes, eletrodialysis, and reverseosmosis [(7,8)].Adsorption is a process confined to the surface area of the adsorbent. The material which is being adsorbed is called adsorbate and the one which adsorbs is called adsorbent.

SCOPE OF THE STUDY

To characterize the heavy metal (Cu) adsorption by the fresh water algae charcoal under various initial concentrations of adsorbate solutions.

MATERIALS AND METHODS

Algae are plant-like organisms. They exist without roots, stems, leaves, vascular tissue and with simple reproductive structures. They are found all around in sea, freshwater and wastewater.

Study Area

Fresh water green algae were collected from fresh water regions like running canals and river sides situated in and around Kancheepuram district, Tamilnadu, India.

Sample Collection

Fresh water green algae were collected from running canals and river sides from 10 places in and around Kancheepuram district. The samples were collected using plastic wire mesh. The trapped algae were then washed with distilled water 5 times to remove other impurities. The washed algae were then spreaded in glass plates and dried fully under hot sun in semi air permeable containers.

Sample preparation

The algae were taken in a container with closed lid. The top of the lid is perforated. The closed lid is kept inside a firing pot. The pot is ignited and the algae in lid are allowed to burn in the firing atmosphere. As the flame heats the lid, the algae burn with fumes which are coming through the perforation. The firing pot is flamed until the fumes through the perforation stops. After the lid is taken out from the pot, it is cooled in atmosphere to room temperature. The algae burnt in to charcoal is taken out and ground to fine powder and packed in polyethylene bags.

Adsorption experiment

Heavy metal Copper (Cu) ion solutions (adsorbate – heavy metal ion) were prepared in four different concentrations in glass beakers and named for identification. Equal amounts of charcoal powder (adsorbent) prepared from fresh water green algae were dropped in to these solutions and stirred well. The adsorbent dropped solutions were let undisturbed for 24 hours at room temperature for adsorption process to occur.After 24 hours, the charcoal residue is separated and dried for further analysis.

ICP- OES analysis for heavy metal analysis

The charcoal samples both original and soaked were subjected to ICP –OES analysis at SAIF, IITM, Chennai to calculate the heavy metal content in the charcoal powder after and before adsorption. Initially acid digestion of samples was done using Microwave digestion using Microwave Accelerated Reaction System (MARS). After digestion the samples were subjected ICP-OES analysis.

RESULTS AND DISCUSSION

The concentrations of Cu have been determined for charcoal samples which were subjected to adsorption process under various concentrations of Cu in solution. The initial concentration of Cu in the charcoal sample before adsorption was also determined. The variation of Cu concentration values were recorded and measured elemental concentrations after adsorption is compared with the

value before adsorption and the variation of adsorption of Copper (Cu) with concentration by the charcoal is discussed.

Variation of adsorption of Cu with concentration

The variation of elemental concentration with respect to different concentration of metal solution is shown in figure1.

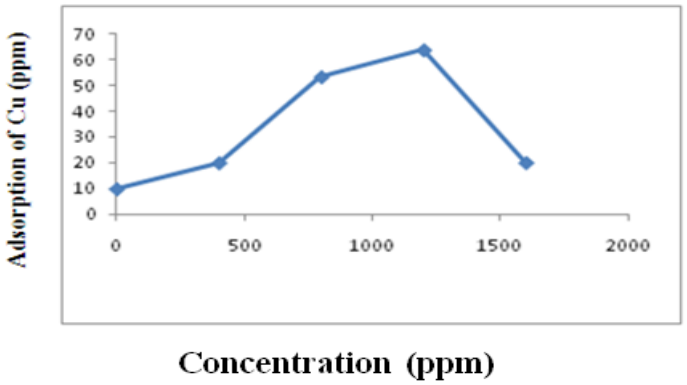

Fig.1Adsorption of Cu at various concentrations

From the fig. 1 it is observed that the Cu adsorption increases with initial concentration of Cu solution and reaches maximum at 1200 ppm. The adsorption for higher initial values of concentration starts decreasing beyond 1200ppm and comes to a minimum at 1600 ppm. The above results may be due to the changes in forces between adsorbent and adsorbate material. Once a layer of adsorbate is formed over the surface of adsorbent, the further adsorption may be affected. Similarly the variation in concentration of adsorbate in solutions may influence the nature and magnitude of force of interactions which are responsible for adsorption processes.

REFERENCES

1. Trivedy, R. K. (1995). 'Environmental pollution and control', I. Karad, Enviro-media, Maharastra, India.
2. Vennilamani, N., Kadirvelu, K., Sameena, Y. and Pattabhi,S. (2005). 'Utilization of activated carbon prepared from industrial solid waste for the removal of chromium(VI) ions from synthetic solution and industrial effluent', Adsorption Science and Technology, vol. 23, no. 2, pp. 145–160.
3. Chakraborti D, Sengupta MK, Rahman MM, Ahamed S, Chowdhury UK, Hossain MA, Mukherjee SC, Pati S, Saha KC, Dutta RN, Quamruzzaman Q. (2004). 'Groundwater arsenic contamination and its health effects in the Ganga-Meghna-Brahmaputra plain', J. Environ. Monitor. 6: pp 74N–83N.
4. Tchobanoglous G. (1987). 'Aquatic plant systems for wastewater treatment; Engineering considerations. In': Smith W.H., Reddy K.R., editors. Aquatic Plants for Waste Treatment and Resource Recovery. Springer; pp. 27.
5. Kiff, R. S. (1987) "General inorganic effluents: In survey in industrial waste water treatment manufacturing and chemical industries", Vol. 31, Longman, Newyork.
6. Bowers, A. R. and Huang, C. P. (1980). "Progress in water technology", Vol. 12, pp. 629-650, Tata McGraw hill, New Delhi, India.
7. Lalvani, S.B., Wiltowski, T., Hubner, A.H., Weston, A., Mandich, N. (1998). 'Removal of hexavalent chromium and metal cations by a selective and novel carbon adsorbent', Carbon 36 , pp1219–1226.
8. Kobya, M. (2004). 'Removal of Cr(VI) from aqueous solutions by adsorption onto hazelnut shell activated carbon: kinetic and equilibrium studies', Bioresour. Technol. 91, pp 317–321.

FLEXIBLE ELECTRONICS TECHNOLOGY- AN OVERVIEW

N. Om Muruga*, D. Sathes Kumar*, A. Balamurugan[§] and S. Dinesh Kumar[§]

**Department of Electronics and Communication Systems, Government Arts College, Udhagamandalam-643002*

[§]Department of Physics, Government Arts College, Udhagamandalam-643002

Abstract

This paper provides an overview of the history, concepts, and possible applications of flexible electronics from the perspectives of materials and fabrication technology. The focus is on large-area capable electronic surfaces. These are made of backplane and front plane optoelectronics that are flexible electronics, and reaches back to rigid-substrate precursor technology.

Introduction to Flexible Electronics

Flexible electronics a s along history. Anything thin is flexible. Forty years ago single-crystalline silicon solar cells were thinned to raise their power/weight ration for use in extraterrestrial satellites. Because these cells were thin , they were flexible and warped like corn flakes. Today, silicon-integrated circuits are thinned to become complaint so that the owner of a smart card does not break it when he sits on it. Flexible can mean many qualities: bendable, conformally shapped , elastic, light weight, no breakable, roll-to-roll manufacturable , or large area. The field has open boundaries that move with its development and application. In this paper we cover a newly emerging segment of flexible electronics that is largely connected with active thin –film transistor(TFT) circuits. Therefore, this survey is representative but incomplete. To the industrial community today, flexible electronic means flexible displays and X-ray sensor arrays.

Materials for Flexible Electronics

A generic large- area electronic structure is composed of (1) a substrate, (2) back-plane electronics, (3) a frontplane, and (4) encapsulation. To make the structure flexible, all components must comply with bending to some degree without losing their function. Two basic approaches have been employed to make flexible electronics(1) transfer and bonding of complete circuits to a flexible substrate and (2) fabrication of the circuits directly on the flexible substrate.

In the transfer-and- bond approach, the whole structure is fabricated by standard methods on a carrier substrate like a Si wafer or a glass plate. Then it is transferred to or fluidic self assembled on a flexible substrate. The transfer –and –bond approach has been extended to the bonding ribbons of Si and GaAs devices to stretched elastomer, which upon relaxation forms a “wavy” semiconductor that can be stretched a and relaxed reversibly. The transfer approaches have advantage of providing high-performance devices on flexible substrates. These process are sophisticated advances over the original flexible wafer-based solar cell arrays. Their drawbacks are small surface area coverage and high cost. Bonded circuits will likely be added to large-area electronic surfaces at low density for high speed communication and computation, lasing, and similarly demanding functions. In many applications, the majority of the surface will be covered with electronics fabricated directly on the

substrate. There are many approaches to integrating disparate materials and often times flexible substrates are not fully compatible with existing planar a silicon fabrication processes.

Substrates

Flexible substrates that are to serve as drop-in replacements for plate glss substrates must meet many requirements.

(i) Optical properties

(ii) Surface roughness

(iii) Thermal and thermo mechanical properties

(iv) Chemical properties

(v) Mechanical properties

(vi) Electrical and magnetic properties

Thin glass

Glass plate are the current standard substrates in flat plane display technology. Plate glass becomes flexible when its thickness is reduced to several 100 μm. Glass foils as thin as 30 μm can be produced by the down draw method.

Plastic film

Polymer foil substrates are highly flexible, can be inexpensive, and permit roil-to-roll processing. However, they are thermally and dimensionally less stable than glass substrates and are easily permeated by oxygen and water. A glass transition temperature Tg , compatible with the device process temperature is essential.

Metal foil

Metal foil substrates less than υ125 μm thick are flexible and are attractive substrates for emissive or reflective displays, which do not need transparent substrates. Stainless steel has been most commonly used in research because of its high resistance to corrosion and process chemicals, and its long record of application in amorphous silicon solar cells. Stainless steel substrates can tolerate process temperature as high 1000˚C , are dimensionally stable, present a perfect permeation barrier against moisture and oxygen , can serve as heat sink, and can provide electromagnetic shielding. Certain magnetic steels lend themselves to magnetic mounting and handling. In general, stainless steel substrates are more durable than plastic and glass foils.

A typical stainless steel foil comes with sharp rolling marks and micrometer-size inclusions, which may cause devices to fail. The most carefully rolled steel has a surface roughness of υ1οοnm , in contrast to display glass with less than 1nm. To ensure the electrical integrity of the thin-film devices made on them, steel foil substrates must be either polised well olr planarized with a film.

Silicon thin film transistors

Silicon-based materials benefit from the advantages of a well-established technology and a native oxide that isz a high-quality insulator. Three approaches can be taken to preparing TFT-grade

silicon on foil substrates: (1) direct deposition of the channel semiconductor, (2) deposition of a precursor film followed by crystallization, and (3) physical transfer of separately fabricated circuits. Techniques (1) and (2) are explored for large-area display applications. Direct deposition can provide the full range of devices, from low OFF current amorphous silicon(a-Si:H) TFTs to CMOS capable TFTs of nanocrystalline silicon (nc-Si-H). The highest ON current is obtained in TFTS of both polarities in polycrystalline silicon (poly-Si) made by the crystallization of an amorphous silicon precursor film.

Organic thin film transistors

The first demonstration of the field effect in a small –molecule organic materials dates back to 1964 . In 1983 , the filed effect in a polymer structure made by a solution proceeds. Since then the performance of organic thin film transistors(OTFTs) as been raised impressively by the introduction of new organic channel materials and by improved fabrication. In the late 1990s, OFTSs with ON currents comparable to those of a Si: TFT were reported. In 2000, pentacene TFTs with a hole field-effect mobility of 3.2 cm2 Vs and an ON/OFF ratio of > 109 were demonstrated . Because in most organic materials the hole mobility is higher than the electron mobility, most OFTTs are p-channel devices. Organic polymers are soluble, and a small molecules can be derivated to soluble precursors. Therefore, OTFTs and circuits have been made on flexible plastic substrate.

Transparent Thin-Film Transistors

TFTs made of transparent materials may not need shielding from visible light to suppress photo conductance, and can raise the pixel aperture of transmissive displays, for example on windscreens of cars. They have been developed from the conventional wide-band gap compound semiconductors. GaN or SiC, and from the transparent oxide semiconductors. ZnO, In_2O_3 and SnO_2. The first flexible transparent TFT was made in 2004 from the amorphous In-Ga-Zn-O system on PET. Saturation mobilities reached 6-9 $cm^2\ V^{-1}s^{-2}$, and device characteristics were stable under mechanical bending. More recently, flexible transparent TFTs have been demonstrated wioth organic channel materials, including a conductive polymer and sinlge-walled carbon nanotubes (SWNT). SWNTs have enabled flexible transparent organic TFTs with mobilities comparable to that of a Si:H TFTs

Growth and Characterization of Pure, L-Lysine doped and L-Leucine doped TGS Crystals

K.Balasubramanian[1*], A.Ponchithra2, T.Karpagam[2], S.Sivapriya[2].
[1] *Department of physics, The M.D.T Hindu college, pettai, Tirunelveli.*
[2] *Research Scholar, Department of physics, The M.D.T Hindu college, pettai, Tirunelveli.*

1. Introduction

Triglycinesulphate (TGS), crystals are expected to play a major role in the fabrication of capacitors, transducers and sensors. It also finds application in burglar alarms, medical visions, Fourier transform infrared (FTIR) instrumentation and in pyro-electric detector. The crystal system for TGS is monoclinic below and above the Curie temperature (49°C). The space group transforms from $P2_1$ the ferroelectric phase to centrosymmetrical $P2_{1/m}$ in the paraelectric phase TGS single crystals can easily be grown from aqueous solutions and exhibit, among ferroelectric materials, one of the best examples of a second order phase transition with order-disorder character. The material is therefore ideal to test a wide range of theoretical predictions on critical phenomena and has been extensively studied in the past.An attempt has been made to grow pure and amino acids doped TGS crystals.The effect of amino acid doping in TGS has been studied extensively. In the case of L-lysine doped TGS dielectric permittivity and spontaneous polarization decrease with improved pyroelectric properties. In addition L-lysine doped TGS crystals possess higher mechanical hardness when compared to pure TGS.

2.Experimental methods

Sample preparation:

Growth of undoped TGS crystal and L-lysine and L-leucine doped TGS crystals were carried out by solution method with slow evaporation technique. The 1 mol % dopants have been incorporated into TGS crystals, and the various studies have been compared with that pure (undoped) TGS crystal. The mother solution of TGS was prepared by dissolving AR grade glycine and sulphuric acid in the molar ratio 3:1. The synthesis of pure and doped TGS salts was explained previously. The synthesized and twice re-crystallized salts of undoped and impurity- doped TGS were used to prepare the saturated solutions separately in accordance with the solubility data. The solutions were constantly stirred for about 2 hours using a magnetic stirrer and were filtered using 4 micro Whatmann filter papers. Then the filtered solutions were taken in borosil beakers (growth vessels). The growth temperature was maintained at 30º C and this temperature was maintained constant by placing the growth period was about 30 days. The photographs of pure, L-lysine doped and L-leucine doped TGS crystals were displayed in the figure 1.

3. Results and discussion

3.1 Solubility Test

The solubility of TGS in various solvent and found that water is the best solvent for crystallization of TGS.to determine the equilibrium concentration, the solution of TGS was prepared. The solubility of TGS increases with increasing temperature as shown in fig1.

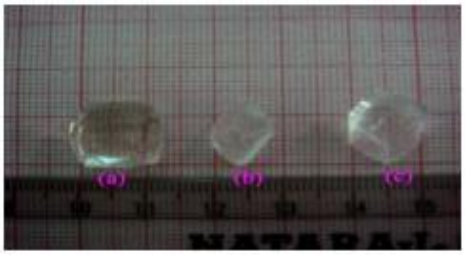

Fig1: Photograph of the (a) Pure, (b) L-Leucine and c) L-lysine doped TGS crystals

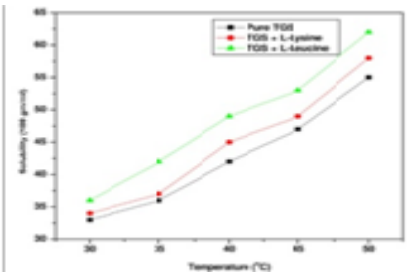

Fig2. Solubility curve of TGS.

3.2. X-Ray Diffraction studies

The effect of amino acids (leucine and lysine) on the structural properties of TGS has been studied by the X-ray powder diffraction analysis. The finely crushed powders of pure and doped crystals were subjected to intense X-ray of wavelength 1.5418 Å (Cu K_α) at a scan speed of 1° min^{-1} with a maximum scan range of 60 ºC. The powder diffraction patterns of Pure and amino acid doped TGS crystals are shown in fig3.

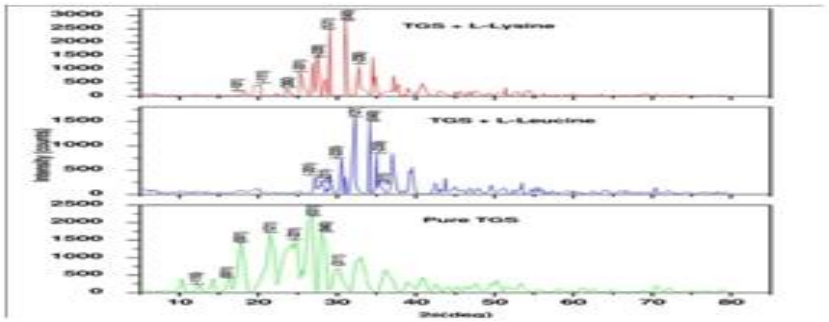

Fig 3. XRD Pattern for pure and doped TGS crystals

The changes in a relative intensity of the peak and their positions confirm the presence of leucine and lysine within the crystal lattice. The lattice parameter values of pure, leucine doped TGS and lysine doped TGS were determined using UNIT CELL software and listed in table and the powder XRD studies were done, Peaks were indexed.

The prominent peaks of pure TGS were (011), (-121), (-221), (031), (040) and (311).
The prominent peaks of L-Lysine doped TGS were (111), (-220), (031), (040), (-230).
The prominent peaks of L-Leucine doped TGS were (111), (-220), (-221), (031).

Table1: Lattice Parameters for pure and doped crystals

Sample Name	a(Å)	b(Å)	C(Å)	Beta(Å)	Cell volume(Å)^3
Pure TGS	9.5203	12.6983	5.7213	110.2020	649.1032
TGS + L-Leucine(1mol%)	11.1849	12.0256	5.4993	100.9852	726.1365
TGS + L-Lysine(1mol%)	10.2521	12.6269	5.7803	94.7180	745.7415

The spectra shows slight changes in peak intensities and peak positions, which may be attribute to strain in lattice. The slight increase in lattice parameter and volume of unit cell of the doped crystals is attributed to the replacement of smaller lattice glycine molecules by larger L-leucine and L-lysine molecules and the lattice could be strained.

3.3. FTIR analysis

The presence of functional groups in the pure TGS and amino acid doped TGS can be confirmed by FTIR analysis. FTIR spectra of pure and doped TGS recorded for a powder samples using KBr pellet technique in the frequency range of 400 – 4000 cm^{-1} are shown in fig4.

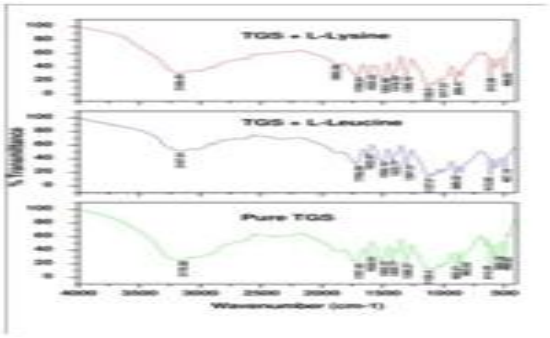

Fig4: FTIR analysis of grown crystals

In the TGS, the NH stretch, OH stretch and aliphatic CH stretch overlaps to each other at a frequency of 3201cm^{-1}. The absorption in the range of 1700-1870cm^{-1} is mainly due to the C=O stretching of the carboxylic acid (COOH) group. The bending mode due to NH_3^+ is clearly seen at 1425, 1503 and 1537 cm^{-1}. The strong absorption in the range 1018 – 1126 cm^{-1} is mainly due to the SO_4^{2-} ion. The peak due to NH^{3+} oscillation occurs at 614,572 and 499cm^{-1}. The peak at 1376cm^{-1} is due to the presence of CH_2 bending. The presence of L-leucine in TGS is confirmed by resolving of NH, OH and CH peaks. Hence it is presumed that the L-leucine molecules would be brought near the NH_3^+ and COOH groups of TGS through its alcoholic OH group. L-lysine doped TGS shows the same effect as L-Leucine doped TGS. There is no major difference in the FTIR spectra of L-leucine doped TGS and L-lysine doped TGS because both are isomers and the presence of dopants (leucine and lysine) in the growth solution with low concentration (1mol %) does not affect much in the FTIR spectrum. If the concentration is high, then the solution becomes unstable. But the presence of low concentration of dopant influences the ferroelectric properties of TGS crystals

3.4. UV- visible-NIR spectroscopy

The UV-visible-NIR spectroscopy was performed on the samples by using UV-1700 SHIMADZU SPECTROPHOTOMETER. The recorded transmittance spectra of pure & doped crystals in the wavelength range 200-1100nm areshown in fig5.

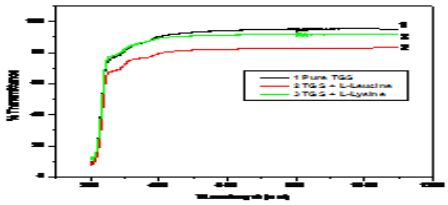

Fig5: UV Transmittance spectra of Pure TGS, L-Lysine doped TGS and L-Leucine doped TGS

This property enables the material for electro-optic application the percentage of transmittance has reduced in the case of doped crystals. The abrupt decrease in transmittance at 228nm corresponds to the fundamental absorption edge and this value is same for both pure and doped TGS crystals. This value obtained in our work is observed to be in good agreement with the literature values using the formula E_g=1240/λ (nm), the band gap is calculated to be 5.51eV.

3.5. Microharness Test

In order to study the mechanical properties, microhardness measurements were carried out on the (100) face of L-lysine and L-leucine doped TGS crystals. At lower loads, hardness is relatively low and it increases for higher loads and remains constant up to a load of 25gm. Above 25gm load significant cracking occurred due to release of internal stress generated locally by indentation. Doped crystals have relatively higher hardness values than pure crystals. Increase in the bond energy with doping is believed to cause the higher hardness values.Selected smooth surface of the cleaved plates of the b-plane was subjected to Vickers hardness measurements. The hardness number was calculated using the relation

$$H_v=1.8544P/d^2 \text{ kg/mm}^2$$

Where, H_v is the Vickers hardness number, P is the applied load and d is the diagonal length of the indentation impression. The load dependence of the microhardness number for pure and doped TGS crystal measured on the b-plane is shown in fig6.

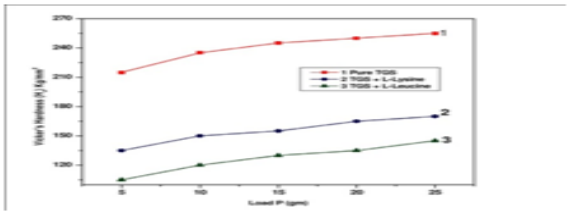

Fig6: Micro hardness for Pure and doped TGS crystals

The hardness of the L-lysine doped TGS crystal was found to be less than that of pure TGS crystal and the hardness of L-leucine doped TGS crystal was much less than L-lysine doped and pure TGS crystal. This is attributed to the incorporation of the doped ions into TGS lattice, which makes the doped crystals loosely bound.

3.6. Dielectric studies

L-lysine doped TGS crystals shows changes in the dielectric properties due to local strain created by the higher dipole moment of L-lysine molecules. Dielectric permittivity measurement was

carried out on the polarizing plane in the temperature range 30 º C-70 º C at a frequency 1 KHz. The temperature dependence of dielectric constant for pure, L-lysine doped and L-leucine doped TGS crystals were illustrated in fig7.

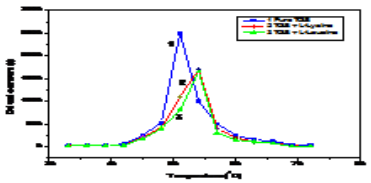

Fig7: Dielectric constant for Pure TGS and doped TGS for various temperatures

The dielectric constant for doped crystals decreases when compared to pure TGS. In the case of pure TGS, Curie temperature (T_c) is 51ºC.The T_c for L-lysine doped and L-leucine doped are 55ºC. Dielectric constant is reduced for doped crystals. The lowering of $\varepsilon_{max}$and shifting of Tc to higher temperatures in the case of doped TGS crystals may be understood in the following way. When a large size molecule goes substantially in TGS lattice replacing some of the glycine molecules, it produces local strains. The decrease of dielectric constant is also attributed to the increasing of dipole moments of the molecules.

2.Conclusions

The pure and L-leucine, L-Lysine doped TGS crystals were grown by slow evaporation method. The size of the grown crystals for pure TGS is 13×12×6mm^3, TGS+Leucine is 13×7×3mm^3 and TGS+Lysine are 9×7×6mm^3. The powder X-ray diffraction confirms the changes in a relative intensity of the peak and their positions due to the presence of leucine and lysine within the crystal lattice.The functional groups and the modes of vibrations were identified by FTIR spectroscopy. From the UV visible spectral analysis of the grown TGS crystals a strong absorption is observed at 228nm for all grown crystals and the forbidden energy gap is5.51eV. The hardness value of doped crystals is less when compared to TGS which confirms that the doped crystals loosely bound. From the dielectric studies,Dielectric constant is reduced for doped crystals.The decrease of dielectric constant is also attributed to the increasing of dipole moments of the molecules.

Reference:

1. Brice, J.C.(1986) Crystal growth process [johnWiley and sons, NewYork].
2. Freeda,T.H (2001) studies on KDP single crystals added with some ammonium compounds[Ph.D. thesis submitted to ManonmaniumSundranar university Tirunelveli]
3. Aggarwal, M.D and LAL, R.B.(1983). Sci.Instrum,54,pp772.
4. Freeda,T.H and Mahadevan,C.(2000)proc.Intlo.Workshop Prep.&Charact.Tech.Imp. Single Crystals,pp350.
5. Mahadevan,C.K. and Meena, M.(2008) Mater.Lett.62,pp3742.
6. JAyakumari,K.(2002)Growth and Characterization of (Nacl)x(kcl)y-x(kbr)l-y single crystals [[Ph.D thesis submitted to ManonmaniumSundranar university Tirunelveli]
7. Jayakumar, K. and Mahadevan,C.(2005)j.phys.Chem.Solids 66,pp1705.
8. Mahadevan,C., MaragathaSelvi ,S. and Vincent Jerin,C.(2005)Indian J.phys.79.pp377.
9. Mahadevan, C.K and Meena ,M(2008) Mater.Lett62,pp3742.
10. Mahadevan,C.K. and padma, C.M.(2007) Mater.Manuf.process.22,pp362.
11. Mahadevan, C.K and priya,M (2008) physica B 403,pp67.
12. Mahadevan, C.K and perumal, S(2005) physica B 369,pp89.

Synthesis and biological activity of Schiff base metal (II) complexes

A. Charles[a,b], P. Aravindan[c], A. Rubas Albert Pitchai[d], P. Saravanan[e], M. Vimalan[f] and K. Sivaraj[g*]

[a]*Department of Chemistry, Thirumalai Engineering College, Kilambi, Kancheepuram.*
[b]*Research and Development Centre, Barathiyar University, Coimbatore.*
[c]*Department of Chemistry, Christian College of Engineering and Technology, Dindigul.*
[d]*Department of Chemistry, SSM institute of Engineering and Technology, Akkaraipatti, Dindigul.*
[e]*Department of Physics, Arignar Anna Government Arts College, Cheyyar.*
[f]*Department of Chemistry, Thirumalai Engineering College, Kilambi, Kancheepuram.*
[*g]*Department of Chemistry, Sri Subramanya College of Engineering and Technology, Palani.*

Abstract

The transition metal complexes of Cu (II) with Schiff base ligand derived from 2-Amino benzaldehyde with primary amine has been synthesized in ethanolic medium for biological activities such as anti-bacterial, anti-fungal, anti-tumour and anti-inflemalory activities. The functional group of the solid complexes are confirmed by FTIR and the biological activity has been also studied. The details of the spectral studies are discussed.

1. INTRODUCTION

Synthesis of new metal complexes of the ligand plays crucial role in chemical, biological and medical field [1]. In recent decades, research in the field of co-ordination chemistry of biological important material which is due to metal complexes play a major role in the chemistry of living matter. On the industrial scale, they have a wide range of application such as dyes and pigments. However its Synthetic Utility and Versatile nature of pharmacological activities it can be prepared by a number of methods usually involving formation of the N - C - N unit as the key step [2]. Significantly, the Schiff base ligands are prepared by the condensation of aldehyde / Ketone using a primary amine. The azomethine (C =N -) linkage present in Schiff base ligand and its metal (II) complexes exhibit a broad range of biocidal activities namely anti – bacterial, antifungal, anti – inflammatory anti cancer, anti – diabetic and antitumor activities [3]. Among all metal ions, Cu (II) is a significant metal due to its versatile use. The obtained data of chemical analysis showed the formation of [M : L] ratio and a square planar geometry was suggested for Copper (II). The importance of Schiff bases with transition metals in the form of co ordination complexes for the successful treatment of various diseases [4]. In this present works are mainly focused on the synthesis and biological activity of Schiff base metal complexes of 2-Amino benzaldehyde and ethylene diamine.

2. EXPERIMENTAL

2.1 General procedure for the synthesis of ligand

All the chemicals were used throughtout the work are of sigma Aldrich, solvents used were ethanol, acetone and double distilled water. Equimolar solution of pure ethylene diamine and 2-Amino benzaldehyde were prepared separately in aqueous ethanol (1:1) and the resulting solution was refluxed with glacial acetic acid for 5h in a RB flask which was cooled with ice water. Desired Schiff

base compounds are obtained by filtration (Scheme 1) and washes several times with water and absolute alcohol. The above 80 % of yield was achieved.

2.2 Syntheris of Schiff base metal (II) compleals

1 mol of the Schiff base ligand was taken in ethenol and stirred gently for 45 minutes to get a homogeneous solution and sample of1 mole of Cu (II) Perchlorate hexahydrate in ethanol is added drop wise and stirred well. The mixture was then refluxed for 5–7 h. The obtained solids were filtered off from the ice – cooled reaction mixture by filtration (Scheme 2). It was washed several times with water and ethanol. The achieved yield was 49.5 %.

Scheme 1

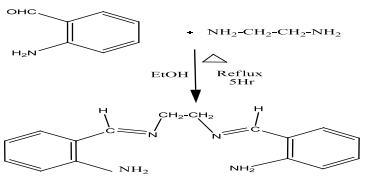

Scheme 2

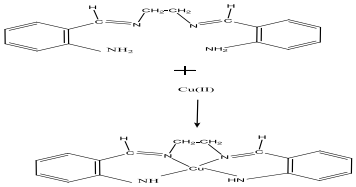

3. RESULTS AND DISCUSSION

FT-IR measurements were taken for the samples in solid state using Perkin-Elmer spectrometer in the range of 400-4000 cm^{-1}. The striking feature common to all the spectrum of the complexes is a broad band at 3350- 3450 cm^{-1}. This band is assigned to –NH stretching frequency. Commonly, the Schiff base complexes contain the characteristic band at 1645 cm^{-1} which is assigned to C=N bond stretches. This band is present in the spectrum of the complexes indicating the presence of this group. The bands due to the vibrations of the aromatic ring are found in the 1450-1600 cm^{-1} region. The other bands fall in the finger print region. When the spectrum of the complexes are examined, it is found that the bands typically indicated to the -NH group is shifted to lower frequencies, A further examination of the infrared spectrum of the copper(II) reveal a peak in the 960 – 980 cm^{-1} region which are used as ligands for the preparation of the complexes. The synthesized compounds were screened for their antibacterial activity using disc diffusion method against four strains of bacteria (Bacillus subtillis and Pseudomonas aeruginosa). According to the antibacterial studies, the efficacy of the compounds against Gram positive bacteria is higher than Gram negative bacteria. Interestingly, the antibacterial activity of their metal complexes is higher than the ligand.

4. CONCLUSION

The Schiff base ligand obtained from the condensation of 2-Amino benzaldehyde and ethylene diamine and its Cu (II) metal complexes have been successfully synthesized. The functional groups of the complexes are confirmed by FTIR spectroscopy. The biological activity study shows that the Cu (II) metal complexes have higher activities compared to the ligand.

References

1.Toggi A.E., Hafez A.M., Wack H., Young B. and Lectka D., J. Am. Chem. Soc., **2002**, 124, 6626-6635.
2. Rodriguez, M. L. L., B. Benhamu, M. J. Morcillo and M. I. Martin., J. Med. Chem., **1999**, 42, 5020-5028.
3. M.S.Habibi., E.Ashari, Synth. React. Inorg. Met. Org. Nano- Met. Chem, **2013**, 43, 406-411.
4. N. Raman, S. Sobha, L. Mitu, J. Saudi Chem.Soc., **2013**, 17(2), 151-159.

Nonlinear Optical and Photoconductivity Studies of L-Leucine Hydrobromide (Lehbr) Single Crystal

I. *Epsy Devakirubai*[a,d], P. Saravanan[b], S. Tamilselvan[b], M. Vimalan[c] and S. M. Ravi Kumar[d*]

[a]*Department of Physics, Voorhees College, Vellore, 632 001.*

[b]*Department of Physics, Arignar Anna Government Arts College, Cheyyar, 604 407.*

[c]*Department of Physics, Thirumalai Engineering College, Kilambi, Kancheepuram, 631 551.*

[*d]*PG and Research Department of Physics, Government Arts College, Tiruvannamalai, 606 603.*

Abstract

Good quality single crystals of L-leucine hydrobromide (LEHBr) of size $10 \times 2 \times 2$ mm^3 were grown by slow evaporation solution growth technique at room temperature. The crystal system and the lattice parameters were analyzed by single crystal X-ray diffraction studies. The SHG efficiency of the grown crystal was found to be 4 times higher than that of KDP crystal. Photoconductivity studies of LEHBr divulged its negative photoconducting nature.

1. INTRODUCTION

There have been significant advances towards the search and synthesize of newer variety of acentric crystalline materials that could produce green/blue laser light. Synthesis of such materials is of great importance from both scientific and technological points of view because of their innovation concerning nonlinear optical (NLO) and electro-optic device applications [1]. Among the various amino acids, L-leucine is the simplest molecule having SHG efficiency of about one-third of the standard KDP material. The importance is due to the fact that amino acids contain chiral carbon atom and crystallize in the noncentrosymmetric space groups; therefore they are potential candidates for optical second harmonic generation. In semiorganic crystals, high optical non linearity of a purely organic ion is combined with the favourable mechanical and thermal properties of an inorganic counter ion [2]. L-leucine hydrobromide (LEHBr) is a semiorganic compound from the amino acid family. Crystals of L-leucine hydrobromide (LEHBr) were first crystallized and structure was solved by Subramanian [3]. In the present investigation, attempt has been made to grow single crystals of L-leucine hydrobromide (LEHBr) by slow evaporation method at room temperature and the characterization studies such as single crystal X-ray diffractometry (XRD), NLO, and photoconductivity. The NLO property of the crystals has been confirmed and second harmonic intensity was measured using Kurtz and Perry powder technique.

2. EXPERIMENTAL PROCEDURE

2.1 Synthesis and Growth of LEHBr

The starting materials for synthesis are of AR grade and used as purchased. L-leucine (Lobachimie) and hydrobromic acid (Merck) are taken in 1:1 stoichiometric ratio. The calculated amount of L-leucine salt is dissolved in deionized water. Then the appropriate amount of HBr is added to the solution. The reaction is as follows,

$$C_6H_{13}NO_2 + HBr \longrightarrow C_6H_{14}NO_2^+ . Br^-$$

In order to purify the synthesized salt it was recrystallized two to three times.

The synthesized salt of LEHBr was purified by repeated crystallization and saturated solution was prepared in accordance with the solubility data. The solution was continuously stirred for few hours and kept for nucleation. Due to the spontaneous nucleation, single crystals of LEHBr with appreciable size were grown in a period of 25– 30 days. In order to achieve single crystals of good optical quality and relatively large size, many growth attempts have been made. The resulting crystals were thin colorless needles. The grown crystals are stable, do not decompose in air and non-hygroscopic in nature. Fig. 1 shows the photograph of the as grown crystals of LEHBr. An important observation during the growth of LEHBr is the absence of any kind of microbial contamination during the growth period even when the solution was kept for nearly 2-3 months. This could be attributed to the high concentration of hydrobromic acid used in the solution.

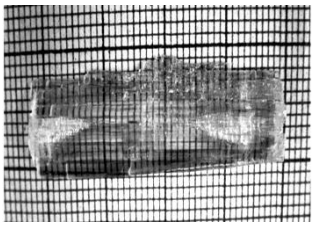

Fig.1 Photograph of as grown single crystal of LEHBr

3. RESULTS AND DISCUSSION

3.1 Single crystal XRD analysis

Single crystal XRD of LEHBr was carried out using ENRAF NONIUS CAD4-F single crystal X-ray diffractometer. The SHG efficiency of the LEHBr crystal was estimated by Nd:YAG Q-switched laser with first harmonic output of 1064 nm. The XRD data reveals that LEHBr crystal belongs to orthorhombic structure with noncentrosymmetric space group of $P2_12_12_1$. The unit cell parameters of LEHBr are given in Table 2. The single crystal X-ray diffraction data of the crystal is in good agreement with the reported values and thus confirming the grown crystal [3].

3.2 NLO studies

Second harmonic generation test was done on the LEHBr sample using Kurtz and Perry (1968) technique. The source used was Q-switched, mode-locked Nd^{3+}:YAG laser emitting 1.06 μm fundamental radiation. The input laser beam was passed through IR reflector and then directed on the microcrystalline powdered sample packed in a capillary tube of diameter 0.154 mm. For the SHG efficiency measurements, microcrystalline material of KDP was used for comparison. When a laser input of 10.8 mJ was passed through LEHBr, second harmonic signal of 210 mV is produced and the experiment confirms a second harmonic efficiency of nearly 4 times that of KDP (53 mV). Thus SHG efficiency of LEHBr sample is comparable with other promising amino acid based NLO crystals.

3.3 Photoconductivity studies

The photo current and dark current of the crystal was recorded using Keithley 485 picoammeter. Photoconductivity study of the LEHBr single crystal was carried out by using Keithly

485 picoammeter. By not allowing any radiation to fall on the sample and by varying the applied field from 60 to 1700 V/cm, the corresponding dark current values shown by the picoammeter were recorded. The sample was then exposed to the radiation from a 100 W halogen lamp containing iodine vapour and tungsten filament. The photo current was recorded for the same range of the applied voltage as done in the case of dark current measurements. The photo current and dark current are plotted as a function of the applied field (Fig. 2). It is observed from the plot that the dark current is always higher than the photo current, hence it is concluded that LEHBr exhibits negative photoconductivity. The Stockmann model also explains the phenomenon of negative photoconductivity successfully with specific references to semiconducting crystals [4].

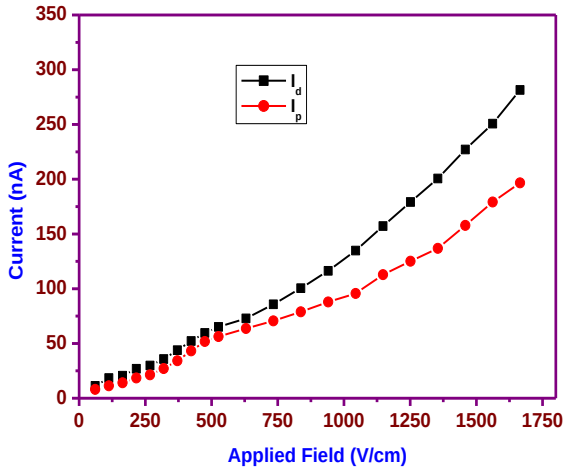

Fig. 2 Field dependent photoconductivity of LEHBr single crystal

CONCLUSION

Single Crystals of L-leucine hydrobromide (LEHBr) are conveniently grown by slow evaporation technique at room temperature. A solvent of deionized water is used for the growth process. The single crystal XRD data proves that LEHBr crystal belongs to orthorhombic in structure with a noncentrosymmetric space group $P2_12_12_1$. The SHG efficiency of LEHBr sample is 4 times better than KDP. The negative photoconducting nature of LEHBr is studied by photoconductivity investigations.

References

1. P. Gunter, (1990), 'Nonlinear Optical Effects and Materials', Springer, Berlin.
2. R. Masse, J. Zyss, J. Mol. Eng. 1 (1991) 141.
3. E. Subramanian, Acta Cryst. 22 (1967) 910–917.
4. V.N. Joshi, Photoconductivity, Marcel Dekker, New York, 1990.

Visible Light Induced Photocatalytic Activity Of Thiourea Doped Tio_2 Nano Particles

M. Ganapathy[a], P. Saravanan[b], M. Vimalan[c], R. Jeyasekaran[d] and I. Vethapotheher[e*]

[a]*Department of Physics, Alpha College of Engineering, Thirumazhisai, Chennai-24.*

[b]*Department of Physics, Arignar Anna Government Arts College, Cheyyar-07.*

[c]*Department of Physics, Thirumalai Engineering College, Kilambi, Kancheepuram-51.*

[d]*Department of Physics, VHNSN College(Autonomous), Virudhunagar-01.*

[*e]*Department of Physics, BIT campus Anna University, Trichy-24.*

Abstract

Carbon, Nitrogen and Sulphur (CNS) tridoped TiO_2 nanoparticles were successfully synthesized by facile, cost effective solvothermal method. The prepared samples were annealed at 430 ^oC for 2 hr to improve the ordering. Grain sizes were determined by X-ray powder diffraction measurements. Optical characterization was done by UV-Vis absorption. The surface area of the doped TiO_2 nanoparticles was done by Brunauer-Emmett-Teller (BET) and found to be 57.0212 m^2/g and 75.0404 m^2/g .The present studies indicates the possible occurrence of nano-confined states in the CNS doped TiO_2 nanoparticles studied.

1. INTRODUCTION

Titania is the naturally found in oxide of titanium from the well known minerals of rutile, anatase and brookite. The need of making Titanium dioxide (TiO_2) nanoparticle from our laboratory for the purpose of solar energy conversion, air purification, and wastewater treatment due to its stability and relatively low price along with its unique properties, such as high refractive index, excellent optical transmittance in the visible and near-infrared regions, high photo-chemical and corrosive resistance, high dielectric constant and photocatalytic activity. Due to wide band gap of TiO_2 (3.2 eV), it requires ultraviolet (UV) irradiation for photocatalytic activation, which available for only a small fraction (about 8%) of the solar energy. To increase the photocatalytic activity of TiO_2 under visible light irradiation, abundant of efforts concerned with shifting of band gap have been focused on doping of the TiO_2 with either transition metallic or nonmetallic elements [1-3]. Doping anions, like N, S, and C alters the conductivity and optical properties as they introduce new surface states that may lie close to the conduction band or valence band of TiO_2. Recent reports have shown that TiO_2 doping with N, C, S, etc., showed high photo catalytic activity under visible light due to band gap narrowing. These applications demand TiO_2 with specifications of a band gap in the visible range. In the present work, a facile, cost-effective solvothermal method was used to synthesize carbon, nitrogen and sulphur doped TiO_2 nanoparticles at two different dopant ratios. Thiourea and urea have often been used as nonmetal ion sources because they can supply sulphur, nitrogen, and carbon [4]. The as prepared doped TiO_2 nanopartilces crystallite size was calculated by Scherer formula using X Ray Diffractogram. Surface area was measured from BET. Band gap narrowing was confirmed by UV-Vis study.

2. EXPERIMENTAL

Analytical Reagent (AR) grade titanium tetra isopropoxide (TTIP), thiourea along with ethanol and water were used for the preparation of CNS doped TiO_2 nanocrystals. Titanium tetra isopropoxide and thiourea in 1:0.5 molecular ratio was mixed and dissolved in mixed solvent of

ethanol and water (1:1).Titanium and water was maintained at 1:4.This mixture was vigorously stirred for an hour to get pale yellowish slurry. Then it was transferred to Teflon coated autoclave with optimized conditions and kept in a muffle furnace at 160^o C for 2 hour. Then it was allowed to cool to the room temperature in open atmosphere and collected as yield. Further it was calcined at 430^o C for 2 h.

3. RESULTS AND DISCUSSION

Several techniques were employed to characterize the sample after drying. X-ray diffraction analysis was done using RICH SEIFER with monochromatic nickel filtered CuK_α (λ=1.5461 Å) radiation to identify the structural and phase composition. Fig. 1 shows the powder XRD pattern of as-prepared CNS doped TiO_2 nanoparticles. The peak positions and their relative intensities in sample are consistent with the standard powder diffraction pattern of TiO_2. All the peaks 2θ = 25.12^o, 25.24^o, 38.04^o, 38.08^o, 48.0^o, 48.28^o, 54.24^o, 54.28^o, 62.54^o and 62.2^o are attributed to (1 0 1), (1 1 2), (2 0 0), (1 0 5) and (2 0 4) crystal planes. The presence of sharp diffraction peaks in the XRD confirms that the products are highly crystalline. The broadening of the peaks was attributed to the nanoscale size of the nanocrystals. The Brunauer-Emmett-Teller (BET) technique was employed to evaluate the specific surface area of the sample by MICROMERITICS ASAP 2020 using nitrogen as the adsorbate at 77 K. The specific surface area of the as prepared CNS doped TiO_2 nanoparticles are estimated to be A_s= 57.0212 m²/g and 75.0404 m²/g. The photon absorption property of the sample in the UV-visible range was recorded using the Shimadzu UV-2400 PC spectrophotometer. The optical behavior of particles can be studied by measuring their UV-vis absorption, in which the characteristic absorption band of CNS doped TiO_2 should be assigned to the intrinsic transition from the valence band (VB) to the conduction band (CB). The absorption spectrum of CNS doped TiO_2 nanoparticle is shown in Fig. 2. It shows that the optical absorbance of pure and CNS doped TiO_2 minimum range starts from 300 -800 nm and 339 -800 nm. The absorption edge of pure and CNS doped TiO_2 nanocrystal was at 400 nm and 445 nm, corresponding to a band gap of 3.1 eV and 2.79 eV, which is usually ascribed to charge-transfer from the valence band to the conduction band.

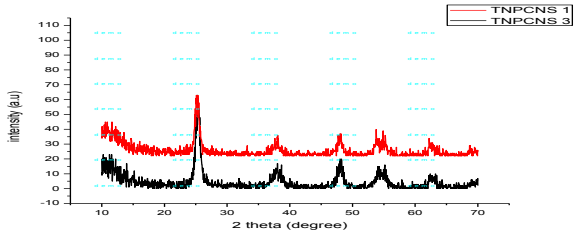

Fig 1. The PXRD pattern for CNS doped TiO2 nanoparticles

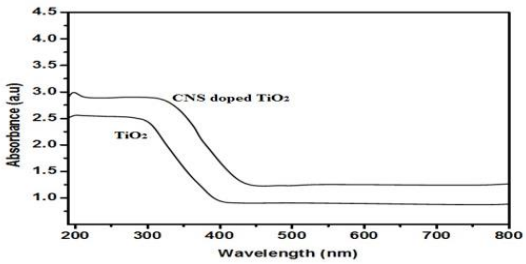

Fig. 2. Optical absorption spectra of CNS doped TiO2 nanoparticles

4. CONCLUSION

We have successfully synthesized CNS tridoped nanoparticles by facile solvothermal method and annealed at 430 ^{o}C. The annealed samples were characterized by the techniques like X Ray Diffractogram (XRD), Brunauer-Emmett-Teller (BET) and UV-Vis absorption. XRD showed that the products are at nanoscale and highly crystalline. Brunauer-Emmett-Teller (BET) study confirmed that the surface area increased when doping ratio is increased. Optical study reveals that the band gap value of as prepared CNS doped TiO_2 samples decreased as compared to undoped TiO_2. It can be suggested that CNS doped TiO_2 can be used for visible light induced photocatalytic activity.

Reference

[1] M.R. Hoffmann, S.T. Martin, W.Y. Choi, D.W. Bahnemann, Chemical Reviews 95(1995) 69–96.

[2] R.W. Matthews, Water Research 24 (1990) 653.

[3] M.A. Fox, M.T. Dulay, Chemical Reviews 93 (1993) 341–357

[4] C. Lettmann, K. Hildenbrand, H. Kisch, W. Macyk, W.F. Maier, Appl. Catal. B: Environ. 32 (2001) 215.

Optical and Mechanical Properties of L-Lysine-L-Tartaric acid (LLLT) Nonlinear Optical Single Crystals

N. Y. Maharani[a,b], I. Vetha Potheher[c], M. Vimalan[d], S. Tamilselvan[e] and A. Cyrac Peter[f*]

[a]*Department of Physics, Gopalan college of Engineering and Mamangement, Bangalore.*
[b]*Research and Development Centre, Barathiyar University, Coimbatore.*
[c]*Department of Physics, Bharathidasan Institute of Technology Campus, Anna University, Trichy.*
[d]*Department of Physics, Thirumalai Engineering College, Kilambi, Kancheepuram.*
[e]*Department of Physics, Arignar Anna Government Arts College, Cheyyar.*
[*f]*Department of Physics, Raja Doraisingam Government Arts College, Sivagangai.*

Abstract

Optically good quality single crystals of amino acid based organic L-lysine-L-tartaric acid (LLLT) have been grown by slow solvent evaporation technique at room temperature. The single crystal X-Ray Diffraction (XRD) study confirms the grown crystal belongs to the noncentrosymmetric space group $P2_1$. Optical transmission studies show that the grown crystal has a fairly wide transparency range which is suitable for nonlinear optical applications and the band gap energy of the sample is found to be 5.39 eV. Normal Indentation Size Effect (ISE) was confirmed from micro hardness studies.

1. INTRODUCTION

Recently, Nonlinear optical (NLO) materials have attracted a great deal of attention because of their potential application in optical devices such as optical switches, optical modulators, electro-optical devices, etc. Recently, amino acids and their complexes belong to the family of organic materials have overcome the most of the drawbacks, which are potential candidate materials for NLO applications [1]. However, the presence of Zwitter ions influences the physical and chemical properties of amino acids. Most of the natural amino acids are permanently having the nonlinear optical properties because they have a proton donor carboxyl acid (COO) group and the proton acceptor amine (NH_2) group with them. Due to this dipolar nature, they possess good mechanical and thermal stabilities, which create them ideal candidates for various NLO applications [2]. Significantly, the NLO property is enhanced in some amino acid materials by combining them with L-tartaric acid. In the present study, organic NLO crystals of L-lysine-L-tartaric acid (LLLT) have been grown from an aqueous solution by the slow solvent evaporation technique and the grown crystals are subjected to single crystal XRD, optical and mechanical studies and reported for the first time.

2. EXPERIMENTAL

2.1. Crystal growth

The LLLT materials were synthesized by dissolving equimolar ratio of high purity amino acid L-lysine-L-tartaric acid with double distilled water as a solvent and stirred well for about 6 hours using a magnetic stirrer at room temperature. The required salt of LLLT was estimated according to the following reaction:

$$C_6H_{14}N_2O_2 + C_4H_5O_6 \rightarrow C_6H_{15}N_2O_2^+C_4H_4O_6^-$$

The saturated solution was prepared based on the solubility data. The solution was filtered using high quality filter paper. Single crystal with perfect external bulky needle shape was obtained

by spontaneous nucleation. Optically good quality single crystal was successfully grown by slow evaporation of the solvent under room temperature in a period of 35 – 40 days. The dimension of the as grown single crystal is 23 x 9 x 4 mm^3. The photograph of the as grown single crystal of LLLT is shown in Fig. 1.

Fig. 1. Photograph of as grown LLLT single crystal

3. RESULTS AND DISCUSSION

3.1. Single crystal X-ray diffraction

In order to confirm the crystal data of LLLT crystals, single crystal X-ray diffraction studies were carried out using Enraf Norius CAD4 diffractometer with MoKα radiation. The lattice parameters of the grown crystal confirmed the crystallinity of LLLT and the calculated values are a = 5.114 Å, b = 17.461 Å, c = 7.553 Å, β = 97.67° and V = 674.45 $Å^3$. It is observed that LLLT crystallizes in Monoclinic with space group of $P2_1$. The single crystal XRD data are in good agreement with the literature values [3] and thus confirming the grown crystal of LLLT.

3.2. Optical studies

Shimadzu UV-1061 UV–Vis spectrophotometer was used to find the optical quality of the grown crystals in the range of wavelength 190–1100 nm. Measurable parameter of the resultant spectrum is transmittance and absorbance which is shown in the Fig. 2. It is observed that the wide optical transmission window occurs from 230-1100 nm without any remarkable absorption in the entire region of the spectrum. The cut off wavelength of LLLT crystal has been identified as 230 nm. The lower cut off wavelength is to be useful to make them potential materials for optoelectronic device applications [4]. The band gap energy of the LLLT crystal is found to be 5.39 eV.

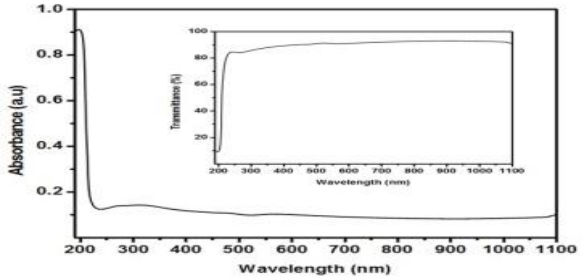

Fig. 2. Optical spectrum of LLLT

3.3. Mechanical study

The mechanical strength of the grown crystal was identified using a Lietz Wetzlar microhardness tester fitted with a Vicker's diamond pyramidal indentor. The static indentation tests were done on the LLLT crystal at room temperature with a constant indentation time of 10 s for all indentations. The applied load was varied from 10 to 50 g. The Vickers's hardness number of the

grown crystal was calculated using the relationship $H_v = 1.8544\ P/d^2\ kg/mm^2$, where H_v is the Vicker's microhardness number, P is the applied load and d is the average diagonal length of the indentation. The variations of H_v for various applied load is shown in Fig. 3. The plot indicates that the microhardness number decreases with increasing load. The decrease in microhardness number with the increase in load satisfies normal indentation size effect (ISE). The value of the work hardening coefficient n was found to be 1.43 from the linear fit plot and it is illustrated in Fig. 4. According to Onitsch [5], the value of n < 2, the fact that LLLT crystal exhibits normal ISE is further confirmed. Therefore, the crystal belongs to the category of hard material which is added advantage for the possibilities towards the device fabrication of the material for NLO applications.

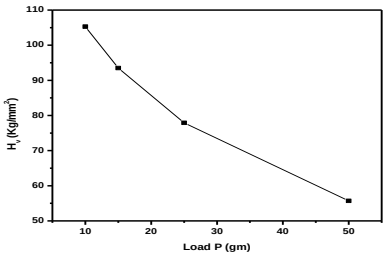

Fig. 3. Vicker's hardness profile of LLLT as a function of applied load

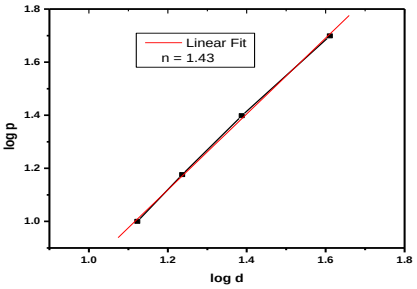

Fig. 4. Mayer index of LLLT single crystal

4. CONCLUSION

Optically good quality single crystals of LLLT are successfully grown by solution growth technique at room temperature. Single crystal structure analysis shows that LLLT crystal belongs to a monoclinic system having space group $P2_1$. The optical studies reveal that the crystal has wide optical transmission window in the entire visible region with the lower UV cut off around 230 nm. Microhardness study exposes the hard nature of the LLLT crystal. Thus, the optical and mechanical properties indicate the suitability of LLLT crystal for photonic device fabrications.

References

[1] G. Ramesh Kumar, S. Gokul Raj, R. Mohan, R. Jayavel, Cryst. Growth. Des. 6, 1308 (2006).
[2] J. Casdo, J. T. Lopez-Navaratee, F. J. Ramirez, J. Raman Spectrosc. 26, 1003 (1995).
[3] S. Debrus, M.K. Marchewka, J. Baran, M. Drozd, R. Czopnik, A. Pietraszko, H. Ratajczak, J. Solid State Chem. 178, 2880 (2005).
[4] P. Anandan, T. Saravanan, S. Vasudevan, R. MohanKumar, R. Jayavel, Journal of Crystal Growth 312, 837 (2010).
[5] E. M. Onitsch, Mikroskopie 95, 12 (1956).

Synthesis and Characterization of Amino Based Organic Nonlinear Optical L-Lysine-L-Aspartic Acid (LLA) Single Crystal

N. Y. Maharani[a,b], I. Vetha Potheher[c], M. Vimalan[d], R. Sathishkumar[e], S. Tamilselvan[e] and A. Cyrac Peter[f*]

[a]*Department of Physics, Gopalan college of Engineering and Mamangement, Bangalore.*
[b]*Research and Development Centre, Barathiyar University, Coimbatore.*
[c]*Department of Physics, Bharathidasan Institute of Technology Campus, Anna University, Trichy.*
[d]*Department of Physics, Thirumalai Engineering College, Kilambi, Kancheepuram.*
[e]*Department of Physics, Arignar Anna Government Arts College, Cheyyar.*
[*f]*Department of Physics, Raja Doraisingam Government Arts College, Sivagangai.*

Abstract

Organic nonlinear optical single crystal of L-Lysine-L-Aspartic acid (LLA) has been successfully grown from solution by slow evaporation technique at room temperature. Single crystal X-ray diffraction (XRD) and Fourier transform infrared (FTIR) spectral analyses are carried out to confirm the LLA crystal. Thermal stability of the crystal is up to 212 °C. Laser damage threshold of the grown crystal was studied. The Kurtz powder second harmonic generation test indicates that the grown crystal is nearly 2 times more efficient than KDP, which is a prospective crystalline material for second order nonlinear optical application.

1. INTRODUCTION

Over the past three decades, Non-Linear Optical (NLO) materials capable of efficient second harmonic generation have been intensely investigated due to commercial importance of these materials in the fields of optical modulation, optical switching, optical logic, frequency shifting, color displays and optical data storage for the developing technologies in telecommunication and in efficient signal processing, sensing and instrumentation. Organic materials have attracted much attention because the NLO responses in this broad class of materials is microscopic in origin, offering an opportunity to use theoretical modeling coupled with extremely synthetic flexibility to design and breed new materials [1]. In this respect amino acids are interesting organic materials for NLO applications. Most of amino acids naturally possess nonlinear optical effect because which contain an asymmetric carbon atom and crystallize in noncentrosymmetric space group. Among these, l-lysine and l-aspartic acid are one of the most promising NLO candidates. For further enhancement of NLO property many efforts have been made on developing l-lysine and l-aspartic acid complexes. However, the combinations of different amino acids have been much less explored. Therefore efforts have been taken to combine amino acids of l-lysine with l-aspartic acid to produce outstanding materials to challenge the existing prospective materials. The crystal structure of L-lysine mixed with l-aspartic acid in the ratio 1:1 has been already reported [2]. On the basis of this, in the present investigation single crystal of L- Lysine- L-Aspartate (LLA) has been grown from its aqueous solution by solvent evaporation method at room temperature. There is no further investigation available to our knowledge in literature. For the first time, the grown crystal is characterized using single crystal X-ray diffraction, thermal and NLO studies.

2. EXPERIMENTAL PROCEDURES

L-lysine aspartate (LLA) was synthesized by dissolving one mole of high purity l-lysine salts in double distilled water containing one mole of maximum quality l-aspartic acid. Since these materials are rich in nutrient, microbes are formed on the surface of the solution when exposed to an open atmosphere thereby inhibiting normal growth of the crystals. In order to prevent microbial contamination, three drops of H_2O_2 were added in the mother solution of LLA.

The chemical reaction is as follows

$$C_6H_{14}N_2O_2 + C_4H_7NO_4 \longrightarrow C_{10}H_{21}N_3O_6$$

Single crystals of LLA are grown from saturated solution of the synthesized salt of LLA using the slow evaporation solution growth technique at room temperature. In order to achieve the crystals with perfect shape and free from defects were formed by spontaneous nucleation in the saturated solution. Optically quality transparent single crystals have been conveniently grown in a period of 40-45 days with dimensions up to 13 x 4 x 3 mm^3. The photograph of grown single crystal of LLA is shown in Fig. 1.

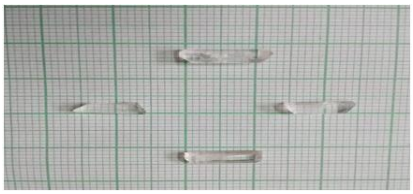

Fig. 1. Photograph of as grown LLA single crystal

3. CHARACTERIZATION

Single crystal X-ray diffraction data were collected by using ENRAF NONIUS CAD4-F single crystal X-ray diffractometer with MoK_α radiation to confirm the cell parameters of LLA single crystal. The SHG efficiency was found by employing Kurtz powder technique with Nd:YAG laser of 1064 nm [3]. The thermal behavior of the grown crystal was investigated using NETZSCH STA 409C AND PERKIN ELMER thermal analyzer in a nitrogen atmosphere.

4. RESULTS AND DISCUSSION

The single crystal XRD analysis data of LLA indicate that LLA crystal belongs to monoclinic structure with a noncentro symmetric space group of $P2_1$ which satisfies one of the basic and essential material requirements for the SHG activity of the crystal. The unit cell parameters values are a = 5.48 Å, b = 7.86 Å, c = 15.29 Å, β = 98.7° and V = 658.58 $Å^3$. The single crystal XRD data determined in the present work for LLA was found to be in good agreement with the reported values [2].

The SHG efficiency of LLA crystals was determined using the powder technique developed by Kurtz and Perry [4]. The second harmonics generation of LLA was confirmed the non-linear nature of the crystal by the emission of green light. Similarly, the potassium dihydrogen phosphate (KDP) was also powdered with the same particle size of the experimental sample to use as the

reference material in the present measurement. The relative SHG efficiency of LLA with that of KDP has been measured. It is observed that the efficiency of the LLA crystal is 115 mV which is two times greater than that of KDP (55 mV). The SHG result is also supporting for further studies. In the present study, the laser damage threshold values of solution grown LLA crystal was also determined by using Q-switched Nd:YAG laser at a wavelength of 1064 nm. The observed damage threshold value of LLA has been found to be 6.3 GW/cm^2.

The TGA and DTA traces are shown in the Fig. 2. There is the absence of the weight loss around 100 °C, which indicates the absence of water of crystallization in the molecular structure. Three stages are observed in the TGA curve. The DTA curve of LLA shows an endothermic peak at 212 °C which can be due to the melting point of the sample. The first stage of decomposition with a weight loss of 18 % from 215 to 292°C in TGA curve is due to liberation of ammonia molecule which almost coincides with an endothermic peak at 212 °C in DTA curve. The second stage takes place in the temperature range 292 to 402 °C with a major weight loss of 32% due to the decomposition of the main carbon chain. An endothermic peak at 284 °C in DTA curve due to the carbon dioxide. The third stage of decomposition with a major weight loss of 40 % is attributed to the release of C_2H_4 in the range of 402- 494 °C which indicates as an endothermic peak at 395 °C in the DTA curve. The LLA crystal is finally decomposed after 495 °C. From the results it is confirmed that the LLA crystal is stable up to 212 °C. The stability of this crystal can be useful property for its possible opto-electronic and NLO application.

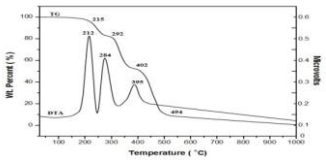

Fig. 2. TGA and DTA curves of LLA

5. CONCLUSION

Successfully, Optical quality single crystals of LLA are grown by solution growth technique at room temperature. Single crystal X-ray diffraction study confirms the crystallinity and the LLA crystal belongs to monoclinic system with space group of $P2_1$. Thermal analysis indicated that the LLA crystal is thermally stable up to 212 °C. The second harmonic conversion efficiency of LLA is 2 times better than KDP and laser damage threshold is found to be about 6.3 GW/cm^2. Therefore, the present LLA crystal can perform as a promising NLO material for opto-electronic and photonic device fabrication.

References

[1] P.N. Prasad, D.J. Williams, Introduction to Nonlinear Optical Effects in Organic Molecules and Polymers, Wiley, New York, 1991.

[2] T. N. Bhat and M. Vijayan, Acta Cryst. B32 (1976) 891.

[3] B. Sridhar, N. Srinivasan and R. K. Rajaram, Acta Cryst. E58 (2002) 1372.

[4] S.K. Kurtz and T.T. Perry, J. Appl. Phys. 39 (1968) 3798.

Green Synthesis and Dielectric Characterization of Tio_2 Nanoparticles

P. Saravanan[a], M. Ganapathy[b], A. Charles[c], S. Tamilselvan[a] and M. Vimalan[d*]

[a]*Department of Physics, Arignar Anna Government Arts College, Cheyyar, 604 407.*

[b]*Department of Physics, Alpha College of Engineering, Thirumazhisai, Chennai, 600 124.*

[c]*Department of Chemistry, Thirumalai Engineering College, Kilambi, Kancheepuram, 631 551.*

[*d]*Department of Physics, Thirumalai Engineering College, Kilambi, Kancheepuram, 631 551.*

Abstract

Titanium dioxide (TiO_2) nano particles are successfully synthesized by the green synthesis with simple solvothermal method using a domestic microwave oven, for the first time, the prepared samples were annealed at 400 ^oC for 3 hr to improve the ordering. Grain sizes and nano particles structure are confirmed by carrying out X-ray powder diffraction measurements. Electrical measurements are done on pelletised samples at various temperatures ranging from 308 K- 368 K. The present study indicates the possible occurrence of nano-confined states in the TiO_2 nano particles studied.

1. Introduction

Nanostructured materials play an important role in the field of electronics, optoelectronics and memory devices. Many researchers have reported on the metal nano particles using different techniques for various device fabrications [1]. Among them, enormous efforts have been devoted to the research of Titanium dioxide (TiO_2) material, which has led to many promising applications. Titanium dioxide (TiO_2) is considered very close to an ideal semiconductor for photocatalysis because of its high stability, low cost and safety toward both humans and the environment. Synthesis of TiO_2 nanostructures may be achieved by various routes including sol–gel methods, template-assisted methods, hydro/solvothermal approaches, and by electrochemical methods. Recently, an eco friendly green mediated synthesis method of nano material is a fast growing research in the limb of nanotechnology. The biosynthesis method employing plant extracts have drawn attention as a simple and viable alternative to chemical procedures physical methods [2]. Therefore, it is necessary to adopt proficient modified methods to enhance the photocatalytic performance of TiO_2, In the present work, TiO_2 nanoparticle have been prepared by using some green synthesis with simple solvothermal methods and characterize the prepared samples, for the first time.

2. Experimental

Fresh plant leaves of *Anisomeles Malabarica* were collected and washed thrice with tap water and double distilled water and kept in the room temperature for air dry. After drying the known amount of leaf samples were grained into fine powder. The powdered *anisomeles malabarica* leaves (3g) were dissolved in distilled water (25 ml) with ethanol (25 ml) and stirred magnetically at room temperature for 1 hr and then filtered.

Analytical Reagent (AR) grade titanium tetra isopropoxide (TTIP) and urea in 1:3 molecular ratio was mixed and dissolved in mixed solvent of ethanol and water (1:1) with continuous stirring at 30 mints until homogeneous solutions were obtained. Then the finely leaf extract of *anisomeles*

malabarica (25ml) was added to precursor solutions and kept in a domestic microwave oven. 2.45 GHz microwave irradiation was carried out till the solvent was evaporated completely. The semi-colloidal precipitate formed was cooled and washed several times with distilled water and then with acetone to remove the organic impurities present, if any. The sample was then dried in open atmosphere and collected as yield. Finally, the resulting fine powder was annealed at 400 ^{o}C done for 2 hr to improve the ordering.

3. Results and Discussion

The X-ray diffraction analysis was done using RICH SEIFER with monochromatic nickel filtered CuK_{α} (λ=1.5461 Å) radiation to identify the structural and phase composition. The grain sizes were determined by using the Scherrer formula [3]. The powder XRD pattern of the green synthesized of TiO_2 nanoparticles are shown in Fig. 1. The peak positions and their relative intensities in sample are consistent with the standard powder diffraction pattern of TiO_2. The peaks are observed in the diffractrogram around at 2θ = 24.95^{o}, 37.44^{o}, 47.70^{o}, 53.60^{o} and 62.41^{o} corresponding planes (1 0 1) (1 1 2) (2 0 0) (1 0 5) and (2 0 4) respectively. These 2θ values could be well indexed to anatase with tetragonal crystal structure (JCPDS no. 21-1272). The products are pure in phases with the calculated lattice constants, a = b = 3.77 Å and c = 9.53 Å. These parameters are in good agreement with the values given in literature [4]. The broadening of TiO_2 peaks is due to the small particle size. The crystallite size of the TiO_2 nanoparticle calculated by applying the Scherrer's equation yielded a value of about 18 nm.

The dielectric measurements were carried out for the pellet of TiO_2 nano particles at different temperatures in the present study using using HIOKI 3532-50 LCR HITESTER instrument from 50 Hz to 5 MHz at different temperatures (308 K- 368 K).

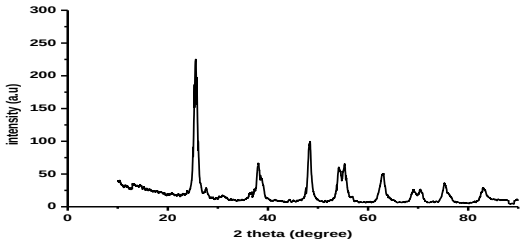

Fig. 1. The PXRD pattern for TiO_2 nano particles

The electrical parameters, viz. ε_r and tanδ observed in the present study are shown in Figs. 2-3. It is seen from the plot that the dielectric constant has high values in the low frequency regions for the TiO_2 nanoparticles and then it decreases with increasing frequency. In high frequency region both dielectric constant and dielectric loss are fairly remaining constant. The high dielectric constant at low frequency is due to the existence of different types of polarization mechanisms like electronic, ionic, orientation and space-charge polarization [5]. The low value observed for ε_r indicates that the polarization mechanism in the nanocrystals considered is mainly due to the space charge polarization.

At high frequencies, the very low dielectric loss exhibited may be associated to the purity of the nanomaterial. So, it can be understood that there seems the occurrence of nano-confined states in the case of TiO_2 nanocrystals considered in the present study which may substantially contribute to the electrical properties.

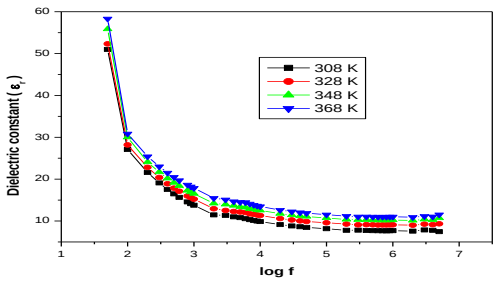

Fig. 2. Variation of dielectric constant with log frequency at different temperatures for TiO_2 nano particles (pelletised)

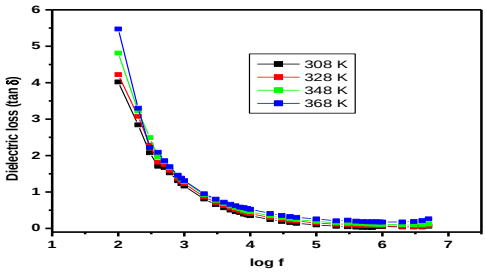

Fig. 3. Variation of dielectric loss with log frequency at different temperatures for TiO_2 nano particles (pelletised)

5. Conclusion

The TiO_2 nano particles were synthesized via a convenient microwave assisted solvothermal with green synthesis method using domestic microwave oven and characterized by PXRD, and electrical measurements. The low value of dielectric constant at higher frequencies is important for the fabrication of materials for ferroelectric, photonic and electronic devices.

References

[1] Jung-Min Kim, Ik-Soo Shin, Seok-Hyun Yoo, Jun-HoJeun, Jihee Lee, Ayoung Kim, Han-Soo Kim, ZiyiGe, Jong-In Hong, Jin Ho Bang, Yong-Sang Kim, Microelectronic Engineering **2012**, 98, 305.

[2] A. Lalitha, R.Subbaiya and P.Ponmurugan, *Int. J. Curr. Microbiol. App. Sci.*, **2013,** 2 (6), 228.

[3] B. D. Cullity, Elements of X-ray diffraction (2nd edn.), Addison Wesley, New York, **1978.**

[4] N. S. Anwar, A. Kassim, H. N. Lim, S. A. Zakarya and N. M. Huang, *Sains Malaysiana.*, **2010,** 39 (2) 261.

[5] D.K. Dwivedi, V. Kumar, M. Dubey, H.P. Pathak, *Chalcogenide Lett.*, **2011,** 8, 521.

Structural, optical and electrical properties of organic stilbazolium family single crystal: 4-N, N-diethylamino-4-N-methyl-stilbazolium tosylate (DEST)

Mohamed Racik, Priya Antony, S. John Sundaram, P. Sagayaraj*
Department of Physics, Loyola College (Autonomous), Chennai -34
psagayaraj@hotmail.com

Abstract

Organic stilbazolium family single crystal 4-N, N-diethylamino-4-N-methyl-stilbazolium tosylate (DEST) has been successfully grown from aqueous methanol solution by adopting slow solvent evaporation technique. Single crystal X-ray diffraction analysis was carried out and it shows that DEST crystal belongs to triclinic structure with P-1 space group. Its absorption spectrum was found by UV-Vis spectrum. Dielectric studies were also carried out for different temperature by varying the frequency.

Keywords: Organic compound; X-ray diffraction; Dielectric

Introduction

The design and synthesis of organic materials for high second order nonlinear optical effect has become an important research area due to their potential and wide applications in the fields of optical signal processing, integrated photonics, optical switching, optical data storage, bioimaging, electro-optic modulation, spectroscopy and THz wave generation and detection. Further, the presence of styryl pyridinium compounds is being mainly used as antibacterial drugs, herbicides, environmental disinfection, disinfection in hospital environments and food industry due to their low toxicity to humans and animals. Hence, the efforts have been made to engineer the novel π-conjugated organic molecules because of their second and third-order nonlinear optical activities. Ionic organic crystals with high chromophore density are of special interest for large NLO effect. The stable packing of chromophores in these crystals results in high thermal, mechanical and photochemical stability. The design of NLO chromophore crystals has an electron withdrawing group that bear an electron donating group interacting through the π-conjugated system with parallel alignment in the crystal structure. The formation of the carbon-carbon bridge (C=C) with π-conjugation chromospheres of an organic molecule can be obtained by Knoevenagel condensation reaction. This method is most favorable and easy method for to form a carbon–carbon double bond. By engineering the organic chromophore many crystals has been grown, among that one such material is 4-N, N-diethylamino-4-N-methyl-stilbazolium tosylate (DEST). This single crystal has been grown by adopting slow evaporation solution growth technique. In this article, we report the Structural, optical and electrical properties of the title compound.

Synthesis and Crystal growth

DEST was synthesised by employing, the condensation of 4-methyl-N-methyl pyridinium tosylate, which was prepared from 4-picoline and methyl tolunesulfonate and 4-N-N-diethylamino-benzaldehyde in the presence of piperidine. The resultant material was kept in an oven, and the temperature was maintained around 100 °C for 1 h. Afterwards, the DEST was purified by successive recrystallization from methanol. In a 250 ml beaker 2g of the DEST was dissolved in methanol. After

getting the homogeneous solution its sealed with appropriated cover and kept in the temperature bath. The growth temperature was maintained at 35 °C. after a period of 10-15 days the crystals were harvested shown in Fig 1.

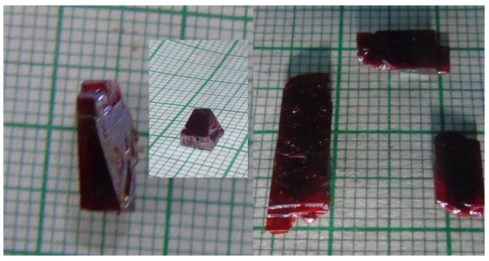

Figure 1 Photograph of DEST crystal

RESULTS AND DISCUSSION

Single crystal X-ray Diffraction analysis

The grown crystal was subjected to single crystal X-ray diffraction studies using Bruker Kappa APEXII single crystal X-ray diffractometer with MoK_{α} radiation (λ = 0.7170 Å) to solve the structure. The calculated lattice parameters of grown DEST crystals are presented in Table. The XRD data indicates that the crystal is t*riclinic* structure and it belongs to centrosymmetric space group P-1.

Table Single XRD data of DEST crystal

Compound	**Parameters**
Formula	$C_{25}H_{30}N_2O_3S$
Formula weight	438.58
Crystal system	triclinic
Space group	P-1
a (Å)	7.88
b (Å)	15.41
c (Å)	17.30
α (deg)	75.54
β (deg)	87.59
γ (deg)	89.75
V ($Å^3$)	2033

Optical absorption spectral analysis

The absorption spectra of the DEST crystal recorded in the solid phase as well as in solution phase (methanol) are shown in Figure 2. It is observed that absorption spectrum of bulk crystalline DEST has a single strong absorbance band below 552 nm; which is due to J-type organization of chromophores within the crystalline structure of DEST. The absorption spectrum of DEST in methanol is different from that of crystalline form which shows two distinct absorption peaks. The minor peak at 271 nm corresponds to the n-π* transition and the major peak with maximum absorption at around 487 nm represents the π-π*. The major absorption peak of the title compound in

the visible region is good agreement with the stilbazolium chromophore with the unsaturated bond. Absence of absorption in the region between 487 and 800 nm for this crystal suggests it is an essential requirement for optoelectronics applications.

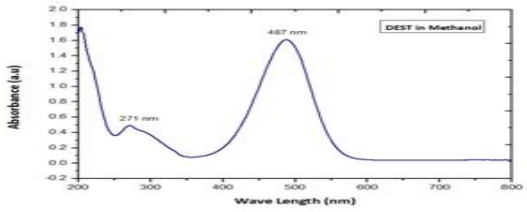

Fig Absorption spectrum of DEST single crystal

Dielectric Studies

Dielectric permittivity measurements were carried out for DEST crystals. The sample was silver coated and then placed inside a dielectric cell and the capacitance measurements were done for temperature at 40, 50, 75, 125 and 150 ^{o}C in the frequency range 50 Hz to 7 MHz. Figure 3 of log dielectric constant ε′ as a function of log frequency and the plot of dielectric loss (D) as a function of log frequency for grown DEST crystals. It is observed that both dielectric constant and dielectric loss exhibits similar variation with frequency. The graphs show that the dielectric constant and the dielectric loss are both inversely proportional to frequency. This is a normal dielectric behaviour that both ε′ and D decrease with increasing frequency. This can be understood on the basis that the mechanism of polarization is similar to that of conduction process. Further, the dielectric constant value of DEST sample is found to increase with increasing temperature. In DEST, as temperature increases it normally becomes more ionic in nature.

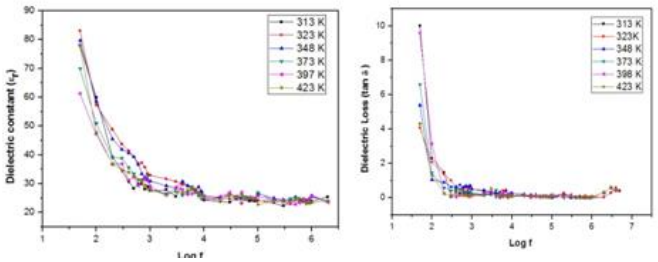

Figure 3 Dielectric constant and Dielectric loss measurement as the function of frequency

Conclusion

Single crystal of DEST has been successfully grown by slow evaporation method. XRD study confirms that DEST belongs to the *triclinic* crystal system with *P-1* space group. The optical properties were measured by UV-Vis spectra. The dielectric studies prove that the sample has low dielectric constant and dielectric loss values at high frequency.

References

1. Narissara Kaewmanee, Kullapa Chanawanno, Suchada Chantrapromma and Hoong-Kun Fun, Acta Cryst. (2010). E66, o2639–o2640.
2. K. Senthil, S. Kalainathan, A. Ruban Kumar, Spectrochimica Acta Part A: Molecular and Biomolecular Spectroscopy 125 (2014) 335–344.
3. R. Jerald Vijay, N. Melikechi, Tina Thomas, R. Gunaseelan, M. Antony Arockiaraj, P. Sagayaraj, Mater. Chem. Phys. 132 (2012) 610-617.
4. K. Senthil, S. Kalainathan, A. Ruban Kumar, Spectrochimica Acta Part A: Molecular and Biomolecular Spectroscopy 124 (2014) 603–610.
5. Jerald V. Ramaclus, Tina Thomas, S. Ramesh, P. Sagayaraj, E. A. Michael, CrystEngComm 16 (2014) 6889-6895.

Growth, Optical and Electrical Properties of DASC Single Crystal Grown By Adopting Capillary Rise Technique

S. John Sundaram[a], A. Antony Raj[a], Dominique[b], P.Sagayaraj[a*]
[a]*Department of Physics, Loyola College, Chennai – 34*
[b]*Department of Physics, St. Joseph's college, Trichy - 02*
psagayaraj@hotmail.com

Introduction

Terahertz (THz) technology has entered into an unprecedented revolutionary era with ever growing applications in biology and medicine, monitoring and spectroscopy in pharmaceutical industry and science, medical imaging, material spectroscopy and sensing, security, and high-data-rate communications. High power and reliable THz sources and high performance THz spectroscopy and imaging systems have been developed over the past few years making it possible to explore new areas in science and technology (Sherwin 2002). Organic non-centrosymmetric nonlinear optical (NLO) crystals are attractive due to their superior NLO properties when compared to semiconductors and inorganic materials. THz spectrometers based on popular ionic organic crystal, 4-N,N-dimethylamino-4-methyl-stilbazolium tosylate (DAST) is now available commercially. Since DAST has few issues like hydration and undesired crystal morphology led to the development of derivatives of DAST with similar structure. So research has been initiated and observed that a minor modification of substituents on the counter anion can considerably change the crystal structure and SHG activity of stilbazolium salts. By this various derivatives of DAST have been synthesized, among them; N,N-dimethylamino-N'-methylstilbazolium p-chlorobenzenesulfonate (DASC) is the one which has high NLO and which is not get hydrated. We have grown thin plate like crystal by capillarity method coupled with slow solvent evaporation method and its structural, optical and electrical properties has been investigated.

Synthesis & Crystal growth

DASC was prepared by metathesization of the 4-N,N-dimethylamino-N'-methylstilbazolium iodide (DMSI) salt with sodium p-chlorobenzenesulfonate. DMSI was synthesized by the condensation of 1,4-dimethyl pyridinium iodide (2.35 g, 10 mmol), methanol (30 ml) and 4-N, N-dimethylamino-benzaldehyde (1.79 g, 10 mmol) in the presence of piperidine (0.2 ml). The total mixture was taken in a round-bottom flask and refluxed for 12 hours and cooled to room temperature. The product was filtered and recrystallized from methanol at least three times. .

The metathesizaton reaction was carried out as follows: Initially, 0.732 g (2 mmol) of DMSI was dissolved in 100 ml of distilled water by heating and simultaneously 0.4292 g (2 mmol) of sodium p-chlorobenzenesulfonate was dissolved in 30 ml of water with continued heating. These two hot solutions were mixed and further heated for 30 minutes at 70° C and then cooled to room temperature. The reaction resulted in the appearance of a red precipitate and the left out aqueous sodium iodide was separated from the former by vacuum filtration. The purity of DASC was further improved by successive recrystallization.

The crystal growth of DASC was a challenge since it dissolved well in various solvents but did not yield single crystal. It was speculated in this case that mixed solvent may provide a solution to this problem. Crystal growth was performed by employing Capillarity method combined with slow solvent evaporation technique. The solution was prepared with 3.35 g of DASC dissolved in 150 ml of mixed solvent of water and methanol (1:1) at 40^{o} C. After a period of time the thin plate like crystals were grown and its showed in the figure 1.

Figure 1 The photograph of DASC crystal

Results& Discussions

Single crystal X-ray diffraction analysis

The crystallographic structure of DASC was determined via single X-ray diffraction analysis using a Bruker Kappa APEX II diffractometer. The structure was determined from the single crystal XRD, it is found that DASC single crystal belongs to *Monoclinic* Crystal system, with the space group Cc. The unit cell parameters are a = 10.395Å, b = 11.201Å, c = 17.86 Å, $\alpha = 90^{o}$, $\beta = 92.06^{o}$, $\gamma = 90^{o}$, Volume of 2081$Å^3$ and it well matched with the reported data.

Optical absorption analysis

Figure 2 shows the absorption spectrum of DASC recorded in solid phase between the wavelength region 200 to2100 nm. Since the DASC crystal is iso-structural to DAST one may not expect much deviation in the optical absorption property. DASC indicates strong absorption upto 700 nm, it correlating with the charge transfer process. This crystal is very transparent in higher wave lengths but at 1700 nm weak absorption observed for DASC crystal which is most probablydue to the overtones of the C-H stretching vibrations. This crystal shows weak absorption at 700-1600 nm which makes the DASC is the potential crystal for NLO applications.

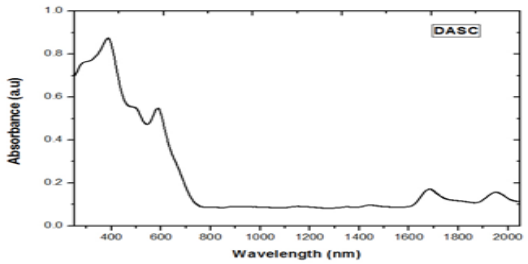

Figure 2 UV absorption spectrum of DASC crystal

Photoconductivity study

The variations of both photo current (I_{ph}) and dark current (I_d) with applied field are shown in Figure 3. It is seen from the plot that both the photo and darks current of the DASC increase linearly with the applied electric field. In the present study, it is observed that the photo current is higher than the dark current at all the applied field values, hence it can be concluded that DASC exhibits positive photoconductivity. This phenomenon can be attributed to the generation of mobile charge carriers caused by the absorption of photons.

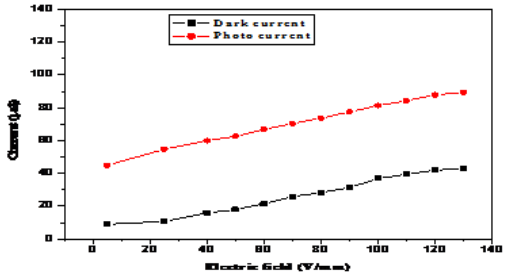

Figure 3 conductivity measurement of DASC crystal

CONCLUSION

An efficient stilbazolium derivative crystal of DASC was successfully grown by Caplillary rise combined with slow evaporation technique. The single crystal X-ray diffraction analysis confirmed the noncentrosymmetric space group and the *monoclinic* structure. The optical absorption property was found for the developed material. The photoconductivity of the crystal was measured and it's found that this DASC crystal exhibit positive photoconductivity.

References

1. Jerald Vijay R., Melikechi N., RajeshKumar T., Joe G.M. Jesudurai and Sagayaraj P., Journal of Crystal Growth, 312, (2010), 420-425.
2. Brahadeeswaran S., Onduka S., Takagi M., Takahashi Y., Adachi H., Kamimura T., Yoshimura M., Mori Y., Yoshida K and Sasaki T., Crystal Growth and Design, 6, (2006), 2463-2468.
3. Jerald Vijay R., Melikechi N., Tina Thomas., Gunaseelan R., Antony Arockiaraj M., and Sagayaraj P., Material chemistry and physics, 132, (2012), 610-617.
4. Z. Sun, X. Liu, X. Wang, L. Li, X. Shi, S. Li, C. Ji, J. Luo, M. Hong, Cryst. Growth Des. 12 (2012) 6181-6187.
5. R. Gunaseelan, A. Antony Raj, P. Sagayaraj, Optik 125 (2014) 3791-3797.
6. Jerald Vijay R., Melikechi N., Tina Thomas., Gunaseelan R., Antony Arockiaraj M., and Sagayaraj P., 338, (2012), 170-176.

Investigation on the Synthesis, Growth and Properties of a Novel Organic Nonlinear Optical Crystal: L-Threonine Diacetate (LTDA)

G. Viju [a,b], R. Uthrakumar [c], C. Inmozhi*[d]

[a] *Department of Physics, DMI College of Engineering, Chennai-600 123. India*

[b] *Department of Physics Periyar University (P.Ex), Salem-636 011 India*

c Department of Physics Govt. Arts College(Autonomous), Salem-636 007 India

[d]**Department of Physics Govt. Arts College for Women, Salem-636 008 India*

**Corresponding author mail: cvesta19@yahoo.com*

Abstract

L-threonine Diacetate (LTDA), a novel organic nonlinear optical crystal has been synthesized and grown by slow evaporation technique. The grown crystals were subjected to powder X-ray diffraction studies. Functional groups present in the material were identified by FT IR spectral analysis. Absorption spectrum shows that the crystal is found to be transparent in the visible region. Thermal analysis was performed to study the thermal stability of the crystal. The SHG efficiency of the grown crystal was confirmed by Kurtz–Perry powder technique.

1. Introduction

Nonlinear optics is at the forefront of current research because of its importance in providing the key functions of frequency shifting, optical modulation, optical switching, optical logic, and optical memory for the promising technologies in areas such as telecommunications, signal processing, and optical interconnections [1, 2]. The properties of organic compounds relevant to non linear optics can be refined using molecular engineering and chemical synthesis [3]. The main advantages of organic materials are that their structure can be modified to get the desired NLO properties [4]. Moreover, it has been demonstrated that organic crystals have large nonlinear susceptibilities compared with inorganic crystals. Particularly, amino acid family crystals are of great interest due to their attractive nonlinear optical properties [5]. When the organic acid mixed with amino acid, NLO property has been increased due to the zwitter ionic nature and high transparency range [6]. Our present work reports the growth of L-threonine Diacetate by slow evaporation technique and the grown crystals have been subjected to X-ray diffraction, Fourier transform infrared spectral analysis, optical absorption, thermal and second harmonic generation efficiency studies.

2. Experimental

2.1 Synthesis and Growth

The L-threonine Diacetate (LTDA) was synthesized from L-threonine and acetic acid in the stoichiometric ratio of 1:2. The calculated amount of L-threonine and acetic acid were dissolved in a mixed solvent of acetone and water. The reactants were stirred well for two hours using a temperature-controlled magnetic stirrer to yield a homogenous mixture of the solution. The product was re-crystallized twice to remove the impurities. The transparent crystals were harvested in a period of 15 days. The photograph of the grown crystals is shown in Fig.1.

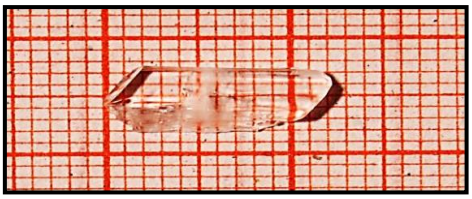

Fig.1. As-grown crystals of LTDA

3. Results and Discussion

3.1, Single crystal X-ray diffraction

Single X- ray diffraction studies of LTDA were carried out using CADENTRAF NONIUS X- ray diffractometer with MoK_{α} (λ = 0.7107 Å). The Crystal belongs to monoclinic system. The cell parameters are a=5.1447Å, b=13.6104Å, c=7.745Å, and volume V =542.3224Å^3.

3.2 Powder X- ray diffraction

Powder X-ray diffraction analysis has been carried out using Rich Seifert X-ray diffractometer with CuKa (λ = 1.5418Å) line radiation and the recorded XRD pattern is shown in Fig.2. The X– ray diffraction peaks were indexed for the lattice parameters. The prominent peaks in the powder X-ray diffraction confirm the crystalline nature of the grown crystals. The peak corresponding to (011) has maximum intensity per second.

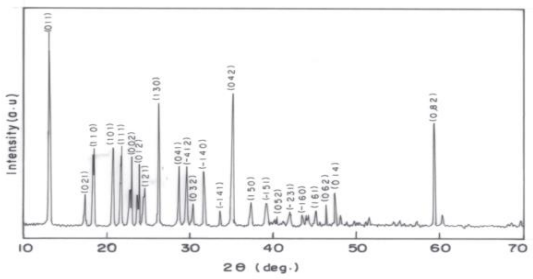

Fig. 2. X-ray diffraction pattern of LTDA

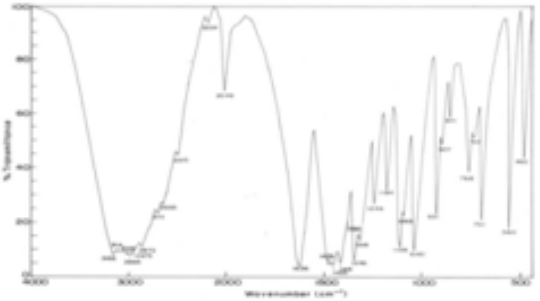

Fig.3. FTIR Spectrum of BDP

3.3 FTIR Analysis

The FTIR Analysis of LTDA crystal was recorded using BRUKER IFS 66V model spectrophotometer by KBr pellet method in the wave number range from 4000 to 500 cm^{-1} and the recorded spectrum is shown in Fig.3. The peak at 3116 cm^{-1} is assigned to N–H symmetric stretching vibration. The C–H symmetric stretching is observed at 2873 cm^{-1}. The C-N stretching vibration appears as a very sharp peak at 2049 cm^{-1}. The peak at 1626 cm^{-1} is assigned to N-H bending. The peaks at 1346 cm^{-1}, 1246 cm^{-1}, 1184 cm^{-1} 1109 cm^{-1} and 1049 cm^{-1} are attributed to C-N stretching. The peak at 931cm^{-1}, 871 cm^{-1} and 768 cm^{-1} corresponds to C-H bending. The peak at 701 cm^{-1} corresponds to N-H wagging. The C-N out of plane bending appears at 560cm^{-1}.

3.4. UV-Vis-NIR absorption spectrum

The UV-vis-NIR studies at room temperature in the wavelength range from 200 to 1000 nm using a Shimadzu UV–vis spectrophotometer and the recorded spectrum is shown in Fig4. From the

absorption spectrum, it was found that the lower cut-off wavelength is 340 nm. The crystal is found to be transparent in the region of 400–800 nm which is an essential parameter for frequency doubling applications [7].

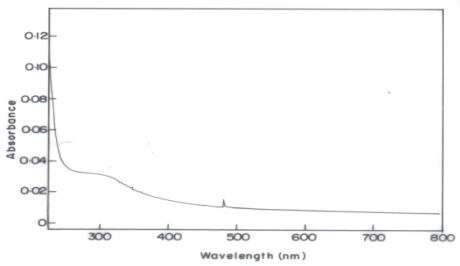

Fig.4.UV-Vis- Spectrum of LTDA

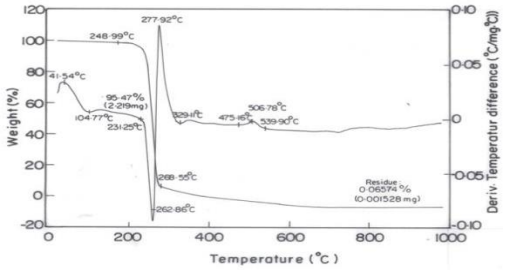

Fig.5. TGA of LTDA

3.5. Thermal behavior

The thermal behavior of LTDA was studied using ZETZSCH – Geratebau GmbH thermal analyzer and the thermogram is shown in Fig.5. TGA graph shows that there is a sharp weight loss at 264.37ºC. It was observed that the material is thermally stable upto 248.99º C.

3.6 NLO studies

The NLO property of the powder sample was confirmed by the Kurtz and Perry powder technique [8]. A Q-switched Nd-YAG laser beam of wavelength 1064 nm was used with an input power of 2.0 mJ and pulse width of 10 ns, the repetition rate being 10 Hz. The SHG behavior is confirmed from the output of the laser beam having the bright green emission (λ=532 nm) from the crystal. The SHG relative efficiency of L-threonine Diacetate crystal was found to be 0.85 times higher than that of KDP.

4. CONCLUSION

Single crystal of L-threonine Diacetate was synthesized and grown by slow evaporation technique. The X-ray diffraction studies reveal that the crystal belongs to monoclinic system. FTIR spectroscopic studies were used to identify the functional groups present in the compound. Absorption spectrum shows lower cut off at 340 nm. Thermal behavior shows that the material is thermally stable up to 248.9º C. The SHG efficiency of the powdered sample of the crystal is 0.85 times higher than that of KDP.

References

[1] Z.G. Hu, N. Ushiyama, Y.K. Yap, M. Yoshimura, Y. Mori, T. Sasaki, J. Cryst. Growth, 237 (2002) 654.

[2] P.N. Prasad, D.J. Williams, Introduction to Nonlinear Optical Effects in Organic Molecules and Polymers, Wiley, New York 1991.

[3] G. De Matos, V. Venkataraman, E. Nogueria, , M. Belsley, P. A. Criado, M. J. Dianez, E. Perez Garrido, Synth. Metals , 115 (2000) 225-228.

[4] J. Zyss, J.F. Nicoud, M. Coquillay, J. Chem. Phys. 81 (1984) 4160.

[5] M. Kitazawa, R. Higuchi, M. Takahsshi, Appl. Phys. Lett. 64 (1994) 2477.

[6] M.N. Bhat, S.M. Dharmaprakas, J. Cryst. Growth 236 (2002) 379.

[7] C. Justin Raj, S. Jerome Das ,J.Cryst Growth, 304 (2007) 191–195.

[8] S.K. Kurtz, T.T. Perry, A powder technique for the evaluation of nonlinear optical materials, J. Appl. Phys. 39 (1968) 3798.

Investigation of Silver Substituted Cobalt Ferrite Nanoparticles

A.PersisAmaliya, S.Blessi and Dr.S.Pauline
Department of Physics,Loyola college, Chennai

Abstract

In the recent years new medical diagnostics and therapeutics are enabled by nanoscience. In particular, magnetic nanoparticles or composites of nano cobalt ferrite with silver is of considerable interest. This study focuses the effects of silver substitution on the structure of as prepared cobalt ferrite nanoparticles by sol-gel method. Formation of nanoparticles was confirmed by x-ray powder diffraction (XRD) and Fourier Transform Infrared Spectroscopy (FTIR) analysis. Surface morphology was analyzed by Scanning electron microscopy (SEM) technique. Magnetic behavior to determine the various magnetic parameters of the as prepared sample were investigated by Vibrating Sample Magnetometer (VSM).

1. Introduction

Nanosized ferrites have been studied for decades because of their wide range of applications in medicine and industries. Ferrite based materials which are biocompatible plays a remarkable role as MRI contrast agent, drug carrier, cell labeling, cell tracking,..,etc. In the present study cobalt ferrite, a member of spinel group is substituted with silver, the antibacterial agent for medical application. There are various reports on the substitution of divalent, trivalent and tetravalent cations in Cobalt ferrite. Transition metal is substituted as it was found that they enhance antibacterial property [1]. Among them there are only a few research works on substitution by silver. M. Kooti et al synthesized silver-coated cobalt ferrite nanocomposite and studied its antibacterial activity. The antibacterial activity of Ag@CoFe2O4 composite against almost all tested bacteria is slightly higher than that of AgNPs. Ag@CoFe2O4 composite compared with AgNPs possesses an extra advantage of easy removal from water by using a magnetic field to avoid contamination of surroundings [2]. Sheena Xavier et al synthesized Silver Substituted Cobalt Ferrite Nanoparticles**.** The antibacterial activity of the nanocomposite materials was investigated against selected Gram negative and Gram positive bacterial strains. An enhancement in the activity is observed with the addition of silver into cobalt ferrite nanoparticles [3]. The biomedical and clinical applications of silver nanoparticles are well established in the literature [4-6]. Okasha et al. [7] studied the effect of silver substitution in magnesium ferrite and observed an enhancement in its thermal and electrical conductivity. Sun et al. [8] have shown that the biological activity of Fe3O4 nanoparticle was improved by coating a thin film of silver onto it and the magnetic properties were helpful in the recovery of the material from the site of action. The aim of the present work is to provide a ferrite material with good magnetic behaviour and enhanced antimicrobial activity.

2. Synthesis procedure

The silver substituted $CoFe_2O_4$ nanoparticles were synthesized by one pot sol-gel route using silver nitrate, cobalt nitrate and ferric nitrate precursors. Typically cobalt nitrate, ferric nitrate and silver nitrate were taken in the mole ratio 0.05:0:95:2. Required quantity of ethylene glycol (EG) was

added and stirred to get clear solution. This solution was transferred to pettri dish and heated at 60º-80ºC. The obtained gel was transferred to a silica crucible and heated for 2 hours at 200ºC. The resulting powder was calcined for 3 hours at 600ºC and fine black powder was obtained.

3. Results and discussion

3.1 XRD analysis

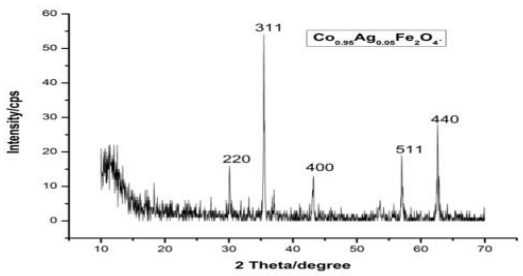

Fig. 1. XRD pattern of $Co_{0.95}Ag_{0.05}Fe_2O_4$.

The XRD pattern of silver substituted $CoFe_2O_4$ nanoparticles is shown in figure.1. Typical reflections from the planes (220), (311), (400), (511) and (440) are observed [JCPDS No:22-1086] and no extra peak is observed. The sharpness of XRD peaks reveals good crystallinity of the sample [9]. The particle size calculated from the prominent peak by Scherrer's equation is 39 nm. Lattice parameter of as prepared cubic spinel structured nanoparticles is found to be a=b=c=8.387 Å which is greater than that of pure cobalt ferrite.

3.2 FTIR

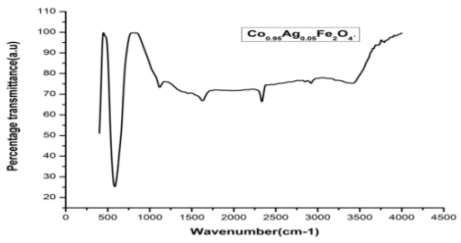

Fig. 2.FTIR pattern of $Co_{0.95}Ag_{0.05}Fe_2O_4$.

FTIR pattern in figure 2 shows the absorption bands near 400 $cm^{-1}$and at 584 cm^{-1}which are attributed to the vibrations in both tetrahedral (A) and octahedral (B) coordination of the spinel structure respectively[10]. The absorption band at 1121 is due to C-O bending vibration [11,12]. The bands at 1394-1595 $cm^{-1}$are assigned to C-O stretching vibration. Bands at 2916-2352 cm^{-1} are assigned to asymmetric and symmetric stretching of CH_2 groups. The band at 3418 cm^{-1} is assigned to asymmetric and symmetric vibration of hydroxyl group.

3.3. SEM

SEM picture of the sample shows the formation of nanosized particles mixed with bulk counterparts. If the calcination temperature is reduced there might be reduction in the grain growth

into the bulk form. EDAX spectrum confirms the proportionate distribution of the elements Fe, Co, O and Ag.

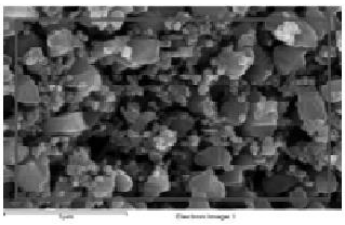

Fig.3.(a) SEM Image

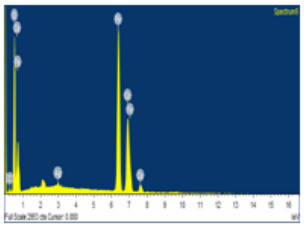

(b) EDAX spectrum

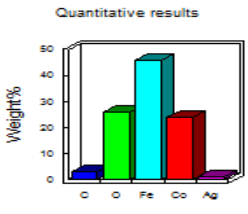

(c) Weight % diagram of $Co_{0.95}Ag_{0.05}Fe_2O_4$

3.4 VSM

Using vibration sample magnetometer, the hysteresis loop was taken for the sample at room temperature and is shown in figure 4. The magnetic properties of as synthesized silver substituted nanoparticles were studied. Saturation magnetization (Ms) observed for the sample is 19.82 emu/g, remnant magnetization (Mr) is 9.72 emu/g and coercivity (Hci) is about 1802 G.

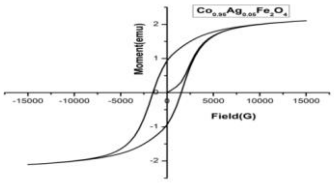

Figure 4. Hysteresis loop of silver substituted cobalt ferrite

Conclusion

Silver substituted cobalt ferrite nano particles were synthesized by sol-gel method. The sample was subjected to XRD, FTIR, SEM and VSM analysis. XRD confirms the spinel structure with no distortion upon silver substitution. There are no additional absorption peak (be it even of low intensity) seen in the FTIR spectra thereby confirming the fact that silver has gone as a substituent. SEM shows the presence of nanoparticles. Also flakes are seen. The EDAX spectrum brings out the right proportion of the elements in the spinel structure. VSM brings out a drastic decrease in all three magnetic parameters when compared to the bulk counterpart.

References

[1] NoppakunSanpo, Cuie Wen, Christopher C. Berndt and James Wang, Microbial pathogens and strategies for combating them: science, technology and education (A. Méndez-Vilas, Ed.)
[2] M. Kooti ,S.Saiahi , H.Motamedi Journal of Magnetism and Magnetic Materials 333 (2013) 138–143.
[3]Sheena Xavier, Harry Cleetus, Nimila PJ, SmithaThankachan, Rintu Mary Sebastian and Mohammed EM,Research Journal of Pharmaceutical, Biological and Chemical Sciences.
[4] Gao M, Sun L, Wang Z, Zhao Y. Mater SciEngg C 2013; 33: 397 – 404.
[5] Sondi I, Sondi BS. J Coll Inter Sci 2014; 275: 177 – 182.
[6] Das R, Gang S, Nath SS. J BiomaterNanobiotechnol 2011; 2: (472 – 475).
[7] Okasha N. J Mater Sci 2008; 43: 4192 – 4197.
[8] Sun S, Zeng H, Robinson DB, Raoux S, Rice PM, Wang SX. J Am Ceram Soc 2004; 126: 273 – 279.
[9] Z.H. Zhou, J.M. Xue, J.Wang, H.SO.Chan, T.Yu, Z.X. Shen, J. Appl.Phy.91(2002) 6015.
[10] M. Kooti, S. Saiahi, H. Motamedi, Journal of Magnetism and Magnetic Materials 333 (2013) 138–143
[11] P.Balakrishnan, P.Veluchamy, International Journal of ChemTech Research, Vol.8, No.1, pp271-276, 2015.

Synthesis and Structural Studies of Fe_2CoSn Heusler Alloy Nanoparticles for Spintronics Applications

V. Asvini[1], G. Saravanan[2], R.K.Kalaiezhily[3] and K. Ravichandran*[4]

[1,2,3,4] *Department of Nuclear Physics, University of Madras, Chennai 600 025, India*

**E-Mail of the corresponding author: ravi21068@unom.ac.in*

Abstract

Fe_2CoSn inverse heusler alloy nanoparticles were synthesized by co-precipitation method. The as-prepared sample was annealed at various temperatures (700°C, 750°C, 800°C, 850°C, and 900°C) in N_2 atmosphere. The structural properties of Fe_2CoSn heusler alloy nanoparticles were analyzed by using powder X-ray diffraction techniques. The structure of the Fe_2CoSn heusler alloy nanoparticles was found to be XA disorder structure. The Fe_2CoSn heusler alloy is zero gaps at the Fermi level of the spin gapless semiconductor in the electronic structure. The grain size increases due to the annealing temperature increases. The Fe_2CoSn heusler alloy nanoparticles, average grain size was found to be 28 nm. Dislocation density was calculated and obtained the value of 6.86 X $10^{15}m^{-2}$ for 700°C annealed sample.

Key words: Heusler alloy, SGSs, dislocation density.

Introduction

Heusler compounds are multifunctional magnetic materials have been studied extensively due to potential spintronics device applications. Half-metallic ferromagnet is the behavior of the majority spin band of metallic behavior and minority spin band structure of the semiconductor behavior [1]. The stoichiometric ratio formulas X_2YZ is full-Heusler alloys are usually X and Y compounds by using transition metals and Z is the main group elements. The half heusler alloy compounds are used XYZ formula is an atom are occupied and the inverse heusler alloy structure formula XY_2Z is an atom are occupied [2]. Fe-based heusler alloy compounds have been high saturation magnetization, high Curie temperature and low coercivity. Fe-based heusler alloy compounds are mostly spin gapless semiconducting electronic structure in nature [3]. The spin gapless semiconducting are novel materials that combine of the ternary and quaternary heusler alloys on the half–metallic ferromagnetic behaviors. Spin gapless semiconductors with a zero gap at the Fermi energy level in one of the spin channels can make electrons easy to exit from the valence band to the conduction band with 100% spin polarization [4]. The Fe-based Heusler compounds predicted to possess a large magnetization and high Curie temperature for potential magnetic memory device applications. The Fe_2CoSn Heusler alloy has attracted our attention because it was predicted to have a considerably large magnetic moment and inexpensive.

Experimental method

The Fe_2CoSn Heusler nanoparticles were synthesized using the chemical method. The precursors used here are $FeCl_2.4H_2O$ (99%), $CoCl_2.6H_2O$ (99%) and $SnCl_2.2H_2O$ (99.9%). Stoichiometries proportions are taken and dispersed in 300 ml of methanol with sonication treatment for 30 min further with methanol removal using a rotary evaporator. The obtained from the precipitate solid sample is completely dry at 80°C for 3 hours and further the solid sample is gently ground to

fine powder. Later the samples are taken in proportional weight for a further annealing process under N_2 atmosphere at various temperatures for 5 hrs to obtain a heusler phase and stability. Samples are cooled and collected for characterization for structural studies and magnetic properties. The Fe_2CoSn nanoparticles heusler alloy for structural details was performed using powder x-ray diffraction pattern. The structural details were observed dislocation density and number of crystallites per unit surface area to be Fe_2CoSn heusler alloy nanoparticles.

Results and Discussion

Figure1.shows the XRD patterns of the Fe_2CoSn heusler alloy nanoparticles. The diffraction intensity peaks value in 2θ = 29.57°, 34.64°, 36.27°, 42.21°, 44.21°, 52.48°, 55.81°, 61.23°, and 72.48° and corresponding diffraction planes (1 1 1), (2 2 0), (3 1 0), (2 0 2), (3 2 1), (1 1 3), (2 2 2), (0 0 4) and (2 0 4) respectively. The obtained reflection planes were confirms that body centered cubic structure. The structure of the Fe_2CoSn heusler alloy nanoparticles was found to be XA disorder structure. The grain size increases due to increasing the annealing temperature. The grain size was only dependence on dislocation density. The grain size was calculated by using Debye-Scherrer equation.

$$D=\frac{0.9\,\lambda}{\beta\,cos\theta} \qquad ; \qquad \delta=\frac{1}{D}$$

The grain size was inversely proportional to the dislocation density with respect to the various annealing temperature. The dislocation density average value $3.51x10^{15}m^{-2}$ was obtained from measurement.

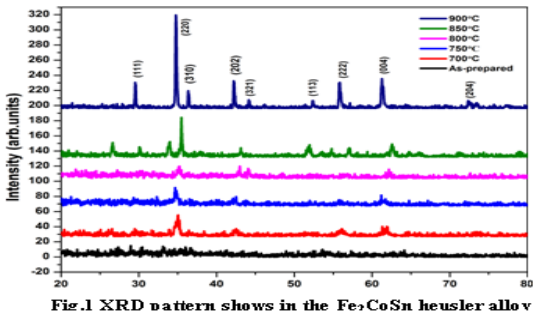

Fig.1 XRD pattern shows in the Fe_2CoSn heusler alloy

The Fe_2CoSn heusler alloy nanoparticles of the space group ($F\bar{4}3m$) for inverse heusler alloy structure. The grain size is high value was observed in the 900°C annealing temperature of the N_2 gas atmosphere. The lattice constant of the Fe_2CoSn inverse heusler alloy nanoparticles at 5.465Å. Fig.1 shown at the peak (310) in 2θ = 35.05° value is shifted due to the annealing temperature are increasing.

Conclusion

Fe_2CoSn inverse heusler alloy nanoparticles of the synthesis by chemical root method. The studies were observed in highest grain size of the 58nm and the dislocation density was inversely proportional to the grain size of the low value at $0.29x10^{15}m^{-2}$ for 900°C annealing temperature. The obtained structure was well crystalline nature due to increasing the annealing temperature. The

Fe_2CoSn heusler alloy nanoparticles of the zero-gap at the Fermi level structure and for a large magnetic moment can possible to use Spintronics device applications.

Acknowledgments

Thanks to Mr B. Nagarajan, XRD - technical officer helped me to do XRD measurements using XRD-instrumental facility in the department of Nuclear Physics, University of Madras, Guindy Campus, Chennai-25, Tamilnadu.

Reference

[1] W. Zhu, E. K. Liu, C. Z. Zhang, Y. B. Qin, H. Z. Luo, W. H. Wang, Z. W. Du, J. Q. Li, and G. H. Wu, *Acta Phys. Sin.* 61 (2011) 027502.

[2] Ayuela, J. Enkovaara, K. Ullakko, and R. M. Nieminen, *J. Phys.: Condens. Matter* 11 (1999) 2017.

[3] T. Gasi. A. K. Nayak, M. Nicklas, and C. Felser, *J. Appl. Phys.* 113 (2013) 17E301.

[4] M. Zhang, E. Brück, F. R. de Boer, and G. Wu, *J. Magn. Magn. Mater.* 283 (2004) 409.

GROWTH, SYNTHESIS AND CHARACTERIZATION OF NONLINEAR OPTICAL L-HISTIDINE CADMIUM BROMIDE CRYSTAL (LHCB)

T. Kubendiran and S.M. Ravikumar*

PG & Research Dept. of Physics, Govt. Arts College, Tiruvannamalai-606603

Corresponding author: smravi78@rediffmail.com

Abstract

L-Histidine cadmium bromide crystals are grown from solution growth by slow evaporation method. It has been successfully synthesized. The variation functional groups are presented in the grown sample has been identified by Fourier Transform Infrared Spectroscopy (FTIR). The transmitted spectrum reveals that the transparency and cutoff wavelength was measured by UV-VISIBLE-NIR spectrum. The dielectric measurements for the crystals were performed for various frequencies and temperature. Photoconductivity nature of the crystal was identified by photoconductivity studies.

1 INTRODUCTION

Nonlinear optical materials have attracted much attention because of their potential applications in emerging optoelectronic technology [1,2]. In this respect, amino acids and their salts belong to a family of organic material that have wider NLO applications [3,4]. The importance of amino acids for NLO applications lies on the fact that almost all amino acids contain as asymmetric carbon atom and crystallize in non-centro symmetric space group. These applications depends upon the various properties of the materials, such as transparency, bifriengence, refractive index, dielectric constant, thermal, photochemical and chemical stability. Organic crystals have large nonlinear susceptibilities compared to inorganic crystals. In last several years, considerable interest in growth and characterization of non linear optical materials (NLO) due to their important contribution in areas of optical modulation, OSptical switching, optical logic, optical data storage and frequency. Several attempts have been made for exploration of nonlinear optical materials which found various applications in optoelectronics[5-10]. In recent years, researchers put their attention to find Out semi organic family crystals using amino acids with inorganic or metal complexes for improving their quality and properties [11]. For the metallic port, the focus is on group II B metals (Cd,Zn and Hg) as the compound formed by such metals usually have a high transparency in the UV-Vis region because of their closed shell [12]. In this present study, the synthesis, growth and physical properties of non-linear optical crystal has been discussed.

2. EXPERIMENTAL PROCEDURE

2.1. SYNTHESIS

LHCB crystal is synthesized by dissolving AR grade L-Histidine and AR grade cadmium bromite in the equimolar ratio 1:1 in distilled water. The saturated solution of Cadmium bromide was slowly added to the saturated solution of L-Histidine. This was stirred well to get a clear solution. Pure LHCB crystal was synthesized according to the reaction.

$$C_6H_9N_3O_2 + CdBr_2 \rightarrow Cd\,[C_6H_9N_3O_2]Br_2$$

2.2. GROWTH OF L-HISTIDINE CADMIUM BROMIDE

The saturated solution of LHCB was prepared in double distilled water solvent at room temperature. The solution stirred well for more than 8 hours using magnetic stirrer to obtain a homogenous mixture. The saturated solution was filtered using ashless whatman filter paper. The filtered solution was taken in a beaker and covered with good quality perforated polythene cover to restrict the fast evaporation it is kept at room temperature in a dust free compartment for slow evaporation. After the period of 40-45 days, colorless crystals with dimension 8mm×3mm×2mm were obtained and. The crystal is non-hygroscopic and optically transparent. After a span of 45days, well-faced good quality crystals of LHCB were harvested and shown in the figure 1.

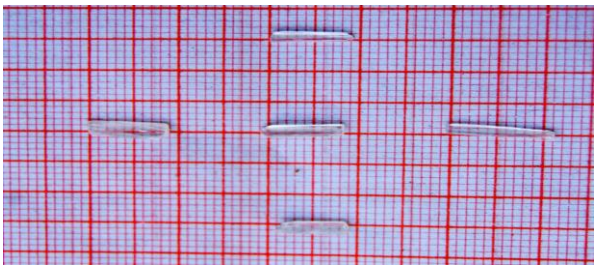

Figure 1.. photograph of LHCB crystal

3. CHARACTERISATION

FTIR spectra of LHCB were recorded using a bruker IFS66 FTIR spectrometer at room temperature in the range 400-3500cm^{-1} by KBr pellet method. To confirm the non-linear optical property, Kurtz and perry powder SHG test was carried out of the grown crystal using Nd:YAG laser with the first harmonics output at 1064 nm. The dielectric constant and dielectric loss wave carried out by using HIOKI model 3532-50 LCR HITESTER. The photoconducting nature of the grown sample was investigated by PICO AMMETER (Keithley 485).

3.1. FOURIER TRANSFORM INFRARED SPECTROMETER (FTIR)

The FTIR spectroscopy studies are effectively used to identify the functions groups presents in the crystal and to determine the molecular structure. In order to analyze qualitatively the presence of functional groups in LHCB. The FTIR spectrum was using thermo Nicolect V-200 FTIR spectrometer by KBr pellet method in the range 400-3500 cm^{-1} as shown in figure 2. It is clearly seen that the existence of COOH is illustrated by the very strong infrared bond located at 1611.57 cm^{-1}. The facts that some of the COOH groups are ionized implicates an appearance of the NH_3^+ group in histidine molecule. The strong shoulder at 1634 cm^{-1} and very strong bond at 1611 cm^{-1} in the infrared spectrum are attributed to stretching vibration of NH_3^+ group. The peak at 1420 cm^{-1} is due to symmetry type of stretching vibration. The peak value of IR spectrum at 1142 cm^{-1} is C-O stretching vibration. The peak obtained at 1111.70 cm^{-1} is also C-O stretching vibration. A peak at 910 cm^{-1}is represent the C-H deformation and mono substituted group. The peak at 834 cm^{-1} C-H

deformation is tri substituted and 707 cm^{-1} .is C-H deformation also di substituted group. The C-Br stretching vibration get in 623 cm^{-1}

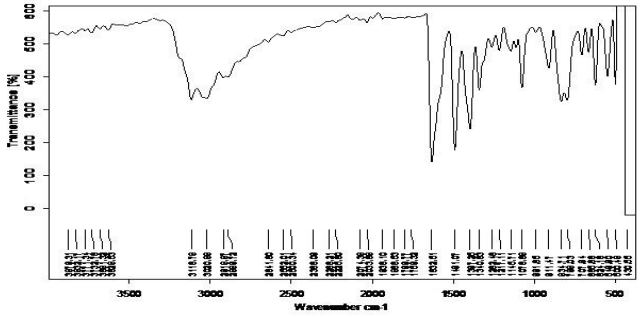

Figure 2. FTIR Spectrum of LHCB crystal

Table 2: Bonds assignments of FTIR spectra of LHCB

Wavelength (cm^{-1})	**Assignment**
3119,3015	N-H stretching
1634,1580	C=C stretching
1611	N=O stretching
1492,1420,1396	C-H deformation
1340,1217,1077	C-O stretching
910,834	C-H deformation
623,548	C-Br stretching

3.2. NLO TEST

Powder SHG test offers possibility of assessing the non-linearity of new materials. Kurtz-perry powder second harmonic generation (SHG) measurements was carried out using a spectra-physics quanta-ray prolab 170 Nd:YAG laser with the first harmonics input at 1064nm and a pulse width of 10ns at repetition rate of 10Hz. The second harmonic signal generated by the compound was confirmed by emission of green radiation and the powder SHG efficiency of LHCB was found to be comparable to that of Potassium Dihydrogen Phosphate (KDP). The SHG behavior was confirmed from the emission of bright green radiation (532nm) by the sample show that the SHG efficiency of LHCB is 3.62 mJ which is comparable with SHG efficiency output of known KDP of 8.8mJ.

3.3. Dielectric study

Figures 3 and 4 show the variation of dielectric constant and dielectric loss of LHCB crystal at different temperatures ranging from 308 to 408 K, as a function of frequency. At low frequencies, the dielectric constant is found to be maximum and then it decreases with increasing frequency. Dielectric constant and loss increases slowly with temperatures as shown in Figures 3 and 4. In high frequency region both dielectric constant and dielectric loss are fairly remaining constant. The high dielectric

constant at low frequency is due to the presence of all types of polarizations viz., electronic, ionic, orientation, space charge polarization, etc. The space charge polarization will depend on the purity and perfection of the sample. Its influence is large at high temperature and is noticeable in the low frequency region. The larger values of Dielectric constant and loss at lower frequencies may be attributed to space charge polarization due to charged lattice defects.

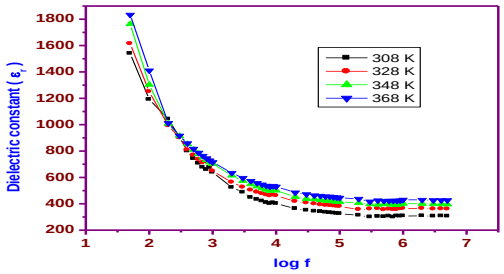

.**Figure. 3 Variation of dielectric constant with log frequency at different temperatures for LHCB single crystal**

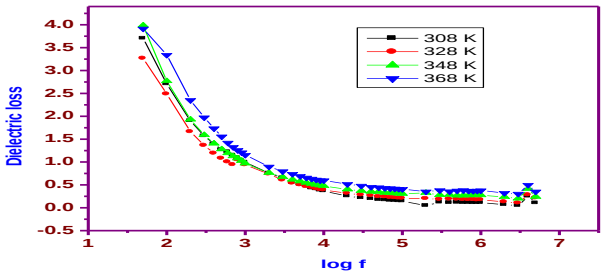

Figure. 4 Variation of dielectric loss with log frequency at different temperatures for LHCB single crystal

3.4. Photoconductivity study

Field dependence of dark and photo currents of LHCB crystal is shown in Figure 5. It is observed that both dark and photo currents of LHCB single crystal increase linearly with the applied voltage. The dark current of the crystal is more than the photo currents which is termed as negative photo conductivity.The negative photo conductivity exhibited by the sample may be due to the reduction in the number of charge carriers in the presence of radiation.

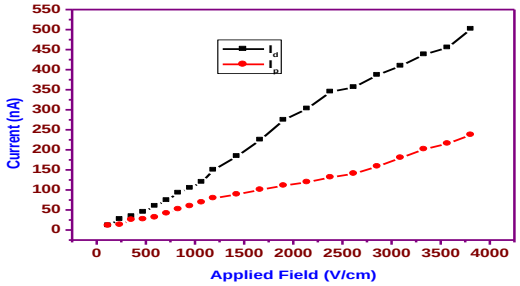

Figure. 5 Field dependent photoconductivity of LHCB single crystal

Conclusion

Single crystal of LHCB, an semiorganic NLO crystal has been grown by slow evaporation method. FTIR analysis confirms the presence of all the functional groups in grown crystal. The nonlinear optical study confirms the SHG property of the material. The dielectric property of LHCB crystal has been analysed which indicates that the sample has higher dielectric constant at lower frequency and attain saturated with increasing frequency. The grown crystal has negative photoconduvity nature.

References

1. Cheng L.K., Bosenberg W. and Tang C.L. (1990), 'Growth and characterization of nonlinear optical crystals suitable for frequency conversion', Prog. Crystal Growth and Charact, Vol. 20, pp. 9-57.
2. Giordmaine J.A. (1962), 'Mixing of light beams in crystals', Phys. Rev. Lett., Vol. 8, pp. 19-20.
3. Chemla D.S. and Zyss J. (1987), 'Nonlinear optical properties of organic molecules and crystals', Vol.1-2, Academic Press, Orlando, New York.
4. Nalwa H.S. and Miyata S. (1996), 'Nonlinear Optics of Organic Molecules and Polymers', CRC Press Inc., New York.
5. Davydov B. L., Kotovschikov S.G., Nefedov V.A. (1977), 'New nonlinear optical materials for second harmonic generation of neodymium laser radiation', Soviet J. Quantum Electron. Vol.7, pp.129-131.
6. Newman P.R, Warren L.F., Cunningham P., Chang T.Y., Copper D.E., Burdge G.L., Polak dingels P. and Lowe-Ma C.K. (1990), 'Semi Organics, a new class of NLO materials', in "Advanced Organic Solid State materials", Ed. Chiang C.Y., Chaikan P.M. and Cowan D.O., Materials Research Society Symposium Proceedings, Vol. 173, pp. 557-561.
7. Velsko S.P. (1990), Laser Program Annual Report, Lawrence UCRL-JC 105000 (Lawrence Livermore National Laboratory, Livermore, California).
8. Kurtz S.K. and Perry T.T. (1968), 'A Powder technique for the evaluation of nonlinear optical materials', J. Appl. Phys., Vol. 39, pp. 3798–38l3.
9. Kurtz S.K. (1968), 'New nonlinear optical materials,' IEEE, J. Quantum Electron, Vol. 4, pp. 578–584.
10. Shaw M.C. (1973), 'The Science of Hardness Testing and its Research Application', Ed. By Westbrook J.H. and Condrad H, ASM. Ohio, pp. 1-11.
11. Westbrook J.H and Conrad H. (1971), 'The Science of Hardness testing and its Research
12. Applications', American Society for Metals, Ohio.

Photonic Crystal Displacement Sensor

P.Ramadoss and R.Tamilselvi

PG & Research Department of Physics, Government Arts College,Tiruvannamalai-606603

ABSTRACT

Photonic crystal sensors have recently drawn much attention due to their inherent compactness and high sensitivity .Different types of photonic crystal sensors rely on one main transduction mechanism perturbations in environmental condition alter index of refraction or periodicity of the structure which is transferred to detectable change in optical power or spectrum. This transduction mechanism facilitates utilization of photonic crystal for sensor applications ranging from pressure and displacement measurement to detection of chemical composition change and binding events. Here we discuss the theory, modeling of photonic crystal fiber, its advantages and also its limitations of technology.

INTRODUCTION

The photonic crystal fiber sensors are a class of optical fibers. It has a large potential for sensing applications. This type of novel structure with a lattice of air holes running along the length of the fibers. It offers the wave guiding properties are highly controlled, but it's not possible with conventional optical fibers. In this work, we have proposed a variety of novel photonic crystal fiber designs for replacing conventional optical fiber to improve the efficiency and accuracy when compared with other different types of interferometric methods.

REFERACTIVE FIBER OPTIC DISPLACEMENT SENSOR: MEASUREMENT OF

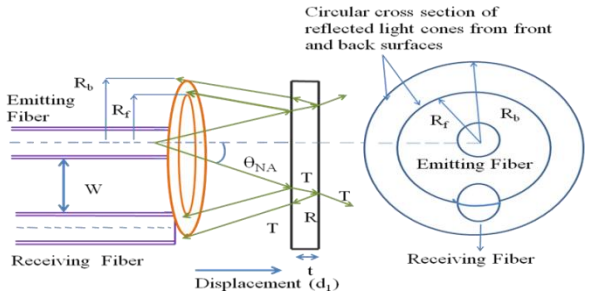

Fig.1.3 Reflective fiber optic displacement sensor for thickness measurement and cross sectional view.

THICKNESS

In Fig.1.1, ' W ' is a separation between the fibers and ' r_e ' and ' r_r ' are emitting fiber radii, respectively. ' S ' is the distance between the fiber core centers.

The output of the sensor is given by the efficiency power factor as

$$\eta(2d,n_0)=\frac{p_0(2d,n_0)}{p_i}=2\int_{R_1}^{R_2}\int_0^{\phi_c}R_m T_i(n_0)T_0(r,2d,n_0)\frac{2}{\pi R^2(d)}\left(1-\frac{r^2}{R^2(d)}\right)rd\phi dr \quad (1.1)$$

The power factor $\eta(2d,n_0)$ is defined as the ratio between the light power captured in the receiving fiber $P_0(2d,n_0)$ and the total power P_i launched into the emitting fiber. $T_i(n_0)$ and $T_0(r,2d,n_0)$ are Fresnel transmittance coefficients and 'n_0' is the refractive index of air medium. 'ϕ' is the azimuth angle.

' R_m' is the mirror reflectivity and ϕ_c is the azimuth angle at maximum overlap position

$$\phi_c = \cos^{-1}(s^2 + r^2{}_e - r^2 / 2r^2{}_e s) \quad (1.2)$$

where ' r ' is the distance from the emitting fiber axis.

The radiated power P_i is expressed with the intensity distribution I(r, 2d) which is considered as parabolic, on the plane surface at a distance 2d from the fiber end by the following equation:

$$p_i = 2\int_0^R \int_0^{2\pi} I(r,2d) r d\phi dr \quad (1.3)$$

Where ' R ' is the radius of the reflected light cone at the fiber end.

The radius could be expressed as

$$R = r_e + 2d \tan(\sin^{-1} NA) \quad (1.4)$$

Where NA is the numerical aperture.

The maximum emitting angle θ_{NA} is given by

$$\theta_{NA} = \sin^{-1}\left(\frac{NA}{n_0}\right) \quad (1.5)$$

The efficiency power factor due to reflected light from the front surface.

$$\eta_f = 2\int_{R_1}^{R_2} \int_0^{\phi_c} R_{mf} T_i(n_0) T_0(r,2d_1,n_0) \frac{2}{\pi R^2{}_f(d_1)} \left(1 - \frac{r^2}{R^2{}_f(d_1)}\right) r d\phi dr \quad (1.6)$$

R_1 and R_2 are the radii of the reflected light cone at receiving fiber end before and after overlapping with the core of the fiber. Where ' R_{mf} ' is the front surface reflectivity and ' d_1 ' is the distance between the glass plate and fiber end.

' R_f ' is the radius of circular cross section of a reflected light cone from the front surface at the fiber end, which is given by

$$R_f = r_e + 2d_1 \tan(\sin^{-1} NA) \quad (1.7)$$

The efficiency power factor due to reflected light from the back surface

$$\eta_b = 2\int_{R_1}^{R_2} \int_0^{\phi_c} T^2 R_{mb} T_i(n_0) T_0(r,2(d_1+t),n_0) \times \frac{2}{\pi R^2{}_b(d_1+t)} \left(1 - \frac{r^2}{R^2{}_b(d_1+t)}\right) r d\phi dr \quad (1.8)$$

Where ' T ' is the transmittance coefficient of the front surface and ' R_{mb} ' is the reflectivity of the back surface. ' R_b ' is the radius of circular cross section of a reflected light cone from the back surface at the fiber end, which is given by

$$R_b = R_f + 2t \tan\left(\sin^{-1}\frac{NA}{n_g}\right) \quad (1.9)$$

Where ' n_g ' is the refractive index of the glass plate and ' t ' is the thickness of the glass plate.

The total efficiency power factor is given by

$$\eta_t = \eta_f + \eta_b \quad (1.10)$$

The output power of the sensor is

$$P_0 = \eta_t P_i \tag{1.11}$$

The output characteristics of the proposed sensor obtained theoretically with R_{mf} = R_{mb} = 3%, NA=0.39, n_c= 1.47012 (refractive index of fiber core), n_g = 1.52 (refractive index of glass plate) and W = 1.2mm (separation between emitting and receiving fibers) for various thickness of the glass plate.

FINITE ELEMENT METHOD

Finite element method is a numerical technique for solving partial differential equations. For irregular domain this method is well suited. In particular, this method is better than the other methods if the transverse structure exhibits high refractive index differences. So, it meets the requirements well PCF modeling where the index difference is substantial. The FEM allows the PCF cross-section in the transverse x-y plane. It can be divided into a patchwork of triangular elements, which can be of different sizes, shapes, and refractive indices. This way different kinds of PCF geometry can be accurately described. The triangular boundaries can be connected with the help of transition conditions. This scheme leads to a matrix eigenvalue system, which can be solved numerically [21]. The FEM provides a full-vector analysis and then it is necessary to model PCFs with large air-holes and high index variations. This method is used to accurately predict their properties.

From Maxwell's equations the basic equation for the FEM analysis is given as

$$\nabla \times ([\mu_r]^{-1} \nabla \times E) - k_0{}^2 [\varepsilon_r] E = 0 \tag{1.12}$$

Where $[\mu_r]$ is the relative magnetic permeability and $[\varepsilon_r]$ is the dielectric permittivity tensors. When applying full-vector FEM, the PCF cross section is divided into sub-domain with triangular element where any refractive index profiles can be properly represented [10]. The dividing cross section PCF having a number of triangular elements, from Eq. (2.1) to obtain the following equation

$$([A] - n^2{}_{eff} [B])\{h\} = 0 \tag{1.13}$$

Where {h} is the discretized electric field vector. It consists of edge and nodal variables. Where [A] and [B] are the finite element matrices. The matrices [A] and [B] are used to allow the efficient resolution of the equation, it means high performance algebraic solvers for both real and complex problems. The computational domain without affecting the numerical solution. The outer boundary, is placed before the anisotropic Perfectly Matched Layers (PML). The formulation is used to able to deal the anisotropic material. Both are in terms of magnetic permeability and dielectric permittivity, allows the anisotropic PML to be implemented directly.

RESULT AND DISCUSSION

EFFECTIVE INDEX

For a given frequency, the magnitude of the wave vector of a ray will increase as it passes from a vacuum into a optically dense medium, since the wavelength decreases. If the ray enters not a uniform medium but rather a waveguide, its wave vector along the waveguide axis will increases

further, as the ray is reflecting back and therefore effectively traveling even more slowly. The relationship is easily seen for the symmetric dielectric. For more complicated geometries, the relationship will not be so simple, but in all case it is possible to define an effective index(n_{eff})such that

$$n_{eff} = \frac{\beta}{k}$$

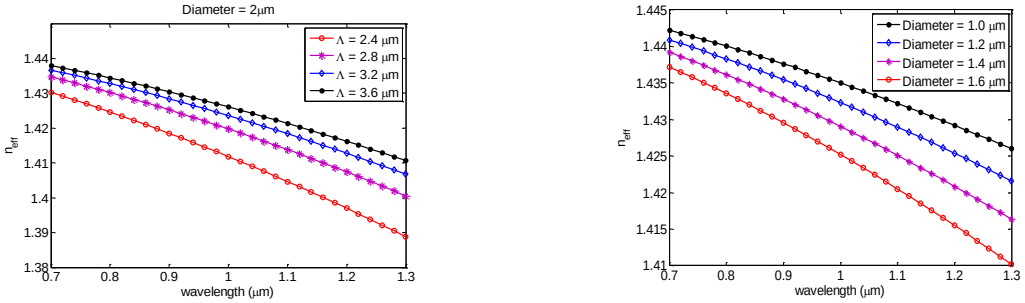

Fig.2.2 Variation of effective refractive index with respect to wavelenth for (a) constant pitch and (b) constant diameter

The effective refractive index of PCF is mainly depending upon the pitch (Λ) and diameter of the air hole (d). We have utilized finite element method to solve maxwell's equation for PCF to obrain refractive for various design. In the first condition, we have calculated n_{eff} value for various pitch (Λ) value with constant and diameter. In the second case, we have calculated n_{eff} for the variation of diameter with fixed value of pitch. Fig. 33 show how the effective index varied with respect to the wavelength and different pitch diameter. It is obvious that both the case effective refractive index and hence effective cladding index are decreasing as the wavelength increases.

NUMERICAL APERTURE

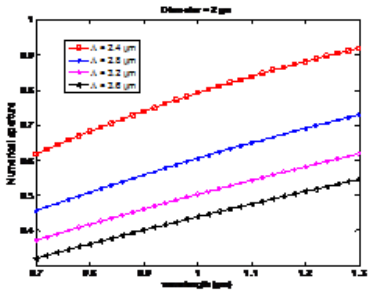

Fig.2.3 Variation of numerical aperture and acceptance cone with respect to wavelength for constant diameter value

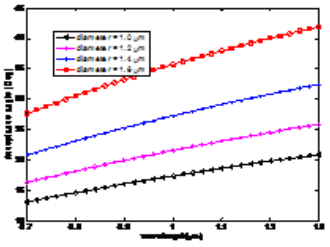

Fig.2.4 Variation of numerical aperture and acceptance cone with respect to wavelength for constant diameter value

Conventional fibers have a strong limit on the core size and the numerical aperture (NA) in a single mode regime. A numerical aperture for PCF is given by modifying above formula

$$NA = \sqrt{n_s^{\,2} - n_{cl}^{\,2}}$$

where n_s and n_{cl} are the refractive index of the silica (core) and effective cladding index respectively. Numerical Aperture of PCF mainly depends on varying pitch length and diameter of core and cladding. Fig. 2.3 and Fig.4.4 depicts the variation of numerical aperture value and acceptance cone for various design of PCF. From these figures, it is observed that if numerical aperture of the PCF increases, corresponding acceptance angle also increases. Also, the numerical aperture value increases with respect to wavelength due to the different pitch and diameter. Compare to different pitch value for a fixed diameter, the NA value is maximum for the small pitch. As a result, the numerical aperture of PCFs can vary over a wide range from 0.1 to more than 0.9 and hence the acceptance angle could be vary from 10^0 to 70^0. Hence, one can can vary the acceptance cone by choosing proper air hole diameter and pitch value.

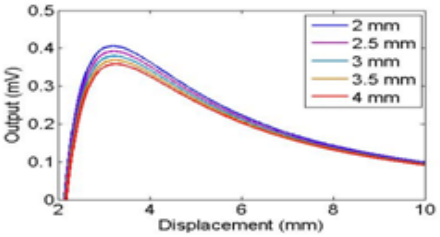

Fig.2.5 Output characteristics for different thickness of glass plate

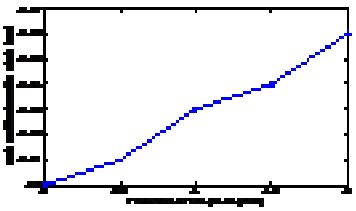

Fig.2.6 Variations of peak position

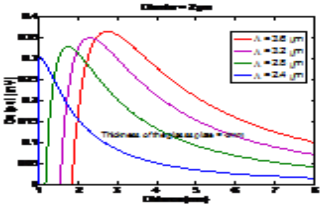

Fig.2.7 Output characteristics of photonic crystal fiber

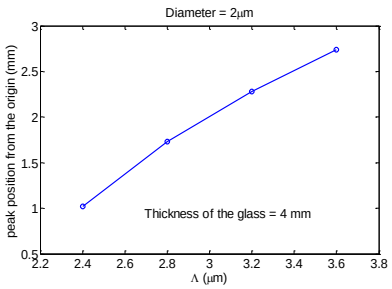

Fig.2.8 Variations of peak position

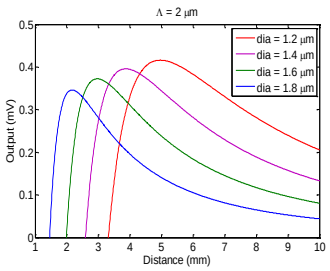

Fig.2.9 Constant pitch length and varying diameter

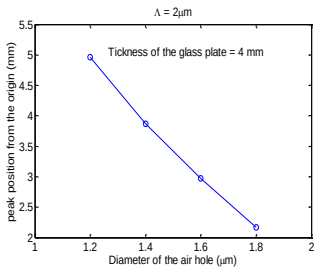

Fig.2.10 Variation of peak position

CONCLUSIONS

A novel photonic crystal fiber sensor is used for measuring the thickness of the transparent thin film. The finite element method is used to calculate effective refractive index for various design of PCF by varying the pitch length (Λ), diameter (d) of the air hole and also varying the wavelength. From the obtained cladding refractive index value, the numerical aperture values have been calculated. The output characteristics of sensor shows that the efficiency of measurement of thickness of the glass plate is purely depend on numerical aperture and acceptance cone of PCF. The simulation results show that the efficiency, sensitivity and accuracy of this PCF sensor is more higher than the conventional fiber optic sensor to find the thickness. Advantages of this work are PCF sensor provides more accurate thickness measurement of transparent thin film than the finding of thickness by the different types of interferometric methods. However, the PCF sensor is limited by thickness of the thin film where one cannot measure less than micrometer scale thickness of the transparent plate.

REFERENCES

[1] Jonh crisp, Introduction to fiber optics, 1(2001)
[2] N. Subramanyam brijlal, M.N. Avadhanulu, A text book of Optics, 627 (2003)
[3] http:/physicsweb.org/article/world/13/8/9/www.neci.nj.nec.com/hompage.
[4] A.M. Zheltikov, Uspekhi Fiz Nauk **170**, 1203 (2000).
[5] J. Broeng, S.E. Barkou, T. Sondergaard, and A. Bjarklev, Opt. Lett. **25**, 96 (2000).
[6] Masato Ohmi, Takehisa Shiraishi, Hideyuki Tajiri, Masamitsu Haruna, Simultaneous measurement of refractive index and thickness of transparent plates by low coherence interferometry, Optical review, **4**, 507 (1997).
[7] Takashi Fukano, Ichirou Yamaguchi, Separation of measurement of the refractive index and the geometrical thickness by use of a wavelength-scanning interferometer with a confocal microscope, J. Phys. D: Appl. Phys, **38**, 4065 (1999).
[8] Giuseppe Coppola, Pietro Ferraro, Mario Iodice, Sergio De Nicola, Method for measuring the refractive index and the thickness of transparent plates with a lateral-shear, wavelength-scanning interferometer, J. Phys. D: Appl. Phys, **42**, 3882 (2003).
[9] Hideki Maruyama, Shogo Inoue, Teruki Mitsuyama, Masato Ohmi, Masamitsu Haruna, Low-coherence interferometer system for the simultaneous measurement of refractive index and thickness, J. Appl. Optics, **41**, 1315 (2002).
[10] Supriya S, Patil P.B, Buchade A.D, Shaligram, Theoretical modeling, simulation and experimental studies of fiber optic bundle displacement sensor, *J. Elsevier*, **201**, 79 (2013).
[11] Bushra R. Mhdi, Nahla A, Aljaber, Suad M. Aljwas, Abeer H. Khalid, Design and construction of optical fiber sensor system for detection of the stress and fine motion, *IJ-Nano*, **1**, 25 (2012).
[12] Mingguang Shan, Rui Min, Zhi Zhong, Ying Wang, Yabin Zhang, Differential reflective fiber-optic angular displacement sensor, *J. Elsevier*. **68**, 124 (2015).
[13] Joao M.S. Sakamoto, Gefeson M, Pacheco, Claudio Kitano, Bernhard R. Tittmann,Geometrical parameter analysis of a high-sensitivity fiber optic angular displacement sensor, J. Appl. Optics, **53**, 8436 (2013).
[14] Jao-Hwa Kuang, Pao-Chuan Chen, Yung-Chuan Chen, Plastic Optical Fiber displacement sensor based on dual cycling bending, J. Sensors, **10**, 10199 (2010).
[15] Yasin .M, Harun S.W, Ahmad .H, Fiber optic displacement sensor based on micro-thickness measurement using bundled fiber and cancave mirror, J. Optoelectronics and advanced materials, **13**, 933 (2011).
[16] Wen H. Ko, Kow-Ming Chang, Gwo-Jen Hwang, A fiber-optic reflective displacement micrometer, J. Elsevier, **49**, 51 (1995).
[17] Anmad .A, Yasin.M, Thambiratnam.K, Harun.S.W, Fiber optic displacement sensor for micro-thicknesss measurement, Sensor Review, **32**, 230 (2012).
[18] Suhadolnik A, Babmk A, Mozina, J. Optical refractometer. Sensors Actuators B, **29**, 428 (1995).
[19] Chadhari AL, Shaligram D, Multi-wavelength optical fiber liquid refactometry based on intensity modulation. Sensors Actuators A, **100**, 160 (2002).
[20] Gobi G, Gokul Raj S, Sastikumar D. Measurement of refractive index of liquids using fiber optic displacement sensors.J Am sci, **5**, 13 (2009).
[21] Sastikumar D, Gobi G, Renganathan B. Determination of the thickness of a transparent plate using a reflective fiber optic displacement sensor. J Elsevier, **42**, 911 (2010).
[22] Vasantha Jayakantha Raja R, Nonlinear pulse propagation through photonic crystal fiber: pulse compression and supercontinuum generation.
[23] Vasantha Jayakantha Raja R, Porsezian K. A fully vectorial effective index method to analyse the propagation properties of microstructured fiber. J Elsevier, **5**, 171 (2007).
[24] N.A. Issa, Appl. Opt **43**, 33 (2004).

GROWTH AND CHARACTERIZATION OF DYE DOPED GLYCENE LITHIUM SULPHATE (GLS) CRYSTALS FOR NLO APPLICATIONS

K.Sahadevan[1], D.Narayanasamy[2], J.Logeswari [3], P.Kumaresan[4*] & P.M.Anbarasan[5]

[1, 4]Department of Physics, Thiru.A.Govindasamy Government Arts College,Tindivanam- 604 002,

[2]Department of Physics, SKP Engineering College, Tiruvannamalai,

[3]Department of Chemistry ,Adhiparasakthi Engineering College, Melmaruvathur-603 319,

[5]Department of Physics, Periyar University, Salem-636 011

E.mail : logeshkumaresan@yahoo.com

Abstract

The ideal material that could have potential applications in non-linear optical (NLO) devices should possess the combination of large non-linear figure of merit for frequency conversion, high laser damage threshold, fast optical response time, wide phase matchable angle, architectural flexibility for molecular design and morphology, optical transparency and high mechanical strength. The stability of Glycene Lithium Sulphate (GLS) single crystal was improved by doping organic dyes. The structural, chemical, optical, mechanical and non-linear optical properties of the dye doped crystals were analyzed with the characterization studies such as powder XRD, FT-IR, UV-Visible, SEM and SHG measurements, respectively.

1. INTRODUCTION

A nonlinear optical material has many applications like image application using photorefractive crystals, frequency multipliers and mixers, fiber optics, parameter oscillators, optical switches, etc., laser in a modern wonder, whether it is in the field of information transformation or in the field of medicine. The interaction of laser with matter has advanced capabilities in optical spectroscopy. The discovery of laser itself is a result of crystal growth.

In recent years more emphasis is given to semiorganic materials due to their much matured NLO applications than organic materials and owing to their good transparency, chemical stability, and mechanical properties. The large nonlinearity arises from the strong charge transfer and high polarisibility. To enable a material to be potentially useful for NLO applications the material should be available in bulk single crystal form. Also research into the growth of large single crystals from aqueous solution is currently serving as the important avenue to general progress in understanding many fundamental concepts of crystallization.Compared with inorganic NLO materials, organic materials may fulfil many of these requirements, but there are also some drawbacks with organic NLO materials such as environmental stability, poor chemical and mechanical stability, red-shift of the cut-off wavelength, low laser damage thresholds and poor phase matching properties. In order to overcome these drawbacks and improve the properties, the growth of semi-organic crystals has nowadays come into prominence.

The semi organic crystals have some advantages such as higher second order optical non-linearities, short transparency cut-off wavelength and stable physio-chemical performance over the traditional inorganic and organic crystals. Considering all the above mentioned facts, Glycene lithium sulphate Crystals have been synthesized and grown moderately at low cost.

2. EXPERIMENTAL PROCEDURE

2.1 CRYSTAL GROWTH

A solution of glycine lithium sulphate was prepared by dissolving equimolar amount of glycine and lithium sulphate. The solution was continuously stirrer using a magnetic stirrer of room temperature. The chemical reaction may be represented as,

$$C_2H_5NO_2 + Li_2SO_4 \rightarrow [Li_2(SO_4)(C_2H_5NO_2)]$$

The prepared solution was filtered and kept undisturbed in a constant temperature bath maintained at a temperature of 40 °C. When evaporation taken place slowly, supersaturation is activated. As a result, crystals with dimensions 7.5 × 5 × 2.75 mm^3 were harvested in a period of 40 days. GLS crystals were grown from aqueous solution by slow evaporation method. The solubility of dyes doped GLS water was measured. It was found to be 16.5 g/100 ml at 40^oC for Coumarin doped GLS. The amount of GLS salt to be dissolved was determined from its solubility curve at an average temperature of 38^oC. The solution was stirred long enough to ensure complete dissolution of the solute, and filtered. Subsequently the solution was cooled at a rate of 0.1^oC/day. The seed crystals were prepared at low temperature by spontaneous nucleation (Fig.1).

Figure 1. Photograph of Coumarine doped GLS Crystal

The seed crystals with perfect shape and free from macro defects were used for growth experiments. Seed crystals of pure GLS and doped GLS were grown using constant temperature bath controlled with an accuracy of ± 0.01^oC. A supersaturated solution of Coumarin doped GLS was prepared in distilled, deionized water. Seed crystals were introduced into the solution using thin nylon thread at the appropriate supersaturation condition. Experiments were allowed to run for considerably longer duration of the time (20 days) would grow large crystals.

3. RESULTS AND DISCUSSION

Powder X-ray diffraction studies were carried out for the as grown crystals using a Rich Seifert X-ray diffractometer with CuK_α (λ = 1.5405 Å) radiation (Kurtz 1968). Powder XRD spectra for the pure and doped GLS revealed that the structures of the doped crystals were slightly distorted compared to the pure GLS crystal. The (h k l) planes satisfy the general reflection conditions of space group observed from the structure determination of the crystal.The FT-IR spectra of pure and dye doped GLS crystals on a Bruker IFS 66V model spectrophotometer using 1064 nm output of a cw diode pumped Nd: YAG laser as a source of excitation in the region 500 – 4000 cm^{-1} operating at 200 mW power at the samples with a spectral resolution of 2 cm^{-1}. The observed FT-IR spectra of pure and doped GLS are shown in Fig.2. In doped GLS spectra, broad peak around 3650 cm^{-1} was due to free –OH stretching vibration. It reveals that at least one of the –OH group of GLS was remain

unaltered after that doped with GLS. Due to the greater mass of sulphur in GLS the C=S stretching vibration was expected to occur at 625 cm^{-1}, it was considerably lower frequency than the usual C=O stretching vibration at 1710 cm^{-1} because of the C=S group is less polar than the C=O group and has a considerably weaker band. The strong vibrational coupling was operative in the case of nitrogen containing thiocarbonyl group of glycene and that the C=S vibration was not located in the spectra.

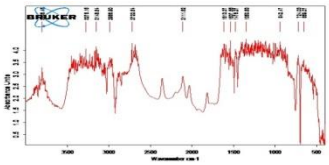

Figure 2. FT-IR spectrum of Coumarin doped GLS crystal

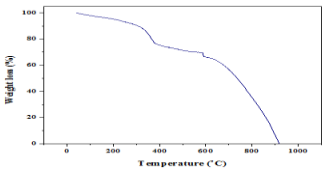

Figure3. TG Curve of Coumarin doped GLS Crystal

The TG curve(Fig.3) of this sample indicates that the sample is stable up to 210°C and above this temperature the weight loss occurred due to self-degradation of doped GLS but merely to its evaporation after its melting. The highest symmetry phase compatible with the ferroelectric structure is termed as the prototype phase also called paraelectric phase Although it is not necessary of non-polar character, it was proves to be the greatest majority of known ferroelectrics so far. Most of the phases actually exist as the highest temperature phase of the crystal, although in some instances the structure may melt before the prototype phase would otherwise become stable. As a result of its small structural displacement from the prototype, a typical ferroelectric material possesses a spontaneous polarization P_s which decreases with the increase of temperature $T_{c.}$

4. CONCLUSION

Good optical quality single crystals of Coumarin dye doped GLS have been grown from solution by slow solvent evaporation technique for the first time. Experiments were allowed to run for considerably larger duration of the time (20 days) for the growth of large crystals. The functional groups present in the grown crystals have been confirmed by FT-IR spectral analysis. Optical transmission UV-Visible spectral range of dye doped GLS was measured and the doped GLS crystal has a good optical transmission in the entire visible region. The powder SHG measurement shows that the grown doped GLS crystal has 1.65 times higher SHG efficiency than KDP. Vickers micro hardness was calculated in order to understand the mechanical stability of the grown crystals. Each type of constituent chemical bond is regarded as one part of the whole crystal that has contributions to the total nonlinearity. The fundamental beam of 1064 nm from Q-switched Nd:YAG laser was used to test the SHG property of the grown crystal.

REFERENCES

[1] S. Hoshino, Y. Okaya, and R. Pepinsky, Phys. Rev. 115 (1959) 1955.
[2] S. Natarajan, K. Ravikumar, and S. S. Rajan, Z. Kristallogr. 168 (1984) 75.
[3] R. Pepinsky, Y. Okaya, D. P. Eastman, and T. Mitsui, Phys. Rev. 107 (1957) 1538.
[4] R. Pepinsky, K. Vedam, and Y. Okaya, Phys. Rev. 110 (1958) 1309.
[5] S. Hoshino, T. Mitsui, F. Jona, and R. Pepinsky Phys. Rev. 107 (1957) 125.
[6] K. Ravikumar and S. S. Rajan, Z.Kristallogr. 171 (1985) 201.
[7] S. Natarajan and J. K. Mohan Rao, Z. Kristallogr. 152 (1984) 179.
[8] J. Baran, M. Drozd, A. Pietraszko, M. Trzebiatowska, and H. Ratajczak J. Polish.Chem. 77 (2003) 1561.
[9] A. Deepthy and H. L. Bhat, J. Cryst. Growth 226 (2001) 287.

Non-Linear and Thermal Properties of Γ- Glycine Single Crystal: in The Presence Of 2-Aminopyridine Potassium Chloride

R. Srineevasan[1]*, T. Revathi[2], R.Jayavel[3], D.Rajanbabu[4], and S.M.Ravi kumr[5]

[1,2,5] *P.G & Research Department of Physics, Government Arts College,Tiruvannamalai,606603,India*

[3]*Dean, Acedemic Research, Anna university, Chennai, India*

[4]*Professor, School of Science,VIT University, India*

e-mail ID: ***rsrinee61@gmail.com***

Abstract

In this research paper, an overview of polymorph γ-form glycine single crystal crystallization in the presence of 2-aminopyridine potassium chloride as an additive at an anambient temperature by slow evaporation solution growth technique (SEST) has been presented. Powder XRD study confirms crystalline nature of the grown γ-glycine crystal. The single crystal XRD study shows that the grown crystal possesses hexagonal structure and belongs to space group $P3_1$ with the cell parameters a=7.09 Å; b=7.09; c=5.52 Å; α = β = 90˚; and γ = 120˚. Thermal studies have been carried out to identify the elevated thermal stability and decomposition temperature of the grown sample. Enhanced SHG efficiency of the grown crystal was confirmed by the Kurtz powder technique using Nd:YAG laser and found 1.6 times greater than that of inorganic standard potassium dihydrogen phosphate.

1. Introduction

Highly polarizable conjugated system of organic molecule possesses non-centro symmetry structure. The inorganic molecule (anion), linking through hydrogen bond with organic molecule (cation) yields strong mechanical and high thermal stability [1,2]. Molecular charge transfer induced in semiorganic complex by delocalized π electron, such that moving between electron donor and electron acceptor which are in opposite sides of the molecules [3,4]. In the base acid interaction of organic and inorganic molecules, there is a high polarizable cation derived from aromatic nitro systems, linked to the polarizable anion of inorganic molecules through hydrogen bond network yields a noncentrosymmetric structural systems and this hydrogen bonding energy between organic and inorganic molecules made the dipole moment in parallel fashion ensures the increase of second harmonic generation activity [5]. The structures of 2-aminopyridine complexes have already been studied by Chao and his co-workers [6]. In recent years metal organic complexes have been played reasonable attention in advancement of technology [2,7]. Growth of 2-aminopyridine complex crystals is widely used in the rapid advancement in technology, such as ultra-fast phenomena, optical communication and optical storage devices , frequency doublers and optical modulators [8]. Optical properties of 2-aminopyridine complexes and their suitability for optoelectronic devices have been reported [9-14]. Metal organic nonlinear optical crystals possess good second harmonic generation efficiency, hence rich demand in optical storage devices, color display units and optical communication systems [7]. Recent research focus is on designing of new materials capable of attaining SHG processes by strong interaction with an oscillating field of light. Amino acids with ionic salt complex crystals have been investigated and recognized as materials having good nonlinear optical properties. In this present work, synthesis and crystallization of glycine into γ-form glycine in

the presence of aqueous solution 2-aminopyridine potassium chloride and their suitability for device fabrication with various enhanced optical and thermal properties are reported.

2. Experimental Procedure

2.1 Material synthesis

The title compound was synthesized by taking analytical grade glycine, 2-aminopyridine and potassium chloride in the stoichiometric ratio (1:1:1) with Millipore water of resistivity 18.2 mega-ohm.cm^{-1} as a solvent. In this synthesis, protonation of nitrogen in pyridine ring facilitates hydrogen bonding interaction between potassium chloride and glycine such that 2-aminopyridine is linked to the metal K^+ ion through pyridine ring nitrogen, rather than amino group nitrogen leaving $(Cl)^-$ ion.

$C_5H_6N_2 + KCl + NH_2CH_2COOH \rightarrow [(K^+) + C_5H_6N_2COOCH_2NH_2(Cl)^-]$

[(2-aminopyridine) + (potassium chloride) + (glycine)]→ [(γ-glycine crystal)]

2.2 Crystal Growth

The prepared mother solution was stirred vigorously for 4h using magnetic stirrer. High degree of purification of synthesized salt was achieved by successive recrystallization process. Synthesized saturated solution was filtered using filter paper of micron pore size. The filtered solution was pored in different petri dishes and covered with porous paper for slow evaporation. After a time span of 15 days, quality crystals of average size 13mm x 12mm x 3mm were harvested. The as grown crystal is shown in figure 1.

Figure 1 As- grown γ-glycine crystal

3. Results and discussion

Single crystal and powder XRD analysis were carried out on a PHILIPS X PERT MPD system. **TGA and DTA analysis were carried out using NETZSCA STA 409 instrument at a heating rate of 20°C min^{-1} from ambient to 500°C.** The NLO efficiency of the grown crystal was tested by KURTZ powder technique using Nd: YAG laser of wavelength 1064 nm

3.1Powder XRD studies

The grown γ-glycine crystal crushed to a uniform powder and subjected to powder x-ray diffractrometer with CuKα (λ=1.540598 Å) radiations for structural analysis study. The powder form sample was scanned over the range 10-45° **at the rate of 2°/min.** The indexed powder XRD pattern of grown crystal is shown in figure 2. Peaks in the XRD without any broadening confirm that the grown sample is higher order of crystalline nature.

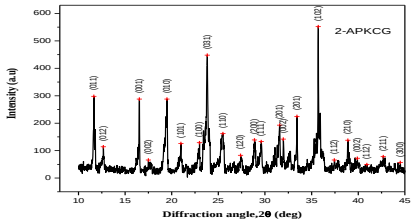

Figure 2 Powder XRD pattern of as grown crystal γ-glycine

3.2 Single crystal XRD analysis

Single crystal **X-ray diffraction analysis** confirms the hexagonal structure of the γ-glycine crystal with space group $P3_1$. The unit cell parameters of the grown γ-glycine are a = 7.09Å; b = 7.09Å; c = 5.52Å; α = β = 90˚; γ = 120˚ and volume of the unit cell was found to be 278 $Å^3$. These values are in-line with the literature values [15-17]. Further, it is evident that the presence of 2-aminopyridine potassium chloride in the aqueous solution, without enter into the grown crystal lattice, yields the polymorph form γ-glycine, as a physical change.

3.3Thenarmal analysis

Thermo gravimetric (TG) and Differential thermal analysis (DTA) gives information regarding phase transition, water of crystallization and different stages of decomposition of the crystal. Samples of γ-glycine crystals were weighed in an Al_2O_3 crucible with a microprocessor driven temperature control. TGA and DTA curves of grown crystals were recorded in nitrogen atmosphere between ambient temperature to 500˚C shown in Figure 3. There is no weight loss up to 216.6˚C indicating that there is no inclusion of solvent (water) in the crystal lattice. The thermogram reveals that the major weight loss (42.4%) starts at 216.6˚C and continues up to 484.4˚C with 1.255mg (57.6%) as residue. The nature of weight loss indicates the decomposition of the material. Below 484.4˚C no weight loss was observed. DTA curve shows that the decomposition point of as grown γ-glycine crystal is 270˚C.

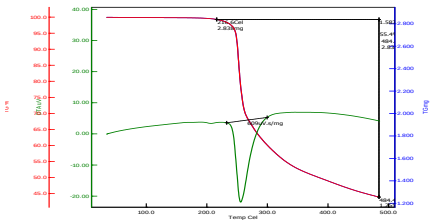

Figure 3. TGA & DTA graph of as grown γ-glycine crystal

3.4 NLO studies

In order to confirm the NLO property, powdered sample of grown crystal was subjected to KURTZ and PERRY powder technique, which is a powerful tool for initial screening of the materials for second harmonic generation (SHG) [18]. The beam of wave length λ =1064 nm from Q-switched Nd:YAG laser was made to fall normally on the prepared powdered sample of grown γ-glycine crystal , which was packed between two transparent glass slides. Suitable solution ($CuSO_4$) was used to

absorb the transmitted beam and the optical second harmonic signal was detected by a photomultiplier and displayed on CRO. Here powder form of KDP crystal of identical size to grown γ-glycine crystal powder particles were used as standard in the SHG measurement.The SHG behavior was confirmed from the emission of bright green radiation (532nm) by the sample. The measured amplitude of second harmonic green light for as grown γ-glycine crystal was 14.9mJ as against 8.8mJ of KDP and 8.9mJ of UREA. The enhanced powder SHG efficiency of as grown γ-glycine crystal is about 1.65 times that of KDP and 1.63 times of UREA. This value is relatively high when compared to the SHG values reported for γ-glycine crystals grown with other additives and comparision is given in Table 3.4. This enhanced lasing performance of as grown γ-glycine crystal is due to the additive influence of 2-aminopyridinium potassium chloride. The good second harmonic generation efficiency of as grown γ-glycine crystal in the presence of 2-aminopyridine potassium chloride attests, that the grown crystal is a potential candidate for nonlinear optical applications.

4. Conclusion

We have successfully grown polymorph γ-form of glycine single crystals by slow evaporation solution growth technique at ambient temperature. Powder and single crystal XRD studies reveal that the grown γ-glycine crystal is having higher order of crystallinity. Thermal studies show the sample is thermally stable up to 270°C (elevated temperature) and this makes the grown crystal's suitability for possible application in laser, where the material is required to with stand high temperatures. NLO studies of the grown sample show that the enhanced SHG efficiency is greater than KDP (1.65 times) and Urea (1.63 times) crystals.

References:

[1].S.Debrus, H.Ratajczak ,J.Venturini, N.Pincon ,J.Baran, J.Barycki,T.Glowiak, A.pietraszko, Synthetic Metals 127 (2002) 99 – 104.

[2] Ch.Bosshard, K.Sutter, Ph.Pretre, J.Hulliger, M.Florsheimer, P.Kaatz, P.Gunter, organic Nonlinear optical materials,Gordon and Breach,Basel,1995.

[3] M.C.Etter, J.ChemPhy. 95 (1991) 4601.

[4] C.B.Aakeroy, P.B.Hitchcock, B.D.Moyle, K.R.Seddon, J.Chem.Soc., Chem.Commun. (1989)1856.

[5] C.B.Aakeroy, P.B.Hitchcock, B.D.Moyle, K.R.Seddon, J.Chem.Soc., Chem.Commun. (1992) 553.

[6] M.Chao, E.Schemp and R.D.Rosenstein, Acta cryst.B31, (1975).2922-2924

[7] D.S.Chemla, J.Zyss(Eds), Nonlinear optical optical properties of organic molecules and crystals,Academic press,New York,1987.

[8] Yari S. Kivshar, Optics Express, 16, (2008)22126-22128

[9] B. K. Periyasamy, R. S. Jebas, and B. Thailampillai, Materials Letters, 61 (2007) 1489-1491.

[10] K.P.Bhuvana, S.Robinson and T.Balasubramanian,Cryst. Res. Technol,45 (2010) 299-302

[11] Z.kotler, R.Hierle, D.Josse, J.Zyss, R.Masse, J.Opt. Soc. Am. B9(1992) 54

[12] Y.Lefur, M.Bagiue-Beucher, R.Masse, J.F.Nicoud, J.P.Levy, Chem.Mater. 8 (1996) 68.

[13] H.Ratajczak, J.Baran, J.Barycki, S.Debrus, M.May, A.Pietraszko, H.M.Ratajczak, A.Tramer, J.Mol.Struct. 55 (2000) 149

[14] H.Ratajczak, , S.Debrus, M.May, J.Barycki, J.Baran, Bull. Pol. Acad. Sci. Chem. 48 (2000) 189.

[15] T.P.Srinivasan,R.Indirajith, R.Gopalakrishnan, J.Cryst.Growth 318 (2011)762-767.

[16] S.Sankar, M.R.Manikandan, S.D.G.Ram, T.Mahalingam, G.Ravi, J.Cryst.Growth 312 (2010)2729-2733.

[17] G.R. Dillip, P. Raghavaiah, C. Madhukar Reddy, G. Bhagavannaraya, V. Ramesh Kumar, B. Deva Prasad Raju, Spectrochimica Acta Part A 79 (2011) 1123-1127.

[18] S.K.Kurtz and T.T.Perry, J.Appl. Phys. 39, (1968). 3798

OPTICAL AND DIELECTRIC PROPERTIES OF SEMIORGANIC NONLINEAR OPTICAL CRYSTAL GLYCINE BARIUM NITRATE (GBN)

S.Varalakshmi[1], S.M. Ravi Kumar[2], G. Senthilkumar[3], J.Jebasinghkores[4] and R. Ravi Sankar[2*]

[1]Department of Physics, Kamban Arts & Science College of women, Tiruvannamalai-606 601

[2]PG and Research Department of Physics, Government. Arts College, Thiruvannamalai- 606 603

[3]Department of Physics, University College of Engineering Arni (A Constituent College of Anna University, Chennai), Thatchur, Arni-632326

Department of Physics, Pope's College, Sawyerpuram-628251, Thoothukudi Dist, Tamilnadu

**Corresponding Author: ravisankarphysics@gmail.com*

Abstract

Transparent crystal of glycine barium nitrate (GBN) has been grown from aquous solution by slow evaporation techniques at room temperature. Powder XRD study reveals the crystalline nature of the grown sample. Single crystal XRD study shows that the GBN is orthorhombic crystal system. The presence of wide transparency window in the UV-visible region makes GBN suitable for opto-electronic device application. The grown sample has SHG efficiency is 0.8 time that of standard KDP crystal. Dielectric studies reveal that both dielectric constant and dielectric loss decreases with increase in frequency.

1.0 INTRODUCTION

Nonlinear optical materials for optical second harmonic generation (SHG) have received attention owing to their practical applications in the domain of optoelectronics and photonics [1-3]. Materials answering for high optical nonlinearity are a potential area which has attracted many theoretical and experimental researchers. Amino acid based semiorganic compounds have been recently recognized as potential candidates for second harmonic generation (SHG) [4-6].

At present the trend is towards semiorganic material compared to inorganic and organic since they posses higher mechanical strength and chemical stability [7]. Hence, recent search concentrated on new class material called semi-organic materials due to their large nonlinearity, high resistance to laser induced damage, low angular sensitivity and good mechanical hardness. Semi-organic materials are used in device fabrication technology due to their enhanced chemical and physical properties such as high thermal stability wide transparency range, less deliquescence's excellent nonlinear optical coefficient. Semi-organic crystals possess both the good qualities at host organic and additive inorganic materials [8, 9].

Glycine is an organic compound is the simplest amino acids which is existing in three phases α, β, γ [10]. Glycine can be readily combined with variety of acids, orgnic and inorganic components to produce a host of materials with interesting properties .

In these semiorganic hybrids the weak forces of organic solids are replaced by stronger ionic forces forming a complete new class of semiorganic materials suitable for electronic industries. The presence of donor NH2 group, acceptor COOH group and due to intra molecular charge transfer, many naturally occurring amino acids themselves exhibit NLO behaviour [18, 19]. In the present

investigation single crystal of glycine barium nitrate (GBN) were grown by slow evaporation method. The grown crystals were characterized by single crystal and powder X-ray diffraction, FTIR, UV-vis NIR studies, SHG, dielectric and studies.

2. EXPERIMENTS

2.1 Synthesis

Commercially available AR grade (E-merk, purity > 98.0%) chemicals were used as the starting materials. The synthesis component of glycine barium nitrate (GBN) was carried out by carefully using glycine and barium nitrate in molar ratio 1: 1 using double distilled water as a solvent. The solution was stirred well using magnetic stirrer to form a clear solution. GBN was synthesized according to the relation

2.2 Growth of GBN

The saturated solution was taken in a beaker and the solvent evaporation technique was employed to grow single crystals of GBN. Since glycine has coordinating capacity to form different phases of metal glycine complexes. The mixtures of reactants had to be stirred to avoid co-precipitation of multiple phases. Hence, the solution was then filtered and allowed to evaporate at room temperature. Optical good quality triangle shaped crystals of GBN were harvested in a span of 10-20 days with dimension is 12×12×3 mm^3. The photographs of the as grown crystals of GBN are shown in figure 1.

Fig. 1 Photograph of as grown crystals of GBN

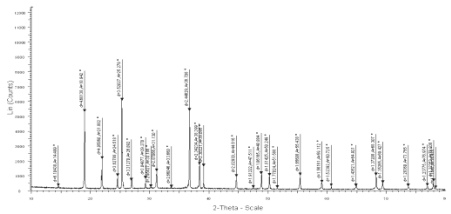

Fig. 2 Powder XRD pattern of GBN

3. Results and Discussion

3.1 Single crystal and powder XRD studies

It is observed from the single crystal XRD studies that GBN is belonged to orthorhombic crystal system. The calculated lattice parameter are a = 8.26 A°, b = 9.300A°, c = 14.838A° and volume = 1140.4$A^{\circ 3}$. Powder XRD of grown crystal GBN is shown in figure 2. The peaks in the XRD without any broadening confirm that the grown sample high order of crystalline nature.

3.2 UV-visible spectrum analysis

The selective electronic transmission spectrum of GBN crystal was recorded in the range 190-900 nm. Optically polished single crystal of thickness 3 mm was used for this study. The recorded spectrum gives limited introduction about the structure of the molecule, because the absorption of UV and visible light involves promotion of the electron in the σ and π orbital from ground state to higher energy state. The transmission spectrum of as grown crystal of GBN is shown in the figure 3. UV-

visible spectral analyzing shows that crystal is transparent in the entire visible region. The UV cut off wavelength occur at 210 nm. It is well known that an efficient NLO crystal has an optical transparency lower cut off wavelength between 200-400 nm [20].

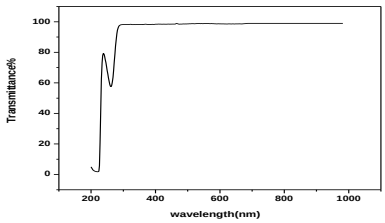

Fig. 3 Optical absorption spectrum

3.3 Kurtz powder SHG test

In order to confirm the nonlinear optical property, powdered sample of GBN was subjected to KURTZ and PERRY techniques, which remains powerful tool for initial screening of materials for SHG efficiency [21]. A Q-switched Nd; YAG laser emitting 1.06µm, with power density up to 1 GW/cm^2 was used as a source of illuminating the powder sample. The sample was prepared by sandwiching the graded crystalline powder with average particle size of about 90µm between two glass slides using copper spices of 0.4mm thickness. A laser produced a continuous laser pulses repetition rate of 10Hz. The input power was fixed at 0.68 J and the output power was measured as 6.9 mJ, which was compared to output 8.8 mJ of standard KDP. The diffusion of bright green radiation of wave length k = 532 nm ($P_2\omega$) by the sample confirms second harmonic generation (SHG). The powder SHG efficiency of GBN crystal is about 0.8 times of KDP. The good second harmonic generation efficiency indicates that the GBN crystals can be used as suitable material for nonlinear optical devices.

3.4 Dielectric studies

Figures 4 & 5 shows the variations of dielectric constant and dielectric loss of glycine barium nitrate crystal at different temperatures as a function of frequency. The dielectric constant decreases with increasing frequency and becomes almost saturated beyond 3.5 KHz for all temperatures. The decrease in dielectric constant of glycine barium nitrate crystal at low frequencies may be attributed to the dependence of electronic, ionic, orientation and space charge polarizations [22]. The space charge contribution will depend on the purity and perfection of the material and it has noticeable influence in the low frequency region. Hence, the larger values of dielectric constant exhibited by sample at low frequencies may be attributed to space charge polarization arising due to the crystal defects at grain boundary interfaces. At low frequencies, the charge on the defects can be rapidly redistributed so that defects closer to the positive side of the applied field become negatively charged, while defects closer to the negative side of the applied field become positively charged. This leads to a screening of the field and an overall reduction in the electric field. As capacitance is inversely proportional to the field, this reduction in the field for a given voltage results in the increased value of capacitance when the

frequency is lowered. However, at high frequency, the defects no longer have enough time to rearrange in response to the applied voltage, and so the capacitance decreases.

The variations of dielectric loss (tan δ) with frequency are shown in Figure 8. It is observed that the dielectric loss decreases with increasing frequency. Similar trend was observed for all the recorded temperatures. Among the all four polarizations, electronic and space charge polarizations are predominant in the low frequency region. The characteristic of low dielectric constant at higher frequency suggests that the sample possesses improved optical quality with lesser defects and this parameter is most important for different nonlinear optical materials and their applications [23].

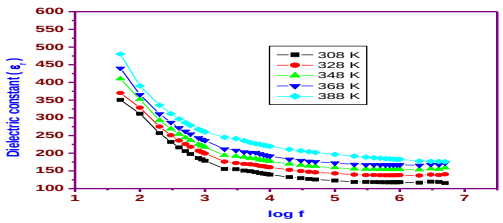

Fig. 4 Variation of dielectric constant with frequency at different temperatures of GBN crystal

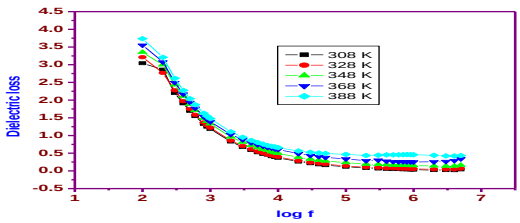

Fig. 5 Variation of dielectric loss with log frequency at different temperatures of GBN crystal

CONCLUSION

Good optical quality semiorganic crystal of glycine barium nitrate (GBN) was grown successfully by slow evaporation technique with the dimension 12 ×12 ×3 mm^3. Powder XRD analysis reveals that GBN crystal highly crystalline nature and belongs to orthorhombic crystal system. UV-visible transmission spectral study shows wide range of optical transmission bands and the lower cutoff wavelength at 210 nm. SHG studies on the grown GBN crystal shows that it is having NLO property and the SHG efficiency is 0.8 times that of KDP. The dielectric property of GBN crystal has been analyzed as a function of frequency at different temperature is discussed.

References

1. A.Deepthy, H.L. Bhat, Journal of Crystal Growth 226 (2001) 287.
2. R. Rajasekaran, P.M. Ushashree, R. Jayavel, P. Ramasamy, Journal of Crystal Growth 229 (2001) 563.
3. D. Prem Anand, M. Gulam Mohamed, S.A. Rajasekar, S. Selvakumar, Joseph Arul Pragasam, P. Sagayaraj, Mater. Chem. Phys. 97 (2006) 501–505.
4. S. Dhansukodi, A.P. Jeyakumari, S. Manivannan, Journal of Crystal Growth 282 (2005) 72.
5. T. Balakrishnan, K. Ramamurthi, Spectrocimica Acta Part A 68 (2) (2007) 360.
6. R. Ramesh Babu, N. Vijayan, R. Gopalkrishnan, P. Ramasamy, Crystal Research and Technology 41 (2006) 405.
7. D.Xu, M.Jiang and Z.Tan, Acta. Chem. Sin., 41(1983)570.
8. S.M. Ravi Kumar, N. Melikechi, S. Selvakumar, P. Sagayaraj, Physica B, 403 (2008) 4160–4163.
9. S. Selvakumar, S. M. Ravi Kumar, K. Rajarajan, J. Madhavan, Ginson P. Joseph, S. A. Rajasekar and P. Sagayaraj**,** Materials Chemistry and Physics 103 (2007) 153-157.
10. J. Nayeem, H. Wakabayashi, T. Kikuta, T. Yamazak, N. Nakatani, J. Korean. Phys. Soc. 42 (2003) 1063.
11. M.D. Aggarwal, J. Stephens, A.K. Batra, R.B. Lal, J. Optoelectronics. Adv. Mater. 5 (2003) 555.
12. C. Razzetti, M. Ardoino, L. Zanotti, M. Zha, C. Paorici, Cryst. Res. Technol. 37 (2002) 456.
13. Y.Le Fur, R.Masse, M.Z.Cherkaoui, J.F.Nicoud, Z.Kristallogr. (1993)856.
14. S.K. Kurtz, T.T. Perry, J. Appl. Phys. 39(1968)3798.
15. J.S. Pan, X.W. Zhang, Acta Mat. 54 (2006) 1343.

INVESTIGATION OF $_L$-LYSINE DOPED TRIGLYCINE BARIUM CHLORIDE SINGLE CRYSTAL FOR NONLINEAR OPTICAL APPLICATIONS

S. Chennakrishnan[1], D. Sivavishnu[2], J.Johnson[2], S.M. Ravi Kumar[2,*]

[1]*Department of Physics, Idhaya Arts & Science College for women, Pudupalayam, Tiruvannamalai.*

[2]*PG & Research Department of Physics, Government Arts College, Tiruvannamalai*

Corresponding author: smravi78@rediffmail.com

Abstract

The single crystal of $_L$-Lysine doped TGBC crystal, a semiorganic crystal has been grown from an aqueous solution by slow evaporation technique at room temperature. Good optical quality single crystal of size 7×9×2 mm^3 was harvested in a period of 31 days. The lattice parameters and crystal system have been measured by single crystal XRD study. The crystalline nature has been confirmed by powder XRD study. Fourier Transform Infrared (FTIR) spectroscopy study confirmed the presence of functional groups in grown crystal. Transmission spectrum has been recorded and the cut-off frequency has been determined as 251 nm. The powder SHG efficiency of $_L$-Lysine doped TGBC crystal is about 0.5 times that of KDP.

1. Introduction

The search of new frequency conversion materials over the past decade has led to the discovery of many organic non-linear optical materials with high non-linearity susceptibility. Hence, recent search is concentrated on semiorganic materials due to their large non-linearity, high resistance to linear induced damage,low angular sensitivity and good mechanical hardness [1-3]. Amino acids with inorganic compounds are promising material for non-linear optical applications [4]. Especially natural amino acids of aspartic acid, $_L$-Lysine, $_L$-Alanine, glutamic acid and γ-glycine evidently showing non-linear activity because of an additional COOH group in first and NH_2 in second carbon [5].

Some complexes of glycine with HCL [6,7], benzoyl glycine [8] forms single crystal with non-linear property. So we report that growth of $_L$-Lysine doped triglycine barium chloride crystal for the first time. The grown crystals were characterized using single crystal XRD and powder X-ray diffraction, fourier transform infrared (FT-IR) analysis, and UV-vis spectroscopy. In order to confirm the nonlinear optical property, powdered sample of $_L$-Lysine doped TGBC was subjected to KURTZ and PERRY techniques

2 .SYNTHESIS AND GROWTH

The single crystals of L-Lysine doped triglycine barium chloride crystal (TGBC) were grown by conventional slow evaporation method. The solubility of $_L$-Lysine doped triglycine barium chloride crystal was held by double distilled water. A super saturated solution of $_L$-Lysine doped triglycine barium chloride crystal were prepared in beaker with stirrering upto 8 hours and then filtered using whatmann filter paper. After filteration the supersaturated solution in the beaker was covered with a perforated polythene sheet then kept at a room temperature. The grown crystal was synthesized on the following equation ,

$CH_2N(CH_2)_4CH(NH_2)$ + Ba $(NH_2\text{-}CH_2\text{-}COOH)_3\,Cl_2$ → Ba. $CH_2N(CH_2)_4CH(NH_2)$ $(NH_2\text{-}CH_2\text{-}COOH)_3\,Cl_2$

A good quality of seed crystal were obtained, optically transparent single crytal were harvested after 31 days in the dimension 7x9x2 mm^3. The grown crystal were shown in figure 1.

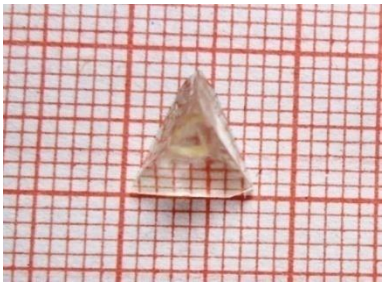

Figure 1. As grown crystal of $_L$-Lysine doped TGBC

3. Characterization

3.1 Single and Powder X-Ray Diffraction analysis

Single crystal X-ray diffraction analysis of L-lysine doped Tri glycine barium chloride was recorded .The calculated lattice parameters are a=5.23Å, b=8.67Å, c=13.67 Å, α=β=γ=90^o and volume V= 619.85 $Å^3$ which confirm that grown L-lysine doped Tri glycine barium chloride crystal belongs to the orthorhombic crystal system. The grown crystal were characterized by powder x-ray diffraction to confirm the crystalline nature of the grown crystal by using BRUCKER, Germany (model D8 Advance) X-ray diffractometer with CUK_{alpha} (wavelength = 1.5405Å) radiation. The sample were scanned for 2θ value for 10 º to 90º at a range of 2º per minute. Figure 2 shows the powder XRD pattern of grown crystal. The presence of sharp well-defined Bragg's peaks conforms the good crystalline nature of the grown crystal.

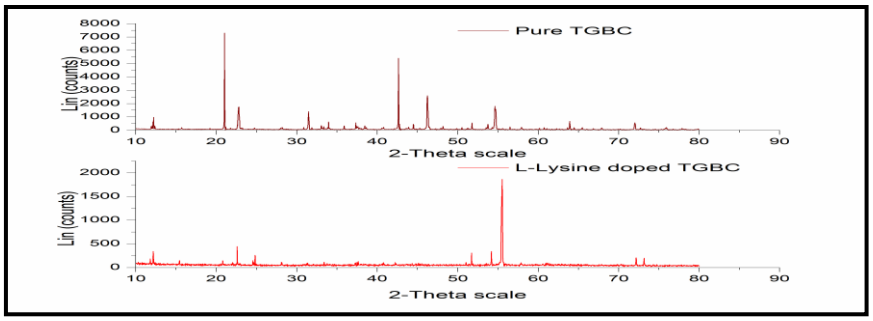

Figure 2 shows the powder XRD pattern of grown crystal

3.2. Linear Optical Studies

Well polished defect free good transparent crystals are subjected to linear optical study. Both the crystals have thickness around a and b respectively used for the optical studies. The observed spectrum of pure and doped are shown in figure 3. From the spectrum it is observed that the grown pure and $_L$-Lysine doped TGBC crystal has good transparency and cut-off wavelength is around 234 nm and 251nm. The addition of $_L$-Lysine with pure TGBC may induced the transparency with higher

value. Also observed from the spectrum of both compounds are having wide transparency may have advantages for these crystals to be utilized in the field of photonics and opto-electronics.

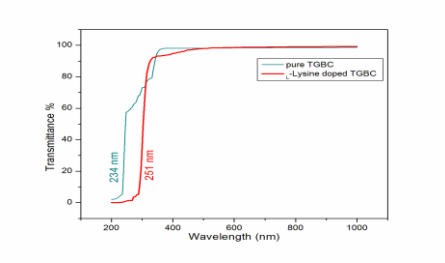

Figure 3. Optical transmission of pure and doped TGBC

3.3. Nonlinear optical study

In order to confirm the nonlinear optical property, powdered sample of $_{L}$-Lysine doped TGBC was subjected to KURTZ and PERRY techniques, which remains powerful tool for initial screening of materials for SHG efficiency. The powder SHG efficiency of Tri-GBC crystal is about 0.5 times that of KDP. The good second harmonic generation efficiency indicates that the $_{L}$-Lysine doped TGBC crystals can be used as suitable material for nonlinear optical deviceses.

Conclusion

Well developed good quality transparent crystal of $_{L}$-Lysine doped Tri-GBC was grown successfully by slow evaporation technique. Unit cell constants and crystal system were determined by single crystal X ray diffraction technique confirmed the identity of the synthesised material. Powder XRD shows good crystallinity of the grown crystal. The various functional groups presence in the grown crystal was identified by FTIR study. The UV cut off wavelength of $_{L}$-Lysine doped Tri-GBC crystal is found to be around 251 nm, which reveals grown crystal is potential candidate for NLO applications. The powder SHG efficiency of Tri-GBC crystal is about 0.5 times that of KDP.

Reference:

1. I. Ledourx, J. Badan, J. Zyss, A. Migus, D. Hulin, J. Etchepare, G. Grillon, A. Antonetti, J. Opt. Soc. Am. B4 (1987) 987–997.
2. S. Boomadevi, H.P. Mittal, R. Dhansekaran, J. Cryst. Growth 261 (2004) 55–62.
3. M.D. Aggarwal, J. Choi, W.S. Wang, K. Bhat, R.B. Lal, A.D. Shields, B.C. Penn, D.V. Frazier, J. Cryst. Growth 204 (1999) 179–182.
4. G.Xing, M.Jiang, Z.Shao, D.Xu, Chin.J. Lasers 14[1997] 302-308.
5. A. Kandasamy, R. Siddeswaran, P. Murugakoothan, S.P. Kumar, R. Mohan, Synthesis, Growth, and Characterization of l-Proline Cadmium Chloride Monohydrate (l-PCCM) Crystals: A New Nonlinear Optical Material, Cryst. Growth Des. 7 (2007) 183-186.
6. K. Ambujan, K. Rajarajan, S. Selvakumar, I. vetha potheher, G.P. Joseph, P. Sgayaraj Growth, Optical, Dielectric and Fundamental Properties o NLO active L-histidinium Perchlorate Single Crystals, J. Crystal.Growth 286 (2006) 440-444.
7. D. Eimerl, S. Velsko, L. Davis, F. Wang, G. Loiacona, G. Kennedy, Deuterated L-arginine phosphate: a new efficient nonlinear crystal, IEEE Quantum Electron. 25 (1989) 179-193.
8. K. Meera, R. Muralidharan, R. Dhanasekaran, Prapun Manyum, P. Ramasamy, Growth of nonlinear optical material: L-arginine hydrochloride and its characterization, J. Cryst.Growth 263 (2004) 510-516.

Synthesis and Characterisation of 4-(5-Chlorothiophen-2-Yl)-1, 2, 3-Selenadiazole

S.Sankari

Sri Sarada College for Women, (Autonomous), Salem-16.

Abstract

Bisheterocycles received considerable attention in recent times because of their pharmacological importance. Thiophene derivatives represent a class of important and well studied heterocycles. Hence it has been planned to synthesise hitherto unknown bisheterocycle 4-(5-Chlorothiophen-2-yl)-1,2,3-selenadiazole **3** in which selenadiazole unit is linked to thiophene ring at C-4. The structure of the 1,2,3-selenadiazole **3** was established from ^{1}H,^{13}C, 2D NMR, IR, mass and Single Crystal X-ray crystallographic study.

Introduction

In the last few decades the chemistry of thiophenes has received considerable attention owing to their synthetic and effective biological importance. 1,2,3-Selenadiazole derivatives possess a broad spectrum of biological activities [1-5]. Hence, it was thought that it would be worth preparing molecules having both 1,2,3-selenadiazole and thiophene units. The present work deals with the synthesis of bis heterocycle having a 1,2,3-selenadiazole in combination with a thiophene unit at C-4. Our synthetic procedure for hitherto unknown 1,2,3-selenadiazole derivative 4-(5-Chlorothiophen-2-yl)-1,2,3-selenadiazole **3** started from ketone **1** containing α-keto methylene group that was first converted into its corresponding semicarbazone. Subsequently the semicarbazone was converted into 1,2,3-selenadiazole derivative by the selenium dioxide oxidative ring closure [6](**Scheme1**).

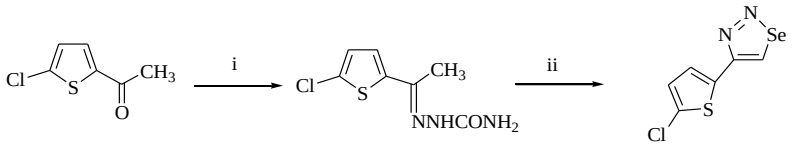

i. $NH_2NHCONH_2$. HCl / CH_3COONa / EtOH-Reflux
ii. SeO_2/THF- Reflux

Scheme1 Synthesis of 4-(5-Chlorothiophen-2-yl)-1,2,3-selenadiazole

Experimental

The NMR spectra were recorded on a JEOL GX 400 Spectrometer using TMS as internal standard and $CDCl_3$ as solvent. Chemical shifts are given in parts per million (δ-scale) and the coupling constants are given in Hertz. IR spectrum was recorded on a FT-IR-Shimadsu instrument (KBr pellet). The vibrational frequencies are reported in reciprocal centimeter. Mass spectrum was recorded on a JEOL GC mate instrument and Electro spray ionization (ESI) mass spectrum was obtained on Agilent mass spectrometer. The single crystal X-ray data were collected on a Bruker SMART APEX CCD detector diffractometer. The structure was solved by direct methods from SHELXS-97 and refined by full matrix least squares on F2 by SHELXL-97.

A mixture of acetyl thiophene **1** (1 mmol), semicarbazide hydrochloride (2 mmol) and sodium acetate (3 mmol) in ethanol (10 ml) was refluxed for 4 h. After completion of the reaction as monitored by TLC, the mixture was poured into crushed ice and the resulting semicarbazone **2** was

filtered off and dried. Then, a mixture of semicarbazone (1 mmol) and SeO_2 (2 mmol) in tetrahydrofuran (10 mL) was refluxed on a water bath for 1h. The selenium deposited on cooling was removed by filtration, and the filtrate was poured into crushed ice and purified by column chromatography using silica gel.

4-(5-Chlorothiophen-2-yl)-1,2,3-selenadiazole (3). Colourless solid; Yield - 73%; m.p. 156-158 ^oC; IR (KBr): 1585, (N=N), 702 (C-Se) cm^{-1}; ^1H NMR (300 MHz, $CDCl_3$) δ_H (ppm): 6.97 (d, *J* = 4 Hz, 1H), 7.40 (d, *J* = 4 Hz, 1H), 9.21 (s, 1H, H-5); ^{13}C NMR (75 MHz, $CDCl_3$) δ_C (ppm): 125.2; 126.9; 131.4; 133.2; 135.1; 156.5. MS: m/z 250.90 (M+1).

Results and Discussion

The formation of cyclised product is evident from the absence of signals due to methylene protons (δ 2.45-2.55 ppm) and acetyl protons (δ 2.50-2.56 ppm) in the ^1H NMR of **3**. Disappearance of characteristic peak due to carbonyl group in the IR spectra (1650-1680 cm^{-1}) and ^{13}C NMR spectra (189-190 ppm) further confirmed the formation of products. The IR spectrum of selanadiazole displayed bands around 1550 cm^{-1} (N=N), and 700 cm^{-1} (C-Se) indicating the formation of selanadiazole ring.

The structure of the 1,2,3-selenadiazole **3** was established from ^1H, ^{13}C and two dimensional NMR spectroscopic data (**Figure1**).

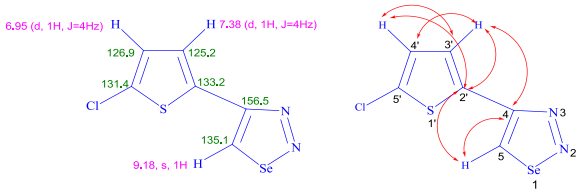

Figure 1 Selected HMBCs and ^1H and ^{13}C chemical shifts in compound **3**

The appearance of a strong singlet around δ 9-9.2 ppm and a weak doublet, centered on the singlet characteristic of 4-substituted selenadiazoles [7] are due to the ring selenadiazole hydrogen. This doublet is assigned to the splitting caused by the presence of the selenium isotope ^{77}Se with a natural abundance of 7.5%.

1) In the ^1H NMR spectrum, the H-5 proton appears as a strong singlet at 9.18 ppm and a weak doublet, centered around the singlet. This signal correlates with the signal at 135.1 ppm in C,H-COSY. This also shows HMBC contours with carbons at 133.2 and 156.5 ppm which are assignable to C-2' and C-4 respectively.

2) The H-3' proton appears as a doublet at 7.38 ppm (*J* = 4.0 Hz). This shows C,H-COSY correlation with the signal at 125.2 ppm assignable to C-3' and HMBCs with carbons at 126.9, 133.2 and 156.5.

3) The H-4' proton appears as a doublet (*J* = 4.0 Hz) at 6.95 ppm. It exhibits

i. H, H-COSY correlation with the doublet at 7.38 ppm.
ii. C,H-COSY correlation with C-4`at 126.9 ppm
iii. HMB correlation with C-3' at 125.2 ppm and C-2' at 133.2 ppm

4) Now, the signal at 131.4 ppm in the ^{13}C NMR spectrum is conveniently assigned to C-5'.

Table 1. Crystal data and structural refinement for 3

Empirical Formula	$C_6H_3ClN_2SSe$
Formula Weight	249.57
Temperature	293 K
Wave length	0.71073 Å
Crystal system	Monoclinic
Space Group	*P*21/*c*
Unit cell dimensions	$a = 6.0412\ (3)$ Å $b = 19.5870\ (11)$ Å; $\beta = 110.257\ (3)°$ $c = 7.2010\ (4)$ Å
Volume	799.38 (7) Å^3
Z	4
Density calculated	2.074 Mg m^{-3}
Absorption coefficient	5.22 mm^{-1}
F(000)	480
Crystal Size	0.22 × 0.20 × 0.18 mm
Theta range for data collection	2.1–28.3°
Reflections collected	1558

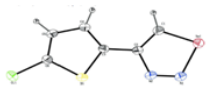

Figure 2 ORTEP diagram of 3

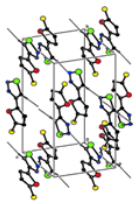

Figure 3 The crystal packing of 3.

The results of single crystal X-ray crystallographic study of 4-(5-chlorothiophen-2-yl)-1,2,3-selenadiazole **3** [7] are presented in Table1. The ORTEP diagram is shown in **Figure 2**. In the title compound, the selenadiazole and chlorothiophene rings are almost coplanar. The bond lengths [Se1—N1] 1.870 Å and [Se1—C1] 1.825 Å are comparable with the values reported in the literature [8]. The packing of the molecules is shown in **Figure 3**. The crystal packing is stabilized by C—H····N intermolecular interactions, linking the molecules to chains extending along the *b* axis.

Conclusion

The synthesis and complete characterisation of 4-(5-Chlorothiophen-2-yl)-1,2,3-selenadiazole was described. As bisheterocycles are expected to have enhanced biological activities because of the two heterocyclic moieties present in its structure, the synthesized compound can be evaluated for its biological activities.

References

1. Lalezari, I.; Shafiee, A.; Yalpani, M. *J. Org. Chem.* **1971**, *36*, 2836.
2. Lalezari, I.; Shafiee, A.; Khorrami, J.; Soltani, A. *J. Pharm. Sci*. **1978**, *67*, 1336.
3. Lalezari, I.; Shafiee, A.; Yazdani, S. *J. Pharm. Sci*. **1976**, *65*, 628.
4. Chitra, S.; Paul, N.; Muthusubramanian, S.; Manisankar, P.; Yogeeswari, P.; Sriram, D. *Euro. J. Med. Chem*, **2011**, *46*, 5465.
5. Arsenyan, P.; Rubina, K.; Shestakova, I.; Domracheva, I. *Eur. J. Med. Chem.* **2007**,*42*,635.
6. Padmavathi, V.; Mahesh, K.; Nagendra Mohan, A. V.; Padmaja, A. *Chem.Pharm.Bull.***2009**,*57*,561.
7. Sugumar, P.; Sankari, S.; Manisankar, P.; Ponnuswamy, M. N. *Acta Cryst.* **2013**, *E69*, o65.
8. Allen, F. H.; Kennard, O.; Watson, D. G.; Brammer, L.; Orpen, A. G.; Taylor, R. *J. Chem. Soc. Perkin Trans.* **1987**, *2*, 1.

Growth and Characterization of Succinic Acid Doped Potassium Hydrogen Phthalate (KHPSA) Crystal

R. Arul jothi[a], R.U. Mullai[a], E. Vinoth[a], G.Selvi[a], S. Vetrivel[a*]

[a]Raman Research Lab, PG & Research Department of Physics, Government Arts College, Tiruvannamalai-606 603, India.

**Corresponding author: vetrivelsivaraman@yahoo.com*

ABSTRACT

Succinic acid doped Potassium hydrogen phthalate (KHPSA) semi-organic single crystals were grown by slow evaporation method at room temperature. Powder X-ray diffraction pattern was recorded for conformation of crystalline nature of the grown crystal. FTIR spectral analysis confirms the presented functional groups in the synthesized compound. The UV–Vis–NIR spectrum showed that the grown crystal is transparent in the entire visible region. TGA/DTA analysis were carried out to characterize the melting behavior and Thermal stability of the title compound. The dielectric constant and dielectric loss of the crystal were studied as function of frequency. Morphology and compositions of the KHPSA crystal was carried out by SEM with EDS.

Keywords: crystal growth, X-ray diffiraction, thermal analysis, dielectric materials and SEM.

1. INTRODUCTION

The search for new conversion materials for various device applications has led to the discovery of many organic, inorganic and semi organic materials. Among these Semi organic crystals have attracted considerable interest due to their large nonlinear optical (NLO) coefficients, high resistance to laser induced damage, low angular sensitivity, excellent mechanical hardness fluorescence properties because of their potential applications such as, telecommunication, optical computing, optical data storage, light emitting diodes, and optical information processing [1, 2].

Potassium hydrogen phthalate (KHP) is also called as potassium acid phthalate (KAP) is a semi-organic material. It is also one of the important NLO crystals in the alkali metal acid phthalate (MAP) family [3]. It belongs to the orthorhombic class of alkali acid phthalate series. The crystal structure of KAP is assigned to the Pca21 [4] space group, consisting of potassium ions and alkali phthalate ions. Recently KAP crystals are used as substrate for epitaxial growth of oriented polymers [5, 6] and for hierarchical growth of organized materials [7]. KAP crystals are playing an important role in the field of non linear optical materials, they are known second harmonic generating materials that have long stability in devices due to their electro-optical properties [8] and exhibit interesting piezoelectric, pyroelectric and elastic properties that are useful in many application [9,10]. Its higher chemical stability and economic viability with good kinetic growth properties have made to pay attention on it in past decades.

Generally Succinic acid has wide applications in many fields, like industry, medicinal, organic intermediates for the pharmaceutical, engineering plastics, resins. Particularly in the chemical industry it is used for the production of dyes, alkyd resin, glass fiber reinforced plastics, ion exchange resins and pesticides. By using these potential sites, in the present work, the effect of succinic acid on thermal, optical and electrical properties of KHP have been analysed. The grown crystals were

subjected to different characterization such as Powder XRD, UV-visible, FTIR spectral studies, Thermal, SEM and Dielectric study.

2. EXPERIMENTAL PROCEDURE

2.1. SYNTHESIS AND GROWTH

The KHPSA salt was obtained from an aqueous solution containing potassium hydrogen phthalate and succinic acid in a 1:1 molar ratio. The calculated amount of starting materials for the synthesis was obtained according to the reaction ,

$$K(C_6H_4COOH\text{-}COO) + C_4H_6O_4 \rightarrow KC_8H_5O_4.\ C_4H_6O_4$$

The calculated amount of KHP was first dissolved in Millipore water of 18.2 MΩ cm resistivity. The calculated amount of succinic acid added to the solution slowly and stirred well using a temperature controlled magnetic stirrer about 18 hours to yield a homogenous mixture of solution. Then it was double times filtered with Wattmann filter paper and poured into petri dishes. Then the filtered solution was allowed to evaporate at room temperature and the mixed salt was obtained by slow evaporation technique. The purity of the synthesized salt was further improved by successive recrystallization process. By this method the seed obtained has been used for the bulk growth. Good quality single crystals with size 13 × 5 ×2 mm^3 was harvested at the period of 23 days with appropriate growth rate of 0.56 mm/day. The photograph of as grown KHPSA crystals are shown in figure 1.

Figure 1. As grown KHPSA crystals

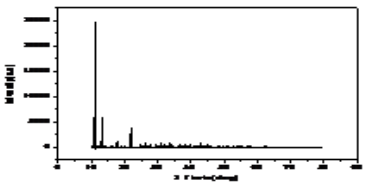

Figure 2 powder X-ray diffraction pattern of KHPSA crystal

3. RESULT AND DISCUSSION

3.1 POWDER X-RAY DIFFRACTION

Powder X-ray pattern for NLO single crystal was recorded and shown in figure 2. To identify the reflection planes and to check the crystalline perfection of the grown crystal, powder X-ray diffraction patterns of the powdered sample have been recorded using a Reich Seifert diffractometer with CuKα (λ = 1.5418 Å) radiation at 30 kV, 40 mA. The synthesized grown crystal was scanned over the range from 10° to 80° diffraction angle at a scan rate of 2°/minute at room temperature.

The powder X- ray pattern of KHPSA crystal consist a set of prominent sharp peaks as shown in figure 2. The well-defined peaks at specific 2-theta values show high crystallinity of the grown crystal.

3.2 FTIR SPECTRAL STUDIES

The FTIR is used to identify the different functional groups present in the compound of the grown crystal. The FTIR spectrum of KHPSA crystal was recorded in the region 500–4000 cm^{-1} from KBr pellets on a Perkin Elmer FTIR spectrometer as shown in figure 3.

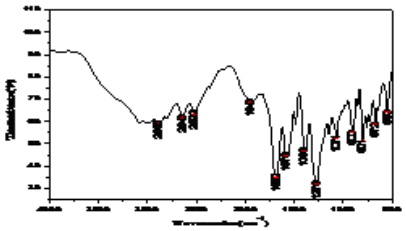

Figure 3 FTIR spectrum of KHPSA crystal

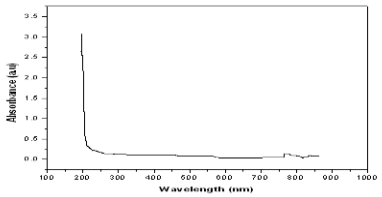

Figure 4 UV-Vis absorption spectra of KHPSA crystal

The band 2885cm^{-1} has been assigned to the C-H stretch. The 2648 cm^{-1} is characteristic of C-H stretch. The other peak at 2522 cm^{-1} is assigned to O-H bending. The peak at 1949 cm^{-1} represents C=C asymmetric stretch. The peak at1680 cm^{-1} represents -C=C- stretching. The peak at 1579 cm^{-1} is assigned to N-H bending. The peak at 1398 cm^{-1} is assigned to C-C stretching. The very strong peak observed at 1279 cm^{-1} is attributed vibration of the C-H Wag. The peak at 1071 cm^{-1} is assigned to C-N stretching. The predominant peaks appeared between 903 and 553 cm^{-1} may be due to the vibrations involved by metal atoms in the crystal [11].

3.3 OPTICAL ABSORBTION SPECTRA

The optical absorbtion spectrum of the grown KHPSA was recorded using Perkin Elmer Lambda 35 UV-Visible spectrophotometer in the wavelength range from 200 to 900 nm. The recorded spectrum is shown in figure 4. The KHPSA crystal has the lower cut-off wavelength at 210 nm in the UV region. The crystal does not exhibit any absorption band in the entire visible region up to 850 nm. Absence of absorption between 220 nm and 870 nm is an advantage, as it is the key requirement for materials possessing SHG properties. As a result, it can be used as a potential candidate for the SHG device applications in the visible region [12].

3.4. THERMAL ANALYSIS

In order to study the thermal stability of the grown crystals, thermo gravimetric (TG) and differential thermal analysis (DTA) have been carried out using a Seiko TG-DTA 6200 model thermal analyzer in an inert nitrogen atmosphere. Powdered sample of about 3.437 mg was used for the analysis in the temperature range of 30 - 500°C with a heating rate of 20°C/minute. The TG-DTA pattern recorded for the KHPSA crystal as shown in figure 5.

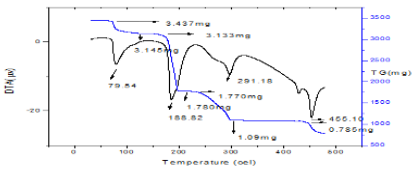

Figure 5 TG-DTA Curves of KHPSA crystal

The above TG curve major weight loss occur at three stages. First weight loss occur with 8.84% at 75°C is due to water molecules which exist in the crystal. The second weight loss occur with 43.18% at 165°C and the third weight loss occur with 38.41% at 189°C. This weight losses are conformed for sharp endothermic peaks of a DTA trace. The three endothermic peaks occurring at different temperatures. These three different stages indicate the decomposition of the substance. This indicates that the crystal have high melting point(188.82°C) and it exhibit high thermal stability.

3.5 DIELECTRIC STUDIES

Dielectric is an important property to support an electrostatic field while dissipating minimal energy in the form of heat. Figure 6 shows that the dielectric loss varies inversely proportional to frequency of the KHPSA crystal.In figure 6 the amount of loss decreases when frequency increases for all temperatures. At low temperature 40 ºC the dielectric loss has a high value 7.55. At high temperature 85 ºC the dielectric loss has a value is very very low (ie.,negative value). Due to this reason the KHPSA crystal used for high temperature.The variation of dielectric constant with log of frequency for the KHPSA crystal at different temperatures has been recorded as shown in figure 7. The high value of 'ε_r' at lower frequencies may be due to the presence of all the four polarizations, namely space charge (Interfacial), orientation, electronic and ionic polarization and its low value at higher frequencies may be due to the loss of significance of these polarizations gradually. The electronic and ionic polarizations are due to the displacement of electrons and ions respectively under an applied electric field and are temperature independent. The orientational polarization occurs due to alignment of permanent dipoles which are otherwise randomly oriented; under the action of electric field. The interfacial polarization occurs when mobile charge carriers are obstructed by a physical barrier that inhibits charge migration. As the frequency increases the dipoles do not completely with the varying external field. The polarization decreases and hence the dielectric constant decreases as the frequency increases.

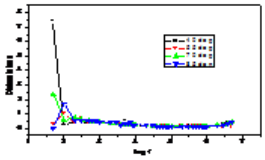

Fig. 6 Variation of dielectric loss with log frequency for KHPSA crystal

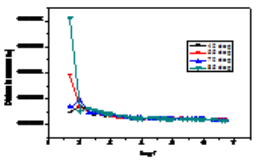

Fig.7. Variation of dielectric constant with log frequency for KHPSA crystal

From the above dielectric constant figure, one can notice that the ε_r has high values in the very lower frequency and then decreases with applied frequencies. Generally the low value of dielectric loss at high frequency for these samples suggests that the samples possess enhanced optical quality and this parameter is vital importance for NLO materials in their application [13-14].

3.6 SEM WITH EDS ANALYSIS

SEM analysis provided information about the nature, suitability for device fabrication and also it is used to check the presence of imperfections. SEM analysis was carried out using JEOL JSM-5610 LV scanning electron microscope with an accelerating voltage of 20 KV, at high vacuum mode and secondary electron image (SEI). since semi organic crystals are non-conducting in nature, gold coating(JEOL auto fine Coater JFS-1600) was done for 120 s before subjecting KHPSA crystal surface to electron beam [15]. KHPSA crystal has well developed morphology with several habit faces (figure 8.). It exhibiting layered growth and it is observed that the basic units are arranged in different layers, which is a clear evidence for the stacking of fundamental units during crystal growth. KHPSA crystal was also analysied by energy dispersive spectroscopy (EDS) for qualitative and quantitative information and shown in figure 9. From the EDS spectra potassium (k) metal present in the KHPSA crystal.

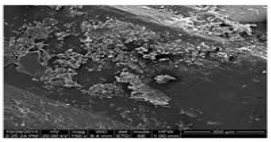

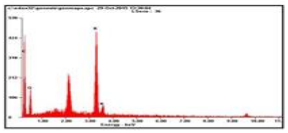

Figure 8 SEM image of KHPSA crystal **Figure 9 EDS spectrum of KHPSA crystal**

CONCLUSION

Good quality single crystals of the succinic acid doped KHP crystal were grown by slow evaporation solution growth technique. Powder XRD studies reveals that the grown KHPSA crystal is having good crystallinity. The optical transmission spectrum showed that succinic acid doped KHP crystal has good transparency in the UV-Vis region. The FTIR spectrum reveals the various functional groups presented in the grown crystal. The TG/DTA analysis shows that the thermal stability of the grown KHPSA crystal. The surface morphology and some elemental compositions of the crystal were reported by SEM with EDS analysis.

REFERENCES

1. Wiliams J (ed) (1983) American Chemical Society Symposium Series 233, American Chemical Society, Washington DC
2. Chemla DS, Zyss J (eds) (1987) vol 1 and 2. Academic press, New York
3. Kumaresan, P; Moorthy Babu, S; Anbarasan, P.M;. Optical Materials. 2008, 30, 1361-1368
4. Y.Okaya, Acta Crystallogr.19 (1965) 879
5. S.Timpanaro, A.Sassella, A.Borghesi, W.Porzio, P.Fontaine, M.Goldmann, Adv.MATER. 13 (2001)127
6. T.Haber, R.Resel, A.Thierry, M.Campione, A.Sassela, M.Moret, Physica E41 (2008) 133
7. Y.Oaki, H.Imai, Chem.Commun.48 (2005) 6011
8. N.Kejalakshmy, K.Srinivasan, J.Phys.D:Appl.Phys.36 (2003) 177
9. A.Miniewicz, S.Bartkiewicz, Adv.Mater.opt.EWlectron.2 (1993) 157
10. N.Kejalakshmy, K.Srinivasan, Opt.Mater.27 (2004) 389
11. A. M. Petrosyan, R. P. Sukiasyan, H. A. Karapetyan, S. S. Terzyan, R. S. Feigelson, J. Crystal Growth, 213, 103 (2000)
12. K.Kirubavathi, K.Selvaraju, N.Vijayan, S.Kumararaman, spectrochim. Acta A 71 (2008) 288
13. K. Jagannathan, S. Kalainathan, T. Gnanasekaran. Mater. Lett. 61, 4485 (2007)
14. C. Balarew, R. Duhlew, J. Solid State Chem. 55, 1 (1984)
15. R. Jerald Vijay, N. Melikechi, T. Rajeshkumar, M. Jesudurai, P. Sagayaraj , J. cryst. Growth (2010) 420-425

Growth, Structural, Spectral, Mechanical, Electrical and Optical Properties of Potassium Hexacyano Ferrate (KHF) Single Crystals

A. Asha[1], E. Vinoth[1], T. Suresh[1], k.kanagasabapathy[2], S. Vetrivel[1*]

PG & Research Department of Physics, Government Arts College,Tiruvannamalai-03.

[2] PG & Research Department of Physics , Arignar Anna Government Arts College,Villupuram-02.

**Corresponding author: vetrivelsivaraman@yahoo.com*

Abstract

Single crystal of potassium hexacyano ferrate (KHF) have been successfully grown by the slow evaporation technique at room temperature has dimensions 23 ×10 ×3 mm^3. The grown crystal was characterized structurally, optically, thermally, mechanically and electrically. Lattice parameters of the grown crystal were determined by X-ray diffraction analysis. The functional groups present in the crystal were identified using Fourier Transform Infrared spectral analysis. UV-Vis-NIR spectrum was recorded to estimate the UV cut-off wavelength and transparency. Second harmonic generation study confirms the NLO property. Thermal stability and decomposition of the crystal has been studied by TG/DTA analysis. Micro hardness measurement indicates the grown crystal exhibits normal indentation size effect. The frequency and temperature dependence of dielectric constant and dielectric loss were also studied.

Keywords: Single crystal XRD, powder XRD analysis, FT-IR, UV-Vis-NIR spectrum, Thermal analysis, microhardness and Dielectric properties.

1. Introduction

In last few decades, the researchers are interested in Non- linear optical material, due to their application in the field as optical communication, signal processing instrumentation [1]. The organic NLO material play on important role in second harmonic generation, Electro optic modulation [2,3]. Extremely large number of organic compounds with non localized - electron system large dipole moment has been synthesized to realize the non linear susceptibilities [4,5]. Many investigations are being carried out to synthesize new material the large second order optical nonlinearities in order to satisfy, day to day technological demands [6-9]. In search of new frequency conversion materials, recent interest focused on inorganic materials due to their NLO properties [10-12]. From the literature survey investigation are focused on potassium hexacyano ferrate material due to its various desired applications . In the present of investigation, the potassium hexacyano ferrate single crystal by slow evaporation technique studied the cell parameter using single crystal XRD. Mechanical behavior was analyzed using vicker's micro hardness test. The NLO property of the grown crystal was confirmed by Kurtz powder SHG method [13]. Dielectric constant and dielectric loss measurements were carried out at different temperaturs and frequencies.

2 .Experimental procedure

Saturated solution of PHF was prepared at room temperature. The solution was continuously stirred for 4 hours using magnetic stirrer and the solution was filtered using whatman filter paper and

transferred into a petri dish and allowed to evaporate slowly in room temperature. The PHF single crystals of size 23×10×3 mm^3 were harvested after the 18 days as shown in figure.

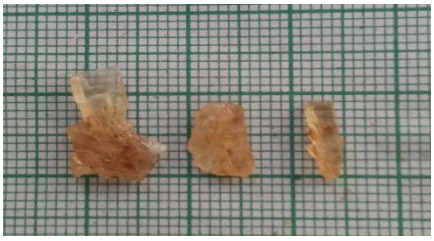

3.Charactrization

3.1 Single Crystal X-Ray Diffraction Studies

A fine quality KHF crystal was kept on an Xcalibur Eos diffractometer at 293(2) K. Single crystal X-ray diffraction analysis of these single crystal have been carried out and the unit cell parameters are given in the Table 1.

Table 1. Lattice parameter of grown KHP Crystal

Lattice parameter	Obtained valus
Crystal system	Triclinic
Space group	P
a (?)	7.401
b (?)	7.487
c (?)	13.436
A	96.25°
B	98°
Γ	90.85°
V(Å^3)	733α

3.2 FT-IR Studies

The FT-IR spectral study used to identify the different functional groups present in the compound of the grown crystal. The FT-IR spectrum of KHF crystal was recorded in the IR region 400–4000 cm^{-1} from KBr pellets on a Perkin Elmer FT-IR spectrometer as shown in Fig.1. The band 3439cm^{-1} has been assigned to the NH–Symmetric &Asymmetric stretch. The 2506, 2292 cm^{-1} is characteristic of OH stretch. The other peak at2118 cm^{-1} is assigned to C=C stretch. The peak at 1822 cm^{-1} represents the C=O – Symmetric & Asymmetric stretch, the peak at1631 cm^{-1} represents -C=O- stretching. The peak at 1390 cm^{-1} is assigned to CH3 C-H bending. The peak at1103 cm^{-1} is assigned to C-O stretching. The very strong peak observed at 791 cm^{-1} is attributed vibration of the = C-H bend. The peak at 593 cm^{-1} is assigned to C-Br stretching. The predominant peaks appeared may be due to the vibrations involved by metal atoms in the crystal [14].

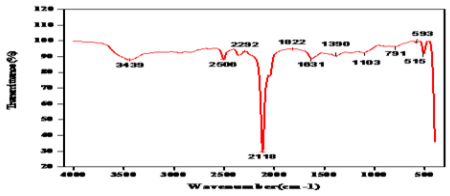

Fig.1. FT-IR Spectrum of pure KHP crystal

TABLE 2.Band assignment of FTIR spectra for KHP Crystal

Wave Number(cm^{-1})	Assignments
2506 ,2292	OH- stretch
2118	C=s tretch
1822	C=O –Symmetric & asym. stretch
1631	C=O stretch
1390	CH3 C-H Bend
1103	C-O stretch
791	=C-H Bend
593,515	C-Br stretch

3.3 Linear Optical Studies

The linear optical studies of potassium hexacyano ferrate (PHF) were carried out using UV-VIS NIR spectrum. From the UV-Vis spectral study a transmission co-efficient are determined. Optical transmission spectrum of PHF crystal was recorded in the range 200-1000 nm.

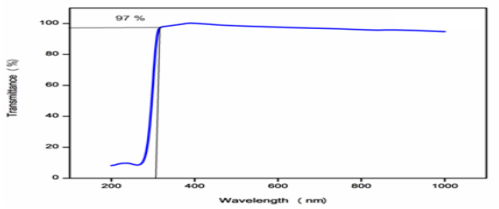

Fig.2. UV-Vis transmittance spectrum of KHF crystal

The recorded spectrum is shown in fig.2. from the optical spectra the UV cut off wave length is 306 nm and the transmittance percentage is 97 %.the high transmission in the entire visible region and short UV-cutoff wavelength evident that the grown crystal KHF to be a potential candidate for non- linear optical applications.

3.4 Thermal Analysis

In order to study the thermal stability of the grown crystal, thermo gravimetric (TG) and differential thermal analysis (DTA) have been carried out using a Seiko TG-DTA 6200 model thermal analyzer in an inert nitrogen atmosphere. Powdered sample of about 15 mg was used for the analysis in the temperature range of 30–800°C with a heating rate of 20°C/minute. The TG-DTA pattern recorded for the KHF crystal as shown in Fig.3.

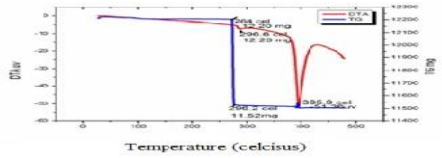

Fig. 3 Thermal Analysis (TG-DTA)KHF Crystal

From the TG curve, there is a weight loss at 296.2°C. The sharp endothermic peak around 395.9°C is assigned to melting point of the KHF. The exothermic peaks are good agreement with TG trace.

3.5 Non-Linear Optical Property Studies

The powdered sample prepared from the grown crystal was subjected to the SHG test by Kurtz and Perry powder technique and the efficiency of the energy (frequency) conversion is

confirmed by the emission of green light. The KDP sample was used as the reference material. The SHG efficiency estimated for both the crystals are given in the Tab. 3

Table 3. SHG Efficiency of KHF Crystal

Sample	Output	SHG efficiency
KDP	8.8	0.14
KHF crystal	1.2	

It is observed from Table 3 the SHG efficiency of mixed crystal, when compared with KDP it is low SHG efficiency. NLO efficiency of KHF crystal has found to be 14% when compared to standard KDP. SHG efficiency has to be increase for enhancing the NLO property for future work.

3.6 Dielectric Studies

Dielectric is an important property, its ability to support an electrostatic field while dissipating minimal energy in the form of heat. The variation of dielectric constant and dielectric loss with log of frequency for the crystal KHF different temperatures has been recorded as shown in Fig.4a & 4b. Figures show that the dielectric constant and the dielectric loss are both inversely proportional to the applied frequency at low frequency range.

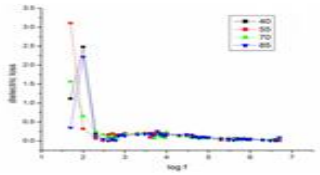

Fig.4a.Log f vs.dielectric loss of PHF

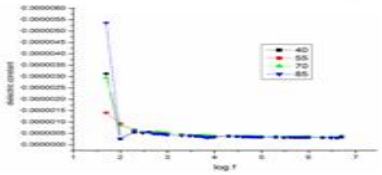

Fig.4b. Log f vs.dielectric constant of PHF

At 85°C the dielectric constant of KHF has high value in the low frequency range. The variation in dielectric loss with frequency within the temperature range 40°C to 85°C is shown in Fig.4a. At low temperature (40°C) the dielectric loss has a high value, at high temperature (85°C) the dielectric loss has a low value. At 55°C the dielectric loss of KHF has high value in the low frequency range (ie.50 Hz). The low value of dielectric loss at high frequency for KHF crystal suggests that the sample possess enhanced optical quality with fewer defects and this parameter is of vital importance for NLO materials in their application [15]

3.7 Microhardness Studies

Micro hardness testing is the one of the best methods for an understanding the mechanical properties of materials, the transparent polished crystal free from cracks was selected for hardness measurement .the indentation, where made soon the felt surface with the load ranging from 25gm to 100gm using shimodzu make-model-HMV_2 filed with Vickers pyramidal indenter and attached to an incident light microscope. The indentation time was kept as 5s for all the loads. The Vickers hardness (Hv) was calculated from the relation.

$Hv = 1.8544p/ d^2$ kg/mm^2

Where p is the applied load in kg and d is average length in mm and Hv is in kg/mm^2 the variation of vickers and MOHS hardness value with increasing load decreasing as shown in Fig.5a.It is observed from the graph, that the hardness value increases with increase in the applied load. Above

50gm, the hardness suddenly decreases, as cracks developed in the material. This may due to the relax of internal stresses generated locally by indentation [16].

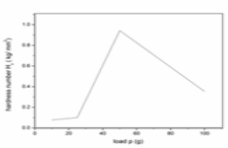

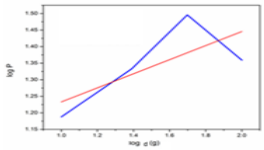

Fig.5a. Variation of H_V vs. Load of PHF crystal **Fig.5b.Plot of log p vs.log d of PHF crystal**

Meyer's index number was calculated from Meyer's law, which relates the load and indentation diagonal length as the $p = K \times d^n$,where k is the material constant and n is Meyer's index. In order to find the value of 'n' a graph of load p against load d is platted as shown in Fig.5b. from the slope of Meyer's index numbers 'n' was calculator too be 0.212. According to on its criteria the value of 'n' lies between 1 and 1.6 of hard material and is greater than 1.6 for hard material [17]. The 'n' values calculated in the percent study is <1.6 suggesting that the potassium hexacyano ferrate III crystal belongs category of hard material.

Conclusion

Synthesis, growth and characteristics of KHF crystal were studied. The KHF crystal was grown from aqueous solution by SEST method at room temperature. The single crystal XRD was recorded, that reveals KHF crystal belongs to Triclinic and possesses P space group. The presence of functional groups in the grown KHF crystal has been confirmed by FTIR analysis. The optical transmission spectrum has been recorded in the wavelength region between 200 nm and 1000 nm. The NLO study was carried out and it reveals the KHF crystal has 0.14 times NLO efficiency than that of KDP. The thermal properties have been studied by obtaining TG-DTA curves. The electrical properties were studied by dielectric constant studies. The mechanical properties were also studied by viker's microhardness study.

Reference

1. AnbuchundarAzhagan, S., Ganesan, S., Recent research in science in technology. 2(6) (2010) 107-109.
2. Badan. J.,Hierle, R.,Perigaud, A.,Zyss.J.,Non linear optics properties of organic molecules and polymeric,materials,3rd ed.Washington: DC: (1993).
3. Chemla, D.S., Zyss, (Eds), NON linear optical properties of organic molecules and crystals, 2nded. New York: Academic press:(1987).
4. Suresh Kumar, M.R., Ravindra, H.J., Jayarama, A., Dharmaprakash, S.M., J. Cryst Growth, 286 (2006) 451.
5. Narayan Bath. M., Dharmaprakash, S.M., J. Cryst Growth, 243 (2002) 526.
6. Meir, U., Bosch, S., Boshard, C., Gunter, P., Synth. Met., 109 (2000) 19.
7. Suresh, S., J. African Review of Physics, 8 (2013) 6.
8. Shen, Y.R., The Principle of Non Liner optics, (Wiley, New, 1984).
9. Ledoux, I., and Zyss, J., Int. J. Nonlinear Opt Phys. 3 (1994) 287.
10. Xing, G., Jiang, M., Zishao, X., aandXu, D., J. Lasers 14 (1987) 357.
11. Versko, S., Laser Programme Annual Report, Lawrence UCRCJC 105000, Lawrence Livermore National Laboratory, Livermore CA. (1990).
12. Warren, L.F., Electronic Materials our future in: Allred, R.E., Martinez, R.J., Wischmann, K.B., (Eds) Procedings of the forth International Sample Electronics Society for the Advanced of Materials and Process Engineering of Materials and Process Engineering, Covina. 4 (1990) 388.
13. Kurtz, S.K., Perry, T.T., J. Appl. Phys, 39 (1968) 3798.
14. Sharda J Shitole and Saraf K. B Bull. Mater, Sci., 24, 461-468 (2001).
15. C. Balarew, R. Duhlew, J. Solid State Chem. 55 1 (1984).
16. Mott, B.W., Micro indentation hardness testing, Butter worth scientific publication, London, (1956).
17. Kalainathan, S., Jagannathan, K., Mechanical and surface analysis of stilbazoliumtosylate derivative crystals. J cryst growth. 310 (2008) 2043-9.

Synthesis, Growth, Optical Studies of Piperazine Doped Succinic Acid (PSA) Single Crystal

G.Periyannan [a], R.Arul jothi [a], R.U.Mullai [a], S. Vetrivel [a],*

[a] Raman Research lab, PG & Research Department of Physics, Government. Arts College, Tiruvannamalai-606 603, Tamil Nadu, India.

** Corresponding author: vetrivelsivaraman@yahoo.com*

ABSTRACT

Optical quality Single crystals of Piperazine doped succinic acid (PSA) were grown and harvested successfully at room temperature by slow evaporation method. Single crystal X-ray diffraction study shows the doped PSA crystal belong to orthorhombic system. Vibration frequencies were assigned from FTIR spectral analysis , which confirms the various presence of functional groups. The transmittance and absorbance of electromagnetic radiation is studied through UV Visible spectrum. Dielectric studies of the compound were also carried out.

KEYWORDS: Crystal growth, Single crystal XRD, FTIR spectral analysis, UV–Vis–NIR spectrum and dielectric studies.

1. INTRODUCTION

Non linear optical (NLO) crystals are of considerable interest and of great demand because of their application in science and technology [1-2]. The organic non linear optical single crystal have usually high melting point, high mechanical strength, but very poor second and third harmonic generation efficiencies. The non linearity of these materials is low compared to organic NLO crystals [3-4]. In contrast organic crystals exhibit higher non linear second and third order co-efficient, Laser damage, threshold, thermal and Mechanical properties [5-6]. In this present investigation we report the synthesis optic properties, crystal growth and characterization of a organic material piperazine succinic acid .

2. EXPERIMENTAL TECHNIQUES

2.1 SYNTHESIS AND GROWTH

The Piperazine and succinic acid was obtained from an aqueous solution in a 1:1 molar ratio. The calculated amount of Piperazine was first dissolved in Millipore water of 18.2 MΩ cm resistivity. Then the amount of succinic acid added to the solution slowly with few drops of HCL stirred well using a temperature controlled magnetic stirrer about 18 hours to yield a homogenous mixture of solution. Then solution was double times filtered with Wattmann filter paper and poured into Petri dishes. The filtered solution was allowed to evaporate at room temperature and the mixed salt was obtained by slow evaporation technique. The purity of the synthesized salt was further improved by successive recrystallization process. By using slow evaporation technique good quality single crystal with size $2.2 \times 0.4 \times 2$ mm^3 was harvested at the period of 20 days as shown in fig.1.

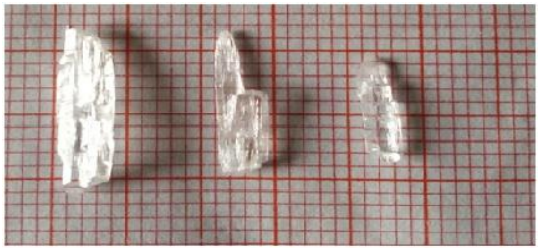

Fig 1.Photograph of PSA crystal

3. CHARACTERIZATION

3.1 SINGLE CRYSTAL X-RAY DIFFRACTION ANALYSIS

In order to estimate the crystal data, single crystal XRD analysis was carried out independently for the grown PSA crystal using CAD4-MV31 single crystal X-ray diffractometer with MoKα radiation. A good quality crystal was selected for the X-ray diffraction analysis studies. The single crystal XRD data of the grown crystal is presented in Table 1.

Table. 1 Lattice parameter of grown crystal

Crystal lattice parameter	Values
Crystal system	orthorhombic
a (?)	5.49
b (?)	7.66
c (?)	8.57
α	90°
β	90°
?	90°
V(Å^3)	361.2

3.2 FOURIER TRANSFORM INFRARED ANALYSIS

FTIR spectrum of piperazine doped succinic acid crystal were recorded using Perkin Elmer spectrum in the range 4000–500 cm^{-1}. FTIR and FT-Raman spectral studies for PSA were carried out to analyze the chemical bonding and molecular structure of the compound. The strong band at1720 cm^{-1}due to (C=O) of carboxylic acid group [7-8] is absent in IR and Raman spectra of PSA, which indicates that succinic acid coordinates to the metal ion through carboxylate (succinate) group[9]. The wave number and the corresponding functional groups are present in PSA crystal are shown in fig.2.

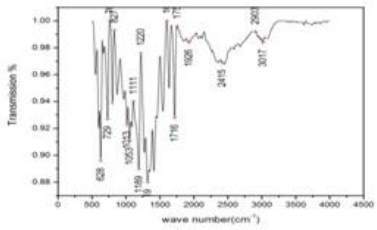

Fig.2 FTIR spectrum of PSA crystal

The band 628 cm^{-1} has been assigned to the C-H bending. The 763 cm^{-1} is C-H bending. The other peak is 827 cm^{-1} C-H bending. The peak at 1053 cm-1 is C-O_C symmetric stretching. The peak at 1220 cm-1 and 1319 cm^{-1} represents asymmetric stretching. The peak at 1603 cm^{-1} and 1669 cm^{-1} represents weak medium N-H bending. The peak at 1716 cm^{-1}represents C-O stretching.

The peak at 2043 cm^{-1} has assigned to C=C stretching. The band 2458 cm^{-1} due to O-H stretching. The peak observed at 2853 cm^{-1} represents O-H stretching. The band 3017 cm^{-1} has been assigned to the medium C-H stretching.

3.3 UV-VISIBLE SPECTRAL STUDIES

The Linear optics study of piperazine succinic acid was carried out using UV-VIS NIR spectrum. From the UV-Vis spectral study a transmission co-efficient are determined.

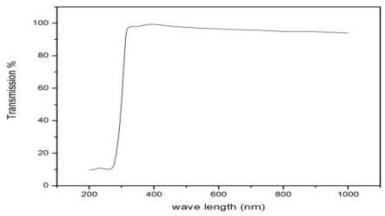

Fig. 3 . UV Transmission spectrum

Optical transmission spectrum of PSA crystal was recorded in the range 200 -1000 nm. The recorded spectra are shown in fig.3. The optical spectrum the UV cutoff wavelength is 255 nm, and the transmission percentage is 95%. The high transmission in the entire visible region and short UV-cut off wavelength evident that the grown crystal PSA to be a potential candidate for non-liner optical applications.

3.4 . DIELECTRIC STUDIES

The study of dielectric constant of a material gives an outline about the nature of atoms ions and their bonding in the material. From the analysis of dielectric constant and dielectric loss as a function of frequency and temperature, the different polarization mechanism in solids can be understood. The dielectric constant and the dielectric loss of piperazine succinic acid crystal were studied at different temperatures using HIOKI 3532 LCR HITESTER in frequency region 50 Hz to 5 MHz. The dielectric constant was measured as a function of frequency at different temperatures ranging from (40^0C, 55^0C, 70^0C, 85^0C) and is shown in fig.4, while the corresponding dielectric losses are depicted in fig.5. The dielectric constant is evaluated using the relation

$$\varepsilon_r = cd/\varepsilon_0 A$$

Where d is the thickness of the sample, A is the area of the sample[10].

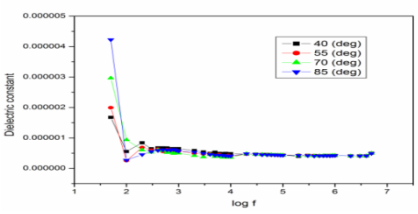

Fig.4 Dielectric constant

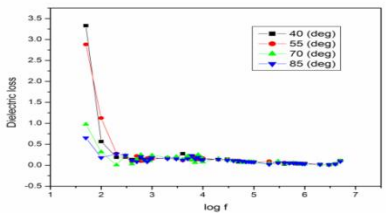

Fig.5 Dielectric loss

It is seen that dielectric constant value is high at low frequencies because, the electronic , ionic, dipolar and space charge or interfacial polarization are predominant. Further, as the frequency

increases, the dielectric constant decreases and for high frequency region, it is almost constant. This can be explained the based on polarization phenomenon. The low value of dielectric constant at higher frequency for a given crystal is a suitable parameter for the enhancement of SHG coefficient [11].From fig.5 it is observed that the dielectric loss decreases with frequency increases the low values of dielectric loss at high frequency suggests that the grown crystal possess good optical quality. This parameter is of vital important for a non linear optical material is the application [12].

4. CONCLUSION

The grown crystal piperazine succinic acid are successfully grown by slow evaporation method. The lattice parameters were found by single crystal X-ray diffraction technique. The fundamental groups presented in Piperazine succinic acid have been confirmed by FT-IR spectral analysis. From the UV-visible spectrum it has a good optical transmittance in the visible IR region. From the dielectric study, it is found that both dielectric constant and dielectric loss of the crystal decrease with an increase in frequency.

REFERENCES

1. Dimitriev UG, Gurzandyan GG, NIkigosyan DN, Hand book of non linear optical crystals [springer series in joptical science 1991, 64]
2. Eimeral D, Vels ko.S, Davis L, Wang F, crystal growth and characterization of materials , ed JB Mullin,20, 59.
3. Ledoux.S, Zyss J (1994) Non linear organic molecules and materials for opto electroni device, Int J Non linear Opt phys 3:287-316.
4. Mostad A, Natarajan S(1995) crystal and molecular structure of DL-Methionine nitsrate. Zkristallogr 210:114-117.
5. Shen YR(1984) The principle of nonlinear optics, wiley, Newyork.
6. Marcy Ho, warren LF, webb Ms, Ebbers CA, vels kosp, catella GC(1992) Second Harmonic generation in zin tris (thiourea) sulfate. Apple opt 31:5051-5060.
7. Raja CR, Kokila G, Joseph A (2009) Growth and spectroscopic characterization of a new organic nonlinear optical crystal:l-alaninium succinate spectrochim. Spectrochim Acta Part A72:753–757.
8. Krishnan S, Raj CJ, Robert R, Ramanand A, Das SJ (2009)Optical and dielectric studies on succinic acid single crystals.Cryst Res Technol 42:344–348.
9. Jisha KR, Suma S, Sudarsanakumar MR (2010) Synthesis,spectral characterization and thermal studies of zirconyl complexes of biologically active molecules. J Them Anal Calorim99:509–513.
10. Sagadevan suresh , The African review of physics (2013) 8 : 0006.
11. Meena.M, Mahadevan.C.K,Archj.Appl.Sci.Res., 2010,2(6),185
12. Balarew .C and dehlew .R , J solid state chem. 55 , 1(1984)

Synthesis and Characterization of Mno_2 Nanoparticles Doped Tio_2 Nanotubes Arrays

R. Mahesh[a], T. Manovah David[a,b] and P. Sagayaraj[a]*

[a]*Department of Physics, Loyola College (Autonomous), Chennai – 600 034*

[b]*Department of Chemistry, Madras Christian College (Autonomous), Chennai – 600 059*

Email: psagayaraj@hotmail.com

Abstract

MnO_2 nanoparticles deposited onto TiO_2 nanotubes array have a wide range of applications especially in the field of supercapacitors. In the present work, we have compared the electrodeposition of MnO_2 nanoparticles over TiO_2 nanotubes through two and three electrode systems, independently. It is observed from the morphological studies using field emission scanning electron microscopy (FESEM), elemental composition using energy dispersive X-ray spectroscopy (EDAX), transmittance spectra using fourier-transform infrared spectroscopy (FT-IR) and thermograms from thermo gravimetry and differential thermal analysis (TG-DTA) that the three electrode system electrodeposition of MnO_2 is better compared to the two electrode system electrodeposition.

Keywords: Titania, Anodization, Manganese oxide, Electrodeposition

Introduction

Recently, significant effort has been taken to produce one-dimensional TiO_2 nanotubes (NTs) through anodization [1,2] due to its noteworthy functionalities in several fields of applications like solar cells, gas sensors, super capacitors and electrochromic switches, etc [3]. The 1D architecture of the TiO_2 NTs provides a huge specific surface area, straight electron pathway, thus making it useful for several applications. However, direct usage of TiO_2 NTs is limited due to its semiconductive behavior. Therefore, to enhance the electronic properties of the NTs several efforts are taken by doping metallic or non metallic nanomaterials [4]. These methods did provide improvement in the advancement of properties but the processes limped in contributing to the orderly and uniform doping of the materials. In the present scenario, electrodeposition of these nanoparticles is observed to cover the surface of the NTs array completely [5].This electrodeposited NTs array has the capacity to beneficially implement it in several applications as such without modification. In this work, we have electrodeposited MnO_2 nanoparticles (NPs) onto TiO_2 NTs array. For comparison, electrodeposition was carried out using two electrode and three electrode system, labeled as MT1 and MT2, respectively. The observation clearly reveals that MT2 has better deposition of MnO_2 as nano spheres over TiO_2 NTs compared to MT1 which has unkempt deposition of MnO_2.The system MnO_2-TiO_2 is very useful in the field of energy storage as it can work as a better supercapacitor. Moreover, the system has merits in terms of usable capacity, high specific energy density, cycling life, cost, safety, environmental friendliness [6]. However, the adherence of MnO_2 plays a crucial role in defining the stability and capacity of the system. Therefore, we aim to compare the adherence of MnO_2 onto TiO_2 NTs electrodeposited through two and three electrode systems.

Experimental Section

TiO_2 NTs were prepared using conventional electrochemical anodization technique, where Ti foil is used as anode and Pt mesh is used as electrode [1]. Prior to the usage of Ti foil, it was

ultrasonically cleaned. The electrolyte comprised of 0.3 wt% of NH_4F and 3 vol% of H_2O in ethylene glycol. The anodization was carried out for 24h. The anodized sample was annealed at 450 ^oC for a period of 5h to obtain crystalline NTs array. Thereafter, for electrodeposition of MnO_2, the electrolyte was based on $Mn(CH_3COO)_2$. The annealed NTs were used as cathode and Pt mesh as cathode two electrode electrodeposition system and was carried out at 5 V. On the other hand, TiO_2 NTs array, Pt wire and Calomel electrode were used as cathode, anode and reference respectively, in a three electrode electrodeposition system at a potential of 1.5 V. For comparison, MnO_2 alone was synthesized using hydrothermal technique at 150 ^oC with $KMnO_4$ as the precursor [7]. Characterization of TiO_2 NTs array, MT1 and MT2 were carried out using FESEM, EDAX, FT-IR and TG-DTA. Pristine MnO_2 was tested for FT-IR and TG-DTA for purpose of assessing MnO_2 doping levels.

Results and Discussion

Morphological and compositional studies

Fig.1 shows the morphology of TiO_2 NTs array, MT1 and MT2. It is understood from the images that the conventional anodization has produced orderly NTs [Fig. 1a]. MT1, where MnO_2 was deposition using two electrode system is observed to have caused damage to the morphology of the NTs. However, deposition has coved a major portion of the surface [Fig. 1b]. In the same manner, MnO_2 deposited through the three electrode system is uniform throughout and is observed as a spherical ball with several accumulated nanorods like structure [Fig. 1c]. The MnO_2 loading is observed to be better than the previous reports [5].The elemental compositional studies also indicated presence of Mn was observed in both MT1 [Fig. 2a] and MT2 [Fig. 2b]. Notably, augmented deposition of MnO_2 is observed in the EDAX spectrum of MT2 compared to MT1 which indicated Mn at higher percentage.

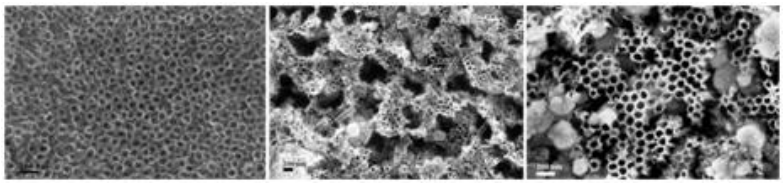

Fig. 1. FESEM images of a) TiO_2 NTs, b) MT1 and c) MT2

FT-IR studies

FI-IR images give much clarity in understanding the level of loading. Fig. 3 depicts the spectrum of TiO_2 NTs array, MT1, MT2 and MnO_2. TiO_2 NTs shows characteristic peaks around 1600 and 450 cm^{-1} [8]. Similarly, MnO_2 shows characteristic peaks around 500 cm^{-1} with a double peak and a peak around 700 cm^{-1}[9]. Strikingly, a remarkable change is observed in both MT1 and MT2. That is, both the spectrum has a shoulder peak around 700 cm^{-1} indicating the decisive presence of MnO_2. Moreover, the sharpening of the peaks around 450 cm^{-1} further supports the concept of MnO_2 loading. Another observation in the MT1 and MT2 spectrum depicts a very shallow peak

around 1600 cm^{-1} indicating the presence of TiO_2. On the whole, the FT-IR spectra denote the effective electrodeposition of MnO_2 in MT2.

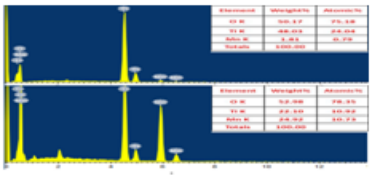

Fig. 2 EDAX pattern of a) MT1 and MT2

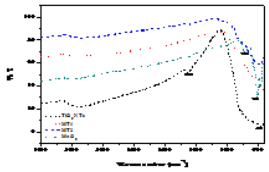

Fig. 3. FT-IR of TiO_2 NTs, MT1, MT2 and MnO_2

TG-DTA studies

Fig. 4a shows the thermograms of TiO_2 NTs array, where there is constant decrease in the weight without any step decrease. MT1 [Fig. 4b] has a steady decrease in the weight loss but the increase in the weight after 700 ^oC could be ascribed to the change of phase from anatase to rutile. Fig. 4c. depicts the temperature behavior of MT2 which indicates a minor rutile formation where the major portion of hindrance could be arrived form electrodeposited MnO_2. Both MT1 and MT2 are observed to be stable for a long temperature range, from 100 to 700 ^oC. Finally, in the case of MnO_2 [Fig. 4d], there are several steps indicating molecular losses at various intervals. The initial step at around 200 ^oC could be ascribed to the fact of dehydration. At 600 ^oC there could be a loss of molecular O_2 from two forming Mn_3O_4 and at 800 ^oC there could a formation of MnO with the loss of oxygen [9]. This could be verified with the formation of black precipitate at the end of the analysis.

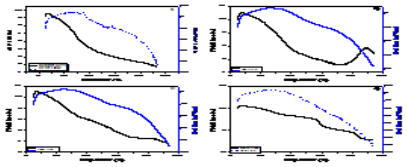

Fig.4. Thermograms of a) TiO_2 NTs, b) MT1, c) MT2 and MnO_2 MPs

Conclusion

The paper deals with the formation of MnO_2 NPs over TiO_2 NTs array through electrodeposition method. FESEM gives details about the better deposition of the MnO_2 NPs in the three electrode system. EDAX confirms the presence of the elements Mn, O and Ti in the as-prepared samples. FT-IR indicates the better loading of MnO_2 with the formation of shoulder peaks in both the samples. TG-DTA displays that the electrodeposited samples are stable for a large temperature range.

References

1. Shibu Joseph and Pappu Sagayaraj. A cost effective approach for developing substrate stable TiO_2 nanotube arrays with tuned morphology: A comprehensive study on the role of H_2O_2 and anodization potential. **New J. Chem.**, 2015, **39**, 5402-5409.
2. Manovah David T, Wilson P, Ramesh C and Sagayaraj P. A Comparative Study on the Morphological Features of Highly Ordered Titania Nanotube Arrays Prepared via Galvanostatic and Potentiostatic Modes. Current Applied Physics., 2014, 14(6), 868-875.
3. Wu H, Xu C, Xu J, Lu L, Fan Z, Chen X, Song Y and Li D. Enhanced supercapacitance in anodic TiO_2 nanotube films by hydrogen plasma treatment. Nanotechnology 2013, 24, 455401.
4. Kim C, Kim S, Lee J, Kim J and Yoon J. Capacitive and Oxidant Generating Properties of Black-Colored TiO_2 Nanotube Array Fabricated by Electrochemical Self-Doping. ACS Appl. Mater. Interfaces.*ACSAppl. Mater. Interfaces*, 2015, *7* (14), pp 7486–7491.
5. Xu X, Zhou X, Li X , Yang F, Jin B, Xu T, Li G and Li M. Electrodeposition synthesis of MnO2/TiO2 nanotube arrays nanocomposites and their visible light photocatalytic activity. Material Research Bulletin, 2014, 32-36.
6. Muralidharsharma K V and Vishal Yadav. Comparison of batteries in automotives. International journal of Advance Research 2016, 4(4), 1316-1321.
7. Mahmoudian M. R, Alias Y, Basirun W. J, Woi P. M and Sookhakian M. Facile preparation of MnO_2 nanotubes/reduced graphene oxide nanocomposite for electrochemical sensing of hydrogen peroxide. Sensors and Actuators B 2014, 201, 526-534.
8. Ali G, Kim H J, Kim J J and Cho S O. Controlled fabrication of porous double-walled TiO_2 nanotubes via ultraviolet-assisted anodization. Nanoscale, 2014, 6, 3632-3637.
9. Zhao G, Li J, Jiang L, Dong H, Wang X and Hu W. Synthesizing MnO_2nanosheets from graphene oxide templates for high performance pseudosupercapacitors. Chem. Sci, 2012, 3, 433-437.

MORPHOLOGICAL STUDY ON BIMETALLIC THIYOCYANATE SINGLE CRYSTAL OF $CdHg(SCN)_4$ IRRADIATED WITH γ-RAYS

T. Rajesh Kumar1*, and P. Sagayraj[2]

[1]*Department of Physics, G.T.N Arts College,Dindigul-624 005, India*

[2]*Department of Physics, Loyola College, Chennai-600 034, India*

E-mail: *rajesh727@gmail.com**

Abstract

Low dose irradiation effects in Single crystals of bimetallic $CdHg(SCN)_4$ (abbreviated as CMTC) irradiated with γ-rays. The crystal was grown by slow cooling method and third order optical nonlinearities are investigated by single beam Z-scan technique with a He:Ne laser operated at 632.8 nm. The nonlinear refractive index, absorption coefficient and third order susceptibility are estimated to be $-1.99x10^{-12}cm^2/W$, $5.62x10^{-6}cm/W$ and $3.94x10^{-9}$esu respectively. The full width at half maximum (FWHM) of the diffraction curves is 5.5 arc s, which is very close to that expected from the plane wave theory of dynamical X-ray diffraction. The surface feature is investigated by AFM.

Keywords: Crystal growth; Z-Scan; HRXRD; Atomic force microscopy

1.1 INTRODUCTION

The search for new materials with enhanced nonlinear optical (NLO) properties has increased considerably over the recent years as a result of wide range of applications in optical communication, photonics, electronics and optical storage systems. Hence, there is a demand for materials with large NLO figure of merit, high resistance to laser damage, good environmental stability and overall high performance [1]. Hence, researchers are focusing their attention on organometallics, which combine the advantages of both organic and inorganic materials. Among the different types of organometallic NLO materials, the thiocyanate (SCN) ligand based bimetallic crystals possess several advantages due to their high transparency, better nonlinear optical response and, moderate mechanical and thermal stability, which make them potential materials for crystal engineering based three dimensional (3D) coordination networks. The organic ligand is usually more dominant in the NLO effect. Especially, the SCN organic ligand with medium sized π-electron systems such as benzene derivatives has its SHG efficiency higher than that of urea. CMTC belongs to tetragonal system, space group $I\bar{4}$ with a=11.445(2) Å, c=4.202(1) Å, V=550.4(2) $Å^3$, Z=2, D_c=3.2148 g/cm^3. High optical quality CMTC single crystals were grown by Yuan et al [2]. Though the growth of CMTC crystal has been achieved by the crystal growers, there are still challenges pertaining to the growth of large size single crystals free from defects. The aim of the present work is to carry out the growth of organometallic crystal of CMTC and investigate its Z-scan study and atomic force microscopic study (AFM) studies are also carried out to expedite the use of the crystal for device fabrication. Crystalline perfection of the grown crystals by high resolution X-ray diffraction (HRXRD) studies

1.2 GROWTH OF CRYSTAL

High purity (E-Merck, AR grade) starting materials were used. The following reaction is expected to take place;

$$4NH_4SCN + HgCl_2 + CdCl_2 \rightarrow CdHg(SCN)_4 + 4NH_4Cl$$

The synthesized product of CMTC was purified by recrystallization and dissolved in mixed solvent of ethanol and water (1:1). In accordance with the solubility data, saturated solution of 200 ml of CMTC was prepared and kept in cryostate for slow cooling. The temperature was then reduced from 45 °C at a temperature lowering rate of 0.1 - 0.2 °C per day and crystals of dimension up to 10 x 9 x 3 mm^3 were obtained. When the samples are irradiated by using ^{60}Co-gamma source with a dose of 200Gy.

1.3 Result and Discussion

1.3.1 Z-Scan Study

Development of high power laser sources has motivated an extensive research in the study of nonlinear optical properties and optical limiting behaviour of materials[3,4]. For the usage of the crystals to be efficient, it is necessary to have quantitative information about their nonlinear optical properties. Such nonlinear optical phenomena as nonlinear refraction and absorption can seriously affect the operation of laser devices. In part, intensity dependent refraction index of laser material causes the changes in the spatial distribution of laser field and can lead to self-focusing of the radiation and breakdown of device. It is the main factor which restricts the light intensities used and output laser power.

In the present investigation, the sample of CMTC was translated in the Z–direction along the axis of a focused Gaussian beam from the He-Ne laser at 632.8 nm and the far field intensity is measured as a function of the sample position. By properly monitoring the transmittance change through a small aperture at the far field position (closed aperture), it is possible to determine the amplitude of the phase-shift. By moving the sample through the focus and without placing an aperture at the detector (open aperture), the intensity dependent absorption of the sample can be measured. When both the methods (open and closed) are used for the measurements, the ratio of the signals determines the nonlinear refraction of the sample.

The real and imaginary parts of the third order nonlinear optical susceptibility ($\chi^{(3)}$) are defined as

Re $\chi^{(3)}$ (esu) =10^{-4} ($\varepsilon_0 c^2 n_0^2 n_2$) /π ($cm^2$/W) (1)

Im $\chi^{(3)}$ (esu) =10^{-2} ($\varepsilon_0 c^2 n_0^2 \lambda\beta$) /$4\pi^2$ (cm/W) (2)

Where, ε_0 is the vacuum permittivity, n_0 is the linear refractive index of the sample and c is the velocity of light in vacuum.

Figure.1 and 2 show the open and closed aperture Z-scan curves for CMTC crystal. In the closed aperture Z-scan curve, the pre-focal transmittance peak is followed by the post focal valley, which is the signature of negative nonlinearity [5]. The nonlinear refractive index, absorption coefficient and third order susceptibility are estimated to be -1.99x$10^{-12}$$cm^2$/W, 5.62x$10^{-6}$cm/W and 3.94x$10^{-9}$esu respectively.

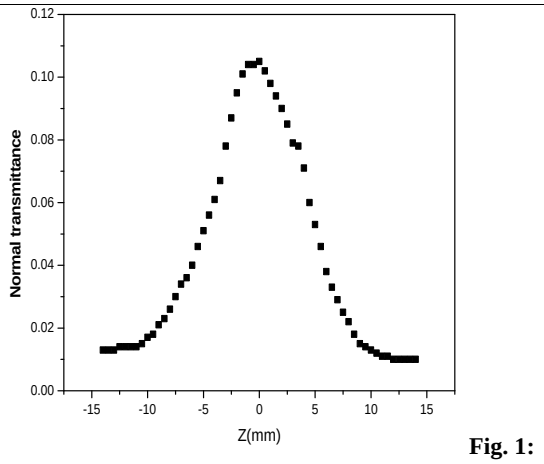

Fig. 1: Open aperture Z-scan curve of CMTC

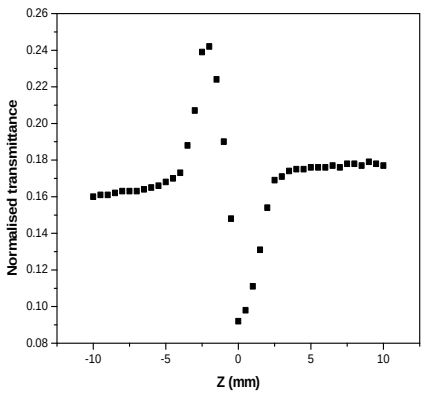

Fig. 2: Open aperture Z-scan curve of CMTC

1.3.2 HRXRD study

Figure 3 shows the DC recorded for CMTC crystal using (2 0 0) diffracting plane in symmetrical Bragg geometry by employing the multicrystal X-ray diffractometer described above. As seen in the figure, the DC is quite sharp without any satellite peaks which may otherwise be observed either due to internal structural grain boundaries due to epitaxial layer which may sometimes form in crystals grown from solution [6].

The full width at half maximum (FWHM) of the diffraction curves is 5.5 arc s, which is very close to that expected from the plane wave theory of dynamical X-ray diffraction [7]. The single sharp diffraction curve with very low FWHM indicates that the crystalline perfection is extremely good. The specimen is a nearly perfect single crystal without having any internal structural grain boundaries. The FWHM of the CMTC crystal grown in the present case is much better than the HRXRD data (32 arc s) reported by Raghavan et al [8] for the CMTC crystal grown by slow evaporation method. It is believed that the two-step process used during the growth of the CMTC crystal has improved the purity as well as crystalline quality. It is further evident that the slow cooling method is better suited than the slow evaporation method for CMTC growth.

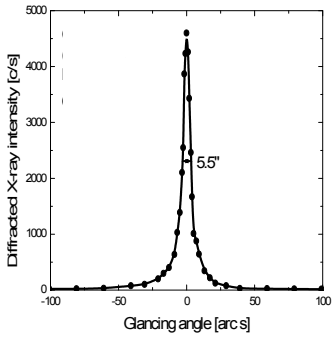

Fig. 3: Diffraction curve for CMTC single crystal for (2 0 0) diffracting plane

1.3.3 Atomic Force Microscopy Study

To better understand the morphology of a surface a quantitative description of the surface topography must be carried out. The topography matrix data should be treated in each profile line (2D) or over all profiles extending the analysis to surface (3D). The surface profile parameters are usually separated in four categories: amplitude, spacing, hybrid and functional.

Figure 3 show the 10, 0000 x 10, 000 nm^2 image morphologies of CMTC crystal on the (110) face of sample. It is evident from the image (Figure.3) for CMTC that the sample possesses almost smooth surface, Surface skewness (S_{sk}) values of CMTC (0.226) and Roughness average (S_a) (4.77 nm). It has been reported that if the height distribution is asymmetrical and the surface has more peaks than valleys, the Skewness moment is positive, and if the surface is more planar and the valleys are predominant then the Skewness is negative [9].

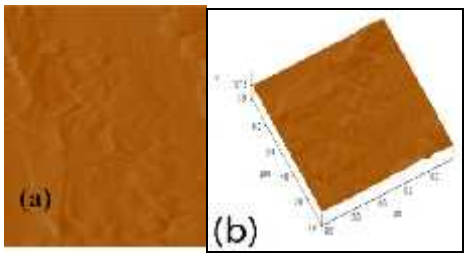

Fig. 4: (a) AFM image and (b) 3D image of CMTC

2. 0 CONCLUSION

Organometallic single crystals of CMTC was grown and by using the open and closed aperture Z-scan curves, parameters like nonlinear refractive index, nonlinear absorption coefficient and third order nonlinear optical susceptibility of these crystals were measured. The large magnitude of the third order nonlinear coefficients of these crystals shows that they are promising candidates for further materials development and possible photonic device applications. The negative sign of the nonlinear refractive index indicates that these materials exhibit self defocusing optical nonlinearity. From the HRXRD, the DC value indicated that the good crystalline quality of the CMTC crystal.

REFERENCES

1. Nalwa Hari Singh, "Organometallic materials for nonlinear optics" *Applied Organometalic Chemistry*, Vol. 5, 1991, pp. 349-77.
2. Yuan D., Zhong Z., Liu M., Xu D., Qi Fang, Bing Y., Sun S. and Jiang M., "Growth of cadmium mercury thiocynate single crystal for laser diode frequency doubling" *Journal of Crystal Growth* , Vol. 186, pp. 240-244.
3. Monaco SB, Davis LE, Velsko SP, Wang FT, Eimerl D, Zalkin A. Synthesis and characterization of chemical analogs of L-arginine phosphate. *Journal of Crystal Growth*, vol 1987;85:252
4. Kiran AJ, Mithun A, Holla BS, Shashikala HD, Umesh G, Chandrasekaran K. "Nonlinear optical studies of 1-3-diaryl-propenones containing 4-methylthiophenyl moieties", Optics Communication, vol.269, 2007,pp. 235.
5. Sutherland R.L., "Effects of multiple internal sample reflections on nonlinear refractive Z-scan measurements" *Applied Optics*, vol. 33,1996, pp. 5576-5584.
6. Bhagavannarayana G., Ananthamurthy R.V., Budakoti G.C., Kumar B., and Bartwal K.S., , "A study of the effect of annealing on Fe-doped LiNbO3 by HRXRD, XRT and FT-IR", *Journal Applied Crystal*, vol. 38, 2005, pp. 768-771.
7. Betterman B.W and Cole H., "Dynamical Diffraction of X Rays by Perfect Crystals", Reviews of Modern Physics. vol. 36, 1964, pp. 681-717.
8. Raghavan C.M., Pradeepkumar R., Bhagavannarayana G., Jayavel R., "Growth of cadmium mercury thiocyanate single crystals using acetone-water mixed solvent and their characterization studies", *Journal of Crystal Growth*, vol. 311, pp. 3174-3178.
9. M. Raposo, Q. Ferreia and P.A. Ribeiro, in *Modern Research and Educational Topics in Microscopy* edited by A. Mendz-Vilas and J. Diaz, Formatex Micorscopic book series, 2007, pp. 758.

Abstracts

Hydrothermal preparation of ZnO/CuO nanocomposites and their antibacterial activities

S.Gnanam*[a], V. Rajendran[b]
*[a] Department of Physics, Sree Sastha Institute of Engineering and Technology, Chembarambakkam, Ch-123, +91-9840159149
[b]Department of Physics, Presidency college, chennai-05
Corresponding author Email address: gnanam.nanoscience@gmail.com

ABSTRACT

ZnO/CuO nanocomposites was successfully synthesized through a facile hydrotherma process under low temperature using a nonionic surfactant PVP. The prepared ZnO/CuO samples were characterized by different techniques such as powder XRD, FTIR, Raman, SEM, TEM, UV–visible absorption and photoluminescence emission studies. The crystal structure and average crystallite size was measured by powder XRD, the peaks conformed that the obtained nanocomposite was ZnO-hexagonal and CuO-monoclinic structures, and there was no external phases involved in the nanocomposite. The Zn-O and Cu-O stretching bands were observed in FTIR studies. SEM and TEM images inferred that the nanocomposite shown high porous nature. The as-synthesized ZnO/CuO nanocoposite may be a promising candidate for antibacterial activities. The efficiency of the samples and their antibacterial mechanism has been discussed in detail.

Keywords: Metal oxide; Nanocomposites; Hydrothermal process; Anibacterial activity

---

Synthesis and Characterization of Lead Sulfide Nanoparticles

L.Kungumadevi*, P.Jeya Kiruba

Department of Physics, Mother Teresa Women's University, Kodaikanal, Tamilnadu-624001.

*E-Mail id:sivarivudevi@gmail.com

ABSTRACT

Lead sulfide is a good IV-VI group semiconductor, which has attracted considerable attention due to its special small direct band gap (0.41 eV) and large excitonic Bohr radius of 18nm. PbS has been widely used in many fields such as Pb2+ ion selective sensor, IR detectors, solar absorber and photography. Nano-particles of lead sulfide have been synthesized recently by different chemical method with controlled particle size distribution. During wet chemical synthesis of nanoparticles organic stabilizers are normally used to prevent them from aggregation by capping their surface. Moreover, the introduction of stabilizers influences on the chemical properties as well as the physical properties of semiconductor materials, from stability solubility and high emission, capping agents with strong binding molecules form dense layer on the particle surface that stabilize nanoparticle better. In this paper, we report the preparation of PbS nanoparticles by using PEG as capping ageent. The synthesized product has been characterized by X-ray diffraction (XRD), FE-SEM, energy dispersive X-ray spectroscopy (EDX) and FTIR and their results have been discussed in detail.

SYNTHESIS, CRYSTAL GROWTH AND CHARACTERIZATION OF LITHIUM IODATE SEMI-ORGANIC CRYSTAL

R. Vinayagamoorthy, A. Albert Irudayaraj*, A. Dhayal Raj, P. Meenatchi, S. Karthick
PG and Research Department of Physics, Abraham Panampara Research Center (APRC) Sacred Heart College (Autonomous), Tirupattur, Vellore District.

ABSTRACT

The semi-organic nonlinear optical material Lithium Iodate was synthesized and crystals of Lithium Iodate were grown by slow evaporation technique using water as solvent. The grown crystals were characterized by Powder XRD, FTIR, UV-Visible, Non linear optical analysis, PL, EDAX, TGA/DTA and dielectric studies. The powder XRD analysis reveals that Lithium Iodate crystal belongs to hexagonal system with unit cell parameters a = 5.481 Å, b = 5.481 Å, c = 5.172 Å, α = β = 90°, γ = 120° and Volume = 155.37 $Å^3$. The functional groups of the crystal were determined using FTIR analysis. The optical transmission range of the lithium iodate crystals was determined by UV-Visible spectroscopy. The lithium iodate was found to be optically transparent in the entire UV-Vis range and its UV lower cut off wavelength was found to be 267 nm. The second harmonic generation efficiency of Lithium Iodate crystal studied by Kurtz and Perry method was 2.3 times that of KDP. The photoluminescence studies reveal that Lithium Iodate emits violet light of wavelength 419 nm when excited by a light of wavelength 267 nm. The chemical composition of Lithium Iodate crystals was confirmed by Energy Dispersive X-ray analysis. TGA/DTA studies indicate that Lithium Iodate was thermally stable up to 258°C. The melting point of the Lithium Iodate was 428°C. Dielectric studies reveal that both dielectric constant and dielectric loss decreases with increase in frequency at room temperature.

Keywords: Semi-organic, XRD, UV-Visible, second harmonic generation, Dielectric.
Corresponding author* - Dr. A. Albert Irudayaraj (vinayaga76@gmail.com)

STUDIES ON THE CHARACTERIZATION OF L-ARGININE ADIPATE CRYSTAL GROWN FROM LIQUID DIFFUSION TECHNIQUE

K. Ramya[1], N. T. Saraswathi[2], C. Ramachandra Raja[3*]
[1]Department of Physics, T.U.K Arts College, Thanjavur-613 002, Tamilnadu, India.
[2]Molecular Biophysics Lab, School of Chemical and Biotechnology, SASTRA University, Thanjavur-613 401, Tamilnadu, India.
[3]Department of Physics, Government Arts College (Autonomous), Kumbakonam- 612 001, Tamilnadu, India.

ABSTRACT

Basically, some salts of amino acid with different organic or inorganic acids are grown from the standard method of synthesizing the aqueous solution of the required materials mixed in a molar proportion, and purifying the solution and then evaporating the solvent by slow evaporation technique. In some cases, this method does not leads to the expected product, in which no reaction takes place between the starting materials, and results in the crystallization of any one of the starting materials. The liquid diffusion technique is employed to overcome such difficulties. Here the single crystals of L-arginine adipate were successfully grown from liquid diffusion technique. The cell parameters were determined by single crystal X-ray diffraction analysis. Fourier transform infrared and Raman spectroscopic investigations were used to characterize the grown crystal. The molecular structure was established from NMR studies. UV-Vis-NIR spectrum and second harmonic generation were used to explore its characteristics optical features. The thermal stability has been analysed by TGA and DTA.

SEM, XRD, FTIR, PL & UV CHARACTERISATION OF KDP SINGLE CRYSTAL BY SLOW EVAPORATION TECHNIQUE

M.Selvapandiyan[a] , N.Suresh[b]
Department of Physics, PG Extension center, Periyar University Dharmapuri
Department of Physics, Periyar University, salem - 11

ABSTRACT

Potassium dihydrogen phosphate (KDP) is a well-known inorganic crystal. It has an interesting property such as NLO, wide frequency conversion, high damage threshold against power laser and good UV transmission. In present study single crystal of pure KDP has been grown by slow evaporation solution growth technique. The crystalline and cell parameters were characterized by X-ray diffraction analysis, the shifting in frequency assignment of different functional groups of KDP was analyzed by FTIR Studies. The optical properties of the products were characterized by UV-Visible spectral analysis and Photo Luminescence spectroscopy (PL).

Keyword: KDP, XRD, UV,FTIR,SEM and PL

Growth and Characterization of Ammonium dihydrogen phosphate single crystals: Non-linear optical material

M.Selvapandiyan[a] , S.Janarthanana[a,b]
[a] Department of Uhysics, Periyar University, P.G Extension centre, Darmapuri,636 705
[b] Department of Physics, Sri Vidya andir arts & science college, Uthangarai,636 902
Email: mselvapandiyan@rediffmail.com
Email:jana.physics@gmail.com

ABSTRACT

Single crystals of ammonium dihydrogen phosphate (ADP) $(NH_4)H_2PO_4$ was grown by slow evaporation solution technique at room temperature. The grown ammonium dihydrogen phosphate single crystal was subjected to various characterizations such as powder X-ray diffraction study, UV-Visible absorption study, Fourier transform infrared spectroscopy study and Photo luminescence study. The grown ammonium dihydrogen phosphate single crystals are very useful to fabricate optical devices and many industries are used in many applications i.e., in the field of optoelectronics, telecommunication, laser technologies and optical storage devices etc.

Key words: Optical material, crystal growth, Fourier transform infrared spectroscopy,

photoluminescence

SYNTHESIS, GROWTH AND CHARACTERISATION OF A NOVEL NONLINEAR OPTICAL SINGLE CRYSTAL OF L- ISOLEUCINIUM HYDROGEN MALEATE HEMIHYDRATE

A.Hemalatha[1,2], N. Indumathi[2], E. Chinnasamy[2], M. Victor Antony Raj[3] and S. Senthil[2,*]

[1]Department of Physics, Quaid-E-Millath Government College for women, Chennai – 02.
[2]Department of Physics, Government Arts College (Men), Nandanam, Chennai-35.
[3]Department of Physics, Loyola College, Chennai-34.
Corresponding author: ssatoms@yahoo.co.in

ABSTRACT

L-- Isoleucinium Hydrogen Maleate Hemihydrate (LIM) nonlinear optical single crystal was grown from aqueous medium by the slow evaporation method at room temperature. The powder XRD analysis confirms the crystallinity of the grown crystal. The second harmonic generation (SHG) efficiency of the LIM was determined using Kutz and Perry powder technique. Thermo-gravimetric and differential thermo gravimetric analysis were carried out to study the thermal behavior of the sample. The optical transparency has been studied using UV-vis-NIR spectroscopy and the band gap value also found from the absorption studies.

Key words: XRD, TGA – DTA, NLO, UV-vis-NIR.

Structural impact of Zinc ions on B_2O_3-Na_2O-ZnO glass system by means of spectroscopic and Ultrasonic studies

L. Balu[a*], R. Amaravel[b] and R. Ezhil Pavai[b]

[a]Department of Physics, Govt. Arts college, C. Mutlur, Chidambaram
[b]Department of Physics, Annamalai University, Annamalainagar- 608 002, Tamil Nadu, India
Corresponding Author mail-*ezhilpavaibalu@yahoo.com*

ABSTRACT

The borate glasses with different compositions of ZnO content have been prepared by melt quenching technique and characterized using The X-ray patterns indicate that the prepared samples were absolutely amorphous. FTIR spectral studies have pointed out the conversion of borate structural units. For all glass samples the glass transition (T_g), crystallization (T_c) and melting(T_m) temperatures were identified from which glass stability and Hruby's parameter were calculated. Ultrasonic parameters were used to understand the mechanical properties of the samples.

Keywords: *XRD, FT-IR, DTA, and ultrasonic velocity measurements.*

SOLAR CELL

Hena Gomathi Priyanka.S.B,
Department Of Physics, Kamban College Of Arts And Science For Women, Thiruvannamalai.

ABSTRACT

The spectrum of solar energy is quite wide and its intensities varies according to the timing of the day and the locations.We review solor energy conversion in to electricity with particular emphasis on photovoltaic systems,solar cell and how to store electricity.

Synthesis of pure hydroxyapatite ($Ca_{10}(PO_4)_6(OH)_2$) by Sol –gel method and drug loaded in presence and absence of polymer for the application of drug delivery

B.Shalini[1], A.Ruban Kumar[2*], A.Mary Saral[2]
School of Advanced sciences, VIT University, Vellore 632014, India

Abstract

The objective of the present paper is to synthesize pure HAp by Sol – gel method. During synthesis the chemical precursors like calcium nitrate tetrahydrate and diammonium hydrogen phosphate was mixed and ammonium hydroxide solution is added to maintain the pH of about 10.5. And the synthesized powders are characterized using XRD, FTIR, TG/DTA, SEM. With this pure Hydroxyapatite the drug was loaded in presence of polymer and in the absence of polymer the powders are characterized again using XRD, FTIR, SEM, Anti bacterial studies, drug loading, drug releasing. Keeping the above points the present study was aimed to produce the biocompatibility and bioactivity of HAp prepared from Sol – gel method.

Keywords: Hydroxyapatite, Sol gel process, XRD, FTIR, TG/DTA, SEM, drug loading, drug releasing.

Ultrasonic Studies of O- and P- Nitrophenols at Various Concentrations

Dr.P.Saritha,
Assistant Professor, Engineering Physics, Annamalai University, Annamalai Nagar – 608 002.
E-mail: psarithaau@yahoo.com

ABSTRACT

To study the ultrasonic parameters of Ortho and Para Nitrophenols in various concentrations at room temperature. This variation in structural formula gives rise to variation in their physical properties. It has been carried out and gives details about the determination of viscosity, density and the preparation of solutions of various concentrations. Of these O- and P- Nitrophenols have been studied at various concentrations by dissolving them in double distilled water. From the study of various parameters it can be concluded that the solute-solvent interactions of O- and P- Nitrophenols with water are prominent at 0.04M concentration. This discussion throws light on the solute-solvent behavior of Nitrophenol with water.

Keywords: Interferometer; Ostwald's Viscometer; Pulse-Echo Technique and Ultrasonic diffraction.

GROWTH AND CHARACTERIZATION OF L-PROLINIUM TARTRATE

Attralarasan S, Shiny Febena A, Madhavan J*
Department of Physics, Loyola College, Chennai-34
Email Id:jmadhavang@gmail.com

ABSTRACT

Single crystals of L-Prolinium tartrate $(C_5H_{10}NO_2)^+$ $(C_4H_5O_6)^-$, a new organic non-linear optical material of size: 15 × 10 × 10 mm3 was grown using submerged seed solution growth method. Characterization of the crystals was made using single crystal X-ray diffraction and density determination. Spectroscopic, thermal, optical and mechanical studies were carried out. These studies show that the crystals are thermally stable upto 161°C, transparent for the fundamental and second harmonic generation of Nd: YAG (λ = 1064 nm) laser and possess good mechanical strength. Second harmonic generation (SHG) conversion efficiency was investigated to explore the NLO characteristics of this material using Kurtz and Perry method and it was found that the SHG conversion efficiency is about 90% of that of the standard KDP crystals. Laser damage threshold study was also carried out.

Keywords: L-prolinium tartrate, FT-IR, thermal studies, micro hardness, SHG, laser damage threshold.

Hydrothermal Synthesis of Nd^{3+}doped TiO_2 nanoparticles and its Optical behaviour

EzhilArasi S, Madhavan J*
Department of Physics, Loyola College, Chennai-34,
Email id: jmadhavang@gmail.com

ABSTRACT

Pure and rare earth ion doped TiO_2nanoparticles were synthesized by hydrothermal method. The synthesized TiO_2nanoparticles were characterized in details by X-raydiffraction, Raman spectroscopy, Fourier transform infrared spectroscopy, UV–vis spectroscopy and photoluminescence emission spectra.From the UV-visible measurement,the absorption edge of Nd^{3+}-$TiO_2$was shifted to a higher wavelength side with decreasing bandgap. The doping reduced the bandgap.Photoluminescence emission studies revealed the obvious peaks and the absorption and emission spectra of Nd^{3+} doped TiO_2 nanoparticles explain energy transfer mechanism.

Keywords: TiO_2 nanoparticles, Hydrothermal technique, Energy level transition.

GROWTH, X-RAY STRUCTURE, SPECTROSCOPIC CHARACTERIZATION AND NLO PROPERTIES OF AMINO ACID SINGLE CRYSTALS OF GLYCINE NICKEL CHLORIDE

Shiny Febena A, Victor Antony Raj M andMadhavan J*
Department of Physics, Loyola College,Chennai-34.
Email id: jmadhavang@gmail.com

ABSTRACT

Highly transparent crystals of Glycine Nickel (II) Chloride dihydrate [GNC] with dimensions 8 mm × 7 mm × 5 mm were grown by slow evaporation technique. Crystals of GNC, a semi organic nonlinear optical (NLO) were grown from aqueous solution at roomtemperature by slow evaporation method.Crystal system and lattice parameters were confirmed by Powder X-raydiffraction analysis. Structural confirmation was done by identifying the vibrational modes using IR and FT-Raman spectroscopic studies. Optical absorption spectrum was recorded in thewavelength region of 190-1100nm. The optical band gap of the grown crystal was found to be 4.84eV. From TG/DTA curve, the crystals were thermally stable and there is an improvement in stability due to dopants added with glycine. SHG efficiency of GNC crystals was examined by Kurtzpowder method. Thus the grown crystals are useful in fabrication of optoelectronic devices.

Keywords: GNC, Powder XRD, FT-IR, FT-Raman, SHG, Kurtz powder method

---

EXPERIMENTAL AND COMPUTATIONAL STUDIES ON L – PROLINIUM PICRATE

Subaranjani R, Victor Antony Raj M andMadhavan J*
Department of Physics, Loyola College, Chennai-34
Email id: jmadhavang@gmail.com

ABSTRACT

L-Prolinium Picrate (LPOP) from L-Proline and Picric acid has been successfully synthesized and grown by slow evaporation solution technique. The presence of functional groups in the LPOP is confirmed by FT-IR vibrational patterns and the good crystallinity indicated by powder X-ray diffraction method. Optical behavior such as UV–visible–NIR absorption and SHG conversion efficiency were investigated to explore the NLO characteristics of the above material. The structural features of the material leading to the large SHG efficiency are discussed. Microhardness measurements and dielectric studies of the compound were also carried out. Using density functional theory (DFT), a systematic study of structure, bonding, vibration, excitation energies and non-linear optical properties has been carried out for noncentrosymmetric L-Prolinium Picrate.

Keywords: LPOP, FT-IR, UV-Vis, NLO, SHG, DFT

INVESTIGATIONS ON QUANTUM CHEMICAL AND VIBRATIONAL SPECTROSCOPY OF L-ARGININE PER CHLORATE - A PROMISING NLO SINGLE CRYSTAL

Vincent femilaa R, Victor Antony Raj M, Madhavan J*
Department of Physics, Loyola College, Chennai-34
Email id: jmadhavang@gmail.com

ABSTRACT

By slow evaporation solution growth method a good quality nonlinear optical crystal (NLO) of L-Arginine Perchlorate (LArPCl) was grown. The powder XRD studies were performed for the confirmation of the grown crystal. Using FT-IR spectrum the crystal was examined for its vibration frequencies. UV-Vis-NIR spectrum determined that the crystal in the visible region has a wide range of transparency. The title compound was investigated theoretically for the HOMO-LUMO analysis using DFT method.

Key words: NLO, FT-IR, XRD, UV-Vis-NIR, HOMO-LUMO, DFT

INVESTIGATION OF STRUCTURAL, OPTICAL AND MAGNETIC BEHAVIOUR OF LITHIUM FERRITE AND VANADIUM DOPED LITHIUM FERRITE

Malathi S and Seenuvasakumaran P
PG and Research department of Physics, Muthurangam Government Arts College (Aut),
Vellore 632002, TamilNadu, India

ABSTRACT

Nanomaterials ferrites have application in making permanent magnets, Magneto Optic displays, Microwave absorbers, High density information storage devices, colour imaging etc. In the present investigation Lithium Ferrite and Vanadium Doped Lithium Ferrite are synthesized by sol-gel process. The X-ray diffraction results show that the structure of Lithium Ferrite is tetragonal and Vanadium Doped Lithium Ferrite is monoclinic structure. The average particle size of lithium ferrite is 18 nm and vanadium doped lithium ferrite is 24nm are calculated from Scherer formula. The lattice parameters and dislocation density (δ) are calculated from XRD data. Strain (ε) values are evaluated from Williamson-hall plot. The FT-IR studies reveal the formation of ferrites showing the significant absorption bands. The UV-Vis spectroscopic data to calculate direct and indirect optical band gap (Eg) by using taue plot at the edge of absorption band has been determined 1.57eV & 1.71eV, 1.01eV & 1.01eV of lithium ferrite and lithium vanadium ferrite respectively. Surface morphology of the synthesize material is studied from scanning electron microscope (SEM). The energy dispersive X-ray analysis spectra showed that the expected elements exist in the material. The magnetic behaviour of the materials studied using vibrating sample magnetometer (VSM).

KEYWORDS: XRD, sol-gel, VSM, color imaging, SEM etc.

OPTICAL PROPERTIES OF NANOCRYSTALLINE STRONTIUM SULPHIDE AND CADMIUM DOPED STRONTIUM SULPHIDE THIN FILMS GROWN BY SILAR TECHNIQUE

Karthik rajan K and Seenuvasakumaran P
PG and Research Department of Physics
Muthurangam Government Arts College (Aut), Vellore 632 002.

ABSTRACT:

The present study focus on Structural and Optical properties of Strontium Sulphide (SrS) and Cadmium doped Strontium Sulphide deposited thin films for Tele communication, Optical coatings, Decorative coatings, Solar cell applications. SrS and SrCdS thin films were deposited by Successive Ionic Layer Absorption Reaction method (SILAR) at room temperature and atmospheric pressure. The synthesized nanomaterials of SrS and Cd doped SrS exhibits the tetragonal structure and its corresponding average particle sizes of thin films are 31nm and 45nm calculated from Debye-Scherrer's formula. The strain and dislocation density of deposited films are calculated using XRD data. Various functional groups of the synthesized nanomaterials are investigated by FT-IR analysis. The optical direct and indirect band gap of SrS and Cd doped SrS are 2.97 eV, 3.51 eV and 2.82 eV, 2.83 eV respectively. The surface morphology of the deposited thin films are studied by scanning electron microscope (SEM). The energy dispersive X-ray analysis (EDAX) spectra showed existence of the expected elements in the deposited thin films.

KEYWORDS: SILAR technique, strain, dislocation density and EDAX etc.

ULTRASONICS

K.MANIMEGALAI
Department of Physics, Kamban College Of Arts & Science For Women,Tiruvannamalai
megakrish05@gmail.com

ABSTRACT

Meaning of Ultrasonic's – transducers – Application In Research Field – Ranging and navigating – The Doppler Effect – Material Testing – High intensity application - Chemical and electrical uses – medical application – Diagnosis – Therapy and surgery

---

SYNTHESIS AND CHARACTERIZATION OF LITHIUM TITANIUM FERRITE AND VANADIUM CADMIUM FERRITE

Ramyapriya R and Seenuvasakumaran P
PG and Research department of Physics, Muthurangam Government Arts College (Aut), Vellore 632002, TamilNadu, India

ABSTRACT

In modern electronic equipments, the ferrite specifies are increasingly requirements due to their properties especially memory capacity. Lithium Ferrite attracts considerable attention of researchers due to feasibility of their application in microwave technology as Circulators, Isolators and Phase shifters due to High resistivity, Low eddy current and in memory device. This comparative study has been undertaken based on the structure, surface morphology, optical and electrochemical properties of Lithium Titanium Ferrite ($LiTiFe_2O_4$) and Vanadium Cadmium Ferrite ($V_2CdFe_2O_4$) synthesized by sol-gel method using stabilizing agent. The synthesized samples are characterized by X-ray diffraction (XRD) to confirm the monoclinic crystal structure and its average particle size are calculated using Debye-Scherrer's formula as 37 nm and 28 nm respectively. The strain and dislocation density are calculated from XRD data. Surface morphology and atomic percentage of the materials is studied from Scanning Electron Microscope (SEM) with Energy Dispersive X-ray Analysis (EDAX). Various functional groups are conformed from Fourier Transform Infrared spectroscopy analysis (FTIR). From the Tauc plot, the direct and indirect band gap of $LiTiFe_2O_4$ and $V_2CdFe_2O_4$ are 1.803 eV, 1.55 eV and 1.01 eV, 1.01 eV using UV-VIS spectroscopic data. From Vibrating Sample Magnetometer (VSM) studied the magnetic behavior of the synthesized materials.

KEY WORDS: Lithium ferrite, sol-gel method, XRD, FTIR, SEM with EDAX, magnetic properties.

INTERFEROMETERS ANALYS AND APPLICATIONS

P.Ramadoss and R.Tamilselvi
Department of Physics, Govt. Arts College, Tiruvannamalai-606 603

ABSTRACT

Fiber optic interferometer to sense various physical parameters including temperature,strain,pressure and refractive index have been widely investigated. In this paper all the four interferometer sensors Fabry-perot ,Mach-zehnder,Michelson and Sagnac are reviewed in terms of operating principles,fabrication,and applications. These sensors have large potential in industrial areas. The new sensor technologies and their descriptions are also discussed here Fabry-perot interferometer,applied in intrinsic and extrinsic structures and mach-zehnder and Michelson interferometric sensors based on photonic crystal fibers are discussed in detail with their remarkable sensingperformance.

Synthesis, Vibrational spectroscopic studies of 2-Amino-4-methylpyridinium 4-aminobenzoate by density functional theory

S. Suresh[1, 3*], S.Venda [3], S. Gunasekaran[2], S. Srinivasan[3]

[1]Department of Physics, Dr.MGR Educational and Research Institute University, Chennai, India.

[2]Research and Development Center, St.Peter's University, Chennai, India.

[3]Department of Physics, Presidency college, Chennai, India.

*Corresponding Author: sureshthanjai2003@gmail.com

ABSTRACT

2-Amino-4-methylpyridinium 4-aminobenzoate (AMPAB), was synthesized and characterized by FTIR and UV–Visible spectra. The non-Centro symmetric single crystal of 2-Amino-4-methyl pyridinium4-aminobenzoate (AMPAB), which crystallizes in Orthorhombic crystal system with space group *P*212121, exhibits second order non-linear optical (NLO) susceptibility, due to intermolecular charge transfer. In the AMPAB crystal, the amino benzoate anions are linked with both of adjacent amino benzoate anions and amino methyl pyridinium cations *via* N—H···O hydrogen bonding, to form the three dimensional supramolecular structure. The crystal structure also contains weak C—H···O hydrogen bonding between adjacent anions. Density functional theory (DFT) calculation has been carried out to study the nature of hydrogen involved in the AMPAB crystal. The bond lengths and bond angles of the structure of AMPAB crystal calculated using B3LYP method with 6-31G (d,p) basis set. A detailed interpretation of the vibrational spectra of this crystal has been made on the basis of the calculated potential energy distribution (PED). The time dependent DFT method employed to study its absorption energy and oscillator strength. The linear polarizability (α) and the first order hyper polarizability (β) values of the investigated molecule have been computed. The electronic properties, such as HOMO and LUMO energies, molecular electrostatic potential (MESP) were also performed. Stability of the molecule arising from hyper conjugative interaction, charge delocalization has been analyzed using natural bond orbital (NBO) analysis. These calculations are compared with experimental values to provide deep insight into its electronic structure and property of grown crystal.

Key words: 2-Amino- 4-methylpyridinium 4-aminobenzoate, DFT, H-bond interaction

---

GREEN SYNTHESIS AND CHARACTERIZATION OF METAL OXIDE(CUO AND ZNO) NANOPARTICLES FROM CENTELLA ASIATICA LEAF EXTRACT

K.Ramya ,S.Ravi, S.Velmurugan, M. Gayathiri, K.Velvizhi, S.Umadevi

Department of Physics, Annamalai University, Annamalainagar-608002, Tamil Nadu, India
Department of Engg. Physics section FEAT, Annamalai University, Annamalainagar-608002, Tamil Nadu, India

ABSTRACT

In recent years the development of metal oxide(CUO and ZNO) nanoparticles in an eco-friendly manner using from centella Asiatica leaf extract.These green synthesized nanoparticles have a range of shapes and sizes compared to those produced by other organisms. The present review is devoted to the possibility of metal nanoparticle synthesis using plant extracts. This review provides a detaited analysis of the various factors affecting the morphology; size and yield of metal nanoparticles.Examples of (proteins, viral particles) to obtain nanoparticles in plant extracts are discussed. The characterized by FE-SEM [Field Emission Scanning Electron Microscopy],X-Ray [X-ray Diffraction] studies. The formation of metal nanoparticles will be confirmed by their XRD spectrum.

Keywords : Metal oxide(Cuo and Zno) nanoparticles,Green synthesis ,centella asiatica,X-ray diffraction technique(XRD)

Synthesis, growth, spectroscopic and SHG studies on new nonlinear Optical crystal: Mercuric Thiocyanate Cadmium Bromide (MTCB)

G.J. Shanmuga Sundar[1], S.M.RaviKumar[2*], S. Selvakumar[3], D.Sivavishnu[2]
[1]*Department of Physics, A.A. Government Arts College, Cheyyar.*
[2]*PG and Research Department of Physics, Government Arts College, Thiruvannamalai.*
[3]*Department of Physics, Government Arts College, Nandanam, Chennai*
[*]Corresponding author: smravi78@rediffmail.com

ABSTRACT

Single crystal of Mercury thiocyanate cadmium bromide (MTCB) was successfully grown by the slow evaporation solution growth technique at room temperature. The title compound was synthesized using mercury thiocyanate and cadmium bromide with molar ratio of 3:1 using double distilled water as a solvent. The size of the crystal 5 x 4 x 2 mm^3 was obtained with in a period of 30 to 40 days.. The lattice parameters of the grown crystal a=11.51Á, b=11.51 Á, c=4.23 Á and volume V= 560.390 $Á^3$ were determined by Single crystal X-ray diffraction analysis. The crystalline nature and perfection of MTCB crystal were observed using Powder X-ray diffraction. A Fourier transform infrared study confirms the presence of functional group in the grown crystal. Transparency and cut off wavelength of crystal was measured using UV-Vis NIR spectroscopy study. Nonlinear optical (NLO) behavior of MTCB crystal has been studied for the first time by Kurtz Perry technique. Remarkable second harmonic generation (SHG) efficiency has been observed in the MTCB crystal, its SHG efficiency is found to be 2.64 times higher than that of known NLO crystal KDP.

Keywords: single crystal XRD; FTIR; UV-vis-NIR; SHG efficiency

---

ACOUSTICAL INVESTIGATIONS ON SOME RARE EARTH METALS

P.Ramadoss and S.Dhanalakshmi
Department of Physics, Govt. Arts College, Tiruvannamalai-606 603

ABSTRACT

Sound velocity and allied parameters have been calculated and presented for Ga, Tb, Dy, Ho, Er and Tm rare earth metals. The results are analysed on the basis of interaction.

INVESTIGATIONS ON SOME SUPERCONDUCTING ALLOYS

P.Ramadoss and M.Kavitha
Department of Physics, Govt. Arts College, Tiruvannamalai-606 603

ABSTRACT

Physical, thermal, mechanical and acoustical properties of some superconducting alloys have been calculated and the results are analysed.

Design and Construction of Vertical Semi Transparent Bridgman Setup

A.Saranraj, R.Murugan, S.A.Martin Britto Dhas*
Department of Physics, Abraham Panampara Research Centre,
Sacred Heart College (Autonomous), Tirupattur- 635601.
Email id: brittodhas@gmail.com, saranrajasj@gmail.com

ABSTRACT

In order to grow single crystals of nonlinear optical materials, a low cost vertical semi transparent Bridgman technique has been designed and constructed with a single zone furnace. The pulling rate of the constructed setup is 27 micro meter per minute. The thermal gradient of the furnace was analyzed by moving the temperature sensor along the axis of the furnace. By using this indigenously developed Bridgman setup a transparent and optical quality acenaphthene single crystal was successfully grown by setting up a suitable thermal gradient achieved by means of analyzing thermal gradient from melting region to bottom region (freezing region). The details will be presented.

Keywords: Nonlinear optical materials, Bridgman technique, acenaphthene single crystal.

Surfactant-liaised variation in ZrO_2 nanocomposites morphology

K. Gnanamoorthi[a], M. Balakrishnan[a]*
[a]PG & Research Department of Physics, Government Arts College, Tiruvannamalai – 606 603, Tamilnadu, India.

ABSTRACT

This paper presents the synthesis of ZrO_2 nanocomposites in chemical precipitation method. This article reports the formation of different morphologies of ZrO_2 nanocomposites with sodium dodecyl benzene sulfonate (SDBS) surfactant. This technique emphasizes the less consumption of time for synthesizing nano powder with smaller particle size. This route for preparing ZrO_2 is simple and cost-effective method. ZrO_2 nanocomposites were characterized by X-ray powder diffraction (XRD), Fourier transform- infrared spectroscopy (FT-IR), TEM measurements, Scanning electron microscope (SEM) and Energy dispersive spectrum (EDS). The particle size extracted from XRD patterns, were around 44 nm. The particle size obtained from TEM image is will consistent with XRD pattern. Analytical potential of these nanocomposites has been used to determine the illustrate levels of polycyclic aromatic compounds in stream waters.

Keywords: ZrO_2; semiconductors; nanocomposites; XRD; TEM

Corresponding author: Tel: +91 9445140029
E-mail address: mbelectronlife@gmail.com.

Study on the structural and optical properties of ZrO_2 nanoparticles using the SDBS surfactant by microwave irradiation route

K. Gnanamoorthi[a], M. Balakrishnan[a*]
[a]PG & Research Department of Physics, Government Arts College, Tiruvannamalai – 606 603, Tamilnadu, India.

ABSTRACT

Zirconium oxide (ZrO_2) nanoparticles using the SDBS surfactant was successfully synthesized by microwave irradiation route and the ZrO_2 nanoparticles were analysed by TG-DTA, XRD, FT-IR, SEM, TEM and HR-TEM techniques. More attention is given for the preparation of ZrO_2 nanoparticles with good optical performance and it has been derived from UV-Visible (UV-DRS) spectra and PL measurements. The X-ray diffraction pattern of the ZrO_2 nanocrystalline has confirmed tetragonal structure with average crystallite size in the range of 48-56 nm. SEM results show the nanoparticles have been good polycrystalline nature. TEM results show the agglomerated particles in the range from 43-58 nm. The HR-TEM images are corresponding to SAED pattern only. The optical studies of UV-DRS spectra of the reflectance peak position of ZrO_2 nanoparticles at about 327 nm and band gap energy values are obtained as 3.79 eV.

Keywords: Zirconium oxide; Microwave irradiation method; Tetragonal; Spherical particles
Corresponding author: Tel: 09445140029
E-mail address: mbelectronlife@gmail.com

ANNEALING EFFECT ON STRUCTURAL, MORPHOLOGICAL AND OPTICAL PROPERTIES OF ZrO_2 NANOPARTICLES

K. Gnanamoorthi[a], M. Balakrishnan[a*]
[a]P.G & Research Department of Physics, Government Arts College, Tiruvannamalai – 606 603, Tamilnadu, India.

ABSTRACT

ZrO_2 nanostructures have been successfully prepared by microwave irradiation method. The crystallite size and morphology of ZrO_2 have been investigated by X-Ray diffraction (XRD), thermogravimetric analysis (TG-DTA), fourier transform infrared spectroscopy (FT-IR), scanning electron microscopy (SEM), energy dispersive spectrum (EDS), and transmission electron microscopy (TEM) techniques. The XRD pattern of average particle sizes of ZrO_2 is estimated to be around 14 nm. Furthermore, ZrO_2 nanoparticles have the crystallite size in the range ~11-50 nm, as confirmed by TEM. Optical and Photoluminescence (PL) properties of the synthesized samples were also compared. Results obtained indicate that the microwave-assisted method is a promising low temperature, cheap, and fast method for the production of ZrO_2 nanostructures.

Keywords: ZrO_2 nanoparticles; Microwave irradiation; Structural; Surface; Optical properties:
Corresponding author: Tel: +91 9445140029
E-mail address: mbelectronlife@gmail.com

Growth and Characterization studies of L- threonine Sodium fluoride (LTSF) a new Semiorganic NLO crystal.

Allen Moses[a], S. Tamilselvan[a*], D. Sivavishnu[b], S.M. Ravi Kumar[b]
[a] Department of Physics, A.A. Govt Arts College, Cheyyar.
[b] Department of Physics, Govt Arts College, Tiruvanamallai.
*Corresponding Author: tamilraji1977@gmail.com

ABSTRACT

The single crystal growth of nonlinear optical crystal L-Threonine Sodium Fluoride (LTSF) has been successfully synthesized by taking equimolar quantity of L-Threonine and Sodium Fluoride, by mixing them thoroughly using deionized water. The crystal has grown by adopting the method of growing in a slow evaporation solution using water as solvent at room temperature. The prepared solution was placed in an undisturbed condition, and it was inspected regularly over a period of a month. A single crystal has been harvested. The single crystal was characterized by different techniques finding out its suitability for device fabrications. The optical studies reveal the transparency of the crystal in the entire visible region. The grownup crystal was subjected to single crystal XRD diffraction technique to examine the crystal system and unit cell parameters. Powder XRD pattern confirms that there is change in the basic structure of materials. Functional groups in crystal lattice were qualitatively identified by FTIR spectrum.Optical behavior of the crystal was identified by UV-Vis analysis. Thermal property of grown crystal was reported in the TGA/DTA analyses. Thermal studies revealed that grownup crystal LTSF is thermally stable. Laser damage threshold and nonlinear optical activity of the grownup crystal were confirmed by Q-switched Nd : YAG laser beam. The second harmonic generation (SHG) efficiency of the LTSF crystal was studied by Kurtz powder method and the efficiency was 2.2 times greater than that of the pure KDP. When compared with the pure L-Threonine crystal, it was found that the efficiency was two times greater than that of L-threonine.

Structural, optical, photocatalytic degradation and antibacterial activity of Ce - doped ZnO nanoparticles prepared via wet-chemical method

R. Bomila [a*], S. Srinivasan [a]

[a,a]Department of Physics, Presidency College, Chennai- 600 005*
Email: bomilar.m.sc@gmail.com

ABSTRACT

The undoped and Ce-doped ZnO nanoparticles were synthesized by the wet - chemical method with Octylamine (OA) as capping agent. Zinc acetate dihydrate and Cerium nitrate hexahydrate was used as precursor materials. The structure, morphology and optical properties were characterized by X-ray Diffraction, Scanning electron microscope, UV-Visible spectroscopic techniques respectively. The presence of ZnO was confirmed by Fourier transform- infrared spectroscopy and Fourier transform-Raman spectroscopic analysis. The band gap value of ZnO was determined from the UV-Vis spectral study. Further we also investigated the photocatalytic degradation of Eosin Yellow, which was well known textile dye by using undoped and Ce-doped ZnO nanoparticles in de-ionized water under sunlight irradiation. The bactericidal efficiency of Ce-doped ZnO nanoparticles were investigated against a Gram positive (Staphylococcus aureus) and a Gram negative bacteria (Escherichia coli).

Synthesis, Growth, Spectroscopy and Optical Studies on Novel Nonlinear Optical Material: $Zn(IO)_3$

D. Sivavishnu[1], T. kubendiran[2], S.M. Ravi Kumar[2]
[1,2] PG and Research Department of Physics, Government Arts College, Tiruvannamalai-606603, Tamilnadu, India.
[*]Corresponding author: smravi78@rediffmail.com

ABSTRACT

Novel nonlinear optical material Zinc iodide ($Zn(IO)_3$) were successfully grown using slow evaporation solution growth technique at constant temperature. The grown $Zn(IO)_3$ crystal is upto the dimension of 6x4x6 mm^3. The lattice parameters of the grown crystal are a=11.137Á, b=5.271 Á, c=11.142 Á, and volume V= 654.07 $Á^3$ were obtained by Single crystal x-ray diffraction analysis, which reveals that the crystal $Zn(IO)_3$ belongs to monoclinic crystal system with space group $P2_1$. The crystalline perfection of $Zn(IO)_3$ was ascertained by Powder x-ray diffraction analysis. Functional groups were identified by FTIR spectroscopy. The $Zn(IO)_3$ crystal were further characterized by UV-Vis-NIR transmission spectrum in the range of 200-1000 nm. The lower cut-off wavelength (212 nm) and the band gap (Eg=5.4 eV) are estimated from the optical studies. Dielectric constant and dielectric loss measurements were carried out at different temperatures and frequencies. Nonlinear optical property of the crystal $Zn(IO)_3$ was studied by Kurtz powder technique using Nd:YAG laser and the crystal exhibits second harmonic generation (SHG) property.

Keywords: XRD analysis, optical property, SHG efficiency

FTIR-ATR, FT Raman and UV- Visible Spectroscopic analyses and the study on Photo Stability and Estimation of Metformin

S. Kamatchi [*1], E. Sailatha[1], S. Gunasekaran[2] and R. Pavithra Marthandam[1]
[1] – *Spectrophysics Research Laboratory, PG & Research Department of Physics, Pachaiyappa's College, Chennai – 600 030.*
[2] – *Sophisticated Analytical Instrumentation Facility, St. Peter's University, Avadi, Chennai – 600 054.*
* E-mail: kamatchi27788@gmail.com

ABSTRACT

Antidiabetic drugs are the medicine prescribed for the treatment of diabetes mellitus. It reduces blood glucose levels and improves insulin sensitivity. Metformin reduces LDL cholesterol and triglyceride levels and is not associated with weight gain and is the only anti-diabetic drug that has been conclusively shown to prevent the cardiovascular complications of diabetes. These drugs can be administrated either orally or intravenously. They are available either in the form of tablets, powder, syrup and injection. Whatever be the form of drug, quality assurance is essential for the safety and efficacy of drugs, modern spectroscopic techniques are sensitive tools for quality and quantity conformation. The FTIR and Raman spectra of metformin have been analyzed in terms of characteristic frequencies of functional groups in the region 4000-450 cm^{-1} and 4000-50 cm^{-1} respectively. To find the quality factor of metformin using UV-Visible spectroscopic technique in the region 200-800 nm, metformin stored in different environmental conditions were analyzed at different concentrations. A comparison after the sample stored in the ideal condition is made with samples exposed to environmental hazards. Further, the internal standard ratios for some specific modes of vibration have also been studied from the FTIR spectra of these samples. A systematic approach has been adopted using UV-Visible Spectroscopic technique for estimation of the active substance of metformin.

Study of Single Human Hair Fiber of Asthmatic Individuals– A spectroscopic approach

P. Sasi Rekha[1*] and S.Gunasekaran[1]
[1] St.Peter's University, Avadi, Chennai-600 054, TN, India.
**Corresponding author: sasirekha77@yahoo.com*

ABSTRACT

Passing from normal tissue to pathological tissue, cellular biochemistry changes. From a diagnostic and therapeutic point of view, it is fundamental to study the physical and chemical changes occurring in tissues and cells due to disease. Spectroscopy has received quite a lot of attention not only for understanding the biological nature of the disease, but also for the diagnosis of the disease in recent times. In this study, it has been demonstrated that the study of FTIR spectra of single Human Hair Fiber is used to differentiate between the healthy and asthmatic individuals. Some clear differences are observed in terms of optical density of absorption bands and a satisfactory analysis has been made.

Characterization of Nano Cellulosic fibrils isolated from Plantain non-wood fibres

R. Pavithra Marthandam[*1], E. Sailatha[1], S. Gunasekaran[2] and S. Kamatchi[1]
[1] *– Spectrophysics Research Laboratory, PG & Research Department of Physics, Pachaiyappa's College, Chennai – 600 030.*
[2] *– Sophisticated Analytical Instrumentation Facility, St. Peter's University, Avadi, Chennai – 600 054.*
* E-mail: pavimarth@gmail.com

ABSTRACT

Cellulose is one of the richest renewable sources obtained from various plants and microorganisms. This study emphasizes the isolation of Nano Cellulosic Fibrils (NCFs) from the non-wood plant resources; agro wastes of Plantains fibres of two different kinds were chosen to isolate NCFs. The NCFs have been obtained using pulping, bleaching and acid hydrolysis and the Lignocellulosic fibres were characterized using FTIR-ATR in the Mid IR region of 4000-450cm^{-1} to learn the chemical modifications after every treatment to the fibres. The crystallinity index of the fibres and NCFs were studied using powder XRD. The NCFs are also characterized using SEM, HRTEM, AFM, DLS and TGA.

FTIR-ATR Spectroscopy in the Analysis of Sugar in Wheat

S.Natchathira[*1], S.Gunasekaran[1], S.Kamatchi[2] and R.Pavithra Marthandam[2]
*1-Deparment of physics, St. Peter's University, Avadi, Chennai-600054.
1- SAIF-SPU, St. Peter's University, Avadi, Chennai-600054
2- PG& Research Department of Physics, Pachaiyappa's College, Chennai-600030.

ABSTRACT

FTIR Spectroscopic technique is evolving as an important technique in analyzing the polysaccharides of grains and cereals .It is yet again proved with analyzing the fiber, glucose and amylose content of wheat flour procured from different source. The qualitative and quantitative Information of Arabinoxylans (fiber), glucose and amylose were, gathered by the FTIR spectral absorption at 1740cm^{-1}, 1077cm^{-1}, and 929cm^{-1} respectively in the Mid IR region of 4000-450cm^{-1}. The quantitative information of the sugar in wheat flour was obtained by performing internal standard ratio calculations over 1740cm^{-1}, 1077cm^{-1}, and 929cm^{-1} to the FTIR absorptions at 3292cm^{-1}, 1536cm^{-1}, 858cm^{-1} and 761cm^{-1}.The commercially available different brands of wheat also compared with the home ground wheat flour, sieved for four times. The glucose, amylose and fiber content of wheat are also compared with raw and boiled rice flour. The obtained sugar profile is also ensured by the available glycemic index rice and wheat.

Analysis over Nutrients in Soil by Fourth Derivative FTIR and UV- Visible DRS Spectroscopy

S.Revathi [a*], S. Gunasekaran [a], R.Pavithra Marthandam [b] and S. Kamatchi [b]
[a]* - Department of physics, St Peter's university, Avadi, chennai – 600054
a - SAIF-SPU, St Peter's university, Avadi, chennai – 600054
b – PG & Research Dept of physics, Pachaiyappa's college, chennai -600030

ABSTRACT

This investigation solely focuses on finding the suitability of soils in growing crops by adopting spectroscopic techniques. There are few different types of soils which enhance the plant growth of certain kind due to its suitability. The nutrient content to the soil to soil is very unique based on its inorganic and organic content. Thus, the investigation is extended in studying the spectral behaviors of soils used for cultivation of different crops in infrared region. The FTIR studies of soils are carried out in the mid IR region of 4000-450cm^{-1}.The FTIR spectral exhibitions of soils, the qualitative analysis has been carried out and the minerals present in the soils were found. The presence of sulfate ions of $ZnSO_4$, $CaSO_4$, $MnSO_4$, and $FeSO_4$ is attributed to the FTIR absorption in the region of 995cm^{-1} in the zeroth order spectra of the soil samples. Further, to classify the sulfate ions of various nutrients, fourth derivative FTIR spectroscopy is employed and the absorption band at 995 cm^{-1} recoded into the absorptions in the regions of 1112 cm^{-1}, 1009 cm^{-1}, 904 cm^{-1}, and 870 cm^{-1} of sulfate ions based on the association. The results obtained from chemical methods is compared with the results of Fourth Derivative FTIR spectral impressions of the soil samples.The soil samples were also investigated for the presence of the sulphate ions UV-Visible DRS spectroscopy technique. The results obtained from reflectance spectroscopy techniques are compared by the conventional spectrometric and titrimetric techniques involved in soil analysis.

ISOLATION AND CHARACTERIZATION OF NANO CELLULOSIC FIBRILS FROM ACACIA NILOTICA

G.B.Anushya[1*], S.Gunasekaran[1], R.Pavithra[2] and S. Kamatchi[2]
*1-Deparment of physics, St. Peter's University, Avadi, Chennai-600054.
[1-] SAIF-SPU**,** St. Peter's University, Avadi, Chennai-600054.
[2-] PG& Research Department of Physics, Pachaiyappa's College, Chennai-600030.

ABSTRACT

In this present work, the cellulosic and nano cellulosic fibrils were successfully isolated from ground wood of Acacia Nilotica. The ground wood, Cellulose and isolated nano cellulosic fibrils are characterized by using Fourier Transform Infrared Spectroscopy (FTIR-ATR), Powder XRD technique, High Resolution Scanning Electron Microscopy (HRSEM), High Resolution Transmission Electron Microscopy (HRTEM). The appearance and disappearance of bands in FTIR spectra shows the removal of lignin and hemicelluloses was successful after the treatment of acid hydrolysis. The XRD patterns obtained shows the enrichment in the percentage of crystalline nature from ground wood to Cellulose and nano cellulose manifests a significant conversion of amorphous to crystalline nature. The surface morphology of ground wood, cellulose and nano cellulose of Acacia Nilotica is observed by using HRSEM analysis. The dimension of isolated nano cellulose was obtained by HRTEM analysis.

Discrimination of Diabetic and Normal Human Scalp Hair Fibre Using Single bounce ATR - FTIRSpectroscopic Technique

A.Rajeswari[a*], S. Gunasekaran[a], S. Kamatchi[b]and R.PavithraMarthandam[b]
a* - Department of physics, St Peter's university, Avadi, chennai – 600054
a - SAIF-SPU, St Peter's university, Avadi, chennai – 600054
b – PG & Research Departmentof physics, Pachaiyappa's college, chennai -600030

ABSTRACT

Diabetes is the faster growing long term disease that affects millions of people worldwide.Diabetes mellitus is a chronic metabolic syndrome or disorder that prevent the body to utilize the glucose completely or partially. Diabetes is known as a disorder of carbohydrates metabolized characterized by high blood sugar level (hyperglycemia). To diagnosis diabetes, hair could be used to detect diabetic by using FTIR-ATR technique. The FTIR-ATR spectra of human scalp hair fibres have been recorded in the mid-infrared region of 4000-450 cm^{-1}. The human hair samples of diabetic patients where chosen for study, because they exhibit distinct changes in the bio- chemical properties, which can be analysed successfully by advanced FTIR-ATR spectroscopic techniques. The FTIR-ATR spectral analysis revealed differences in several major metabolic components glucose, proteins, and lipidsthat clearly demarcated normal and diseased hair fibres. Patients with Diabetes showed increase in the peak height ratio of the $\mathbf{I_{1240/1085}}$, $\mathbf{I_{3285/2930}}$,**and** $\mathbf{I_{1640/1545}}$ of glucose, protein, and lipids bands. In the present study aims at employing FTIR-ATR Spectroscopy for analyzing the Diabetes hair sample with elevated glucose, protein and lipid, levels to detect spectral parameter, which might serve as biomarker for identifying and detecting glucose, protein and lipid. The absorbance values at these specific modes of vibration varied significantly from that of normal subject. To differentiate Diabetes from that of normal subjects, Internal Radio parameter among the absorption bands has been introduced and the results are substantiated by histogram. It has been found that diabetes hair sample is more sensitive to absorb infrared radiation than that of normal hair fibre.

Preparation and characterization of TiO_2 @ carbon nanoroad as anode materials for lithium ion Battery applications

E.Priyadharshini [a*], S. Srinivasan [a]

[a,a*]Department of Physics, Presidency College, Chennai- 600 005
*Email: prydharshini20@gmail.com

ABSTRACT

In this method study provides a simple hydrothermal method. The purpose of this method controlled introduction of carbon to optimize better electrical performance of lithium ion battery using the TiO_2@ carbon nanoparticle as anode materials. Lithium ion battery is prepared by a facile route using titanium tetrachloride and commercial filter paper is the carbon source. The weight ratios between carbon nanoparticle and TiO_2, nanoparticles, which seriously affect the battery performance, have been demonstrated to be easily tuned by adjusting the different sintering temperature. The electrochemical performance shows that the TiO_2@carbon nanoparticle with the good percentage have been the best performance with the good capacity of 540 mAg^{-1}after 40 cycle at a current density of 100 mAg^{-1}.were calcined at different temperature 400,450,500^oC and characterized using Powder X-ray diffraction (XRD), Thermo gravimetric (TG) & Differential thermal (DT) analyses, Scanning Electron Microscope (SEM), energy dispersive X-ray diffraction, FT-Raman & UV-Visible Spectral analyses and galvanostatic Charge-discharge tests.

Crystal structure analysis of (2'R,3'R,4'R)-3'-(1H-benzo[d]imidazol-2-yl)-4'-(4-bromophenyl)-1'-methyl-2-oxospiro[indoline-3,2'-pyrrolidine]-3'-carbonitrile

K. Elumalai[1], Nataraj Poomathi[2], P. T. Perumal[2], K. Sakthi Murugesan[1*]
[1,1*]Department of Physics, Presidency College (Autonomous), Chennai-600 005, India

[2]Organic Chemistry Division, CSIR Central Leather Research Institute,
Adyar, Chennai-600 020, India

***Corres.author email:** ksakthimurugesan2492@gmail.com

ABSTRACT

The crystal structure of(2'R,3'R,4'R)-3'-(1H-benzo[d]imidazol-2-yl)-4'-(4-bromophenyl)-1'-methyl-2-oxospiro[indoline-3,2'-pyrrolidine]-3'-carbonitrile ($\mathbf{C_{27}H_{26}BrN_5O_3}$). The compound crystallizes in Monoclinic, P21/nspace group with unit cell parameters at 296(2) K as follows: a = 18.660 (2) Å, b =7.5092 (7) Å, c =19.001 (2) Å, α = β =90°, γ =110.26°.Crystal data were collected using BRUKER SMART APEX II CCD X-ray diffractometer. The structure was solved by direct methods and refined on F^2 by full-matrix least-squares procedures to the final R_1 of 0.089usingSHELXL programs.

Key Words:oxoindoline, pyrrolidine and crystal structure.

Infrared study of compositional changes of poorly crystalline hydroxyapatite of bone tissues of fingerlings edible fish

S.Karthikeyan*[1], R. Ravisankar[2], P.Eswaran[3]
[1] Department of Physics, Dr. Ambedkar Government Arts college, Vyasarpadi, Chennai-600039
[2]PG and Research Department of Physics, Government Arts College, Tiruvannamali-606603.
Department of Physics, *Dhaanish Ahmed College of Engineering, 601301 Chennai.*
**Corresponding Author: physicskarthik@gmail.com*

ABSTRACT

The composite nature of bone consists of hydroxyapatite, collagen, water, minerals which surrounds crystals by dense filling. A biological apatite usually has a calcium deficient substituted by either CO_3^{2-} or PO_4^{3-} ions. This characteristic change influence crystallinity, crystal symmetry, and lattice parameters, physical and biological characteristics of bone. Thus quantitative measurement of bone mineral composition varies considerably in relation to bone age, type and its nature. The mineral component of bone is the poorly crystalline hydroxyapatite in which CO_3^{2-} ions substitutions will lead to nonstoichiometric apatite minerals. This substitution creates vacancies and distorts the crystal lattice consequently which affects the mechanical strength of bone. FTIR is a powerful tool for conformation regarding bone minerals and its compositions. This changes is studied by FTIR in the region of 500-650 cm^{-1}, 850-890 cm^{-1}, 900-1200 cm^{-1} and in amide I region. In addition the other parameters such Ca/P ratio, crystallinity Index, Mineralization index and aging of bone can be computed from the FTIR spectra. The study reveals a bone mineral of fingerling is poorly crystalline and its crystallinity increases to the aging of bone. Further changes in the secondary structure protein are studied in the collagen matrix of the bone sample. The study helps in understanding the mechanism of compositional changes in the bone minerals and its crystalline nature using FTIR spectroscopy.

***Key Words**: FTIR, hydroxyapatite, Crystallinity Index, Ca/P ratio, bone minerals*

Comparative Study on Healthy and Anemia Diseased Human Nail Samples using FTIR-ATR Spectroscopic technique.

P. Ramesh [a], S. Gunasekaran [b]
a , b St.Peter's Institute of Higher Education and Research
St. Peter's University, Avadi, Chennai -600 04.
Corresponding author Email: rameshphysics12@gmail.com

ABSTRACT

Generally nails can be an index of health with abnormalities found under diseased conditions. There is a prominent colour change in the anemic diseased patients nail. Possible differences in infrared (IR) spectra of nail samples of anemia patients compared to the healthy subjects were investigated in the present study. The FTIR-ATR spectra of human nail samples have been recorded in the mid-infrared region of 4000-450cm^{-1}. The spectral analysis revealed that differences in several major metabolic components of proteins, lipids and glucose that clearly indicated healthy and anemic diseased nails. There are significant changes in the spectral bands at 3285cm^{-1},1655cm^{-1} and 1545cm^{-1} due to N-H Stretching Vibrations of amide A, Amide I and Amide II respectively for anemic nail with that of the healthy nail. Intensities of IR spectra provide quantitative information, while the frequencies revealed that quantitative analysis about the nature of the chemical bonds and their structure. Infrared spectroscopy may represent an appropriate tool with which to identify the risk factor of anemic diseases.

Magnetic and Electrochemical Behaviour of Cobalt Doped Tungsten Oxide (WO_3) Nanomaterials by Microwave Irradiation Method

V. Hariharan[a], B. Gnanavel[b*], S.Komathi[b] and D.Dhanabalan[b]
[a]Department of Physics, Mahendra Arts and Science College,
Kalipatti – 637 501, Tamilnadu, India
[b] PG & Research Department of Physics, Chikkaiah Naicker College, Erod – 4, Tamilnadu, India
E-mail address: gnanavelphd@gmail.com

ABSTRACT

Nanocrystalline $WO_3.H_2O$ nanopowders, doped with cobalt (2 and 5 wt%) have been synthesized using $CoCl_2.6H_2O$ and $Na_2WO_4.2H_2O$ in a facile microwave irradiation process, followed by the annealing process. The samples were characterized with powder X-ray diffraction, field emission scanning electron microscopy, UV-VIS diffusion reflectance spectroscopy, photoluminescence spectroscopy and cyclic voltammetry (CV). X-ray diffraction patterns showed both undoped and Co doped $WO_3.H_2O$ crystallized with orthorhombic phase. Annealing h-WO_3 at 600˚C 6h in air resulted in the different products, $W_{17}O_{47}$ (monoclinic) for undoped, WO_3 orthorhombic for 2 wt% Co doped and WO_3 (monoclinic) for 5 wt% Co doped. FE-SEM micrographs suggested that the dopants are able to influence the growth rate and morphology of the prepared nanopowders. UV-VIS-DRS spectra revealed that the dopant (Co ion) is incorporated in the intermediate energy level. Blue emissions (450 – 550 nm) were verified using PL at room temperature for the annealed samples ($W_{17}O_{47}$ and WO_3) with excitation wavelength 390 nm. The difference in peak intensity observed through PL spectra attributed to the possible distortions in WO_4^{2-} tetrahedron group during microwave irradiation process. Electrochemical studies showed the possible enhanced catalytic behavior of cobalt doped (5wt.%) as prepared samples than that of others. The temperature dependent magnetic susceptibility (300 K to 2 K) and isothermal magnetization measurements showed the enhancement in magnetic behaviour of the samples for diamagnetic to antiferromagnetic nature which is clearly shows the incorporation of Cobalt ion at tungsten lattice site and in determining the resultant magnetic behaviour of the samples.

Keywords: Tungsten oxide, Microwave irradiation, Cobalt doping, Nanoparticles, Magnetic properties, Cyclic Voltammetry

Growth and Characterization of Pure, L-Lysine doped and L-Leucine doped TGS Crystals

K.Balasubramanian[1*], A.Ponchithra[2], T.Karpagam[2], S.Sivapriya[2].
[1] Department of physics, The M.D.T Hindu college, pettai, Tirunelveli.
[2] Research Scholar, Department of physics, The M.D.T Hindu college, pettai, Tirunelveli.

ABSTRACT

Pure and amino acid doped Triglycine sulphate crystals were grown from aqueous solution by slow evaporation method. The solubility of the TGS increases with increasing temperature. The grown crystals were subjected to powder XRD analysis, and the result shows slight changes in peak intensities and peak position, which may be attribute to strain in lattice. The presence of functional groups in the crystals has been observed by FTIR analysis. Optical transmission studies were carried out by allowing the UV-NIR rays of wavelength between 200-1100nm. Dielectric constants of the grown TGS crystals were determined at various temperatures. Micro hardness studies were carried out by using vickersmicrohardness tester.

Key words: Growth from solution - X-ray diffraction - FTIR studies - Transmittance spectrum - Dielectric constant - Microhardness test.

Tri-block copolymer of Poly (Urethane-Urea) Based on HMDI: Synthesis and Characterization

***M. Kayalvizhi, K. Balaji and A. Arun*[*]**
P.G & Research Department of Chemistry, Government Arts College, Tiruvannamalai – 606603, Tamilnadu, INDIA.

ABSTRACT

A series of polyurethane triblock copolymers were synthesized by reacting a hexamethylene diisocyanate (HMDI) with functionalized polystyrene (OH-PSt-OH, M_n = 2,000 g/mol). Two different amines were used as chain blockers, n-hexylamine (6m) and aniline. The length of the soft segment was varied from 2000 to 9042 g/mol using HMDI as chain extenders. The synthesized copolymers were characterized by viscosity measurements, FT-IR, DSC, TGA, water absorption and solvent resistivity. Depending on the urethane-urea concentration, the melting temperature of the polymers was varied from 273°C to 258°C. The inherent viscosities of the polymer were found to be 0.13 - 0.42 dL/g suggesting that triblock copolymers were of low molecular weight. The solubility of the polymer in chloroform was found to be depends on the concentration of the hard segment. The TGA data reveals that the polymer showed single stage decomposition centered around 400°C.

Keywords: Polystyrene, Poly (urethane-urea), semi-crystalline, thermal stability, solvent resistivity.

Growth aspects, spectral and thermal studies of Cerium (III) doped sulphanilinic acid with tartaric acid based single crystal

E.Vinoth[*], S.Elavarasu, N.Vaigundan, M.Govindharaj and E. Vakees
[*]PG and Research Department of Physics, Government Arts College, Tiruvannamalai 606611, India
Department of Chemistry, Sivagamiammal College of Arts and Science, Krishnagiri 635108, India

ABSTRACT

Growth and characterization of novel crystal based on ammonium ceric sulphate (ACS), sulphanilic acid and tartaric acid. The crystals were grown by slow evaporation technique using water solvent. The grown crystal structure is confirmed by single crystal X-ray, FT-IR, UV-Visible, NMR, TGA, NLO and electrical properties. A single crystal X-ray diffraction study is confirmed by monoclinic structure of system. All the functional groups are confirmed by FT-IR spectroscopy. Structural studies are established by NMR technique. The growth crystal is thermally stable upto 208ºC and melting point is 168ºC. The powder SHG studies were done with the Kurtz powder technique and the NLO efficiency is one times greater than that of standard KDP.

Keywords: X-ray diffraction, crystallization, growth from solution, nonlinear materials
Corresponding author tel.:+91 9442792346
E-mail address:vakees.e@gmail.com

Growth and characterization of HALT single crystal by Sankaranarayanan - Ramasamy (SR) and Slow Evaporation Solution Growth (SEST) method

R. Purusothaman[a], M. Shankar[a], P. Dennis Raj[b], I. Vetha Potheher[a*]
[a]Department of Physics, Bharathidasan Institute of Technology (BIT) Campus, Anna University Tiruchirappalli - 620024, Tamil Nadu, India.
[b]Department of Physics, Mookambigai College of Engineering, Pudukkottai - 622 502, Tamil Nadu, India
* Corresponding author: Dr. I. Vetha Potheher, Assistant Professor in Physics, Bharathidasan Institute of technology (BIT) Campus, Anna University Trichirappalli-6200024.
Mobile: +919942994274, Email: potheher11@gmail.com

ABSTRACT

The HALT single crystal was grown by Slow Evaporation Solution Growth method and Sankaranarayanan – Ramasamy method. The SEST crystal was dimension 5x4x3 mm^3 and their grown crystal growing period 20 days. The seed crystal of SEST was used (010) was SR method. The SR grown crystal was growing period of 40 days and their growing crystal length 50mm diameter 20mm. The HALT grown crystal was confirmed X-ray diffraction method by both single and powder X-ray techniques. The crystal was space confirmed $P2_1$, the mention space group identity helpful behavior for acentric or polar group. The HALT single crystal was optical transmittance SR method grown crystal higher than SEST grown crystal. The Photoluminescencespectrum of grown crystal was SR high intensity to SEST method. The thermal analysis grown crystal was melting point at 130 °C. The piezoelectric coefficient of HALT grown crystal was 0.67 pC/N that time of compared quartz single crystal.

Synthesis and Characterization of ZnO nanorods by using hydrothermal method

N. Senthil Kumar, E. Vivek, S. Sharmila, I. Vetha Potheher*
Department of Physics, Bharathidasan Institute of Technology (BIT campus), Anna University, Tiruchirappalli, Tamilnadu, India
**Corresponding Author e-mail: potheher11@gmail.com*

ABSTRACT

In this present work, ZnO nanorod was prepared by a hydrothermal method. The ZnO nanorods were synthesized by using a 100ml Teflon lined stainless steel autoclave. The Synthesized ZnO nanorods where confirmed and characterized by UV-Visible spectroscopy, Powder X- ray diffraction (PXRD), Fourier Transform Infrared spectroscopy (FTIR), Raman Spectroscopy, TG-DTA analysis, Zeta Potential analysis and Field Emission Scanning Electron Microscopy (FESEM). The UV absorption of the wavelength observed at the peak of 378 nm & Energy band gap of the ZnO nanorods was found to be 3.2eV.The FTIR analysis confirmed the presence of various functional groups in the ZnO nanorods. The synthesized ZnO nanorods are confirmed by the powder XRD analysis and the crystalline size was calculated by the Scherer's formula and it also shows the purity of the synthesized ZnO nanorods. The thermal behavior of the ZnO nanorods was studied by TGA and DTA analysis. The zeta potential analysis shows stability of the synthesized ZnO nanorods. The crystalline size, shape and surface morphology of the ZnO nanorods are determined by using FE–SEM.

A study on Electrochemical Properties of ZnO/Mn_2O_3 Nanocomposite material for Supercapacitor Application

N. Senthil Kumar, E. Vivek, S. Sharmila, I. Vetha Potheher*
Department of Physics, Bharathidasan Institute of Technology (BIT campus), Anna University, Tiruchirappalli, Tamilnadu, India
**Corresponding Author e-mail: potheher11@gmail.com*

ABSTRACT

In this work, ZnO/Mn_2O_3 nanocomposite is synthesized by adopting simple hydrothermal method. The as prepared material was characterized by Powder X-Ray Diffraction, Fourier Transform Infrared Spectroscopy, Raman spectroscopy, TG-DTA analysis, UV-Vis spectroscopy. The UV absorption of the wavelength observed at the peak of 215nm. The FTIR analysis confirmed the presence of various functional groups in the ZnO/Mn_2O_3 nanocomposite material. The synthesized ZnO/Mn_2O_3 nanocomposite was confirmed by the powder XRD analysis and the crystalline size was calculated by the Scherer's formula and it also shows the purity of the synthesized nanoparticles. The surface morphology was studied using Field Emission Scanning Electron Microscopy (FE-SEM). The electrochemical performance of ZnO/Mn_2O_3 was analyzed by employing techniques like cyclic voltammetry, galvanostatic charge discharge and electrochemical Impedance Spectroscopy. Based on the electrochemical results, it shows a specific capacitance of about 675 F/g at the scan rate of 5 mV/s in 1 M KCL electrolyte solution and gives a better cyclic stability even after prolonged cycles (1000 cycles). The efficiency of 90.5 % was obtained and moreover it possess constant efficiency rate from 100 to 1000 cycle , which entails the ZnO/M_2O_3 nanocomposite is as a promising candidate for supercapacitor applications.

FABRICATION OF SN:CEO_2/ TIO_2 HYBRID PHOTO ANODE FOR DYE SENSITIZED SOLAR CELLS

K.Sahadevan[1,2], P.Kumaresan[1], M. Karl Chinnu[3]

[1] Department of Physics, Thiru.A.Govindasamy Government Arts College, Tindivanam- 604 002, Tamil Nadu, India.
[2] Department of Physics, Periyar University, Salem-636 011, Tamil Nadu, India.
[3]Department of Physics, Dr. Ambedkar Government Arts College, Vyasarpadi, Chennai-600039, India.
E.mailID :chinnu0202@gmail.com,logeshkumaresan@yahoo.com

ABSTRACT

CeO_2 and Sn:CeO_2nanocrystals, successfully synthesized by simple Sonochemical method. Their photo voltaic performance was investigated with TiO_2 nanostructure in an effort to enhance the light conversion efficiency of DSSCs. The highest short circuit current was measured among them, which was proved to be related to the fast electrons transferred in the hybrid electrodes. CeO_2 has high band gap energy and conduction band of both stable Ce^{3+} ($4f^15d^0$) and Ce^{4+} ($4f^05d^0$) oxide states, owing to the remarkable redox property and oxygen storage capacity. The Ceria changes in the conduction band of TiO_2, due to the unoccupied Ce-4f trap states in the band gap, and reduction of Ce^{4+} to Ce^{3+} when electrons are injected in the photo anode. The cerium oxide doped photoanodes with special electrochemical properties which strongly influence the performance of DSSCs. The PCE of the Sn:CeO_2-TiO_2anode cell was conspicuously improved by loading the Sn:CeO_2 and the maximum PCE was 5.4 %. The overall solar to electric energy conversion efficiency was about 24% for Sn:CeO_2/TiO_2 (AM-1.5, 100 mW/cm^2) compared with pristine anode.

Keywords: Sn:CeO_2:TiO_2, DSSCs, Photocurrent, impedance, electron life time

---

FTIR, FT – RAMAN ANALYSIS AND QUANTUM CHEMICAL CALCULATIONS ON ACETAZOLAMIDE

M. Suhasini[a*], E. Sailatha[a], S. Gunasekaran[b], G.R. Ramkumaar[c],

[*a]PG& Research Department of Physics, Pachaiyappa's College, Chennai – 600 030.
[b]Research and Development, St. Peter's University, St. Peter's Institute of Higher Education and Research, Avadi, Chennai – 600 054
[c]Head, Department of Physics, C.Kandaswami Naidu college for Men, Chennai – 600 102.

ABSTRACT

The Fourier Transform (FT) infrared and FT-Raman spectra of benzothiazole (BT) have been recorded and analyzed. The equilibrium geometry, bonding features, and harmonic vibrational frequencies have been investigated by ab initio (HF) and density functional theory (DFT) methods. The assignments of the vibrational spectra have been carried out. A detailed interpretation of the vibrational spectra of the molecule has been made on the basis of the calculated Potential Energy Distribution (PED) by VEDA program. The computed optimized geometric bond lengths and bond angles show good agreement with experimental data of the title compound. UV–visible spectrum of the compound was also recorded and the electronic properties, such as HOMO and LUMO energies and λmax were determined by time-dependent DFT (TD-DFT) method. Stability of the molecule due to conjugative interactions arising from charge delocalization has been analyzed using natural bond orbital (NBO) analysis. The thermodynamic functions of the title molecule were also performed using the HF and DFT methods.

FITR – ATR Spectroscopy in Qualitative & Quantitative analysis of different Milk Species

L. Sangeetha[a*], S.Gunasekaran[a], S.Kamatchi[b] and R.Pavithra Marthandam[b]
[a*] Department of Physics, St.Peter's University, Avadi, Chennai-600 054.
[a] SAIF –SPU St. Peter's University, Avadi, Chennai-600 054.
[b] PG & Research Department of Physics, Pachiyappa's College, Chennai – 600 030.

ABSTRACT

FTIR- ATR, having diamond IRE is employed for the identification and quantification of the nutrient composition of milk in different milk species of cattle, such as Goat (SGM), Cow (SCM), Buffalo (SBM), boiled Cow's milk (SBCM) and boiled Buffalo's milk (SBBM). The same is employed in the characterization of various brands of commercially available stored milk procured from grocery shop viz., SAM, SSTM, SSFCM, SAPFCM, SAPTM and SAPSM to study the contents of the constituents of the milk were chosen, based on the results of the fresh cattle milk samples. The FTIR absorption of the constituents of fat, protein, lactose and minerals witnessed in the region of 1744 cm^{-1}, 1644 cm^{-1}, 1451 cm^{-1}, 1066cm^{-1} and 1024cm^{-1} are also quantified to the FTIR absorptions at 1402 cm^{-1} and 892 cm^{-1}. The efforts taken in this quantification work discloses the contents in different brands of commercially available stored milk.

Qualitative and Quantitative Assessment of Pure Honey and Commercial Honey Using FTIR-ATR Spectroscopy

S.Vimala[a*], S.Gunasekaran [a], S.Kamatchi [b], R.Pavithra Marthandam [b]
[a*] - Department of Physics, St. Peter's University, Avadi, Chennai – 600 054.
[a] – SAIF–SPU, St. Peter's University, Avadi, Chennai – 600 054.
[b] – PG & Research Dept of Physics, Pachaiyappa's College, Chennai – 600 030.

ABSTRACT

Honey is an important agricultural product for medicinal properties for centuries. A large proportion of honey's components consist of sugars, mainly Fructose, Glucose, Sucrose and Maltose. The spectral exhibition of pure honey extracted from bee is compared with the procured commercial honey samples VAH, VBHGA2, VDA, VHGA1 and VLH. The spectra of honey samples have been recorded in the Mid- Infrared region of 4000 – 450 cm^{-1}**.** The ratio of the spectral intensities are considered to discriminate the adulterated samples from the pure sample. The spectral signatures of the adulterated samples are also recorded in the Mid IR region. The variations observed in the optical density of the FTIR spectral signatures of the honey samples show the differences in the Fructose, Glucose and Sucrose of honey. The sensitive bands from the honey ie., 1063 cm^{-1} due to stretching vibration of C-O of fructose, 1033 cm^{-1} due to C-O stretch in the C-OH of glucose and 995 cm^{-1} due to C-C and C-O stretching of sucrose**.** The quantitative information of the honey samples are obtained by performing internal standard ratio calculation over the chosen specific modes of vibration $I_{1063/3298}$, $I_{1033/3298}$ & $I_{995/3298}$ and quantified.

Study of antibacterial activity, synthesis and characterisation of silver nanoparticles using *Morinda coreia* leaf extract in green synthesis methods

J. Venugobal[a], K. Anandalakshmi[b*]
[a]Department of Physics, Sir Issac Newton College of Engineering and Technology, Nagapattinam, Tamil Nadu, India.
[b]Department of Engg. Physics, Annamalai University, Annamalainagar 608 002, Tamil Nadu, India

ABSTRACT

Silver nanoparticles (Ag NPs) have involved the interest of researchers because of their unique properties and various field applications such as medicine, catalysis and textile. The green synthesized Ag NPs were analyzed by UV-visible analysis, Fourier transform infrared spectroscopy (FTIR), X-ray diffraction (XRD), Field emission scanning electron microscopy (FESEM), Energy-dispersive X-ray spectroscopy analysis (EDAX) and Transmission electron microscopy. UV-Vis spectroscopy technique used to study the formation of Ag NPs and it exposed the surface plasmon resonance (SPR) at 428 nm. FTIR spectra provide the evidence for the presence of biomolecules responsible for reduction and capping of silver nanoparticles. X-ray diffraction (XRD) analysis revealed the average crystalline size of the synthesized Ag NPs was approximately 20 nm. Field emission scanning electron microscopy (FESEM) depicted the spherical morphology of Ag NPs with size range of 15-25 nm.TEM reveals spherical shape of synthesized Ag NPs. The synthesized silver nanoparticles were found to exhibit high antibacterial activity against the bacteria such as *E. coli*, *K. pheumoniea*, *M. flavus*, *P. aeruginosa*, *B. subtilis*, *B. pumilus*, *S. aureus*.

Kew words: Ag NPs, Green synthesis, Anti bacterial activity.

* Corresponding author. E-mail address: anandhi8888@gmail.com (K. Anandalakshmi) Tel: +91-9842694183

Linear and Nonlinear Optical Properties of L-Glutamic Acid Zinc Chloride (LGAZC) Semiorganic NLO Crystal

S. Chennakrishnan[1], D. Sivavishnu[2], J. Johnson[2], S.M. Ravikumar[2,*]
[1]Department of physics, Idhaya Arts & science College for women, Tiruvannamalai 606 705. Tamilnadu, India.
[2]Department of physics, Government Arts College, Tiruvannamalai 606 603, Tamilnadu, India.
[*]**Corresponding author**: smravi78@rediffmail.com; ravism23@gmail.com.

Abstract

The aim of this work is to investigate the growth and physiochemical properties of nonlinear optical semiorganic crystal of L-Glutamic acid Zinc chloride (LGAZC) optically good grade and defect free crystal was grown by slow evaporation technique under optimized conditions. Single crystal X-ray diffraction studies reveals that the crystal is orthorhombic structure with lattice parameters a = 5.17 Å, b = 6.95 Å, c = 17.35 Å, α = β = γ = 90° and Volume = 623.411Å^3. The spectroscopic properties were investigated by recording the Fourier transform infrared and optical transmission spectra. The thermal decomposition process was investigated by Thermo Gravimetric and Differential Thermal Analysis (TG/DTA). LGAZC crystal exhibit second harmonic generation (SHG) efficiency which is nearly 0.44 times more than that of KDP. The presence of the metal ion in a grown crystal was investigated by EDAX study.

Keywords: NLO, XRD, EDAX, Thermal studies,

Preparation and characterization of TiO_2 @ carbon nanoroad as anode materials for lithium ion Battery applications

E.Priyadharshini [a*], S. Srinivasan [a]
[a,a*]Department of Physics, Presidency College, Chennai- 600 005
Email: prydharshini20@gmail.com

ABSTRACT

In this method study provides a simple hydrothermal method. The purpose of this method controlled introduction of carbon to optimize better electrical performance of lithium ion battery using the TiO_2@ carbon nanoparticle as anode materials. Lithium ion battery is prepared by a facile route using titanium tetrachloride and commercial filter paper is the carbon source. The weight ratios between carbon nanoparticle and TiO_2, nanoparticles, which seriously affect the battery performance, have been demonstrated to be easily tuned by adjusting the different sintering temperature. The electrochemical performance shows that the TiO_2@carbon nanoparticle with the good percentage have been the best performance with the good capacity of 540 mAg^{-1}after 40 cycle at a current density of 100 mAg^{-1}.were calcined at different temperature 400,450,500^oC and characterized using Powder X-ray diffraction (XRD), Thermo gravimetric (TG) & Differential thermal (DT) analyses, Scanning Electron Microscope (SEM), energy dispersive X-ray diffraction, FT-Raman & UV-Visible Spectral analyses and galvanostatic Charge-discharge tests.

Vibrational Spectroscopic and Thermodynamic analysis on 2-(2, 3-dimethylphenyl) amino benzoic acid

R.Padmavathi[1*], B. Rajamannan[2], S.Gunasekaran[3], G.R.Ramkumar[4], G Sankari[5].
[1]Department of Physics, Meenakshi Sundararajan Engineering college, Kodambakkam, Chennai,600024.
[2]Engineering physics, FEAT Annamalai University, Annamalai Nagar, Chidambaram.
[3]Research and development St.Peter's institute of Higher Education and Research ,St.Peter's University, Avadi,Chennai, 600054.
4.Department of Physics ,C.Kandaswaminaidu college for Men, Anna Nagar East, Chennai,600102.
[5]Department of Physics, Meenakshi college for Womens, Kodambakkam, Chennai, 600024,
***E-mail: pathmavathi@gmail.com**

ABSTRACT

Mefenamic acid is a nonsteroidal anti- inflammatory drug (NSAID). Mefenamic acid is a white to greyish-white, odorless, microcrystalline powder with a melting point of 230°-231°C and water solubility of 0.004% at pH 7.1. The molecular weight is 241.29. The FTIR and FT-RAMAN Spectra of 2-(2, 3-dimethylphenyl) amino benzoic acid were recorded in region 4000-450 cm^{-1} and 4000- 50 cm^{-1}respectively. the vibrational parameters were determined by B3LYP/6-31G(d,p),B3LYP/6-31++G(d,p),RHF/6-311G(d,p).Thermodynamic parameters such as zero point vibrational energy (ZPVE) ,thermal energy and specific heat capacity ,entropy of Mefenamic acid at 298 K in ground state have been calculated by HF and DFT methods. The calculated HOMO and LUMO energies indicate that charge transfer occurs within the molecule.

Keywords: Vibrational spectra, DFT, Thermodynamic properties

Ultrasonics for All - A Review on the Recent Industrial Practices and It sApplications

P.Kuppuraj[1]*, S.Gunasekaran[2]

[1]*PG & Research Department of Physics, Pachiyappa's College, Chennai-30, Tamilnadu, India.*

[2] *SAIF, Research and Development, St.Peter's University, Avadi, Chennai-54, Tamilnadu, India.*

* Corresponding Author: wowkr@rediffmail.com

ABSTRACT

Once upon a time we surprised, how great this "new" technology is that we have to see inside people bodies in a non-invasive way!, Yes!, the human body scanning technology developed by Ultrasonic irradiations for medical Imaging Purpose since 1950's but It is taken a long amount of time because the research and development of sound waves and its allied technology slowly enhanced from the way back in the 17 Th Century. But, it is very interesting to look back and see how one of the most widely used medical imaging modalities came about and how it has changed over the decades to become what it is today. Moreover, one can only imagine how ultrasound technology will continue to evolve. Nowadays, Ultrasonics and Its assisted Technologies are entered many Industries Like Medical, Pharmaceutical, Chemical, Petrochemical, Oil & Refineries, Energy, Biodegradation, Biodiesel & Biofuels, Solar, Wind, Hydro, Atomic, Nuclear &, Thermal Power Generation Plants, Road & Transports, Automotive, Railways, Aerospace & Aeronautical, Ship & Marine, Civil & Mechanical Constructions, Manufacturing, Fabrications, Machining, Welding, Moulding, Brazing, Cleaning, Cutting, Waste Management, Water Treatments, etc., From the Economical View Without Ultrasonic Assistance, the development of Industrial Practices are very difficult. That's why, we are interested to review and study the recent Industrial Practices through Ultrasonically Assisted Methods Viz., Production, Processing, Enhancing, Testing, Analysis, Measurements, Quality Control and Assurance activities. By the way, we attempt to identify the Principles, Techniques, Equipments and Application Data's are summarized for these areas and the limitations due to the influence of unwanted variables are identified in some case studies and also we aims to accelerate the forthcoming Technological developments in the field of Ultrasonics.

Keywords: Ultrasonics, Ultrasonic Irradiations, Application of Ultrasonics, Industrial Practices on Ultrasonics, Ultrasonic Assisted methods, Uses of Ultrasonics, Ultrasonic Processor, Sono-process, Physics of Ultrasonics, UFD,UTG, Ux Cleaning, Sonicator,etc.,

---

Growth and Characterization of nickel sulphate admixtured L-alanine crystals (LANS)

[1]R.Jothimani, [2]P. Selvarajan

[1]Department of Physics, Sadakathullah Appa College, Tirunelveli Tamil Nadu.

[2]Department of Physics, Aditanar College of Arts and Science,Tiruchendur, Tamil Nadu.

ABSTRACT

NLO materials have a nonlinear response to the electric field of the light of a laser beam**.** Most of the amino acids are NLO materials that find application in field of optical communication, information technology, signal processing and industrial applications. The NLO active material such as L-alanine is mixed with nickel sulphate in the molar ratio 2: 1 to bring out better NLO active crystals. The reactants are dissolved in double distilled water, stirred well using hot plate magnetic stirrer at 50^{o}C for three hours. The solution was filtered and kept in undisturbed place. Colourless and transparent crystals were formed and they were harvested after growth period of 20 days. The grown crystals are subjected to various characterizations. The structure of LANS was confirmed to be orthorhombic with a non-centro symmetric space group $P2_12_12_1$ by SCXRD analysis. The NLO efficiency of LANS is highly pronounced comparing to that of L-alanine. Good degree of crystallinity of the sample is confirmed by TGA/DTA analysis. UV–visible–NIR transmittance spectrum was recorded for the sample to analyse the transparency in visible and near infrared region (NIR). The optical band gap (E_g) and other optical constants were determined. The grown sample was characterized by Energy Dispersive Analysis by X-rays (EDAX) to confirm the presence of elements. Hardness parameters show the mechanical strength of LANS crystal.

Keywords : SCXRD; NLO; crystallinity; solution growth; optical constants; LDT

EFFECT OF TEMPERATURE, STRUCTURAL AND MAGNETIC STUDIES ON ANILINE CAPPED MANGANESE OXIDE NANO STRUCTURES FABRICATED BY HYDROTHERMAL METHOD

[a]A. Martin Joseph*, [b]R. Thilak Kumar*
[a]Research and Development Centre, Bharathiar University, Coimbatore , Tamilnadu, India
[b]Periyar Arts College, Cuddalore-607001, Tamilnadu, India
*Corresponding author email: manojthilak@yahoo.com

ABSTRACT

Hydrothermal fabrication of pure α-Manganese Dioxide Nanostructures were done by the reduction of 0.2m/L of $KMnO_4$ with 0.2m/L of $Na_2S_2O_3.5H_2O$ at two elevated temperatures (393 and 413K) by passivating with the organic ligand Aniline. The Structural, Functional, Morphological and Chemical Composition of the fabricated Nanorods were investigated by X-Ray Diffractometer (XRD), Fourier Transform Infrared Spectrometer (FTIR), High Resolution Scanning Electron Microscope (HR-SEM) and Energy Dispersive X-Ray Spectrometry (EDX). The XRD analysis indicated high crystalline nature of the product, FTIR confirmed the contribution of the organic ligand in surface passivation. HR-SEM image revealed the morphology of the fabricated α-MnO_2 Nanostructures. EDX confirmed the presence of Mn and O in the material. The Magnetic studies were carried out using Vibrating Sample Magnetometer (VSM) which showed that the α-MnO_2 nanostructures exhibits a paramagnetic behavior with Saturation magnetization around 0.49 and 0.70emu/g . The magnetic properties, like saturation magnetization, coercivity and Retentivity were found to increases with increasing reaction temperature. This enhancement is attributed to the transition from a multi-domain to a single-domain nature of the material were reported.

Keywords: Nanostructures, Hydrothermal Fabrication, X-Ray Diffraction, Vibrating Sample Magnetometer

---

EFFECTS OF ANNEALING TEMPERATURE OF MAGNESIUM DOPED NICKEL FERRITE NANOPARTICLES

K.ELAYAKUMAR[a], R.SAGAYARAJ[b], R.THILAKUMAR[c]
[a]Research scholar, Bharathiar University, Coimbatore, Tamilnadu, India.
[b]Research scholar, ThiruvalluvarUniversity, Vellore, Tamilnadu, India.
Department Of Physics, Periyar Arts college, Cuddalore, Tamilnadu. India.
E-mail: elaya.phys@gmail.com

ABSTRACT

As a promising material for soft magnets, magnesium doped nickel ferrite nanoparticles were prepared by co-precipitation method. The structural, functional groups and morphological studies are carried out for the investigation of prepared nanoparticles . The crystalline size of the nanoparticles are increases by varying the annealing temperature at (650°C,750°C,850°C) are found to be 35,40,52 nm. From the analysis of FT-IR spectra the functional groups are studied, the morphology of the nanoparticles are remarkably varying from mixed spongy state to spine structure.

[a] Corresponding Author E-mail: elaya.phys@gmail.com
Mobile: +919944002801

STUDIES ON THE GROWTH, STRUCTURAL, OPTICAL, MECHANICAL AND SHG PROPERTIES OF DIGLYCINE AMMONIUM CHLORIDE SINGLE CRYSTAL: AN ORGANIC NONLINEAR OPTICAL CRYSTAL

H.JUDE LEONARD HILARY[a], P.C.JOBE PRABAHAKAR[b], A.CHRISTY FERDINAND[c]
[a]Research scholar, Bharathidasan University, Tiruchirappalli, Tamilnadu, India.
Department Of Physics, T.B.M.L.college, Porayar, Tamilnadu. India.
Department Of Physics, Periyar Arts college, Cuddalore, Tamilnadu. India.
E-mail: judeleonard141@gmail.com

ABSTRACT

Single crystals of diglycine ammonium chloride was grown from aqueous solution by low temperature growth technique. The phase purity and crystal structure of the grown crystals were confirmed by Powder X-ray diffraction analysis. The presence of functional groups were confirmed by FT-IR spectrum. The optical absorption and lower cut-off values were ascertained by recorded UV-Visible spectrum of crystals. The mechanical properties of the grown crystal was subjected to Vickers hardness test. The second-order nonlinear optical property was confirmed by Q-switched Nd:YAG laser technique.

Keywords: Solution growth, XRD, FT-IR, Optical absorption, Mechanical, NLO

SYNTHESIS, GROWTH AND CHARACTERIZATION OF ORGANIC NLO MATERIAL: DIGLYCINE TRICHLOROACETATE

H.JUDE LEONARD HILARY[a], P.C.JOBE PRABAHAKAR[b], A.CHRISTY FERDINAND[c], C.YOGAMBAL[d]
[a]Research scholar, Bharathidasan University, Tiruchirappalli, Tamilnadu, India.
[b]Department Of Physics, T.B.M.L.college, Porayar, Tamilnadu. India.
[c]Department Of Physics, Periyar Arts college, Cuddalore, Tamilnadu. India.
[d]Department Of Physics, St.Joseph's college of Arts And Science, Cuddalore, Tamilnadu. India.
E-mail: judeleonard141@gmail.com

ABSTRACT

A nonlinear optical material of Diglycine Trichloroacetatecrystal was grown by slow evaporation method. The form of crystallization was confirmed by powder X-ray diffraction analysis. The presence of all the functional groups of the sample was confirmed by FT-IR spectral analysis. The grown crystal was subjected to Vickers microhardness test. The optical transparency and lower cut-off value of UV transmission **237 nm** were ascertained by recording a UV- Visible spectrum of crystal. The second-order nonlinear optical property was confirmed by Q-switched Nd:YAG laser.

Keywords: Crystal growth, PXRD, FT-IR, UV-Vis-NIR, Nonlinear optical

STUDIES ON GROWTH, STRUCTURAL, OPTICAL AND THERMAL PROPERTIES OF CADMIUM THIOCYANATE DIMETHYL SULFOXIDE NLO CRYSTAL

S. Karthick*, A. Albert Irudayaraj, A. Dhayal raj, R. Vinayagamoorthy

Research and PG Department of Physics, Sacred Heart College,
Tirupattur, Vellore Dist. - 635601.

ABSTRACT

The organometallic crystal,Cadmium Dimethyl Sulfoxide Thiocyanate (CDST) was grown from aqueous solution. The grown CDST crystals are characterized by powder X-ray diffraction for structural analysis.Fourier Transformation Infrared analysis confirms the presence of functional groups in the CDST. UV- Visible analysis reveals that CDST is about 90% transparent in the entire visible region and UV lower cutoff wavelength is 236 nm. TGA and DTA studies reveal thephysicochemical stability of the CDST and NLO study by Kurtz – Perrypowder technique reveals that the CDSTexhibits emission of green light and the second harmonic generation efficiency of CDTS was 1.2 times that of KDP.

Key words: Organometallic crystal, FTIR, UV-Vis, TG/DTA, NLO.

STRUCTURAL, OPTICAL AND ELECTRICAL PROPERTIES OF HYDROTHERMAL SYNTHESIZED VO_2 AND LiV_3O_8 NANOMATERIALS

Suganya A and Seenuvasakumaran P

PG and Research department of Physics, Muthurangam Government Arts College (Aut), Vellore 632002, TamilNadu, India

ABSTRACT

Vanadium dioxide (VO_2) and Lithium Vanadium oxides (LiV_3O_8) have been extensively studied in recent research, because of their potential applications in thermochromic materials and as a cathode material for rechargeable lithium batteries. VO_2 and LiV_3O_8 are successfully synthesized via facile hydrothermal method using vanadium pentoxide (V_2O_5), Lithium nitrate ($LiNO_3$) as a starting materials and NaOH as a reductant. The precursors are kept in stainless steel-autoclave at 120^0C for 20 hours. In the case of hydrothermal method, formation of nanostructured materials depends on concentration of precursors, reaction rate and temperature, reductant and pH. From XRD, the crystalline structure of synthesized nanomaterials VO_2 and LiV_3O_8 monoclinic phase and the crystallite size are 27 nm and 23 nm respectively. The strain is estimated through Williamson-Hall plot which reveals the structural defects of nanomaterials. The morphological and elemental compositions are analyzed from SEM with EDAX diffraction. From FT-IR spectrum, the conformation of absorption band of metal oxide and various functional groups peaks are performed.The measurement of direct and indirect energy gap of VO_2 and LiV_3O_8 are determined from Tauc plot as 1.76 eV & 1.69 eV and 1.57 eV & 1.54 eV respectively. The emission excitation values are studied from Photo Luminescence spectra. The electrical properties are investigated from graphical results of Cyclic Voltameter.

KEYWORDS: hydrothermal synthesis, stainless steel autoclave, VO_2, LiV_3O_8, thermochromic material, Lithium ion batteries.

Dr.S.M.Ravikumar did his M.Sc(Physics) in Madras Christian College, Tambaram, Chennai, Tamilnadu and obtained his Ph.D degree in the field of Crystal growth from Loyola college, chennai which is affiliated to University of Madras. He has about 30 research article published in reputed International Journals and more than 70 papers presented in the National and International conferences. He has guided more than ten students in obtaining M.Phil degree and currently guiding Ph.D scholars for Thiruvalluvar University, Vellore. He is having teaching experience more than 10 years in college levles. At present he is working as Assistant Professor of Physics, Government Arts College, Tiruvannamalai, Tamilnadu, India.

ISBN 9788193156612

JACS DIRECTORY
Research Journals and Book Publishing Group
Tamilnadu. India.
www.jacsdirectory.com/book